

Experimental investigation of electrical domestic heat pumps equipped with a twin-stage oil-free radial compressor

THÈSE N° 6764 (2015)

PRÉSENTÉE LE 26 NOVEMBRE 2015

À LA FACULTÉ DES SCIENCES ET TECHNIQUES DE L'INGÉNIEUR
LABORATOIRE D'ÉNERGÉTIQUE INDUSTRIELLE
PROGRAMME DOCTORAL EN ENERGIE

ÉCOLE POLYTECHNIQUE FÉDÉRALE DE LAUSANNE

POUR L'OBTENTION DU GRADE DE DOCTEUR ÈS SCIENCES

PAR

Jean-Baptiste CARRÉ

acceptée sur proposition du jury:

Dr J. Van Herle, président du jury
Prof. D. Favrat, directeur de thèse
Prof. V. Lemort, rapporteur
Dr D. Hughes, rapporteur
Prof. J. Schiffmann, rapporteur



ÉCOLE POLYTECHNIQUE
FÉDÉRALE DE LAUSANNE

Suisse
2015

Résumé

La consommation mondiale d'énergie a augmenté dramatiquement depuis la fin de la seconde guerre mondiale. La part principale de cette énergie provient de la combustion d'énergie fossile. Le secteur résidentiel consomme environ 30% de la production totale d'énergie et la plus grande part de cette dernière est dédiée au chauffage des espaces de vie et à la production d'eau chaude sanitaire. Dans ce contexte une consommation d'énergie soutenable est requise afin de limiter notre impact sur l'environnement et le climat, l'efficacité énergétique est un facteur clé pour amorcer la transition vers la sobriété énergétique. Les pompes à chaleur alimentées par électricité sont identifiées comme une technologie clé pour augmenter notre efficacité énergétique. Nous avons besoin de pompes à chaleur plus efficaces, plus compactes, plus silencieuses, construites avec moins de matières premières, et utilisant des charges en réfrigérant plus faibles. La phase de compression est responsable de la plupart des pertes d'énergie. Depuis des décennies maintenant, les performances des pompes à chaleur stagnent, principalement parce que l'efficacité de la phase de compression stagne. Par conséquent, il est nécessaire d'améliorer l'efficacité de la phase de compression. Une nouvelle conception d'unité compresseur mono-étagé a été développée, construite, et testée lors d'une thèse de doctorat précédente. La thèse présentée ici utilise une unité compresseurs bi-étagés ayant succédé à l'unité compresseur mono-étagée initiale, et a testé l'unité en question dans deux prototypes de pompe à chaleur domestique sans huile. Ce travail vise à étudier l'intégration d'unités compresseurs radiaux dans des pompes à chaleur domestiques et à démontrer la faisabilité et le potentiel de ces dernières. Les prototypes testés sont une pompe à chaleur domestique Air/Eau sans huile et une pompe à chaleur domestique Saumure/Eau sans huile. Les deux prototypes sont équipés d'une unité compresseurs bi-étagés radiaux sans huile dont l'arbre est en rotation sur des paliers à gaz. La vitesse maximum du rotor de ces unités est de 180000 tours/min. Six points de fonctionnement stables ont été documentés avec le prototype Air/Eau. Notamment, le point de fonctionnement A-7/W35 a été atteint et démontre un coefficient de performance de 2.36 pour une puissance chaleur de 10.7 kW. Le prototype Saumure/Eau a été utilisé pour procéder à des tests partiels d'amélioration apportées aux circuits de pompe à chaleur, afin d'apporter des solutions aux problèmes rencontrés avec le prototype Air/Eau. L'analyse des données expérimentales utilise une modélisation dont l'approche est basée sur les équations de conservation de masse et d'énergie. Cette approche permet d'améliorer le niveau de compréhension des débits internes ou non-mesurables du système. Le modèle propage aussi, à travers les équations, les incertitudes de mesure des données expérimentales. De nouvelles améliorations et circuits de pompes à chaleur innovants, notamment, au niveau de l'économiseur, composant-clé du circuit, sont proposés et intègrent plus intimement l'unité compresseur dans les circuits de la pompe à chaleur bi-étagée, et cela afin de parvenir à des systèmes globalement plus efficaces, plus compacts, plus silencieux, moins gourmand en terme de matières premières, et nécessitant moins de charge de réfrigérant.

Mots clefs: pompe à chaleur, 2 étages, sans huile, lubrifiant, compresseur radial, économiseur, réservoir de décompression

Abstract

The world energy consumption has dramatically increased since the end of the World War II. The main share of this energy comes from fossil fuel combustion. The worldwide domestic sector consumes about 30% of the global energy supply and the biggest share of that is dedicated to space and water heating. In this context where sustainable energy consumption is required to limit our impact on the environment and the climate, energy efficiency is a key factor to successfully transition to energy sobriety. Electrically-driven heat pumps are known to be a key technology to increase our energy efficiency. More efficient, more compact, more silent heat pumps, built with less raw material, and using lower refrigerant charges are needed. In electrically-driven heat pumps, the compression process is responsible for most of the energy losses. However, for decades now, the heat pump performance has been stagnating, mainly because of the compression process efficiency which has not been increasing significantly. Consequently, the improvement of the compression process is indeed needed. A new single-stage compression unit design has been developed, built, and tested in a previous thesis work. This current thesis work uses a twin-stage successor of the initial single-stage compression unit and tests it into two oil-free domestic heat pump prototypes. This work aims at studying the integration of the radial compression units in domestic heat pumps and at demonstrating their feasibility and potential. The tested prototypes are a twin-stage Air/Water domestic heat pump and a twin-stage Brine/Water domestic heat pump. Both of them are equipped with a twin-stage oil-free radial compression unit rotating on gas bearings. By which, the maximum rotor speed of the compression units is 180 krpm. Six stable operating points have been documented with the Air/Water heat pump prototype. More notably so, the operating point A-7/W35 has been reached and demonstrates a coefficient of performance of 2.36 for a heating power of 10.7 kW. The Brine/Water heat pump prototype has been used to perform partial tests of circuit improvements, in order to solve some of the issues observed on the Air/Water prototype. The analysis of the experimental results uses a mass and energy balance modeling approach to improve the level of understanding of the internal and non measurable flows in the heat pump circuits. This model also propagates the uncertainties of the measurements through the equations. New improvements and innovative circuit layouts, notably at the level of the economizer, a key-component of the two-stage heat pump circuit, are offered to integrate further the compression unit in the heat pump circuits, and to make the whole system more efficient, more compact, more silent, less demanding in raw materials and reducing the refrigerant charge needed for the heat pump cycle.

Keywords: heat pump, two stages, twin-stage, oil-free, radial compressor, lubrication, heatpump, economizer, flash tank, gas bearings

License and Acknowledgments

This thesis manuscript is the final thesis version, numbered v1.0.2. The manuscript source files are available online at <https://github.com/speredenn/epfl-leni-oilfree-radial-cp-hp/releases/tag/v1.0.2>. The compiled PDF version is available at [doi:10.5075/epfl-thesis-6764](https://doi.org/10.5075/epfl-thesis-6764). The official printed version of this thesis manuscript is printed in Black & White (B&W). Most of the figures presented in this manuscript have been designed to be readable in B&W, but a few of them are easier to understand in their color version (like fig. 4.13, page 54 or fig. 4.16, page 60). Please refer to the online version on the EPFL website ([doi:10.5075/epfl-thesis-6764](https://doi.org/10.5075/epfl-thesis-6764)) to access the color version of the figures.

License

This thesis work is licensed under [Creative Commons Attribution 4.0 International \(CC BY 4.0\)](https://creativecommons.org/licenses/by/4.0/)¹. Excepted if specified differently in the credits sections of each chapter, graphs, figures, tables, pictures, movies, and photographs are copyrighted by Jean-Baptiste Carré and are licensed under [Creative Commons Attribution 4.0 International \(CC BY 4.0\)](https://creativecommons.org/licenses/by/4.0/). The parts and assemblies designs are copyrighted by Jean-Baptiste Carré and are licensed under [Creative Commons Attribution 4.0 International \(CC BY 4.0\)](https://creativecommons.org/licenses/by/4.0/). The codes developed for the purpose of this thesis are licensed under the [GNU General Public License 3.0](https://www.gnu.org/licenses/gpl-3.0.html)². In order to use all the functions of those codes, some external codes and tools, not licensed under the [GNU General Public License 3.0](https://www.gnu.org/licenses/gpl-3.0.html) or a more permissive license, are needed. Please refer to the specific instructions in each of those codes to know more about those limitations and conditions of use. Those external codes or tools are not provided with the thesis codes.

The sources of this thesis and its codes are available in the repositories listed below:

- Thesis dynamic version:
<https://www.authorea.com/users/54640/articles/71121/>
- Thesis static version, with data analysis codes included:
<https://github.com/speredenn/epfl-leni-oilfree-radial-cp-hp>

Acknowledgments

First of all I want to thank [Professor Daniel Favrat](#) who has supported me unconditionally throughout the whole thesis time. I particularly appreciated his guidance and vision. I also address my gratitude toward Professor [Jürg Schiffmann](#) who supported me in this project with lots of inestimable advice and care on theoretical and technical topics. I am also grateful that he accepted to be one of the co-examiners for this thesis. My thanks equally go to [Professor Vincent Lemort](#) and [Dr. David Hughes](#) for having accepted to be co-examiners for this thesis, and to [Professor Jan Van Herle](#) to have accepted to be the President of the jury. Many thanks to my colleagues [Julien Jakubowski](#) and [Johannes Wegele](#) who have greatly contributed to the success of this project with their help in the laboratory. I also want to thank [Gilles Bernard](#), [Dr. Patrice Dubois](#), and [Professor Jean-François Omhover](#) to have enhanced my perspectives and sharpened my taste for research. Thanks also to [Professor Roger Röthlisberger](#) and

¹ <http://creativecommons.org/licenses/by/4.0/>

² <http://www.gnu.org/licenses/gpl.html>

to my colleagues [Violette Mounier](#), [Antoine Girardin](#), [Noé Bory](#), and [Julien Ropp](#) for their help, tolerance, and support during the last months of my PhD work.

During my work and my research at the [Industrial Energy Systems Laboratory \(LENI\)](#), there were many people who have made my work considerably easier and more enjoyable. Particular thanks (in alphabetic order) to [Alberto](#), [Amalric](#), [Andreas Schöler](#), [Angel](#), [Antoine B. Antonin](#), [Arata](#), [Azadeh](#), [Benjamin](#), [Benoît](#), [Cédric B.](#), [Cédric F.](#), [Christian](#), [Claudia](#), [David](#), [Diego](#), [Emanuela](#), [Emmanuele](#), [Germain](#), [Helen](#), [Henning](#), [Hossein](#), [Irvin](#), [Jakob](#), [James](#), [Johannes](#), [Jonathan](#), [Jorge](#), [Juliette](#), [Laurence](#), [Leandro](#), [Leda](#), [Leonidas](#), [Luc](#), [Manuele](#), [Marco R.](#), [Martin](#), [Matteo](#), [Mathias](#), [Matthias B.](#), [Matthias D.](#), [Matthieu](#), [Nadia](#), [Nasibeh](#), [Nicolas B.](#), [Nicolas D.](#), [Nicolas R.](#), [Nicole](#), [Nordahl](#), [Olivier](#), [Pietro](#), [Priscilla](#), [Raffaele](#), [Raman](#), [Romain](#), [Samira](#), [Samuel Haury](#), [Samuel Henchoz](#), [Simon G.](#), [Sinan](#), [Stefan](#), [Stéphane](#), [Stefano](#), [Tivi](#), [Thierry](#), [Thomas](#), [Yannick](#), [Zacharie](#), [Zlatina](#), and [Zoé](#). Thanks to them for sharing many ideas and good times. I also thank [Dr. Michele Zehnder](#), [Professor Deborah Sills](#), [Professor Cécile Munch-Alligné](#), [Dr. Sami Barbouchi](#) and [Pierre-Alain Giroud](#) for the interesting discussions that we have had each time we met. I also want to thank my colleagues and friends from [Heat and Mass Transfer Laboratory \(LTCM\)](#) and the [Thermal Turbomachinery Laboratory \(LTT\)](#) who have shared with me nice and sweet moments, in addition to their experience with experimental work. My thanks go notably, in [LTCM](#) (in alphabetic order), to [Andrea](#), [Bogdan](#), [Brian](#), [Cécile](#), [Duan](#), [Etienne](#), [Eugene](#), [Farzad](#), [Giulia](#), [Gustavo](#), [Jackson](#), [Jeff](#), [Marco M.](#), [Mathieu](#), [Mirco](#), [Natalie](#), [Nicolas A.](#), [Nicolas L.](#), [Ricardo](#), [Sepideh](#), and [Sylvia](#), and in [LTT](#) (in alphabetic order), to [Achim](#), [Alexandros](#), [Elia](#), [Jonsson](#), [Philip](#), [Sami](#), and [Virginie](#). Thanks also to the people close and dear to me who were there to support me so frequently. I met wonderful people while practicing martial arts, volunteering, or defending the causes dear to me. Thanks for the wonderful times that helped me and made me stand the work load.

My special thanks go to [Marc Salle](#), [Christophe Zurmühle](#), [Nicolas Jaunin](#), [Laurent Chevalley](#), and [Aziz](#), for the help with the manufacturing of the parts and the assembly of the experimental setups.

Many thanks to [Brigitte](#), [Suzanne Z.](#), [Irène](#), and [Faye](#), the amazing [LENI](#) secretaries, who always made things easy with the administrative stuff and who saved the situation many times, despite the tight schedule.

Many thanks to my first aider teammates and friends, notably (in alphabetic order) to [Agnès](#), [Alexandre](#), [Alok](#), [Andreas Schwab](#), [Audrey](#), [Carlos](#), [Christophe](#), [Coralie](#), [Cyrielle](#), [Daniela](#), [Élise](#), [Eric](#), [Frank](#), [Gaëlle](#), [Julien](#), [Leila](#), [Linda](#), [Mahé](#), [Mickaël](#), [Mikael](#), [Monica](#), [Nikita](#), [Nils](#), [Pascal](#), [Pauline](#), [Petr](#), [Pierre-Alain](#), [Philipp](#), [Raphaël](#), [Sabina](#), [Simon D.](#), [Suzanne D.](#), [Thomas](#), and [Yvan](#), for the nice moments during the EPFL events and for really interesting exchanges and discussions. Many thanks to the [Safety, Prevention and Health Domain \(DSPS\)](#) for its top-level first-aid-training program.

My deepest thanks go to you, [Alisa](#), who always supported me and the constraints subsequent to our lives. You have stood unacceptable situations and difficulties, and you have helped me to evolve and grow. For this, I will never thank you enough. Thank you, [Riwen](#), to have been such a patient, understanding, and tolerant child with me. Thanks to have been so frequently nice when I was falling asleep directly on the ground of your room, while we were playing, when I was finally back home after long work days. Thanks to you, [Adam Young](#), for the amazing songs, optimistic and cheerful melodies and lyrics, which guided me through my thesis work and efforts, and which still guide me through my life. Thanks to you, [Dr. David Lefrançois](#), [Dr. Stephen Covey](#), and [Tony Buzan](#), for the amazing guidance and insights you provide and share everyday (or that you provided and shared, [Stephen](#)).

This thesis work is funded by the [Swiss Commission for Technology and Innovation \(CTI\)](#) and [Fischer Engineering Solutions AG](#), which is part of the [Fischer Spindle group](#). The compressor units used in this thesis work have been manufactured by [Fischer Engineering Solutions AG](#). I thank them for their help and support. I thank the [CTI](#) and [Fischer Engineering Solutions AG](#) for the funding that allowed me to perform this thesis work.

Contents

Résumé	i
Abstract	iii
License and Acknowledgments	v
Contents	vii
List of Figures	xiii
List of Tables	xvii
Nomenclature	xix
Glossary	xxi
1 Introduction	1
1.1 The world energy consumption needs to be slowed down	1
1.2 Better domestic heat pumps can help	4
1.3 Scope of this thesis work	4
Bibliography	5
Credits	5
2 State of the art	7
2.1 Types of refrigerant compressors	7
2.1.1 Dynamic versus volumetric	7
2.1.2 Volumetric compressors used in domestic heat pumps	7
2.1.3 Dynamic compressors used in domestic heat pumps	9
2.1.4 About the compression units used in this thesis work	9
2.2 Noise reduction in refrigeration circuits	9
2.3 Variable-speed in refrigeration circuits	11

2.4	Multistage refrigeration circuits	11
2.5	Lubrication in refrigeration circuits	12
2.5.1	Impact of the lubricant on the expansion process	13
2.5.2	Impact of the lubricant on the evaporation process	13
2.5.3	Oil-free heat exchange technologies	14
2.5.4	Impact of the lubricant oil on the compression process	14
2.6	Refrigerant charge reduction in refrigeration circuits	14
2.6.1	Importance of the control strategy in heat pumps with low refrigerant charge	15
2.7	Defrosting strategies	15
	Bibliography	16
	Credits	21
3	Thesis & methodology	23
3.1	Demonstration of feasibility	23
3.2	Demonstration of potential	23
3.3	Limits of the demonstration	24
3.4	Methodology	24
3.4.1	Design and assembly of heat pump prototypes	24
3.4.2	Test of the heat pump prototypes	24
3.4.3	Modeling of those heat pump prototypes	25
3.4.4	Analysis of the experimental results	29
	Bibliography	33
4	Air-Water heat pump Prototype (AWP)	35
4.1	Design of the AWP	35
4.1.1	Specifications	35
4.1.2	Description	36
4.2	AWP components	36
4.2.1	Compression unit	36
4.2.2	Compression stage bypass systems	39
4.2.3	Economizer	39
4.2.4	Evaporator	40
4.2.5	4-way valve	45
4.3	Modeling	45
4.4	Prototype performance	46
4.5	Design issues	47
4.5.1	Gas forced to flow reversely in one side of the axial bearing	48
4.5.2	Excess of compressor thrust forces during deceleration	48
4.5.3	Significant increase of the temperatures in the labyrinth seal with rotation speed	49
4.5.4	Mixing and separating gas and liquid in the economizer:	53

4.5.5	Decreasing the performance by using a 4-way valve	53
4.5.6	Poor exergy efficiency of the evaporator and fluids maldistribution	55
4.5.7	Poor exergy efficiency of the subcooler	57
4.6	Control issues	57
4.6.1	Procedure to start the cycle	57
4.6.2	Procedure to reverse the cycle	58
4.6.3	Procedure to stop the cycle	59
4.6.4	Setting an appropriate gas bearings aeration circuit flow rate	59
4.6.5	Setting an appropriate motor cooling circuit flow rate	59
4.6.6	Controlling the heat pump to reach stable OP	61
4.6.7	Control of an industrialized version of the AWP	63
	Bibliography	64
	Credits	65
5	Brine-Water heat pump Prototype (BWP)	67
5.1	Design of the BWP	67
5.1.1	Specifications	67
5.1.2	Description	68
5.2	BWP components	68
5.2.1	Compression unit	68
5.2.2	Bypass system	71
5.2.3	Motor cooling circuit	71
5.2.4	Gas bearings aeration circuit	72
5.3	Modeling	74
5.4	BWP results and observations	74
5.5	Additional issues	76
5.5.1	Getting enough power to explore the operation range	76
5.5.2	Setting the intermediate pressure to a chosen value while being in bypass-mode	78
5.5.3	Pumping down of the evaporator	78
5.5.4	Keeping the loop clean	80
	Bibliography	81
6	Integration of the compression unit in heat pumps layouts	83
6.1	Topology	83
6.2	Electromagnetic perturbations	83
6.3	Gas bearings aeration circuits	84
6.4	Towards new layouts with improved bypass circuits	84
6.5	Towards more integration, performance, and compactness	87
	Bibliography	88

7 Conclusion & outlook	89
7.1 Conclusion	89
7.1.1 Feasible	89
7.1.2 Promising performance	89
7.1.3 Many challenging improvements needed	89
7.2 Perspectives	90
Appendix A Details about the Air-Water heat pump Prototype	91
A.1 Components	91
A.1.1 Evaporator	91
A.1.2 Pipes and fittings	91
A.1.3 Valves	91
A.1.4 Economizer	91
A.1.5 Subcooler	92
A.1.6 Motor cooling chamber and circuit	92
A.2 Sensors	93
Bibliography	93
Appendix B Details about the Brine-Water heat pump test-rig	95
B.1 History	95
B.1.1 First set of heavy modifications	96
B.1.2 Second set of heavy modifications	96
B.2 Gas bearings aeration circuit layout and topology	96
B.3 Motor cooling circuit layout and topology	97
B.4 Components	97
B.4.1 Expansion devices	97
B.4.2 Load cells	97
B.4.3 First stage separator	97
B.4.4 Economizer	99
B.4.5 Pipes and fittings	100
Bibliography	100
Appendix C Equations set for the simple example	101
Appendix D AWP model set of equations	103
Bibliography	106
Appendix E BWP model set of equations	107
Bibliography	109

Appendix F Experimental data	111
F.1 A-6.8/W31.3 - 170 krpm	111
F.2 A-7.0/W32.3 - 160 krpm	114
F.3 A-7.0/W35.6 - 171 krpm	117
F.4 A-0.5/W20.7 - 130 krpm	120
F.5 A-3.1/W29.5 - 153 krpm	123
F.6 A-6.6/W22.1 - 160 krpm	126
F.7 B8.0/W11.0 - 110 krpm	129
Appendix G Uncertainties and sensors calibration	135
G.1 Stable OP	135
G.2 Sensors calibration	135
G.2.1 Absolute pressure transducers	135
G.2.2 Thermocouples	137
G.3 Uncertainties	138
G.3.1 Propagation of the uncertainties in the calculations	138
Bibliography	139
Appendix H Compressor maps mathematical models	141
H.1 History	141
H.2 Why a mathematical model of the compression maps?	141
H.3 Mathematical model of a compression map	142
H.3.1 Modeling of the compressor iso-speed curves	142
H.3.2 Rotation of the coordinates	143
H.3.3 Modeling of the isentropic efficiency	143
H.4 Errors of the correlations	143
Bibliography	146
CV	147

List of Figures

- 1.1 Final energy consumption in Switzerland 2
- 1.2 Final household energy consumption for the IEA19 3

- 2.1 Trends for high speed electrical drives and turbomachineries. 10
- 2.2 Volume of the twin-stage compression unit 10

- 3.1 Example case – Layout & model 26
- 3.2 Example case – Thermodynamic diagrams 29

- 4.1 Housing and 3D layout of the AWP circuits 36
- 4.2 AWP layout with components numbers 37
- 4.3 AWP model 38
- 4.4 Structure of the compressor unit with the AWP gas bearings aeration circuit I/O layout 40
- 4.5 Views of the AWP 41
- 4.6 Compression unit *cp105*, being mounted in the AWP 41
- 4.7 AWP economizer version #1 to #5. 42
- 4.8 AWP assembly 43
- 4.9 Gas/liquid stream patterns with qualitative flow velocities 44
- 4.10 View of the 4-way reversing valve in the heat pump circuits 45
- 4.11 A-7.0/W35.6 - Sankey diagram for heat pump energy balance (internal frontier) 47
- 4.12 Gas temperatures inside the compression unit 51
- 4.13 A-6.8/W31.3 & A-7.0/W32.3 – Thermodynamic diagrams with and without 4-way valve 54
- 4.14 Refrigerant and air flow maldistribution in the evaporator 56
- 4.15 Air ducting with the fan and the fin-and-tube evaporator 57
- 4.16 A-3.1/W29.5 & A-6.6/W22.1 – Thermodynamic diagrams 60
- 4.17 A-7.0/W35.6 – Thermodynamic diagrams 60
- 4.18 Schematic of the motor cooling chamber filled up with lubricant oil 61
- 4.19 The flow rates of the compression stages are bound together 62

5.1	BWP topology, after the first set of heavy modifications mentioned in appendix B.1.1.	69
5.2	View of the experimental setup in the laboratory.	69
5.3	Layout of the Brine-Water heat pump test-rig	70
5.4	Structure of the compressor unit with the BWP gas bearings aeration circuit I/O layout	71
5.5	Compression unit <i>cp101</i> , mounted in the BWP	72
5.6	Compressors bypass systems in the AWP and the BWP	73
5.7	Modeling of the BWP in bypass mode	75
5.8	Thermodynamic diagrams of the BWP OP and of its closer AWP OP	77
5.9	Simplified layout in an evaporator pump down situation	79
5.10	Lubricant pollution in the BWP	81
6.1	Proposal for a new BWP layout	85
6.2	Proposal for a new AWP layout	86
6.3	Proposal of an integrated topology for a future heat pump prototype	87
A.1	AWP motor cooling inlet/outlet (heating mode)	92
A.2	Extra shielding of the AWP sensor cables	93
A.3	Electro-magnetic perturbation of pressure sensors signals	93
B.1	BWP expansion devices section	98
B.2	Load cell used in the BWP	98
B.3	First stage compressor inlet separator, in the BWP	99
B.4	Economizer of the BWP	100
F.1	A-6.8/W31.3 – Sankey diagram for heat pump energy balance (internal frontier)	111
F.2	A-6.8/W31.3 – Sankey diagram for the compressor unit energy balance	112
F.3	A-6.8/W31.3 – Sankey diagram for the motor energy balance	112
F.4	A-7.0/W32.3 – Sankey diagram for heat pump energy balance (internal frontier)	115
F.5	A-7.0/W32.3 – Sankey diagram for the compressor unit energy balance	115
F.6	A-7.0/W32.3 – Sankey diagram for the motor energy balance	115
F.7	A-7.0/W35.6 – Sankey diagram for the compressor unit energy balance	118
F.8	A-7.0/W35.6 – Sankey diagram for the motor energy balance	118
F.9	A-0.5/W20.7 – Sankey diagram for heat pump energy balance (internal frontier)	121
F.10	A-0.5/W20.7 – Sankey diagram for the compressor unit energy balance	121
F.11	A-0.5/W20.7 – Sankey diagram for the motor energy balance	121
F.12	A-3.1/W29.5 – Sankey diagram for heat pump energy balance (internal frontier)	124
F.13	A-3.1/W29.5 - Sankey diagram for the compressor unit energy balance	124
F.14	A-3.1/W29.5 – Sankey diagram for the motor energy balance	124
F.15	A-6.6/W22.1 – Sankey diagram for heat pump energy balance (internal frontier)	127
F.16	A-6.6/W22.1 – Sankey diagram for the compressor unit energy balance	127
F.17	A-6.6/W22.1 – Sankey diagram for the motor energy balance	127

F.18	B8.0/W11.0 – Sankey diagram for heat pump energy balance (internal frontier)	131
F.19	B8.0/W11.0 – Sankey diagram for the compressor unit energy balance	131
F.20	B8.0/W11.0 – Sankey diagram for the motor energy balance	131
F.21	Pressures and temperatures at the bearings cavity when the breakdown happened	132
F.22	Pressures and temperatures at compression unit inlets/outlets when the breakdown happened	132
F.23	Power consumption and rotational speed records when the breakdown happened	133
G.1	Absolute pressure transducers calibration statistics	137
G.2	Thermocouples calibration statistics	138
H.1	Errors in the first compression stage map correlations	144
H.2	Errors in the second compression stage map correlations	145

List of Tables

3.1	Example case – Thermodynamic points of the heat pump cycle	28
3.2	Example case – Mass flow rates between the components	29
3.3	Example case – Energy flows between the components	29
4.1	Overall performance of the AWP and its main components	47
4.2	AWP and similar industrial domestic heat pumps coefficient of performance	48
4.3	Temperatures and heat energy exchanges inside the compression unit. The uncertainties are not all the same for every experiments because some sensors have been damaged between the different experiments. Indeed, the measurement points were equipped with one, two, or three thermocouples. Consequently, the values measured have not been measured all the time with the same number of sensors.	50
4.4	Isentropic efficiencies for each compression stages	52
4.5	OP comparison with and without 4-way valve	55
5.1	Key values for the comparison of the AWP and the BWP gas bearings aeration circuits	76
5.2	B8.0/W11.0 – Mass flow rates between the components	76
5.3	B8.0/W11.0 – Energy rates between the components	77
F.1	A-6.8/W31.3 – Performance indicators	111
F.2	A-6.8/W31.3 – Thermodynamic points of the heat pump cycle	113
F.3	A-6.8/W31.3 – Mass flow rates between the components	114
F.4	A-6.8/W31.3 – Energy rates between the components	114
F.5	A-7.0/W32.3 – Performance indicators	114
F.6	A-7.0/W32.3 – Thermodynamic points of the heat pump cycle	116
F.7	A-7.0/W32.3 – Mass flow rates between the components	117
F.8	A-7.0/W32.3 – Energy rates between the components	117
F.9	A-7.0/W35.6 – Performance indicators	117
F.10	A-7.0/W35.6 – Thermodynamic points of the heat pump cycle	119
F.11	A-7.0/W35.6 – Mass flow rates between the components	120
F.12	A-7.0/W35.6 – Energy rates between the components	120

F.13	A-0.5/W20.7 – Performance indicators	120
F.14	A-0.5/W20.7 – Thermodynamic points of the heat pump cycle	122
F.15	A-0.5/W20.7 – Mass flow rates between the components	123
F.16	A-0.5/W20.7 – Energy rates between the components	123
F.17	A-3.1/W29.5 – Performance indicators	123
F.18	A-3.1/W29.5 – Thermodynamic points of the heat pump cycle	125
F.19	A-3.1/W29.5 – Mass flow rates between the components	126
F.20	A-3.1/W29.5 – Energy flows between the components	126
F.21	A-6.6/W22.1 – Performance indicators	126
F.22	A-6.6/W22.1 – Thermodynamic points of the heat pump cycle	128
F.23	A-6.6/W22.1 – Mass flow rates between the components	129
F.24	A-6.6/W22.1 – Energy rates between the components	129
F.25	B8.0/W11.0 – Thermodynamic points of the heat pump cycle	130
F.26	B8.0/W11.0 – Performance indicators	132
H.1	Characteristics of the classical and the dimensionless compressor maps	142

Nomenclature

Roman Symbols

\dot{E}	Energy rate, exergy rate	[W]
\dot{M}	Mass flow rate	[kg s ⁻¹]
\dot{Q}	Heat energy rate	[W]
\dot{Y}	Transformation energy rate [eq. (3.6) page 30]	[W]
h	Specific enthalpy	[J kg ⁻¹]
P	Absolute pressure, pressure	[Pa]
s	Specific entropy	[J kg ⁻¹ K ⁻¹]
T	Temperature	[K]

Greek Symbols

ε	Coefficient of Performance, effectiveness [eq. (3.8) page 31]	[-]
η	Exergy efficiency, efficiency [section 3.4.4 page 30]	[-]
κ	Angle of rotation	[rad]
μ	Uncertainty of the reference probe	[K]
ϕ	Angle of rotation	[rad]
Π	Pressure ratio [eq. (3.3) page 30]	[-]
Ψ	Angle of rotation [eq. (H.9) page 143]	[rad]
θ	Angle of rotation	[rad]

Common and global subscripts

axi	axial
cp	compressor
h	heating
imp	impeller
in	Inlet, input

inv inverter

mot motor

out outlet, output

rad radial

rotated used if the value is represented in a rotated axis system

s isentropic (when follows the symbol η)

sc subcooling, subcooler

scaled used if the value is scaled

tip tip of the impeller

trans transmission

Glossary

Air-Water twin-stage heat pump Prototype (AWP)

Air-Water twin-stage oil-free domestic heat pump powered by an oil-free twin-stage radial compression unit, rotating on gas bearings.

Brine-Water twin-stage heat pump Prototype (BWP)

Brine-Water twin-stage oil-free domestic heat pump powered by an oil-free twin-stage radial compression unit, rotating on gas bearings.

heating effectiveness (ϵ_h)

Ratio between heat power supplied to the hot source and the consumed work power, also called heating Coefficient Of Performance (COP_h), defined in section 3.4.4.

economizer

Also called flash tank, this is the second-stage liquid-vapor separator.

Ozone Depletion Potential (ODP)

The ozone depletion potential (ODP) of a chemical compound is the relative amount of degradation to the ozone layer it can cause. R-11 ODP is the reference (ODP=1.0).

Operating Point (OP)

An operating point is a specific set of conditions within the operation range of the heat pump cycle. It is characterized by two level of temperature: the cold source inlet temperature and the hot source outlet temperature. The operating point is named with those two temperatures preceded by the first letter of the source. The first part of the name concerns the cold source while the second part concerns the hot source. A slash separates the two parts. The letter *A* stands for air, the letter *B* stands for brine, and the letter *W* stands water.

Polyolester oil (POE-oil)

Polyolester oil is a synthetic oil used in refrigeration circuits using hydrofluorocarbons refrigerants.

NIST Reference Fluid Thermodynamic and Transport Properties Database (REFPROP)

Program using equations for the thermodynamic and transport properties to calculate the state points of fluids or mixtures.

bold value

In a tabular only, this means that the value is measured. Consequently, its uncertainty is directly a result of the measurement.

underlined value

In a tabular only, this means that the value is guessed by the optimizer directly. Consequently, it does not benefit from the uncertainties propagation.

value with normal font

In a tabular only, this means that the value is computed with the model, but it is not guessed directly. Consequently, it benefits from the uncertainties propagation.

Introduction

This chapter demonstrates why more efficient domestic heating systems are necessary and identifies why heat pumps are one of the best candidates for this improvement.

1.1 The world energy consumption needs to be slowed down

The world energy consumption increases dramatically. In slightly more than 40 years, the global energy consumption has almost doubled. Indeed, from 1973 to 2012, the global final energy consumption increased from 4672 Mtoe¹ to 8979 Mtoe¹ [International Energy Agency, 2014, p. 28]. In order to illustrate the growth at a more local scale, fig. 1.1 presents the evolution of the use of each energy source during the 20th century in Switzerland. Since the end of the World War II, the energy consumption follows a worrying trend. In a context where humanity starts to feel the limits of the Earth resources, changing this trend is a necessity everywhere on the planet.

The domestic sector represents about 30% of the world final energy consumption. Investigating further this energy consumption highlights that the worldwide domestic energy uses are almost as high as the industry uses; they almost reach a third of the global consumption and are mostly provided by fossil fuels. Indeed, the 3 big shares representing most of the global energy consumption are the industry, with 33% of the consumption, the domestic uses, with 29% (which are responsible of 21% - 4.5 Gto of CO₂ - of the carbon dioxide emissions), and the transportation sector, with 26% [International Energy Agency, 2008, p. 17]. Moreover, from 1973 to 2012, the ratio between the different fuels kept approximately the same. The only significant exception concerns the transition from coal to electricity [International Energy Agency, 2014, p. 28], particularly motivated by the development of the nuclear energy. During the period, natural gas and oil consumption ratios also kept approximately constant. Global energy uses in the domestic sector increased between 1990 and 2005 by 19% [International Energy Agency, 2008, p. 44]. Moreover, the domestic sector is the only major end-use sector where the increase in energy consumption since 1990 has been greater in OECD countries (+22%) than in non-OECD countries (+18%) [International Energy Agency, 2008, p. 44].

Space & water heating represent about 70% of the IEA19 domestic sector energy consumption. In the IEA19 countries², space heating remains the most important energy use, responsible for 53% of household final energy consumption, as illustrated in fig. 1.2. This share has decreased a bit (5%) since 1990, but the energy saved has been transferred to the appliance consumption. Space and water heating, as illustrated in fig. 1.2, make

¹ Mtoe: Megatons petroleum equivalent.

² IEA19 is a set of 19 countries where extended energy data is available. Notably those 19 countries have domestic sector final energy consumption statistics available. The 19 countries are Australia, Austria, Canada, Denmark, Finland, France, Germany, Ireland, Italy, Japan, Korea, Netherlands, New Zealand, Norway, Spain, Sweden, Switzerland, United Kingdom, United States of America.

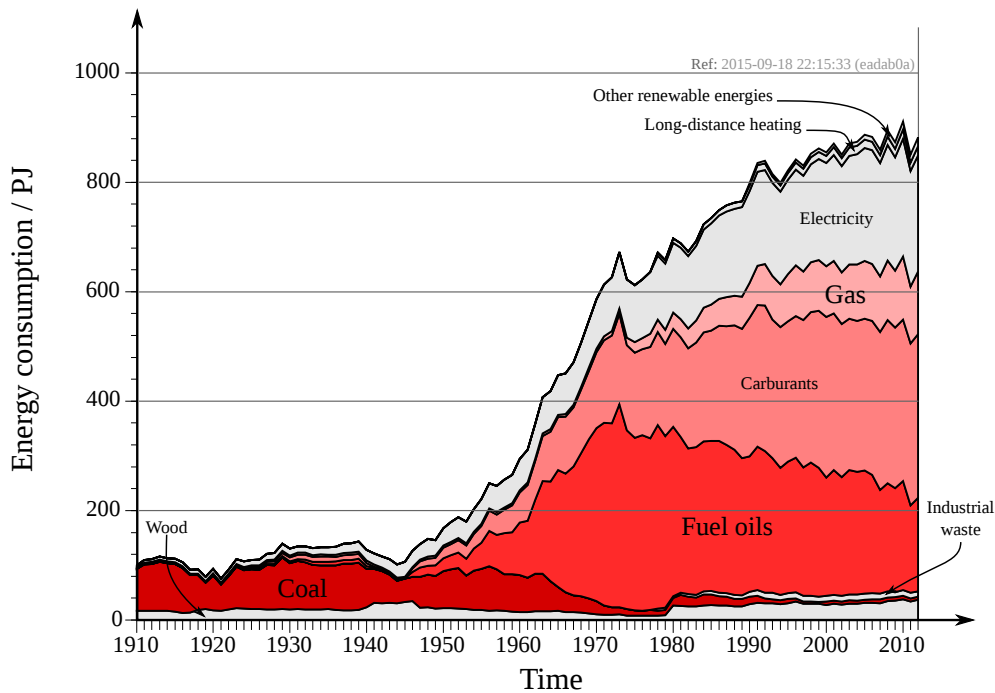


Figure 1.1: Final energy consumption in Switzerland, based on the work of the [Swiss Federal Office of Energy](#) [2012, Fig. 1, p. 4].

together an almost stable consumption of about 70% of the energy used in the domestic sector over the last 25 years. Moreover, the share of the domestic heating is considerably larger for the colder climates where space heating demands higher temperature lifts, which are even higher for the houses heated with conventional hydronic systems³.

Space & water heating technologies for domestic uses. Space and water heating is mostly performed around the world with fuel consumption. The technologies involved are thermally-driven heat pumps, cogeneration, fuel-cells, and of course, boilers. Direct electric heating is also used, as is the use of electrically-driven heat pumps (the latter still representing a small share).

Heat pumps have a great potential to decrease the domestic energy consumption. Direct electric heating is a waste of energy, as that electricity could be better used within an electrically-driven heat pump. Fuel-based technologies play a role in an energy transition, especially the fuel-cells, the thermally-driven heat pumps, and the cogeneration technologies, but the human race needs in any case to dramatically decrease its fossil fuel consumption as soon as possible, in order to limit its carbon dioxide emissions. Most of the climate scientists in the world agreed through countless studies that those emissions have a negative impact on the climate and the planet ecosystems [IPCC, 2014]. Consequently, the use of heat pumps to perform space and water heating in the domestic sector appears as a key-technology for substantially reducing both the energy consumption and the carbon dioxide emissions. And it will be even more the case if the electricity powering those heat pumps is produced in a sustainable way and from renewable sources.

What is a heat pump? A heat pump is a device that extracts heat energy from a source at low temperature and releases it at a higher temperature [Borel and Favrat, 2010, based on def. p. 607–608]. A heat pump is primarily

³ Conventional hydronic systems may usually need water temperatures higher than 60°C while hydronic heating floor systems only need temperature up to 35°C.

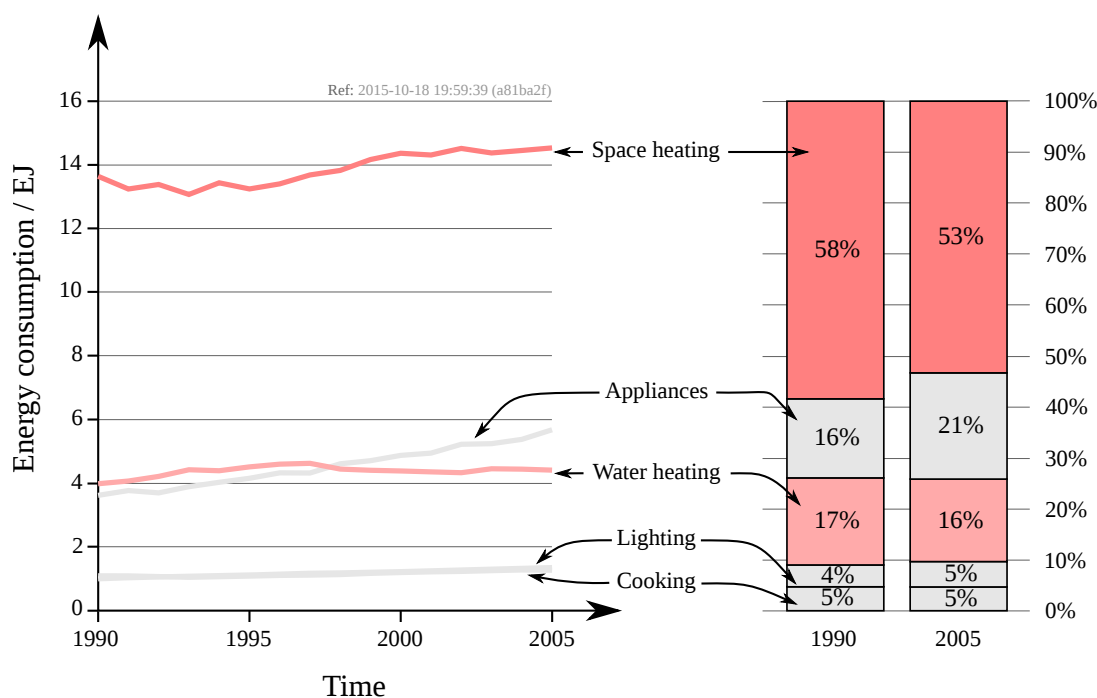


Figure 1.2: Final domestic sector energy consumption for the IEA19, based on the work of the [International Energy Agency \[2008, Fig. 4.3, p. 46\]](#).

based on a reversed Rankine cycle and can be made from different variants (single-stage, two-stage, with internal heat exchangers, etc...). This thesis work focuses on bithermal heating heat pump cycles, also called thermopump cycles. [Borel and Favrat \[2010, p. 639–643\]](#) give an accurate and detailed definition of this cycle. The basics to remember is that the cycle happens in 4 main thermodynamic processes. First, low pressure, low temperature gas is compressed during the compression process, which releases this gas at high pressure, high temperature. This gas is then condensed through a condensation process, which releases the refrigerant in a liquid state, at high pressure, and lower, but still high temperature. Then follows an expansion process, where the high pressure, high temperature refrigerant is expanded. It leaves in a two-phase state at low pressure, low temperature. The last process is the evaporation which takes the two-phase refrigerant and evaporates it completely, in order for it to enter the compression process again. When the refrigerant condenses in the condensation process, it is at a higher temperature than a house heating network. It releases heat energy, usually to a water tank or to a house, in domestic applications. When the refrigerant evaporates, it is at a temperature lower than the temperature of the environment. It takes heat energy from it, as in domestic applications, environment is usually the only source of heat energy, also called cold source⁴. Heat pumps can collect and release heat from and to different medias. Those medias are fluids, in gaseous or liquid state. In domestic applications, the medias used are usually water, brine⁵, or air. It exists all the combinations of those medias in the domestic heat pump world: Air/Water heat pumps, Air/Air heat pumps, Brine/Air heat pumps, Brine/Water heat pumps. Air/Air and Air/Water heat pumps are the most common models, as they are cheaper than the other versions, but they have also the lower performance (the least efficient system being the Air/Air version). The Brine/Air version is pretty uncommon and seldomly encountered. The Brine/Water version is the most effective because the heat source is usually more stable and at a higher temperature than the air energy source, and also because the heat exchange is more efficient in Brine/Water heat pumps, which decreases the losses in the heat exchangers.

About the refrigerants used in heat pumps A refrigerant is a fluid which condenses and evaporates at pressure and temperature levels which are of interest for the application. For domestic heat pumps applications, many fluids

⁴ The hotter environment where the heat pump releases the heat energy is called the hot source.

⁵ Brine is a mixture of water and an antifreeze agent.

can be used as refrigerants. The latter can be natural fluids or synthetic fluids. They can be used pure, or blended together in specific proportions, the blend getting convenient characteristics for the application. The choice of a refrigerant for a thermodynamic cycle is a critical one, as there are technical characteristics to take into account, but also legislative constraints, related to regulations. A refrigerant could have an impact on the atmospheric ozone layer depletion, if released. Most of the forbidden refrigerants had an Ozone Depletion Potential (ODP). Nowadays refrigerants have no ozone depletion potential. Refrigerants could also have a negative impact on the greenhouse effect, if released in the atmosphere. Most of the refrigerants have a global warming potential. The trend worldwide is to use refrigerants with a global warming potential as low as possible. Nowadays, the trend is to use more and more natural fluids as refrigerants, as they have usually lower global warming potentials than synthetic refrigerants (and consequently lower legal constraints related to regulations). The issue with natural fluids is mainly that, often, they are either toxic, flammable, or explosive.

1.2 Better domestic heat pumps can help

Better domestic heat pumps can help to slow down the energy consumption. Better domestic heat pumps are needed. The better domestic heat pumps should be:

More efficient: Zehnder [2004] and Barbouchi [2007] demonstrate in their work the importance of the exergy losses in the compression process. Barbouchi [2007, Fig. I.2 p. 206] demonstrates with his simulation work an exergy loss of 49% for a two-stage compression process, and of 57% for a single-stage compression process. The heat pump thermodynamic cycle being considered in this study was a A5/W48 cycle. Zehnder [2004, p. 227] demonstrates with his simulation work an exergy loss of 60.3% for a single compression process, and of 50.5% for a twin-stage compression process. The heat pump thermodynamic cycle being considered in this study was a A-12/W60 cycle. As a consequence, in order to significantly improve the performance of the domestic heat pumps, the compression process efficiency has to be improved as much as possible. Therefore, to improve the domestic heat pump performance, a technological gap on the compression device is necessary. This is the motivation for the radial compressor development performed by Schiffmann [2008].

More compact: More compact heat pumps opens the way to their use in places where they could not be used before. If they get compact enough, they can be used in flats, replacing boilers, for instance. They could also be used for waste water heat recovery.

Less material: A significant share of the metals used in human machinery becomes harder to extract from the Earth crust, as they rarefy. It increases the cost of production of the machinery and decreases their sustainability. Consequently, the less raw material needed, the better.

Less noise: In order to be used in flat or small homes, the heat pumps need to be as silent as possible.

Decreased impacts of the refrigerant: The refrigerant used in the heat pumps should have a low impact on the environment or the climate, as they are elements to be preserved for our own sake. In the same spirit, the refrigerant charge should be kept as low as possible, in order to decrease the impact of leakages and the security risks.

1.3 Scope of this thesis work

This thesis work focuses on the experimental investigation of two electrical domestic heat pump prototypes equipped with a twin-stage oil-free radial compression unit in the electric power range 1 kW – 50 kW. The two prototypes tested have been designed, built, and tested during this thesis work. They are the first worldwide working prototype of domestic heat pumps powered with radial oil-free compressors. Chapter 1 is the introduction motivating the need for better domestic heat pumps. Chapter 2 is a literature review stating some paths of improvement for the domestic heat pumps. Chapter 3 presents the thesis to validate and the methodology applied. Chapters 4 and 5 present the prototypes, their test results, the issues encountered, and the observations made. Chapter 6 presents additional ways of improvement of the two prototypes and highlights good practices regarding oil-free heat pump design. Chapter 7 concludes this thesis work by validating the thesis proposed in chapter 3. The originality of this thesis work articulates around of the following points:

1. The two prototypes that have been designed, built, and tested are the two first heat pumps powered by oil-free radial compressors successfully tested worldwide in the electric power range 1 kW – 50 kW. This is the first time that such achievement is reached and documented. The two prototypes allowed to gain a lot of experience about the issues related to oil-free systems and knowledge about good practices for the design of such devices (chapter 4 & chapter 5).
2. An original design of economizer has been developed for the Air-Water twin-stage heat pump Prototype (AWP). This economizer is equipped with an efficient liquid/gas separator and combines directly with the volute of the compression unit, already starting an integration process of the heat pump parts together (chapter 5).
3. Building onto the experience gained during the experiments, original designs are offered for advanced concepts of bypass systems and first stage separator. An original integrated design concept of compression unit module including the first stage separator and the economizer is also offered (chapter 4, chapter 5, & chapter 6).
4. The modeling approach offered in this work to analyse the experimental data transposes a software modeling tool to the energy analysis domain. The use of this tool makes the modeling easier by systematizing the generation of the set of equations, making the modeling steps easier and more reliable (chapter 3).

Bibliography

- S. Barbouchi. *Pompe à chaleur air/eau haute température pour la réhabilitation du chauffage dans l'habitat existant*. PhD thesis, Mines Paris ParisTech, 2007. URL <http://www.sudoc.fr/143767712>.
- L. Borel and D. Favrat. *Thermodynamics and energy systems analyses*. EPFL Press, 2010.
- International Energy Agency. *Worldwide Trends in Energy Use and Efficiency: Key Insights from IEA Indicator Analysis*. Technical report, International Energy Agency, 2008. URL http://www.iea.org/publications/freepublications/publication/Indicators_2008-1.pdf.
- International Energy Agency. *2014 Key World Energy Statistics*. Technical report, International Energy Agency, 2014. URL <http://www.iea.org/publications/freepublications/publication/KeyWorld2014.pdf>.
- IPCC. *Climate Change 2014: Synthesis Report. Contribution of Working Groups I, II and III to the Fifth Assessment Report of the Intergovernmental Panel on Climate Change* [Core Writing Team, R.K. Pachauri and L.A. Meyer (eds.)]. Technical report, IPCC, Geneva, Switzerland, 2014. URL <http://www.ipcc.ch/report/ar5/syr/>.
- J. Schiffmann. *Integrated design, optimization and experimental investigation of a direct driven turbocompressor for domestic heat pumps*. PhD thesis, Swiss Federal Institute of Technology - Lausanne, 2008. URL <http://dx.doi.org/10.5075/epfl-thesis-4126>.
- Swiss Federal Office of Energy. *Statistique globale suisse de l'énergie 2012*. Technical report, Swiss Federal Office of Energy, 2012. URL http://www.bfe.admin.ch/php/modules/publikationen/stream.php?extlang=fr&name=fr_468077826.pdf.
- M. Zehnder. *Efficient air-water heat pumps for high temperature lift residential heating, including oil migration aspects*. PhD thesis, Swiss Federal Institute of Technology - Lausanne, 2004. URL <http://dx.doi.org/10.5075/epfl-thesis-2998>. PhD Thesis n°2998.

Credits



Fig. 1.1, page 2 © 2013 Jean-Baptiste Carré, licensed under  4.0 . This figure is based on an original figure from the [Swiss Federal Office of Energy](#) [2012, Fig. 1, p. 4].

Fig. 1.2, page 3 © 2013 Jean-Baptiste Carré, licensed under  4.0 . This figure is based on an original figure from the [International Energy Agency](#) [2008, Fig. 4.3, p. 46].

State of the art

This chapter exposes what are the different ways to improve heat pump systems through a review of the available literature. Multistage, oil-free, and variable-speed technologies show promising perspectives in the heat pumps application fields and allow to make more efficient, more compact, more silent heat pump circuits built with less raw material and using a lower refrigerant charge.

As explained in section 1.1, there are different types of heat pumps. The interest in this chapter is focused on electrically-driven vapor compression domestic heat pumps.

2.1 Types of refrigerant compressors

2.1.1 Dynamic versus volumetric

Refrigeration systems equipped with dynamic compressors are expected to develop better seasonal performance than those equipped with volumetric compressors. Indeed, soon after the scroll compressor technology release, Purvis [1987] described scroll-based heat pump systems capacity response to the residential heating demand. Heat pumps using volumetric compression devices, like scroll compressors (the other types of volumetric compressors are even more concerned by this trend according to ASHRAE [2008]), are characterized by a decrease of their capacity as the outside temperature decreases, while the residential demand evolves inversely. This behavior explains why the heat pumps used for space or water heating in residences must be designed to provide the heating demand for the lowest expected outside temperature in the geographic area. It implies that the heat pump, whose function would be to heat the houses without any auxiliary device (like a boiler or an electric resistor to compensate for the heat pump, or replace it totally when outside temperature becomes too low), will be significantly over-sized, during most of the heating period. As explained by Schiffmann and Favrat [2009, p. 1922], variable-speed dynamic compressors do not behave this way and stick with the residence demand curve. They are also expected to develop better isentropic efficiencies¹. Consequently using dynamic compressors in domestic heat pump circuits would result in a much better energy use and, potentially, in a maximization of the efficiency, since it becomes possible to choose the exact compressor speed which maximizes the compressor efficiency for the given mass flow rate and pressure ratio needed. Additionally, the compression unit would not need to be over-sized which would result in a more rational use of raw materials and result in a smaller compression unit, which also increases the compactness potential.

2.1.2 Volumetric compressors used in domestic heat pumps

The main volumetric compressor (also called positive-displacement compressor) technologies used in refrigeration circuits are:

¹ The isentropic efficiency of a compressor is defined in section 3.4.4, page 30.

Reciprocating compressors: Piston compressors are also known as reciprocating compressors. Linear stroke compressors are also reciprocating compressors. Historically, that compression technology is the first one to have powered vapor compression domestic heat pumps, from after somewhere between the two World Wars [Zogg, 2008, p. 23] to the 1980s, when the scroll compressors have been introduced. From that point in time, reciprocating compressors started to be replaced by scroll compressors in the domestic heat pump application. Scroll compressors were cheaper, more reliable, needed less maintenance, and were less noisy. In the 1990s, most of the vapor compression domestic heat pumps are equipped with scroll compressors, instead of reciprocating compressors. Reciprocating compressors had to be lubricated to work properly and to not fail. With the increase of the accuracy of the manufacturing methods and the development of new design, linear stroke compressors without lubrication start to be produced. They target first the domestic refrigerators application, but are also used in some other applications, like in the study made by Marcinichen et al. [2014]. For instance, Marcinichen et al. [2014] used an oil-free 125W [Marcinichen et al., 2014, Tab. 1, p. 183] linear stroke mini-compressor capable of modulating its volumetric displacement on a share of the stroke [Marcinichen et al., 2014, p. 183] and, an oil-free magnetically driven liquid gear pump to perform two-phase chip cooling. The compressor power of the compressor selected in the paper from Marcinichen et al. [2014] would not fit for domestic heating applications as its power is very low. Generally speaking, totally oil-free linear stroke compressors are limited in power range and are usually dedicated to household refrigerators applications, where they greatly contributed to increase the system performance [Bansal et al., 2011]. However, Marcinichen et al. [2014, p. 186] consider the efficiency of such a compressor still low compared with conventional domestic heating heat pump compressors.

Scroll compressors: A scroll compressor is an involute profile, mounted on a rotor, that rolls onto an other involute profile, which is usually fixed, and that is slightly offset. The involutes are drawn in a way that reduces the volume of the compression space further and further during the rotation of the shaft. The geometry of the scroll compressor has been invented by Creux [1905] at the beginning of the 20th and did not really changed ever since. The involute profile is described mathematically by two Archimedean spirals with the same generating circle, and separated by a constant offset. They also can be generated from hybrid curves. The scroll compressor has not been commercialized until the early 1980s, as it had to wait for the development of effective high-accuracy, high volumes manufacturing techniques to be developed because of the complexity of the shapes involved [Zogg, 2008, p. 16]. Between the 1980s and 1995, the performance of the scroll compressors has been optimized and increased, then, after the introduction of the last generation of scroll compressors between 1992 and 1995, the increase of performance stopped. The data collected by Eschmann [2009]² and summarized in his report of 2008 highlights the stagnation of the heat pump performance since the introduction of this last generation of scroll compressors. Nowadays development of this technology takes new paths, like the one explored by Iglesias and Favrat [2014]. They presented a prototype of oil-free scroll air compressor with two mobile involutes working in synchronized co-rotation one relative to another. The prototype can also work as a turbine, as the compressor is reversible. This concept could theoretically be applied with refrigeration compression, even if the technical challenges are significant. For instance, injection of liquid refrigerant during the compression in the volutes could also be done. Zehnder [2004] has documented this kind of humid vapor injection in his work [Zehnder et al., 2010], but in his case, one of the involutes was fixed, as he was working with an orbital scroll, which was making the process easier. Using co-rotative scrolls greatly limit the efforts on the bearings and results in a balanced setting [Iglesias and Favrat, 2014, Fig. 2 p. 567], which makes it an interesting concept for oil-free applications. Nonetheless, it seems that the development of the scroll compressors reaches technological limits and will not increase its performance significantly, with the current technology state.

Rotary vane compressors: Rotary vane compressors are made of a rotor with blades inserted in radial slots in the rotor. When the rotor turns, the blades slide in and out of the slots, keeping contact with the outer wall of the compressor housing. As the rotor is not at the center of the housing, the gas is being compressed by a reduction of the volume between the blades. Those compression devices are being introduced recently in the domestic heat pump sector as a second compression stage on top of a scroll compressor [Kazuya Kondo et al., 2010, Mitsubishi, 2011, Sato et al., 2012]. A rotary vane compressor can be multistage and is a lot quieter than the reciprocating technology, at equivalent power.

² Eschmann [2009] performed a monitoring study on Brine/Water and Air/Water domestic heat pumps whose performance had been measured at the Swiss heat pump certification center between 1992 and 2007.

2.1.3 Dynamic compressors used in domestic heat pumps

There is no dynamic compressor technology used in the heat pump domestic sector currently, but one is coming with the developments performed since the beginning of the 21st century, notably with the work of Schiffmann [2008].

Radial compressors The first radial compressors were manufactured at the beginning of the 20th century. They were originally developed by steam turbine manufacturers and were widely used for ventilation purposes in deep mining. At that time, the possibilities of producing an impeller were rather limited by the manufacturing technology available. Decades later, the manufacturing technologies had evolved and started to allow the manufacturing of highly efficient radial compressors. Carrier has been the first to work seriously on radial compressors from 1911 for refrigeration applications (at the time, it was for air conditioning). In about 1919, he first tried a German radial compressor with di-chloroethylene, and then a compressor made by Eastman Kodak in the United States with dichloromethane [Zogg, 2008, p. 16]. They have been used in industrial refrigeration circuits from the beginning of the 20th century to nowadays, and they now can be used in domestic heat pump applications due to the recent development of the manufacturing processes and the development of small scale gas bearings sets specially designed for this application, with an integrated-design approach [Schiffmann, 2008].

2.1.4 About the compression units used in this thesis work

Schiffmann and Favrat [2009] presented in 2009 really encouraging experimental results with the testing of a single-stage compression unit. They also presented promising preliminary simulation results for a twin-stage heat pump based on the radial compressor unit that Schiffmann [2008] was developing. That compression unit, and its successors, the twin-stage compression units used in this thesis work, are at the cutting edge of the technique and the technology reachable nowadays, as shown in fig. 2.1. Those compression units are several times lighter and smaller than their equivalent in the scroll technology, as illustrated in fig. 2.2 and are expected to demonstrate the greatest potential in many processes where gas compression is needed. A similar design has been used by Demierre et al. [2014] with a compressor-turbine unit, using a radial compressor and a radial turbine, mounted at the two sides of a same shaft³. The twin-stage compression units powering the Air-Water twin-stage heat pump Prototype (AWP) and the Brine-Water twin-stage heat pump Prototype (BWP) have been developed between 2002, when the feasibility study of the twin-stage unit has been presented by Schiffmann et al. [2002], and 2012, when the first compression unit prototype has been able to power a heat pump cycle in an experimental setup. The results of those first experiments are presented in chapter 4, page 35.

2.2 Noise reduction in refrigeration circuits

As very accurately balanced and high rotation speed devices, the compression unit developed by Schiffmann [2008] and its successors produce no vibrations and can be made very silent. In opposition to typical scroll compressors that produce a lot of vibrations and noise (about 65 dBA, on average, according to ARI compliant measurements, at the nominal compressor speed of 50 Hz [ASHRAE, 2008, Fig. 43, p. 37.26]), widely spread on the audible sound spectrum. This implies that this noise is difficult to insulate, on the contrary to the radial compression units, which produce high frequency noises due to their high rotational speed and the gas bearings technology (no friction). As those high frequencies are easy to staunch with basic sound insulation, radial compression unit rotating on gas bearings can be made very silent. Furthermore, regular Air/Water domestic heat pumps available in the Eurovent Certification [2010] database release between 53 and 83 dBA (with fans), according to ISO 9614 [AFNOR, 2009] and ISO 3744 [ISO, 2010] compliant measurements. Consequently, compressor noise constitutes a significant part of the heat pump noise. Thus, switching to radial compression unit rotating on gas bearings and to silent fans open the way to very quiet heating machinery.

³ Details about this specific design can be found in the thesis work of Demierre [2012].

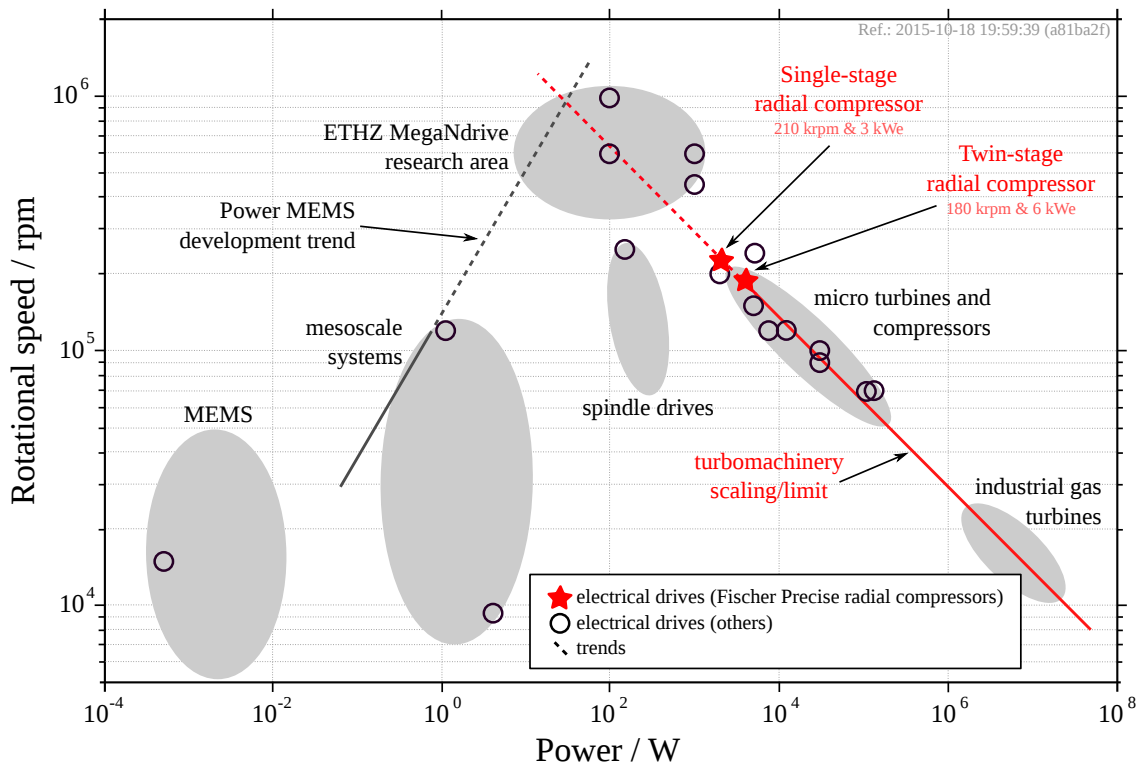


Figure 2.1: Emerging application areas and trends for high speed electrical drives and turbomachineries, based on the work of Zwysig et al. [2009, Fig. 1, p. 565].



(a) Compression unit aside a 1.5-liter water bottle

(b) The compression unit is equivalent to 2 scroll compressors

Figure 2.2: The volume and the weight of the twin-stage compression unit are several times lower than a single-stage scroll compressor. The 6 kW twin-stage compression unit is roughly equivalent to 2 single-stage 3 kW scroll compressors.

2.3 Variable-speed in refrigeration circuits

Variable-speed capacity control has been proven to increase heat pump efficiency [Karlsson, 2003, Karlsson and Fahlén, 2008]. There are different ways to obtain this capacity control.

Heat pump capacity control is performed by reducing the compressor capacity. In domestic heat pumps, most of the compressor used are scroll compressors. Those device are currently using one of the three technologies detailed below to control their capacity.

Variable displacement based capacity control: This mechanism is dedicated to scroll compressors and consists in ports incorporated in the fixed scroll. The control consists in the connection or not of the compression chamber to the suction side by respectively closing or opening the ports. Then, when the ports are all closed, the compressor runs at its full capacity. To provide only a share of the full capacity, some holes are open. The number of different capacities and extent of the capacity reduction available is governed by the locations of the ports.

Pulse Width Modulation based capacity control: This mechanism is also dedicated only to scroll compressors and consists in a device that modulates the axial pressure that maintains sealing contact between the scroll tips and its base. The control is done by cycling the loading and unloading of the fixed scroll without changing the motor speed. The cycle is controlled by an electrical devices which adapt the loading and unloading phases to make the compressor deliver the exact capacity required.

Variable speed based capacity control: The compressor is driven by an inverter to convert the 50 Hz fixed-frequency alternative current coming from the power network to an adjustable voltage and frequency signal. This signal is then used to control the speed of the motor, which is correlated with the mass flow rate of the refrigerant through an equation or a compression map. This capacity control strategy is used on some scroll compressors and is the solution selected for the control of the radial compression units used in this thesis work.

2.4 Multistage refrigeration circuits

Two-stage compression cycles has been proved to reach higher performance than single-stage cycles in various studies [Favrat et al., 1997, Zehnder, 2004]. Moreover, this statement is particularly true for high temperature differences between the hot source and the cold source. Zehnder [2004] presented several twin-stage heat-pump configurations and tested some of them [Zehnder et al., 1998, 2002]. The most promising cycles were the following:

Solution #1: Addition of a separate single-stage heat-pump cycle to a main single-stage heat-pump cycle. The main cycle is dedicated to the heating of the house while the additional cycle uses the subcooled liquid at the outlet of the main condenser as a cold source to produce tap water.

Solution #2: Superposition of two single-stage heat-pump cycles coupled with a shared heat exchanger acting as the condenser for the bottoming cycle and an evaporator for the topping cycle.

Solution #3: A single-stage cycle using a single-stage compressor with intermediate vapor-injection.

#3.1: The vapor injected during the compression process is produced by the expansion of subcooled liquid removed at the outlet of the condenser. Before being injected, the wet vapor is heated up by going through an intermediate heat exchanger, exchanging heat between the main subcooled liquid line and the wet vapor previously expanded [Beeton and Pham, 2003, Zehnder and Favrat, 2002]. When the vapor exchanges heat in the intermediate heat exchanger, its vapor quality increases. Often, the vapor injected in the compressor is just saturated. Wet vapor injection is only needed if the outlet temperatures are getting too high.

#3.2: The subcooled liquid coming from the condenser is expanded to an intermediate pressure and enters a flash tank where vapor and liquid are separated. Liquid is expanded and enters the evaporator while vapor is injected in the compressor, during the compression process.

Solution #4: A twin-stage heat-pump using a twin-stage compressor and an intermediate heat exchanger or a flash tank in order to inject vapor between the two compression stages, as in the two versions of the above solution.

Schiffmann et al. [2005] have analyzed those different concepts in order to design a domestic, high temperature lift, air-water heat pump. They sum up those concepts in a later article [Schiffmann and Favrat, 2009] and conclude notably that the solution #4, with a flash tank acting as an economizer, is the most interesting one, when taking in account the radial compressors characteristics and limitations. Moreover, they pointed out that this solution is an elegant one in terms of number of components and control, and a promising one in term of heating effectiveness (ϵ_h) [Favrat et al., 1997, Schiffmann, 2008]. They also indicate that, with this cycle configuration, inverting the cycle in order to defrost the evaporator, could allow to use the economizer as an internal energy source. Since the final goal is the development of a twin-stage oil-free air-water heat-pump using a twin-stage radial compressor rotating on gas bearings, the configuration #4 is favored. This configuration is referred as a twin-stage compression cycle with flash cooling, as it has been named by the ASHRAE [ASHRAE, 2008, Fig. 49, p. 37.29].

2.5 Lubrication in refrigeration circuits

Youbi Idrissi and Bonjour [2008] highlight that, currently, almost every refrigeration vapor compression systems need a lubrication agent, which is generally a mineral or synthetic lubricant oil depending on the refrigerant used in the system. Oil functions are (1) to protect the mechanical moving elements against the wear with a thin lubricant film, (2) to act as a sealing element, (3) to limit the noise made by the mechanisms, (4) to help the evacuation of chemical impurities or deposits which may be present in the circuits, and (5) to act as a heat transfer medium for cooling the compressor, in many systems. Those favorable or vital functions clearly assert that oil in refrigeration compression systems is generally compulsory and useful. However, that oil brings also severe drawbacks to the refrigeration circuits. Most of the time, it reduces the heat transfer coefficient in heat exchangers, it changes the flow configurations, it increases the pressure drops, and it modifies the thermodynamic equilibrium and the thermodynamic properties of the refrigerant [Youbi Idrissi and Bonjour, 2008].

Migration of the oil inside the heat pump loops

Zehnder [2004] studied the migration of the oil into a twin-stage heat pump loop. He concluded that the oil is migrating from the topping stage compressor to the bottoming stage compressor and could not identify a stable situation where this statement was false. The topping compressor, a scroll compressor, without lubricant oil recovery circuit, dries and is doomed to failure. Moreover, Navarro et al. [2005] studied the oil circulation ratio and its return to the compressor with R290/Polyolester oil (POE-oil) and R407C/POE-oil, on a reciprocating compressor installation and compared their results with mineral oil experiments. They found that the oil would return easier to the compressor if it is a POE-oil than if it is a mineral oil. They concluded also that there is no behavior difference, from the oil point of view, with R290 or R407C but this conclusion is deduced from a single-stage heat pump loop. Winandy and Cuevas [2003] has studied the oil level in two scroll compressor in parallel, in a refrigeration installation. They demonstrated that the oil was not returning equally to the two compressors, especially when working under part load. They also linked the two compressor housings with a straight pipe, welded at the normal height of the oil-levels, allowing an oil-level adjustment between the two compressors and concluded the oil migration phenomenon has to be taken seriously, even more seriously when running under part-load. Unfortunately, in twin-stage heat pumps based on 2 scroll compressors, since the pressure level is not the same for the two compression devices, in opposition to the two scroll compressors in parallel presented by Winandy and Cuevas [2003], this solution is not applicable. The direct consequence of those studies is that it should be a lot easier to make multistage heat pump devices without having to consider the return of the lubricant agent to the compressors. Those heat pumps are likely to be more reliable also, as they won't fail because of lubrication issues. Additionally, using oil-free circuits allows to get free from the design rules of circuits with oil. For instance, the pipe diameters can be increased in the suction lines in order to decrease the pressure drop on the vapor line, generating exergy losses⁴. Those pipes diameters are limited in the circuits with oil because the oil has to be recovered in the compressor housing [Guo et al., 2011, Kesim et al., 2000]. This problem is even more acute with variable flow capacities linked to variable speed compressors.

⁴ Exergy and exergy efficiency are defined in section 3.4.4, page 30.

2.5.1 Impact of the lubricant on the expansion process

Electronic expansion valves

Liang et al. [2009] have established models of electronic expansion valves for R22, R407C and R410a based on Bernoulli equation giving accurate results. The models they propose differ from some conventional models using the two-phase outlet pressure and corrected flow coefficient since they consider metastable phenomena caused by rapid depressurization and employ the throat pressure of the electronic expansion valves and the single-phase incompressible flow coefficient. Park et al. [2007] have used a different approach using a model with a set of parameters and variables including the valve geometry, its inlet and outlet conditions, and the refrigerant thermodynamics properties to describe the valves behavior. Both of those studies are dealing with pure refrigerant or neglect the presence of oil. For now, influence of oil seems not to be documented or considered as negligible, but it could be a problem with oil-free circuits.

Capillary tubes

There are two groups of studies dealing with the effect of oil in the capillary tubes. The first deals with oil-rich mixtures, with typically more than 5% in weight, while the second treats the oil as a contaminant, present in quantities lower than 5% in weight. The studies where important quantities of oil are mixed with the refrigerant are quite seldom but are interesting to understand and interpret the foaming phenomenon occurring in compressors, as the oil concentration is the highest in those devices. For instance, Poiate Jr and Gasche [2006] studied the foaming phenomenon inside small tubes. The second case is more usual and several studies have been published. Most of them aim to improve the knowledge available on the phenomena which occur in capillary tubes, like two-phase flow pressure drop or metastable flow⁵. Motta et al. [2002] performed visual experiments to determine the position of the vaporisation point of a R404a-oil mixture inside a capillary tube and quantified the effect of a given percentage of oil on the capillary tube behavior. Some of the studies observed a reduction in the mass flow rate with an increase of the oil concentration [Fukuta et al., 2003, Motta et al., 2001].

2.5.2 Impact of the lubricant on the evaporation process

The evaporation process is known for decades to be the more sensitive process of the heat pump cycle regarding the presence of compressor lubrication oil in the refrigerant. McMullan et al. [1992] have shown that the viscosity of the lubrication oil has a negative effect on the evaporator performance for a fully miscible oil-refrigerant mixture. For shell-and-tubes evaporators, they concluded that the addition of oil produces a change in the refrigerant two-phase flow regimes and a decrease of the overall evaporator performance. Previous studies [Hughes et al., 1980, 1982, 1984a,b, McMullan et al., 1988a,b], observed the lubricant oil influence on the heat pump performance and concluded that the presence of oil in the evaporator was responsible of a significant decrease of performance. They also concluded that the accumulation of oil at the end of the evaporator (refrigerant vaporizes, oil just flows), has a significant influence on the decrease of the heat transfer coefficient which is observed. They have estimated that, in principle, an evaporator working with no oil at all would allow an increase of the whole evaporator heat exchange coefficient by about 40% [McMullan et al., 1983, p. 123]. Indeed, the more refrigerant evaporates, the more the remaining liquid refrigerant is charged in oil, and the more it is difficult for it to evaporate. The potential improvement of 40% is certainly quite optimistic, but it remains that improvements of the heat exchange coefficient are observed with the decrease of the oil mass fraction. If oil can not be removed, from an heat exchange point of view, McMullan et al. [1983] added that, for low amounts of oil in the refrigerant, a low viscosity oil leads to better results, while for bigger amount of oil in the refrigerant, high viscosity oil would be the better choice. They also observed that the presence of oil increases the pressure drop into the evaporator. Spindler and Hahne [2009] have studied the influence of oil on nucleate pool boiling heat transfer with enhanced surface tubes. They concluded that, except under very specific conditions, oil always decreases the heat transfer coefficient [Spindler and Hahne, 2009, Fig. 19 p. 990] and [Möller, 1998]. The more oil there is, the less efficient the evaporation is. Nidegger et al. [1997] and Zürcher et al. [1998a] have studied the intube flow boiling of R-407C and R-407C-oil mixtures [Zürcher et al., 1998a,b], and the R134a and R134a-oil mixtures [Nidegger et al., 1997, Zürcher et al., 1997], both on plain tubes and microfins tubes, and confirmed the observations of McMullan et al. [1983]: with increasing

⁵ A metastable flow remains liquid over a distance longer than the one predicted by conventional pressure drop models.

oil concentration, the heat transfer coefficient drops. Some authors, like [Cawte et al. \[1996\]](#), observed, in the contrary, an increase of the heat transfer if the oil concentration reaches a certain range (2 to 10% in the case of the study published by [Cawte et al. \[1996\]](#)). [Bandarra Filho et al. \[2009\]](#) reviewed a great number of papers involving refrigerant–oil mixtures that can be found for different test conditions and found that they often present conflicting results, unfortunately. Even so, it is still possible to affirm that some thermodynamic properties of refrigerant/oil mixtures, such as density, viscosity, surface tension and miscibility, can modify, specifically, the heat transfer and pressure drop, and thus affect directly the ϵ_h of the system [[Bandarra Filho et al., 2009](#), p. 186]. [Cawte \[1992\]](#) performed similar heat transfer studies on condensation processes with refrigerant/oil mixtures and observed a big non-linear decrease of the heat coefficient with the increase of the oil concentration. However, he concludes that this change of heat transfer coefficient has little impact on the whole heat pump performance. Of course, it is important to consider that most of those studies have been made on plain tubes, or conventional surfaces.

2.5.3 Oil-free heat exchange technologies

Using oil-free compression devices opens the way to the use of existing or to-develop heat exchangers, which would be more efficient or become usable with oil-free compression technologies. Those heat exchangers include micro-channels heat exchangers, direct ground evaporators, and heat exchangers using enhanced surfaces, like enhanced tubes-based heat exchangers [[Habert, 2009](#), [Ribatski and Jacobi, 2005](#), [Van Rooyen, 2011](#)] or enhanced plate-based heat exchangers [[Furberg, 2006](#)], which would result in a reduction of the heat exchange surfaces, and consequently, in a reduction of the pressure drops inside the circuits and of the whole heat pump size. Furthermore, some of those heat exchange technologies open the way to heat exchangers with reduced temperature pinches between the refrigerant and the heat source and would contribute to decrease the exergy losses coming from the heat exchanges. [Furberg \[2006\]](#) and [Li \[2008\]](#) develop plates heat exchangers with enhanced surfaces with micro patterns [[Furberg et al., 2009](#)]. Enhanced surfaces with micro-patterns are filled with oil, if used with refrigerant-oil mixtures [[Spindler and Hahne, 2009](#), Fig. 10 & 11 p.985–986] and thereby become less efficient. Consequently, the enhanced plate heat exchangers developed by [Furberg et al. \[2009\]](#) mainly target oil-free applications. Oil free heat exchange technologies are in heavy development since the last 20 years [[Bandarra Filho et al., 2009](#), Fig. 1 p. 186], as new market applications emerge. Their application in oil-free compact domestic heat pumps promises to increase even further the potential of the oil-free compression technologies.

2.5.4 Impact of the lubricant oil on the compression process

One of the main effect of oil in the compression process is the foaming phenomenon, which is due to the interactions between the oil and the refrigerant induced by the blade rotation or the vapor blow. The foaming phenomenon has been studied in a hermetic casing simulating a hermetic rotary compressor by [Yanagisawa et al. \[1991\]](#). They observed that the foaming increases and become massive for high compressor blade speed combined with a high mass flow rate. Another effect of the oil on the compression process is the modification of the compressor performance. Indeed, because of the solubility of the oil into the refrigerants⁶, the refrigerant-oil mixture enthalpy may be substantially different from the pure refrigerant enthalpy [[Youbi Idrissi et al., 2003](#), Fig. 2–4, p. 288–289]. As a consequence, the energy balance performed on the compressor may be false and, as shown with the [Youbi Idrissi et al. \[2003](#), Fig. 2–4, p. 288–289] diagrams, it leads to wrong estimations of the refrigerant mass flow rate. Indeed, considering pure refrigerant instead of the real oil-mixture that really flows out of the compressors leads to make a mistake on the enthalpies at the inlet and the outlet of the compressors, which is reflected on the energy balance, and finally on the mass flow rates. As some refrigerant remains dissolved in the oil, some liquid desorbs from the oil during the compression process, inducing a wet compression process. This phenomenon may considerably affect the compressor isentropic efficiency while it has no effect on the volumetric efficiency [[Wang et al., 2006](#)].

2.6 Refrigerant charge reduction in refrigeration circuits

Because of their impact on the environment, European regulation concerning refrigerating systems has become more and more severe and imposes increased constraints related to the refrigerant charge of the installations. As

⁶ The solubility of the oil into the refrigerant is proved to increase with pressure [[Wahlstrom and Vamling, 1997](#)].

a consequence, many studies aimed at minimizing the charge in refrigeration circuits were developed. Studying the behavior of the refrigerant charge in the refrigeration circuits and components aims at understanding it and reducing the charge to its minimal amount. Poggi et al. [2008] made a review of the studies aiming at reducing the refrigerant charge. They conclude that the optimal charge for each installation can be determined and that a reduction of the overall charge can be achieved by reducing the internal volume of exchangers, receivers, and liquid lines. In particular, exchangers with small internal volume should be used; compact exchangers (for instance based on the small channel technology) allow a considerable benefit without performance decline [Poggi et al., 2008, p. 367]. Poggi et al. [2008] explain also that the use of electronic expansion valves allow to decrease the charge. The use of secondary circuits, when possible, also helps. Palm [2007] arrived previously to the same conclusions than Poggi et al. [2008], but added also that in indirect systems, the amount of refrigerant solved in the compressor oil may be comparable to the amount in the (compact) heat exchangers. A possible solution to reduce this amount is consequently to use compressors with less oil. Palm [2007] also suggested that, instead of a high pressure receiver and a thermostatic expansion valve, which is a common heat pump circuit design, a capillary tube may be used in combination with a minimal low pressure receiver. This statement partially goes against the proposal of Poggi et al. [2008], who suggest that using an electric expansion valve, more sophisticated than a thermodynamic valve, would help. In the opposite, Palm [2007] suggested to use a capillary tube instead. Both approaches may be giving good results, as they use the whole circuit components and topology to handle the charge behavior. Obviously, it would be interesting to test them out within the same experimental setup. This is the kind of test that the BWP had been designed for: testing different layouts, topologies, and components, in a domestic heat pump prototype. The specifications of the BWP and its design are detailed in chapter 5, page 67 and appendix B, page 95.

2.6.1 Importance of the control strategy in heat pumps with low refrigerant charge

Increasing the compactness and decreasing the refrigerant charge implies to better control the thermodynamic cycle, in order to prevent system failures and to reach the best performance. While several studies show that an optimized control in refrigeration systems allows to save a significant amount of energy [Abdelghani Idrissi et al., 2001, Jakobsen and Rasmussen, 1998, Leducq et al., 2006, Yao et al., 2004], Fallahsohi et al. [2010] demonstrate the importance of dynamic modeling in the optimization of the control strategies in thermodynamic systems, as the transient phases are of a great importance, especially if low superheat values are favored [Lin and Yeh, 2007, Nanayakkara et al., 2002, Tamainot Telto, 1993, Tamainot Telto et al., 1996].

2.7 Defrosting strategies

Defrosting strategies are needed in the case of Air-Water or Air/Air heat pump circuits. Indeed, when refrigerant colder than 0°C goes through the evaporator coil, the water in the air freezes and accumulates on the coil. The ice blocks the air flow and acts as an insulator, decreasing the coil performance [Dinçer and Kanoglu, 2010, p. 169]. Consequently, to maintain appropriate performance, the coil needs to be defrosted periodically. Bertsch and Hubacher [2002, p. 4] state that the investigation of alternative defrosting strategies and the effects of natural defrosting, in addition to hot gas and reversed-cycle strategies, show that there is a big potential for improvements of the defrosting of evaporators.

Many defrosting strategies are available:

- cycle defrost using a 4-way valve. This technique is commonly used in domestic heat pump devices.
- Electric heater rods inserted into formed holes through the aluminum fins (common solution in small commercial system not reversible).
- If the evaporator can be insulated from the the cold air (in a ducted system, for example), the ice can be melted by warm air coming from the house itself.
- It is possible to run hot water over the coil. In that case a careful design of the water lines around the evaporator is needed to avoid freezing of the water used for the defrosting [Dinçer and Kanoglu, 2010, p. 169]. This technique is usually reserved for large systems.

- hot gas from the compressor discharge. This technique is common in large systems, like the hot water solution.

The heating capacity of Air/Water and Air/Air heat pumps decreases when there is frost formation on the evaporator surfaces in humid climates.

Bibliography

ARI 270-94: Sound Rating of Outdoor Unitary Equipment.

M.A. Abdelghani Idrissi, M.A. Arbaoui, L. Estel, and J. Richalet. Predictive functional control of a counter current heat exchanger using convexity property. *Chemical Engineering and Processing: Process Intensification*, 40(5): 449 – 457, 2001. ISSN 0255-2701. doi:10.1016/S0255-2701(00)00143-4.

AFNOR. ISO 9614-1: Acoustics - Determination of sound power levels of noise sources using sound intensity - Part 1 : measurement at discrete points, 11 2009. URL <http://sagaweb.afnor.org/fr-FR/sw/consultation/notice/1287190>.

ASHRAE. *ASHRAE Handbook - HVAC Systems and Equipment (SI)*, chapter Compressors, pages 37.1–37.38. ASHRAE, 2008.

E. P. Bandarra Filho, L. Cheng, and J. R. Thome. Flow boiling characteristics and flow pattern visualization of refrigerant/lubricant oil mixtures. *International Journal of Refrigeration*, 32(2):185–202, Mar. 2009. ISSN 0140-7007. doi:10.1016/j.ijrefrig.2008.06.013.

P. Bansal, E. Vineyard, and O. Abdelaziz. Advances in household appliances - A review. *Applied Thermal Engineering*, 31(17–18):3748–3760, 2011. ISSN 1359-4311. doi:10.1016/j.applthermaleng.2011.07.023. {SET} 2010 Special Issue.

W. L. Beeton and H. M. Pham. Vapor-injected scroll compressors. *ASHRAE Journal*, 45(4):22–27, 2003. URL http://opac.nebis.ch/F/?local_base=NEBIS&con_lng=FRE&func=find-b&find_code=SYS&request=000042859.

S. Bertsch and P. Hubacher. Verbesserung des Abtauens bei luftbeaufschlagten Verdampfern - Phase 2: Bewertung der Abtauprozesse. Technical report, Swiss Federal Office of Energy, 2002. URL <http://www.bfe.admin.ch/php/modules/enet/streamfile.php?file=000000007564.pdf>.

H. Cawte. Effect of lubricating oil contamination on condensation in refrigerant-R22. *International Journal of Energy Research*, 16(4):327–340, Jun. 1992. ISSN 0363-907X. doi:10.1002/er.4440160407.

H. Cawte, D. A. Sanders, and G. A. Poland. Effect of lubricating oil contamination on evaporation in refrigerants R12 and R22. *International Journal of Energy Research*, 20(8):663–679, Aug 1996. ISSN 0363-907X. doi:10.1002/(SICI)1099-114X(199608)20:8<663::AID-ER181>3.0.CO;2-M.

L. Creux. Rotary engine, 1905. URL <http://www.google.com/patents/US801182>. US Patent 801,182.

J. Demierre. *Theoretical and Experimental Study of a Thermally Driven Heat Pump Based on a Double Organic Rankine Cycle*. PhD thesis, STI, Lausanne, 2012. URL <http://dx.doi.org/10.5075/epfl-thesis-5201>.

J. Demierre, D. Favrat, J. Schiffmann, and J. Wegele. Experimental investigation of a Thermally Driven Heat Pump based on a double Organic Rankine Cycle and an oil-free Compressor-Turbine Unit. *International Journal of Refrigeration*, 44(0):91 – 100, 2014. ISSN 0140-7007. doi:10.1016/j.ijrefrig.2014.04.024.

I. Dinçer and M. Kanoglu. *Refrigeration Systems and Applications*. Wiley, 2nd edition edition, 2010. ISBN: 978-0-470-74740-7.

- M. Eschmann. Monitoring von Klein-Wärmepumpen mittels Normprüfungen 2008 - Schlussbericht. Technical report, Interstaatliche Hochschule für Technik NTB, on the behalf of the Swiss Federal Institute for Energy (OFEN), Feb. 2009. URL http://www.bfe.admin.ch/forschungwkk/02425/02724/02732/index.html?lang=en&dossier_id=03726. Project: 102062 - QS-WP/QP: Monitoring von Wärmepumpenanlagen 2007. Publication 290015.
- Eurovent Certification. Eurovent database - LCP-A-P/S-R-AC/CHF products, Feb. 2010. URL http://www.eurovent-certification.com/en/Certification_Programmes/Programme_Descriptions.php?lg=en&rub=03&srub=01&select_prog=LCP. The LCP program is a test program dedicated to Liquid Chilling Packages. Eurovent certification only applies to refrigeration machinery (to be certified, a product has to be able to have a cooling mode) and is one of the main reference database to compare refrigeration products. Most of the biggest heat pump manufacturers manage to have their products certified by this certification organization. The products used as air/water domestic heat pumps are Liquid Chilling Packages, Air Cooled, Packaged or Split, with Reverse cycle, and used for Air-Conditioning (A7/W45) or Cool Heating Floor (A7/W35). According to this denomination, the products considered here are from the LCP-A-P-R-AC and LCP-A-S-R-AC categories for the A7/W45 operation point and from the LCP-A-P-R-CHF and LCP-A-S-R-CHF categories for the A7/W35 operation point.
- H. Fallahsohi, C. Changenet, S. Placé, C. Ligeret, and X. Lin Shi. Predictive functional control of an expansion valve for minimizing the superheat of an evaporator. *International Journal of Refrigeration*, 33(2):409–418, 2010. ISSN 0140-7007. doi:[10.1016/j.ijrefrig.2009.10.008](https://doi.org/10.1016/j.ijrefrig.2009.10.008).
- D. Favrat, E. Nidegger, D. Reymond, and G. Courtin. Comparison Between a Single Stage and a Two Stage Air to Water Domestic Heat Pump with one Variable Speed Compressor. In *IIR Conference on Heat Pump Systems, Energy Efficiency, and Global Warming, Linz, Austria.*, Oct. 1997. URL <http://infoscience.epfl.ch/record/53338>.
- M. Fukuta, T. Yanagisawa, T. Arai, and Y. Ogi. Influences of miscible and immiscible oils on flow characteristics through capillary tube—part I: experimental study. *International Journal of Refrigeration*, 26(7):823–829, 2003. ISSN 0140-7007. doi:[10.1016/S0140-7007\(03\)00068-9](https://doi.org/10.1016/S0140-7007(03)00068-9).
- R. Furberg. Enhanced boiling heat transfer from a novel nanodendritic micro-porous copper structure. Master's thesis, KTH, Energy Technology, 2006. URL <http://urn.kb.se/resolve?urn=urn:nbn:se:kth:diva-4057>.
- R. Furberg, B. Palm, S. Li, M. Toprak, and M. Muhammed. The Use of a Nano- and Microporous Surface Layer to Enhance Boiling in a Plate Heat Exchanger. *Journal of Heat Transfer*, 131(10):101010, 2009. doi:[10.1115/1.3180702](https://doi.org/10.1115/1.3180702).
- Y. Guo, G. Zhang, J. Zhou, J. Wu, and W. Shen. The refrigerant oil return speed influence on the design of vertical U-Tube ground heat exchanger in the direct expansion ground-source heat pumps. In *Conference of 2011 Asia-Pacific Power and Energy Engineering Conference, APPEEC 2011, Wuhan, March, 25–28th*, 2011. ISBN 9781424462551. doi:[10.1109/APPEEC.2011.5749136](https://doi.org/10.1109/APPEEC.2011.5749136).
- M. Habert. *Falling film evaporation on a tube bundle with plain and enhanced tubes*. PhD thesis, Swiss Federal Institute of Technology - Lausanne, 2009. URL <http://library.epfl.ch/theses/?nr=4341>. PhD Thesis n°4341. Directed by Prof. Dr. John Richard Thome.
- D. W. Hughes, J. T. McMullan, K. A. Mawhinney, R. Morgan, and B. L. Sutcliffe. Influence of lubricant on heat pump performance. In *Proceedings of the Purdue compressor technology conference*, volume 2, page 443, 1980. URL http://opac.nebis.ch/F/?local_base=NEBIS&con_lng=ENG&func=find-b&find_code=SYS&request=000032288.
- D. W. Hughes, J. T. McMullan, K. A. Mawhinney, and R. Morgan. Pressure-enthalpy charts for mixtures of oil and refrigerant R12. *International Journal of Refrigeration*, 5(4):199–202, 1982. ISSN 0140-7007. doi:[10.1016/0140-7007\(82\)90019-6](https://doi.org/10.1016/0140-7007(82)90019-6).
- D. W. Hughes, J. T. McMullan, K. A. Mawhinney, and R. Morgan. Influence of oil on evaporator heat transfer (results for R12 and Shell Clavus 68). *International Journal of Refrigeration*, 7(3):150–158, 1984a. ISSN 0140-7007. doi:[10.1016/0140-7007\(84\)90093-8](https://doi.org/10.1016/0140-7007(84)90093-8).

- D. W. Hughes, J. T. McMullan, K. A. Mawhinney, and R. Morgan. Experimental investigation of the influence of lubricating oil on heat pump performance. *International Journal of Energy Research*, 8(3):213–222, 1984b. doi:[10.1002/er.4440080303](https://doi.org/10.1002/er.4440080303).
- A. Iglesias and D. Favrat. Innovative isothermal oil-free co-rotating scroll compressor–expander for energy storage with first expander tests. *Energy Conversion and Management*, 85(0):565 – 572, 2014. ISSN 0196-8904. doi:[10.1016/j.enconman.2014.05.106](https://doi.org/10.1016/j.enconman.2014.05.106).
- ISO. ISO 3744: Acoustics – Determination of sound power levels and sound energy levels of noise sources using sound pressure – Engineering methods for an essentially free field over a reflecting plane, 2010. URL http://www.iso.org/iso/iso_catalogue/catalogue_tc/catalogue_detail.htm?csnumber=52055.
- A. Jakobsen and B. Rasmussen. Energy-optimal speed control of fans and compressors in a refrigeration system. In *Proceedings of Eurotherm Seminar, Nancy, France*, pages 317—323, 1998.
- F. Karlsson. Integrated control of heat pumps. Master’s thesis, Chalmers University of Technology, Building Services Engineering, Chalmers University of Technology, SE-412 96 Göteborg, Sweden, 2003. URL <http://publications.lib.chalmers.se/publication/20110>. Thesis for the degree of licentiate of engineering. Technical report D - Department of Building Technology, Building Services Engineering, Chalmers University of Technology, n°2003:03.
- F. Karlsson and P. Fahlén. Impact of design and thermal inertia on the energy saving potential of capacity controlled heat pump heating systems. *International Journal of Refrigeration*, 31(6):1094–1103, Sep 2008. ISSN 0140-7007. doi:[10.1016/j.ijrefrig.2007.12.002](https://doi.org/10.1016/j.ijrefrig.2007.12.002).
- Kazuya Kondo, Hajime Sato, and Yoshiyuki Kimata. Two stage compressor having rotary and scroll type compression mechanisms, 2010. URL <http://www.google.com/patents/US7717686>.
- S. C. Kesim, K. Albayrak, and A. Ileri. Oil entrainment in vertical refrigerant piping. *International Journal of Refrigeration*, 23(8):626 – 631, 2000. ISSN 0140-7007. doi:[10.1016/S0140-7007\(99\)00085-7](https://doi.org/10.1016/S0140-7007(99)00085-7).
- D. Leducq, J. Guilpart, and G. Trystram. Non-linear predictive control of a vapour compression cycle. *International Journal of Refrigeration*, 29(5):761 – 772, 2006. ISSN 0140-7007. doi:[10.1016/j.ijrefrig.2005.12.005](https://doi.org/10.1016/j.ijrefrig.2005.12.005).
- S. Li. *Fabrication of Nanostructured Materials for Energy Applications*. PhD thesis, KTH, Microelectronics and Applied Physics, 2008. URL <http://urn.kb.se/resolve?urn=urn:nbn:se:kth:diva-4807>. ISBN-13: 978-91-7178-994-5.
- C. Liang, C. Jiangping, L. Jinghui, and C. Zhijiu. Experimental investigation on mass flow characteristics of electronic expansion valves with R22, R410A and R407C. *Energy Conversion and Management*, 50(4):1033–1039, 2009. ISSN 0196-8904. doi:[10.1016/j.enconman.2008.12.018](https://doi.org/10.1016/j.enconman.2008.12.018).
- J.-L. Lin and T.-J. Yeh. Modeling, identification and control of air-conditioning systems. *International Journal of Refrigeration*, 30(2):209 – 220, 2007. ISSN 0140-7007. doi:[10.1016/j.ijrefrig.2006.08.009](https://doi.org/10.1016/j.ijrefrig.2006.08.009).
- J. B. Marcinichen, D. Wu, S. Paredes, J. R. Thome, and B. Michel. Dynamic flow control and performance comparison of different concepts of two-phase on-chip cooling cycles. *Applied Energy*, 114(0):179 – 191, 2014. ISSN 0306-2619. doi:[10.1016/j.apenergy.2013.09.018](https://doi.org/10.1016/j.apenergy.2013.09.018).
- J. T. McMullan, D. W. Hughes, and R. Morgan. Influence of lubricating oil on heat pump performance. Final report, New University of Ulster, Coleraine, N. Ireland, U.K. BT52 1SA, Dec. 1983. Research financed by the Commission of the European Communities within the frame of the Energy R&D Programme "Energy Conservation". Contract n° EEA-4-028-GB.
- J. T. McMullan, N. Murphy, and D. W. Hughes. The effect of oil on the performance of heat pumps and refrigerators–II. Experimental results. *Heat Recovery Systems and CHP*, 8(2):95–124, 1988a. ISSN 0890-4332. doi:[10.1016/0890-4332\(88\)90004-X](https://doi.org/10.1016/0890-4332(88)90004-X).
- J. T. McMullan, N. Murphy, and D. W. Hughes. The effect of oil on the performance of heat pumps and refrigerators–part one. Experimental test facility. *Heat Recovery Systems and CHP*, 8(1):53–68, 1988b. ISSN 0890-4332. doi:[10.1016/0890-4332\(88\)90041-5](https://doi.org/10.1016/0890-4332(88)90041-5).

- J. T. McMullan, N. J. Hewitt, A. J. Masson, and N. E. Murphy. The influence of oil viscosity and refrigerant quality on evaporator performance. *International Journal of Energy Research*, 16(7):567–581, 1992. doi:[10.1002/er.4440160702](https://doi.org/10.1002/er.4440160702).
- Mitsubishi. Development of the Q-Ton CO₂-Refrigerant Heat Pump for Industrial Water-Heater Systems for Use at Outside Air Temperatures Down to -25 degrees Celsius. *Mitsubishi Heavy Industries Technical Review*, 48(4), December 2011. URL <https://www.mhi.co.jp/technology/review/pdf/e484/e484076.pdf>.
- S. F. Y. Motta, S. L. Braga, and J. A. R. Parise. Experimental study of adiabatic capillary tubes: critical flow of refrigerant/oil mixtures. *HVAC&R Research International Journal*, 7(4):331–334, 2001. URL <http://resourcecenter.ashrae.org/store/ashrae/newstore.cgi?itemid=6793&view=item&categoryid=350&categoryparent=350&page=1&loginid=39870624>.
- S. F. Y. Motta, J. A. R. Parise, and S. L. Braga. A visual study of R-404A/oil flow through adiabatic capillary tubes. *International Journal of Refrigeration*, 25(5):586–596, 2002. ISSN 0140-7007. doi:[10.1016/S0140-7007\(01\)00057-3](https://doi.org/10.1016/S0140-7007(01)00057-3).
- C. Möller. *Blasenbildung und Wärmeübergang beim Behältersieden von Kältemittel/Öl-Gemischen*. PhD thesis, University of Stuttgart, Papierflieger, Clausthal Zellerfeld, 1998. Directed by Prof. Dr.-Ing E. Hahne. ISBN-13 978-3897202153.
- V. K. Nanayakkara, Y. Ikegami, and H. Uehara. Evolutionary design of dynamic neural networks for evaporator control. *International Journal of Refrigeration*, 25(6):813 – 826, 2002. ISSN 0140-7007. doi:[10.1016/S0140-7007\(01\)00090-1](https://doi.org/10.1016/S0140-7007(01)00090-1).
- E. Navarro, J. F. Urchueguía, J. González, and J. M. Corberán. Test results of performance and oil circulation rate of commercial reciprocating compressors of different capacities working with propane (R290) as refrigerant. *International Journal of Refrigeration*, 28(6):881–888, 2005. ISSN 0140-7007. doi:[10.1016/j.ijrefrig.2005.01.010](https://doi.org/10.1016/j.ijrefrig.2005.01.010).
- E. Nidegger, D. Favrat, and J. R. Thome. Local Flow Boiling and Pressure Drop Measurements for R134a/Oil Mixtures - Part 1: Evaporating in a Microfin Tube. *HVAC&R Research*, 3(1):38–53, 1997. URL <http://resourcecenter.ashrae.org/store/ashrae/newstore.cgi?itemid=6679&view=item&categoryid=330&categoryparent=330&page=1&loginid=39874521>.
- B. Palm. Refrigeration systems with minimum charge of refrigerant. *Applied Thermal Engineering*, 27(10):1693 – 1701, 2007. ISSN 1359-4311. doi:[10.1016/j.applthermaleng.2006.07.017](https://doi.org/10.1016/j.applthermaleng.2006.07.017). Heat transfer and sustainable energy technologies.
- C. Park, H. Cho, Y. Lee, and Y. Kim. Mass flow characteristics and empirical modeling of R22 and R410A flowing through electronic expansion valves. *International Journal of Refrigeration*, 30(8):1401–1407, 2007. ISSN 0140-7007. doi:[10.1016/j.ijrefrig.2007.03.011](https://doi.org/10.1016/j.ijrefrig.2007.03.011).
- F. Poggi, H. Macchi Tejada, D. Leducq, and A. Bontemps. Refrigerant charge in refrigerating systems and strategies of charge reduction. *International Journal of Refrigeration*, 31(3):353 – 370, 2008. ISSN 0140-7007. doi:[10.1016/j.ijrefrig.2007.05.014](https://doi.org/10.1016/j.ijrefrig.2007.05.014).
- E. Poiate Jr and J. L. Gasche. Foam flow of oil-refrigerant R12 mixture in a small diameter tube. *J. Braz. Soc. Mech. Sci. Eng.*, 28(4):390–398, 2006. ISSN 16785878 (ISSN). doi:[10.1590/S1678-58782006000400003](https://doi.org/10.1590/S1678-58782006000400003).
- E. Purvis. Scroll compressor technology. In *Heat Pump Conference, New Orleans*, 1987.
- G. Ribatski and A. M. Jacobi. Falling-film evaporation on horizontal tubes - A critical review. *International Journal of Refrigeration*, 28(5):635–653, 2005. ISSN 0140-7007. doi:[10.1016/j.ijrefrig.2004.12.002](https://doi.org/10.1016/j.ijrefrig.2004.12.002).
- H. Sato, Y. Hotta, H. Mizuno, Y. Kimata, T. Goto, and H. Kobayashi. Development of Two-Stage Compressor for CO₂ Heat-Pump Water Heaters. *Mitsubishi Heavy Industries Technical Review*, 49(1), March 2012. URL <http://www.mhi.co.jp/technology/review/pdf/e491/e491092.pdf>.
- J. Schiffmann. *Integrated design, optimization and experimental investigation of a direct driven turbocompressor for domestic heat pumps*. PhD thesis, Swiss Federal Institute of Technology - Lausanne, 2008. URL <http://dx.doi.org/10.5075/epfl-thesis-4126>.

- J. Schiffmann and D. Favrat. Experimental investigation of a direct driven radial compressor for domestic heat pumps. *International Journal of Refrigeration*, 32(8):1918–1928, 2009. ISSN 0140-7007. doi:10.1016/j.ijrefrig.2009.07.006.
- J. Schiffmann, A. Molyneaux, D. Favrat, F. Marechal, M. Zehnder, and J. Godat. Compresseur radial pour pompe à chaleur bi-étagée - Phase 1. Technical report, OFTTech SA, Nov. 2002. URL http://www.bfe.admin.ch/forschungwkk/02425/02724/02727/index.html?lang=en&dossier_id=03092. On the behalf of the Office Fédéral de l'ENergie (OFEN).
- J. Schiffmann, A. Molyneaux, and D. Favrat. Compresseur radial pour pompe à chaleur bi-étagée - Phase 2. Technical report, OFTTech SA, Nov. 2005. URL http://www.bfe.admin.ch/forschungwkk/02425/02724/02727/index.html?lang=en&dossier_id=03093. On the behalf of the Office Fédéral de l'ENergie (OFEN).
- K. Spindler and E. Hahne. The influence of oil on nucleate pool boiling heat transfer. *Heat & Mass Transfer*, 45(7):979–990, May 2009. ISSN 0947-7411. doi:10.1007/s00231-007-0321-0. 6th International Conference on Boiling Heat Transfer, Spoleto, Italy, May 07–12, 2006.
- Z. Tamainot Telto. *Détendeurs thermostatiques de machines frigorifiques. Comportement dynamique et modélisation*. PhD thesis, INSA Lyon, 1993.
- Z. Tamainot Telto, A. Outtagarts, P. Haberschill, and M. Lallemand. Comportement dynamique de détendeurs thermostatiques de machines frigorifiques Behaviour of a thermostatic expansion valve in non-steady state for a refrigerating machine. *International Journal of Refrigeration*, 19(2):124–131, 1996. ISSN 0140-7007. doi:10.1016/0140-7007(95)00084-4.
- E. Van Rooyen. *Boiling on a Tube Bundle*. PhD thesis, STI, Lausanne, 2011. URL <http://dx.doi.org/10.5075/epfl-thesis-5226>.
- A. Wahlstrom and L. Vamling. Prediction of solubility for HFC working fluids in model substances for compressor oils. *Canadian Journal of Chemical Engineering*, 75(3):551–561, 1997. doi:10.1002/cjce.5450750309.
- S. Wang, J. Gu, and T. Dickson. Modeling and experimental investigation of accumulators for automotive air conditioning systems. *International Journal of Refrigeration*, 29(7):1109–1118, 2006. ISSN 0140-7007. doi:10.1016/j.ijrefrig.2006.03.004.
- E. L. Winandy and C. B. Cuevas. Analysis of the oil return in a pair of scroll compressors working in parallel at part load. *Applied Thermal Engineering*, 23(5):623–636, 2003. ISSN 1359-4311. doi:10.1016/S1359-4311(02)00189-8.
- T. Yanagisawa, T. Shimizu, and M. Fukuta. Foaming characteristics of an oil-refrigerant mixture. *International Journal of Refrigeration*, 14(3):132–136, 1991. ISSN 0140-7007. doi:10.1016/0140-7007(91)90066-P.
- Y. Yao, Z. Lian, Z. Hou, and X. Zhou. Optimal operation of a large cooling system based on an empirical model. *Applied Thermal Engineering*, 24(16):2303 – 2321, 2004. ISSN 1359-4311. doi:10.1016/j.applthermaleng.2004.03.006.
- M. Youbi Idrissi and J. Bonjour. The effect of oil in refrigeration: Current research issues and critical review of thermodynamic aspects. *International Journal of Refrigeration*, 31(2):165–179, 2008. ISSN 0140-7007. doi:10.1016/j.ijrefrig.2007.09.006.
- M. Youbi Idrissi, J. Bonjour, C. Marvillet, and F. Meunier. Impact of refrigerant-oil solubility on an evaporator performances working with R-407C. *International Journal of Refrigeration*, 26(3):284–292, 2003. ISSN 0140-7007. doi:10.1016/S0140-7007(02)00129-9.
- M. Zehnder. *Efficient air-water heat pumps for high temperature lift residential heating, including oil migration aspects*. PhD thesis, Swiss Federal Institute of Technology - Lausanne, 2004. URL <http://dx.doi.org/10.5075/epfl-thesis-2998>. PhD Thesis n°2998.
- M. Zehnder and D. Favrat. Migration d'huile dans les pompes à chaleur. Technical report, Laboratoire d'Energétique Industrielle, Ecole Polytechnique Fédérale de Lausanne, Dec. 2002. URL http://www.bfe.admin.ch/forschungwkk/02425/02724/02727/index.html?lang=en&dossier_id=04022. On the behalf of the Office Fédéral de l'ENergie (OFEN). Rapport annuel 2002.

- M. Zehnder, D. Favrat, G. Reiner, and C. Brugnoli. Waermepumpe mit Hilfskreislauf zur Kondensatunterkuehlung, phase 1. Technical report, Bundesamt fuer Energie, 1998. URL <http://infoscience.epfl.ch/record/53356>.
- M. Zehnder, D. Favrat, H. Hohl, C. Olivier, and M. Perevozchikow. High Performance Air-Water Heat Pump with Extended Application Range for Residential Heating. In *7th International Energy Agency, Heat Pump Conference, Beijing*, volume 2, page 702, 2002. URL <http://infoscience.epfl.ch/record/53444>.
- Michele Zehnder, Jürg Alexander Schiffmann, Jean-Baptiste Carré, and Daniel Favrat. Implementation of a scroll booster compressor into a single-stage air-water heat pump for peak winter day. In *Proceedings of the 23rd International Conference on Efficiency, Cost, Optimization, Simulation and Environmental Impact on Energy Systems*, volume 1, 2010. doi:[10.5075/epfl-infoscience-164962](https://doi.org/10.5075/epfl-infoscience-164962).
- M. Zogg. History of Heat Pumps: Swiss Contributions and International Milestones. Technical report, Swiss Federal Office of Energy, 2008. URL <http://www.zogg-engineering.ch/publi/HistoryHP.pdf>.
- C. Zwyssig, J. W. Kolar, and S. D. Round. Megaspeed Drive Systems: Pushing Beyond 1 Million r/min. *IEEE-ASME Transactions on Mechatronics*, 14(5):564–574, Oct 2009. ISSN 1083-4435. doi:[10.1109/TMECH.2008.2009310](https://doi.org/10.1109/TMECH.2008.2009310).
- O. Zürcher, J. R. Thome, and D. Favrat. Local Flow Boiling and Pressure Drop Measurements for R134a/Oil Mixtures - Part 2: Evaporating in a Plain Tube. *HVAC&R Research*, 3(1):54–64, 1997. URL <http://resourcecenter.ashrae.org/store/ashrae/newstore.cgi?itemid=6680&view=item&categoryid=330&categoryparent=330&page=1&loginid=39874521>.
- O. Zürcher, J. R. Thome, and D. Favrat. Intube Flow Boiling of R-407C and R-407C/Oil Mixtures. Part 2: Plain Tube Results and Predictions. *HVAC&R Research International Journal*, 4(4):373–399, 1998a. URL <http://infoscience.epfl.ch/record/53361>.
- O. Zürcher, J. R. Thome, and D. Favrat. Intube Flow Boiling of R-407C and R-407C/Oil Mixtures. Part 1: Microfin Tube. *HVAC&R Research International Journal*, 4(4):347–372, 1998b. URL <http://infoscience.epfl.ch/record/53362>.

Credits

Fig. 2.1, page 10 © 2013 Jean-Baptiste Carré, licensed under © ⓘ 4.0 . This figure is based on an original figure from Zwyssig et al. [2009, Fig. 1, p. 565].

Thesis & methodology

This chapter states first that multistage oil-free variable-speed domestic heat pumps powered by twin-stage radial compressors are feasible and demonstrate a significant potential. Then, it offers a methodology to validate this statement.

Chapter 1 states that better domestic heating systems are needed and that heat pumps are one of the best candidates for this improvement. Chapter 2 demonstrates that multistage oil-free variable-speed technologies show promising perspectives in the heat pumps application fields. Moreover, a twin-stage oil-free radial compressor dedicated to heat pumps applications is being developed based on a previous thesis work [Schiffmann, 2008]. The integration of the single-stage unit in a refrigerant circuit has shown promising results [Schiffmann, 2008, p. 221], even if that refrigerant circuit was not a single stage heat pump circuit yet. Consequently, the purpose of this doctoral thesis is to push further the integration and experiments performed by Schiffmann [2008] with a single-stage compressor unit, using now a twin-stage compressor unit and thus to demonstrate that **multistage oil-free variable-speed domestic heat pumps powered by twin-stage radial compressors are feasible and demonstrate a significant potential**. This chapter describes the methodology used in this work to achieve the demonstration of those two points. The approach chosen is experimental and uses energy modeling to analyze the behavior of the prototypes from laboratory measurements. Two prototypes are being used for this demonstration: a pre-industrial Air-Water twin-stage heat pump Prototype (AWP) (further described in chapter 4) and a more academic Brine-Water twin-stage heat pump Prototype (BWP) (further described in chapter 5).

3.1 Demonstration of feasibility

The feasibility of the heating devices mentioned in the previous section is demonstrated experimentally directly. Two prototypes, the AWP and the BWP, have been designed, assembled, then characterized with one Operating Point (OP), or more (6 OP have been tested for the AWP, including the A-7/W35 OP, and 1 OP for the BWP). The issues encountered and paths of improvement for those prototypes are discussed in chapters 4 and 5.

3.2 Demonstration of potential

In order to quantify the performance of the heat pump prototypes and their components, measurements of physical values are needed at many locations in the circuits of the prototypes. The measured physical values include, from a thermodynamic point of view, pressure, temperature, and mass flow rate measurements. However, many of those locations do not easily allow to measure those physical values: Some locations are very difficult to instrument, some measurements would influence the behavior of the prototypes and/or decrease their performance, some flow

rates are very small and located in inaccessible locations. For instance, the internal heat energy fluxes and gas flow rates inside the compressor unit are complex and hard to measure, especially in locations such as gas bearings and labyrinth seals. An other example is the flow rate measurements in the AWP where compactness matters; it has been decided to leave the main flow rates unmeasured in that prototype in order to match the compactness criteria (report to section 4.1.2 for more details about this choice). In order to compensate for those missing measurements, a modeling approach is proposed. The proposed model propagates the measured physical values and their uncertainties, through mass and energy balance equations, to inaccessible locations. Those enhanced results are used to characterize the performance of the prototypes and spot the elements to improve, thus demonstrating the potential of the technology. Historically, the BWP has been designed and built first, in 2009. It has been tested in 2010 unsuccessfully with defectuous twin-stage compression units, and consequently gave inexploitable OP at the time, but contributed to gain experience with the technology. The BWP was more an academic experimental setup than an industrial prototype, with lots of instrumentation and modularity. Details about the BWP are given in chapter 5, page 67, and appendix B, page 95. The AWP, designed and built in 2011 and 2012, has been tested while the testing of the BWP had been put on hold, and allowed to reach stable OP, detailed in chapter 4. The AWP is also a step into more integration of the compression unit inside the heat pump circuits and was equipped with an economizer coupled with the compression unit directly. The details of this coupling is shown in section 4.2.3, page 39. Details about the AWP are given in chapter 4, page 35, and appendix A, page 91. Building onto the experience gained with the AWP, the original BWP has been modified, mainly to be able to use the last generation of compression unit at the time, and in order to test a new bypass system, likely to solve the issues observed with the AWP. The AWP was more an industrial prototype than an academic experimental setup and took advantage of the ideas and thinking process which led to the design of the BWP, and to some extents, from the experience of the failed experiments performed on the BWP with the defectuous compression units. The modified BWP is presented in chapter 5 and has been tested in 2013. The experience gained with the two first prototypes suggests further integration and ideas for the next prototypes. Those concepts and proposals are exposed in chapter 6, page 83.

3.3 Limits of the demonstration

The methodology proposed allows the demonstration of the feasibility of twin-stage oil-free variable-speed domestic heat pumps and the potential of this technology for heat pumps applications. Autonomous control and switching between modes such as defrosting-mode, heating-mode, cooling-mode and start & stop procedures are only evoked in the form of remarks and comments and need further developments and analysis, as they imply more dynamic tests of the prototypes, which have not been performed so far. They are consequently out of the scope of this thesis work. However, the remarks and comments are inspired by the observations made during the experiments and are summarized in chapter 6.

3.4 Methodology

3.4.1 Design and assembly of heat pump prototypes

The design and assembly of the heat pump prototypes follow traditional heat pumps systems design rules, as detailed in various references [ASHRAE, 2008a,b, Brown, 1997, Rapin et al., 2011, Smith and Zappe, 2004], but add also some specific rules that are related to oil-free technologies. Some of these specific rules add constraints, some give more flexibility. Those additional design rules, often learned while developing the successive versions of the prototypes of the heat pumps presented in this work, are presented in chapter 6. Only the last versions of the prototypes, which have been used for the tests and to generate the results, are presented in details in chapters 4 and 5 and their appendix.

3.4.2 Test of the heat pump prototypes

The prototypes have been tested many times with different versions of the compression units. Most of those units have been destroyed before any interesting OP could be reached, unfortunately. The tests presented in this

work have been performed using two of the first functional twin-stage compression units available during the whole thesis time¹. The units used in BWP and AWP have been destroyed during the tests. The development of the compression units has been carried on, and fully functional twin-stage compression units, with advanced designs, have been finalized between 2013 and 2015, and are now available. Their design have evolved and they are now incompatible with the prototypes of the heat pumps developed during this thesis (mainly because the location of their inlets and outlets have been modified). The prototypes of the heat pumps need to be modified to integrate the new cores. Further details about the compression units and their compatibility with the prototypes of the heat pumps can be found in chapter 6. The OP presented in this thesis work are the OP that could be reached with the prototypes before the compression unit was destroyed, for the case of the BWP, or before the AWP prototype was shipped to the industrial partner. Tests were carried out starting with a steady state system at a given uniform temperature (at the climate chamber temperature for the AWP and at the atmospheric temperature for the BWP). The difference between the sources temperatures being slowly increased gradually during the tests. Every OP presented in this work is stable conditions recorded during those slow increase procedures: when a stable point was found, it was recorded, keeping the system in that stable state for at least 10 minutes. Each stable OP presented is in fact an average of the measurements performed during the more stable 3-minute period during the stable period of at least 10 minutes. The data acquisition rate was at minimum of 1 measurement per second, which gives an interesting level of accuracy of the OP measurements (see appendix G for details about uncertainties and uncertainty calculations).

3.4.3 Modeling of those heat pump prototypes

The modeling methodology follows the steps detailed below:

Draw a layout of the installation and the frontier of the analysis where **all** the flow rates and possible entities appear. All the existing flow rates need to be visible on the layout.

Separate the layout in components. A component is a network, as intended by [Borel and Favrat \[2010, p. 24–25\]](#), and corresponds to an element where flows enter and leave, partially (if there are accumulation) or totally, and that can exchange energy with normal components, or special components like the atmosphere or the environment of the device. The special components have no flow and are infinite reservoir at a given temperature. They can exchange energy with normal components or be the source or the receiver of flows. With this paradigm, a component does not necessarily correspond to a physical element or to a part of the system that can be isolated from the rest. For instance, a heat exchanger, in this paradigm, is made of two components which exchange heat energy. In the next chapters, the compression unit will be modeled as many components exchanging mass or energy (details about this modeling of the compression unit are given in chapter 4 & chapter 5). This thesis work uses steady-state models. In steady state conditions, mass and energy balances are equal to zero for every components, as for the whole system delimited by a frontier. There is no mass change of the components. The components are assigned with a number. The modeling approach presented here could also be used to generate quasi-static models or dynamic models, if enough data is available.

Transform the layout view into the model view. Each component exchanges energy or mass with other components. The representation of the model using the GraphViz modeling paradigm from [Gansner and North \[2000\]](#), typically dedicated to software engineering modeling, is unusual in the thermodynamic modeling field and is a representation analogy proposed by the author of this thesis work. In the opposite, the modeling itself, using mass and energy balances is a common modeling approach in the thermodynamic field. Each type of energy is represented with a bold and colored arrow, and the mass flow rates are represented with thin black arrows. The convention is that positive energy or mass flow rates enter the components. Negative flows leave the components. This means that a negative value results in a flow moving against the arrow. The notation indicates the direction of the arrow with subscripts using the numbers or the components, separated by an arrow.

¹The compression unit mounted in the BWP was the unit named *cp101* and compression unit mounted in the AWP was the unit named *cp105*. Both were issued from the design family of the prototypes of the compression unit named *evo4*. Both have been destroyed during the tests at EPFL. The unit *cp105* has been tested in May 2012. The unit *cp101* has been used in the industrial partners laboratories in 2011 and 2012, for heatpump tests, and has been tested at EPFL only after, in 2013.

Determine the equations. Each component gives two equations: a mass flow rates balance equation, as shown in eq. (3.1), and an energy rates balance equation, as shown in eq. (3.2). By convention, each transformation energy rate² is included in the equation using the outlet specific enthalpy³ of the component being the source of this flow rate. The whole device, at its frontier, also provides a mass flow rates balance equation and an energy rates balance equation. In the case of dynamic modeling, the mass and energy balance equations are not equal to zero. A steady-state approach has been favored in this thesis work because the data collected during the experiments were not enough to solve equations not equal to zero⁴.

$$\sum_{i=1}^n \dot{M}_{x_i \rightarrow y_i} = 0 \quad [\text{W}] \quad (3.1)$$

$$\sum_{i=1}^m \dot{M}_{a_i \rightarrow b_i} \cdot h_{out\ a_i} + \sum_{j=1}^n \dot{Y}_{c_j \rightarrow d_j} + \sum_{k=1}^p \dot{E}_{e_k \rightarrow f_k} = 0 \quad [\text{W}] \quad (3.2)$$

Solve the system of equations. Mass flow rates balance equations have the priority. They are solved first, if possible. When no more equations can be solved, a fitting parameter is added with the introduction of a new relation bounding 2 variables together. For instance, this can be introduced for a flow which is divided in two. The proportion of the entering flow leaving in one of the leaving flows is characterized here with a splitting parameter. When all the mass flow rates are determined, the energy balance equations are written with the same method.

Implement the model. As soon as every variable can be expressed, the model is implemented in a modeling software (here, the MATLAB from MathWorks) and the set of equations is solved with a solver. The solver tries to fit the parameter that were added to express every variable as an expression in order to get the lowest objective function value. If no fit parameter was added, the level of information of the system is sufficient and the set of equations should close, within the limits of the measurement uncertainty ranges. A set of equations is considered closed, in steady state conditions, if every energy and mass balance of every component and the balances at the frontier of the system are equal to zero. If fit parameters were added, the set of equations is now solvable but is not closed. Consequently, a fitting of those parameters is necessary to close the system. This step is performed using a minimization of an objective function under constraints, using a standard optimization algorithm. In this work, the MATLAB *fmincon* [MathWorks, a] function has been used with an interior point algorithm, which was the best suited to solve this problem with this function [MathWorks, b]. The variables of this algorithm are the fit parameters. Constraints on the variables are necessary to bound the fit parameters and to ensure that realistic conditions only are explored by the algorithm. For instance, if a flow is divided into three flows using two fit parameters, the sum of those two parameters can not be greater than one. The starting point of the minimization algorithm is determined randomly. The first valid starting point found randomly is selected as the optimization starting point. Indeed, the fluid properties at each location in the cycles are determined using the NIST Reference Fluid Thermodynamic and Transport Properties Database (REFPROP) [Lemmon et al.] but the latter can only compute properties within given inputs range. When the number of fit parameters starts to be quite high, as this is the case with the AWP model, it is common that a randomly chosen starting point is not defined which implies that the minimization algorithm does not initialize. The objective function minimized by the optimizer is the sum of two aggregates of indicators. The first one has an order of magnitude above 1 and is the sum of an array. This array contains statements penalizing unrealistic conditions in the system, such as an outlet stream enthalpy lower than its inlet stream enthalpy, in a compressor. If an unrealistic condition is observed, the objective function is penalized using the difference between the realistic condition that should be and its current unrealistic state.

² See section 3.4.4, page 29, for a definition of the transformation energy rate.

³ See section 3.4.4, page 29, for a definition of the specific enthalpy.

⁴ Fitting a dynamic model of the prototypes would have required to know the variation of mass of the components. Most of the components mass variation can be neglected, but the variation of mass of the condenser, the evaporator, and the economizer need to be measured (or, alternatively, the mass flow rates entering and leaving those components can be measured, but this is technically far more difficult and inconvenient). Those measurements were planned to be made in the BWP, but most of the experiments have been performed on the AWP. The BWP has only given a single OP and the load cells were not calibrated at the time, as this is a procedure which was planned for the next experiments. For more details, see chapter 4, page 35, and chapter 5, page 67.

In other word, the more the condition is unrealistic the bigger is the penalization. This first term, as soon as the system is realistic, is equal to zero. If this term is not equal to zero, the solution found by the optimizer is not considered, an other starting point is chosen, and the optimizer is run again. The second term of the sum is of an order of magnitude below 1 and corresponds to the sum of the energy balances on every component and on frontier of the system. It is equal to zero when all the balances are equal to zero. Typically, this term is never exactly equal to zero due to the fact that a model never fully represents the reality and due to uncertainties and measurement errors. The optimization problem has been run for every experimental points more that a hundred times in order to provide more confidence in the presented results. For the points presented in this work the sum of those balances is always below 100W.

Analyze the results As soon as the parameters of the system have been fitted, an analysis of the system can be performed.

In order to better understand this modeling approach, a simple example dedicated to illustrate the methodology is offered here. The chosen example is a single stage heat pump using part of the liquid refrigerant leaving the condenser to cool down the motor of the compressor. The partly evaporated flow is then collected at the evaporator inlet. The layout of this heat pump is presented in fig. 3.1. Using the modeling approach proposed above, the example system is modeled using 7 components. This model is described in fig. 3.1. The components are represented on the layout with green markers and are listed in the legend provided with the model.

Unfortunately, the designer of this example experimental setup, for unknown reasons, could not instrument the heat pump with enough sensors. Each component of the system can not be characterized and only some physical values are available. The measurement points are represented on the layout in fig. 3.1. A **bold value** is a value physically measured in the experiment. An underlined value is guessed directly by the optimizer, and a value with normal font is computed with the model⁵. The uncertainties are being propagated through the model⁶. For the example case, the values are presented in tables 3.1 and 3.3.

Component	Location	P / bar	T / °C	h / kJ kg ⁻¹	s / kJ kg ⁻¹ K ⁻¹
1	inlet	3.50 +/- 0.05	8.53 +/- 0.15	404.72 +/- 0.27	1.7359 +/- 0.0020
	outlet	9.12 +/- 0.05	86.01 +/- 0.27	469.78 +/- 0.35	1.8689 +/- 0.0014
2	inlet	4.30 +/- 0.05	11.10 +/- 0.35	243.18 +/- 0.22	1.1526 +/- 0.0014
	outlet	3.70 +/- 0.05	6.64 +/- 0.39	382.00 +/- 0.22	1.6507 +/- 0.0000
3	inlet	9.12 +/- 0.05	86.01 +/- 0.15	469.78 +/- 0.22	1.8689 +/- 0.0010
	outlet	8.52 +/- 0.05	31.01 +/- 0.15	243.18 +/- 0.22	1.1481 +/- 0.0007
4	inlet	3.70 +/- 0.05	6.64 +/- 0.39	245.81 +/- 17.47	1.1639 +/- 0.0015
	outlet	3.50 +/- 0.05	8.53 +/- 0.44	404.72 +/- 0.27	1.7359 +/- 0.0020
5	inlet	8.52 +/- 0.05	31.01 +/- 0.15	243.18 +/- 0.22	1.1481 +/- 0.0007
	outlet	3.70 +/- 0.05	6.64 +/- 0.39	243.18 +/- 0.22	1.1545 +/- 0.0015
6	inlet	1.00 +/- 0.05	10.00 +/- 0.15	407.21 +/- 0.16	3.8055 +/- 0.0149
	outlet	1.00 +/- 0.05	7.00 +/- 0.15	404.20 +/- 0.16	3.7948 +/- 0.0149
7	inlet	2.00 +/- 0.05	30.00 +/- 0.15	125.91 +/- 0.63	0.4367 +/- 0.0021
	outlet	1.70 +/- 0.05	35.00 +/- 0.15	146.78 +/- 0.63	0.5051 +/- 0.0020

Table 3.1: Example case – Thermodynamic points of the heat pump cycle

In order to compensate for the missing measurements, the heat pump system is modeled with the proposed approach. The known mass flows and energy fluxes are identified and used to write the set of equations in a solvable order. The set of equations is detailed for this example case in appendix C, page 101. The set of equations is solved, starting with mass flow rates balance equations. When the resolution is stopped by uncharacterized flows, a fit parameter is added. For instance, in the example case, the refrigerant flow coming from the compressor (component #1) is divided after the condenser circuit (component #3) into two streams. The splitting of this flow between those two streams is unknown. Consequently, a split factor is added and will later be fitted in order to close the set of equations (in the example case, the fit parameter f_{01} is introduced with eq. (C.1)). As soon as every mass flow is

⁵ See the glossary at the beginning of the thesis for details about the signification of those 3 types of values.

⁶ See appendix G, page 135 for more details about uncertainties computation and propagation.

characterized, eventually using fit parameters, the same procedure is applied to energy fluxes, starting with known fluxes, and using equations similar to eq. (3.2). When the resolution is stopped by uncharacterized fluxes, a fit parameter is also added. At the end of this process, the whole system is characterized using the thermodynamic conditions at the measurement points and the measured flows and fluxes. In the example case considered in this chapter, this model allows to determine the values presented in tables 3.1 to 3.3, to draw diagrams such as the ones presented fig. 3.2, and to determine performance indicators, such as the heating effectiveness (ϵ_h), which is here of 3.35, or such as the motor efficiency, which is equal to 96.11 % here⁷.

Name	Value / g s^{-1}	Name	Value / g s^{-1}	Name	Value / g s^{-1}
$\dot{M}_{1 \rightarrow 3}$	32.2336 +/- 1.65904	$\dot{M}_{2 \rightarrow 4}$	0.611456 +/- 0.0314711	$\dot{M}_{3 \rightarrow 2}$	0.611456 +/- 0.0314711
$\dot{M}_{3 \rightarrow 5}$	31.6221 +/- 1.62757	$\dot{M}_{4 \rightarrow 1}$	32.2336 +/- 1.62787	$\dot{M}_{5 \rightarrow 4}$	31.6221 +/- 1.62757
$\dot{M}_{6 \rightarrow en}$	1697.52 +/- 180.24	$\dot{M}_{7 \rightarrow ho}$	350 +/- 10	$\dot{M}_{en \rightarrow 6}$	1697.52 +/- 180.24
$\dot{M}_{ho \rightarrow 7}$	350 +/- 10				

Table 3.2: Example case – Mass flow rates between the components

Name	Value / W	Name	Value / W
$\dot{E}_{2 \rightarrow 1}$	2097.11 +/- 108.52	$\dot{E}_{el \rightarrow 2}$	2182.00 +/- 1.00
$\dot{Y}_{3 \rightarrow 7}$	7304.18 +/- 375.81	$\dot{Y}_{6 \rightarrow 4}$	5122.18 +/- 375.81

Table 3.3: Example case – Energy flows between the components

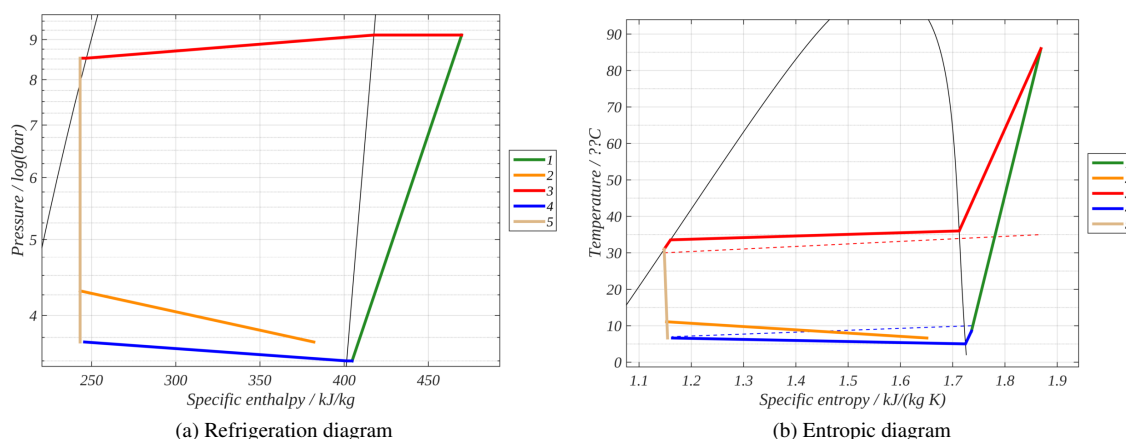


Figure 3.2: Example case – Thermodynamic diagrams. The legend of the numbered lines is available on fig. 3.1. Dashed lines represent the sources.

3.4.4 Analysis of the experimental results

The experimental results are analyzed using diagrams, and performance indicators, which are defined below.

Definitions

Pressure ratio (Π): The pressure ratio is the ratio of the absolute pressure at the compressor outlet to the absolute pressure at the compressor inlet. Consequently, the first stage pressure ratio is the ratio of the absolute pressure at the first stage compressor outlet $P_{1,out}$ to the absolute pressure at the first-stage compressor inlet $P_{1,in}$. The second

⁷ Those performance indicators are defined in section section 3.4.4.

stage pressure ratio is the ratio of the absolute pressure at the second stage compressor outlet $P_{2,out}$ to the absolute pressure at the second stage compressor inlet $P_{2,in}$. Those two ratios are defined in eq. (3.3).

$$\Pi_1 = \frac{P_{1,out}}{P_{1,in}} \quad [-] \quad (3.3a)$$

$$\Pi_2 = \frac{P_{2,out}}{P_{2,in}} \quad [-] \quad (3.3b)$$

Specific enthalpy (h): The specific enthalpy is a state function resulting of the combination of the specific internal energy u , the specific volume v , and the pressure P state functions [Borel and Favrat, 2010, p. 19]. It is computed as described in eq. (3.4). The specific enthalpy is used in the energy rate calculations.

$$h = u + vP \quad [\text{J kg}^{-1}] \quad (3.4)$$

Specific entropy (s): The specific entropy is a state function which may vary as a result of transfers across the system boundary or because of internal processes of the system which result in entropy creation [Borel and Favrat, 2010, p. 37]. The specific entropy unit is $\text{J kg}^{-1} \text{K}^{-1}$. It is used in various thermodynamic calculations, and especially in exergy calculation, via the coenthalpy.

Specific coenthalpy (k): The specific coenthalpy is a state function defined from the specific enthalpy h , the environment temperature T_a and the specific entropy s , as described in eq. (3.5) [Borel and Favrat, 2010, p. 410]. The specific coenthalpy is used in the exergy rate calculations. The environment temperature T_a is the temperature of the air at the inlet of the evaporator, for the AWP, and of the room temperature for the BWP.

$$k = h + T_a s \quad [\text{J kg}^{-1}] \quad (3.5)$$

Transformation energy rate (\dot{Y}): Borel and Favrat [2010, p. 24] define the transformation energy rate as defined in eq. (3.6). Normally, the transformation energy rate is decreased by the derivative of the quantity $U + P_a V$, relative to time, U being the internal energy, P_a being the pressure of the environment, and V being the volume. The derivative of this quantity being equal to zero or being negligible for the system studied here, it is not mentioned in eq. (3.6).

$$\dot{Y}^+ = \sum_j h_j \dot{M}_j^+ \quad [\text{W}] \quad (3.6)$$

Transformation exergy rate (\dot{E}_y): Based on the transformation energy rate, the transformation exergy rate is defined as described in eq. (3.7) [Borel and Favrat, 2010, p. 410]. Normally, the transformation exergy rate is decreased by the derivative of coenergy J relative to time. The coenergy is defined as $J = U + P_a V - T_a S$ with U , the internal energy, P_a the environment pressure, T_a , the environment temperature, V , the volume, and S , the entropy. The derivative of this quantity being here equal to zero or being negligible for the system being studied here, it is not mentioned in eq. (3.7).

$$\dot{E}_y^+ = \sum_j k_j \dot{M}_j^+ \quad [\text{W}] \quad (3.7)$$

Performance indicators

The components numbers which are used in the definitions are defined in fig. 4.2, page 37 for the AWP and in fig. 5.7, page 75 for the BWP.

Heating effectiveness (COP_h): The heating effectiveness ε_h , also called heating Coefficient Of Performance (COP_h), is the ratio between heat power \dot{Q}_h^- supplied to the hot source and the consumed work power \dot{E}^+ . This definition can also be given in energy instead of power, as defined by Borel and Favrat [2010, p. 641]. It is defined in eq. (3.8).

$$\varepsilon_h = COP_h = \frac{\dot{Y}_h^-}{\dot{E}^+} = \frac{\dot{Y}_{3 \rightarrow 15}^-}{\dot{E}_{el \rightarrow 14}^+} \quad [-] \quad (3.8)$$

Motor efficiency (η_{mot}): The motor efficiency is defined as the ratio between the work transmitted to the shaft \dot{E}_{shaft}^- and the electric power consumed by the motor \dot{E}_{mot}^+ . It is defined in eq. (3.24).

$$\eta_{mot} = \frac{\dot{E}_{shaft}^-}{\dot{E}_{mot}^+} \quad [-] \quad (3.9)$$

Isentropic efficiency (η_s): The isentropic efficiency of a compressor is defined as the ratio between the isentropic work power of the compressor $\dot{E}_{cp,s}$, which is the work power required by an adiabatic compressor without dissipation performing an isentropic compression, and the actual work \dot{E}_{cp} required by the compressor. It is defined by eq. (3.10).

$$\eta_s = \frac{\dot{E}_{cp,s}}{\dot{E}_{cp}} = \frac{h_{out,s} - h_{in}}{h_{out} - h_{in}} \quad [-] \quad (3.10)$$

The compressor inlet specific enthalpy h_{in} is computed using the inlet absolute pressure P_{in} and temperature T_{in} . The compressor isentropic outlet specific enthalpy $h_{out,s}$ is computed using the outlet absolute pressure P_{out} and the inlet specific entropy s_{in} . The compressor outlet specific enthalpy h_{out} is computed using the inlet absolute pressure P_{out} and temperature $T_{out} > T_{out,s}$. The isentropic efficiency ranges between 0 and 1 (1 is the ideal unreachable case) and typical values range between 0.7 and 0.8 for nowadays compressors.

In the specific case of the non-adiabatic compression unit tested, we can differentiate the external isentropic efficiency, and the isentropic efficiency of the impeller only. The isentropic efficiency of the impeller only is not accurately known, as the mass flow rates and the inlets and outlets temperatures are deduced from the models presented sections 4.3 and 5.3 and not measured directly. They are defined with eqs. (3.11) and (3.13). The external isentropic efficiencies include the leakage through the labyrinth seal and the gas flux from the axial bearing to the inlet of the first impeller. They are the isentropic efficiencies as measurable from the outside of the unit, at its physical inlets/outlets and take in account the different flows and energy transfers. Those isentropic efficiencies are defined in eqs. (3.12) and (3.14) and are based on the definition offered by Borel and Favrat [2010, p. 201].

$$\eta_{s,cp1} = \frac{\dot{M}_{29 \rightarrow 1} h_{1,out,s} - \dot{M}_{29 \rightarrow 1} h_{1,in} + \dot{Q}_{11 \rightarrow 1} - \dot{Q}_{1 \rightarrow 2}}{\dot{M}_{29 \rightarrow 1} h_{1,out} - \dot{M}_{29 \rightarrow 1} h_{1,in} + \dot{Q}_{11 \rightarrow 1} - \dot{Q}_{1 \rightarrow 2}} \quad [-] \quad (3.11)$$

$$\eta_{s,cp1,ext} = \frac{(\dot{M}_{10 \rightarrow 25} + \dot{M}_{25 \rightarrow 27} + \dot{M}_{25 \rightarrow 8}) h_{1,out,s} - \dot{M}_{22 \rightarrow 29} h_{22,out} + \dot{Q}_{11 \rightarrow 1} - \dot{Q}_{1 \rightarrow 2}}{(\dot{M}_{10 \rightarrow 25} + \dot{M}_{25 \rightarrow 27} + \dot{M}_{25 \rightarrow 8}) h_{1,out} - \dot{M}_{22 \rightarrow 29} h_{22,out} + \dot{Q}_{11 \rightarrow 1} - \dot{Q}_{1 \rightarrow 2}} \quad [-] \quad (3.12)$$

$$\eta_{s,cp2} = \frac{\dot{M}_{28 \rightarrow 2} h_{2,out,s} - \dot{M}_{28 \rightarrow 2} h_{2,in} + \dot{Q}_{1 \rightarrow 2} - \dot{Q}_{2 \rightarrow 10}}{\dot{M}_{28 \rightarrow 2} h_{2,out} - \dot{M}_{28 \rightarrow 2} h_{2,in} + \dot{Q}_{1 \rightarrow 2} - \dot{Q}_{2 \rightarrow 10}} \quad [-] \quad (3.13)$$

$$\eta_{s,cp2,ext} = \frac{(\dot{M}_{2 \rightarrow 10} + \dot{M}_{2 \rightarrow 20}) h_{2,out,s} - \dot{M}_{28 \rightarrow 2} h_{2,in} + \dot{Q}_{1 \rightarrow 2} - \dot{Q}_{2 \rightarrow 10}}{(\dot{M}_{2 \rightarrow 10} + \dot{M}_{2 \rightarrow 20}) h_{2,out} - \dot{M}_{28 \rightarrow 2} h_{2,in} + \dot{Q}_{1 \rightarrow 2} - \dot{Q}_{2 \rightarrow 10}} \quad [-] \quad (3.14)$$

Exergy efficiencies (η): Favrat et al. [2008, based on def. p. 2] give a general definition of the exergy linked to a transfer or a storage of energy and define it as the potential of maximum work which could ideally be obtained from each energy unit being transferred or stored (using reversible processes exchanging heat only with the atmosphere). Borel and Favrat [2010, p. 406–448] give a detailed explanation of the exergy approach applied to system analysis. They develop the concept of exergy efficiency in general [Borel and Favrat, 2010, p. 447–448], and apply it to the specific case of a heat pump [Borel and Favrat, 2010, p. 642]. Written using exergy rates instead exergy, the exergy efficiency of a heat pump is defined as the ratio between the supplied transformation exergy power \dot{E}_{yh}^- and the consumed electrical power \dot{E}_{el}^+ . This ratio is expressed mathematically in eq. (3.15).

$$\eta_{heat\ pump} = \frac{\dot{E}_{yh}^-}{\dot{E}_{el}^+} = \frac{\dot{M}_{17 \rightarrow 15} (k_{15, out} - k_{15, in})}{\dot{E}_{el \rightarrow 14}} \quad [-] \quad (3.15)$$

The exergy efficiency of the first compression stage is defined in eq. (3.16a) for the AWP, and in eq. (3.16b) for the BWP.

$$\eta_{cp1} = \frac{\dot{M}_{22 \rightarrow 29} (k_{25, out} - k_{29, in})}{\dot{E}_{11 \rightarrow 1} - \dot{E}_{1 \rightarrow 2}} \quad [-] \quad (3.16a)$$

$$\eta_{cp1} = \frac{\dot{M}_{19 \rightarrow 1} (k_{25, out} - k_{19, out})}{\dot{E}_{11 \rightarrow 1} - \dot{E}_{1 \rightarrow 2}} \quad [-] \quad (3.16b)$$

The exergy efficiency of the first compression stage is defined in eq. (3.17).

$$\eta_{cp1, imp} = \frac{\dot{M}_{1 \rightarrow 25} (k_{1, out} - k_{1, in})}{\dot{E}_{11 \rightarrow 1} - \dot{E}_{1 \rightarrow 2}} \quad [-] \quad (3.17)$$

The exergy efficiency of the second compression stage is defined in eq. (3.18).

$$\eta_{cp2} = \frac{\dot{M}_{2 \rightarrow 20} (k_{2, out} - k_{2, in})}{\dot{E}_{1 \rightarrow 2}} \quad [-] \quad (3.18)$$

The exergy efficiency of the second stage impeller is defined in eq. (3.19a) for the AWP, and in eq. (3.19a) for the BWP.

$$\eta_{cp2, imp} = \frac{\dot{M}_{28 \rightarrow 2} (k_{2, out} - k_{2, in})}{\dot{E}_{1 \rightarrow 2}} \quad [-] \quad (3.19a)$$

$$\eta_{cp2, imp} = \frac{\dot{M}_{27 \rightarrow 2} (k_{2, out} - k_{2, in})}{\dot{E}_{1 \rightarrow 2}} \quad [-] \quad (3.19b)$$

Component #15 specific coenthalpies are determined using CoolProp 5.0.8 [Bell et al., 2014] Ethylen Glycol / Water mixture fluid properties. Other fluid properties are computed using the NIST Reference Fluid Thermodynamic and Transport Properties Database (REFPROP) [Lemmon et al.]. The exergy efficiency of the condenser is defined in eq. (3.20).

$$\eta_{cd} = \frac{\dot{M}_{20 \rightarrow 3} (k_{3, in} - k_{3, out})}{\dot{M}_{17 \rightarrow 15} (k_{15, out} - k_{15, in})} \quad [-] \quad (3.20)$$

The exergy efficiency of the evaporator is defined in eq. (3.21a) for the AWP, and in eq. (3.21b) for the BWP.

$$\eta_{ev} = \frac{\dot{M}_{ew \rightarrow 16} (k_{16,in} - k_{16,out})}{\dot{M}_{9 \rightarrow 4} (k_{4,out} - k_{4,in})} \quad [-] \quad (3.21a)$$

$$\eta_{ev} = \frac{\dot{M}_{18 \rightarrow 16} (k_{16,in} - k_{16,out})}{\dot{M}_{4 \rightarrow 19} (k_{4,out} - k_{4,in})} \quad [-] \quad (3.21b)$$

The exergy efficiency of the subcooler is defined in eq. (3.22).

$$\eta_{sc} = \frac{\dot{M}_{19 \rightarrow 6} (k_{19,in} - k_{19,out})}{\dot{M}_{18 \rightarrow 22} (k_{18,in} - k_{18,out})} \quad [-] \quad (3.22)$$

The exergy efficiency of the mechanical transmission in the compression unit is defined in eq. (3.23).

$$\eta_{trans} = \frac{\dot{E}_{11 \rightarrow 1}}{\dot{E}_{13 \rightarrow 12}} \quad [-] \quad (3.23)$$

The exergy efficiency of the motor in the compression unit is defined in eq. (3.24).

$$\eta_{mot} = \frac{\dot{E}_{13 \rightarrow 12} + \dot{M}_{3 \rightarrow 7} (k_{7,out} - k_{7,in})}{\dot{E}_{14 \rightarrow 13}} \quad [-] \quad (3.24)$$

Diagrams

Refrigeration diagram A refrigeration diagram is a diagram that represents a thermodynamic cycle and the state of the refrigerant on a two-dimension space. The abscissa is the specific enthalpy, and the ordinate is the logarithm of the absolute pressure [Borel and Favrat, 2010, p. 370–373]. Figure 3.2a shows an example of refrigeration diagram.

Entropic diagram An entropic diagram is a diagram that represents a thermodynamic cycle and the state of the refrigerant on a two-dimension space. The abscissa is the specific entropy, and the ordinate is the temperature [Borel and Favrat, 2010, p. 355–361]. Figure 3.2b shows an example of entropic diagram.

Sankey energy diagram A Sankey diagram is a flow diagram in which the width of the arrows is shown proportionally to the flow quantity. Sankey diagrams are typically used to visualize energy, material, or cost transfers between processes. Figure 4.11, page 47, shows an example of Sankey energy diagram.

Bibliography

ASHRAE. *ASHRAE Handbook - HVAC Systems and Equipment (SI)*, chapter Heat Exchangers, pages 47.1–47.6. ASHRAE, 2008a.

ASHRAE. *ASHRAE Handbook - HVAC Systems and Equipment (SI)*, chapter Valves, pages 46.1–46.14. ASHRAE, 2008b.

I. H. Bell, J. Wronski, S. Quoilin, and V. Lemort. Pure and Pseudo-pure Fluid Thermophysical Property Evaluation and the Open-Source Thermophysical Property Library CoolProp. *Industrial & Engineering Chemistry Research*, 53(6):2498–2508, 2014. doi:[10.1021/ie4033999](https://doi.org/10.1021/ie4033999). URL <http://pubs.acs.org/doi/abs/10.1021/ie4033999>.

- L. Borel and D. Favrat. *Thermodynamics and energy systems analyses*. EPFL Press, 2010.
- R. N. Brown. *Compressors: Selection and Sizing*. Elsevier Gulf, 1997. ISBN-13: 9780884151647.
- D. Favrat, F. Marechal, and O. Epelly. The challenge of introducing an exergy indicator in a local law on energy. *Energy*, 33(2):130–136, Feb 2008. ISSN 0360-5442. doi:[10.1016/j.energy.2007.10.012](https://doi.org/10.1016/j.energy.2007.10.012). 19th International Conference on Efficiency, Cost, Optimization, Simulation and Environmental Impact of Energy Systems (ECOS 2006), Aghia Pelagia, Greece, July 12-14, 2006.
- E. R. Gansner and S. C. North. An open graph visualization system and its applications to software engineering. *Software - Practice and Experience*, 30(11):1203–1233, 2000. doi:[10.1002/1097-024X\(200009\)30:11<1203::AID-SPE338>3.0.CO;2-N](https://doi.org/10.1002/1097-024X(200009)30:11<1203::AID-SPE338>3.0.CO;2-N). <http://www.graphviz.org>.
- ISO. ISO/NP 14617: Graphical symbols for diagrams.
- E.W. Lemmon, M.L. Huber, and M.O. McLinden. NIST Standard Reference Database 23: Reference Fluid Thermodynamic and Transport Properties (REFPROP), Version 9.0, National Institute of Standards and Technology, Standard Reference Data Program, Gaithersburg, 2011.
- MathWorks. fmincon: Find minimum of constrained nonlinear multivariable function (MathWorks MATLAB 2014a), a. URL <http://ch.mathworks.com/help/optim/ug/fmincon.html>.
- MathWorks. Choosing a solver: fmincon algorithms (MathWorks MATLAB 2014a), b. URL <http://ch.mathworks.com/help/optim/ug/choosing-a-solver.html>.
- P. Rapin, P. Jacquard, and J. Desmons. *Technologie des Installations Frigorifiques*. Dunod, 9th edition edition, 2011. ISBN: 978-2-10-055760-8.
- J. Schiffmann. *Integrated design, optimization and experimental investigation of a direct driven turbocompressor for domestic heat pumps*. PhD thesis, Swiss Federal Institute of Technology - Lausanne, 2008. URL <http://dx.doi.org/10.5075/epfl-thesis-4126>.
- P. Smith and R. W. Zappe. *Valve Selection Handbook: Engineering Fundamentals for Selecting the Right Valve Design for Every Industrial Flow Application*. Gulf Professional Publishing, 5th ed. edition, 2004. ISBN-13: 9780750677172.

Air-Water heat pump Prototype (AWP)

This chapter presents the Air-Water twin-stage heat pump Prototype (AWP) designed to demonstrate the statement detailed in chapter 3. It presents the prototype specifications and design, its results, and the encountered issues.

4.1 Design of the AWP

4.1.1 Specifications

The prototype specifications were:

Performance: The prototype had to demonstrate the potential of an oil-free radial variable-speed multi-stage compressor unit for domestic heat pumps applications.

Compactness: The prototype had to fit into the housing of the existing Air-Water heat pump, pictured in fig. 4.1a, chosen and provided by the industrial partner.

Low cost: The prototype was intended to demonstrate the simplicity of the heat pump layout selected, which would have had positive effects on the costs of the industrial product¹. The selected layout is among the simplest possible layouts.

Those 3 guidelines led to the following design choices:

Basic measurements capability: The prototype was intended to be equipped only with pressure and temperature sensors in order to get close to the compactness of an industrial product and to limit the costs of the prototype itself. Originally, none of the prototype internal refrigerant flow rates were measured. The only flow rate being measured was the water flow rate at the condenser. With the issues encountered during the tests², Coriolis mass flow meters were added on the motor cooling refrigerant flow and on the gas bearings aeration refrigerant flow. The flow rates in the main circuits were not measured and were deduced from the condenser energy balance³ and from the global energy balance⁴, in steady state conditions.

Components merged together: The economizer has been merged with the volute of the compression unit in order to obtain one element only. Details about this component merging are given in section 4.2.3.

Compact cycle inversion circuit: The circuit for the cycle inversion, in this twin-stage heat pump, meant for defrosting the evaporator or for cooling applications, is made with a set of 4 check valves⁵ and a 4-way valve⁶, which makes it very compact. This circuit and cycle inversion solution can be observed on fig. 4.2.

¹ The choice of the two-stage heat pump layout is discussed in section 2.4, page 11.

² The issues encountered during the tests are detailed in section 4.4, page 46, and section 4.6, page 57.

³ See eqs. (D.1) to (D.3) page 103 for details about the AWP condenser energy balance.

⁴ See eqs. (D.4) and (D.5), page 103 for details about the AWP global energy balance.

⁵ The 4 check valves are easily seen on fig. 4.8c page 43.

⁶ The 4-way valve can be seen on fig. 4.8b page 43.

4.1.2 Description

The Air-Water twin-stage heat pump Prototype (AWP) is the second prototype to be built⁷ and has been designed to be integrated into one of the industrial partner's single-stage Air/Water heat pump housing. The industrial partner's Air-Water heat pumps are designed for cold climates. Consequently, their heat pump circuits and components are located below the air ducting (fig. 4.1), which is made of the ducting itself, the fan, and the evaporator, as illustrated in fig. 4.15. This design allows to keep the air ducting above snow level. As a consequence of this design choice, the heat pump layout topology for the AWP had to fit into the space available below the air ducting, as illustrated in figs. 4.1a and 4.1b. The topology of the AWP, designed to fit into the volume available under the air ducting can be seen in fig. 4.1b.

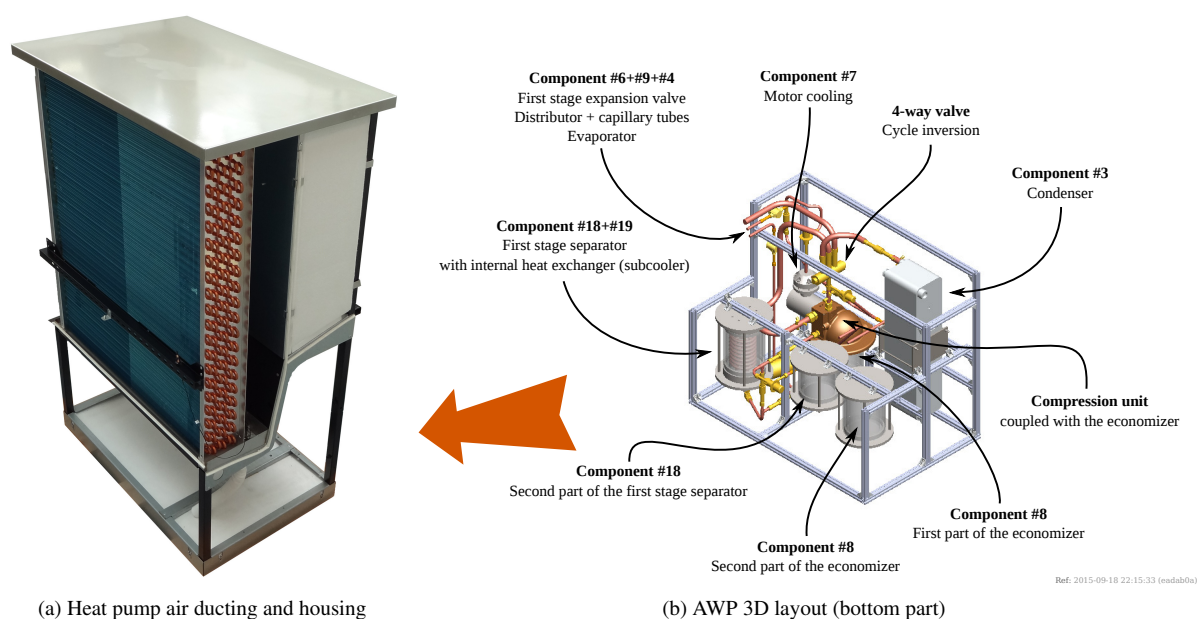


Figure 4.1: Housing and 3D layout of the AWP circuits, as they were expected to be built. The differences between the expected layout and the layout that has been tested are detailed in section 4.2.

4.2 AWP components

This section gives details of the main components in order to make the understanding of the sections 4.3 to 4.6 easier. Further details about the components and the topology of the circuits are given in appendix A, page 91.

This section only displays the details of some of the AWP main components. The level of detail given in this section corresponds to the mandatory level needed to understand the contents of sections 4.3 to 4.4. Appendix A extends those details and displays information about the components that have not been described here, or only partially.

4.2.1 Compression unit

The compressor is a main component of vapor compression heat pump cycles and has two main functions:

- Compress the refrigerant vapor from the evaporator so that the desired temperature and pressure can be maintained in the evaporator [Dinçer and Kanoglu, 2010, p. 109].

⁷ See section 3.2, page 23 for details about the timeline of the experimental setups in the project.

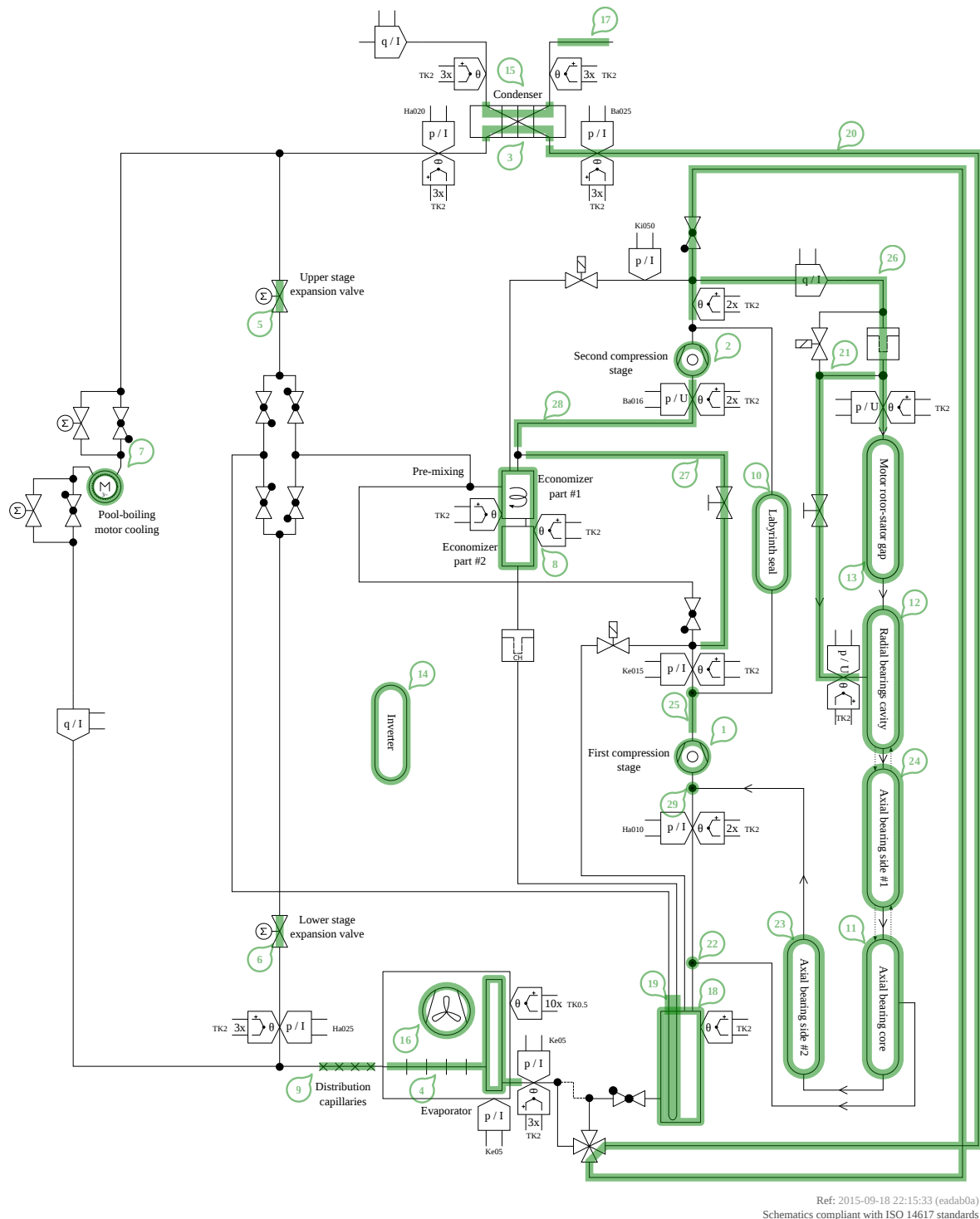
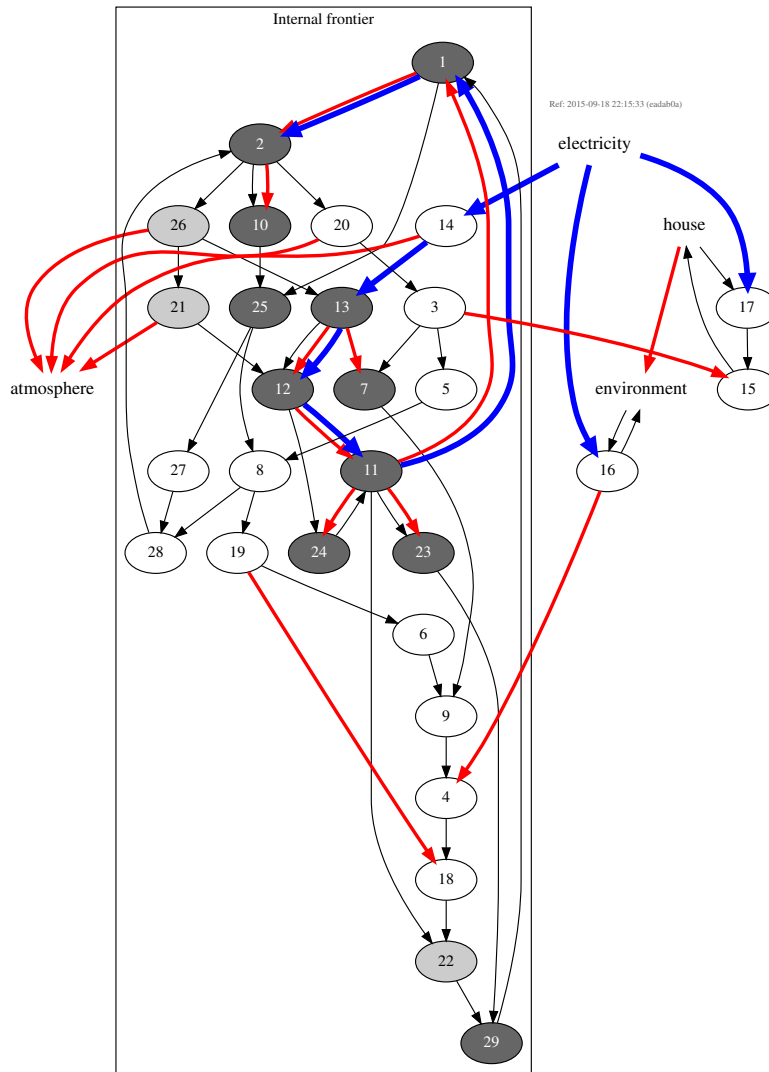


Figure 4.2: AWP layout, with components numbers



Legend

Ref: 2015-09-18 22:15:33 (eadab0a)

24 Elements from the compression unit

26 Elements from the auxiliary circuits

6 Elements from the main circuit

← Flow rate

← Work energy

← Heat or transformation energy

- 1: First stage impeller
- 2: Second stage impeller
- 3: Condenser, refrigerant stream
- 4: Evaporator, refrigerant stream
- 5: Second stage expansion
- 6: First stage expansion
- 7: Motor cooling circuit
- 8: Economizer
- 9: Capillary tubes (second expansion phase)
- 10: Labyrinth seal
- 11: Axial bearing zone
- 12: Radial bearings zone
- 13: Rotor/stator zone
- 14: Inverter
- 15: Condenser, hot source stream
- 16: Evaporator, cold source stream (with fan)
- 17: Hot source circuit and pumps
- 18: First stage separator, vapor-side
- 19: First stage separator, liquid-side
- 20: Piping and fittings between the second stage impeller and the condenser
- 21: Piping and valve between the gas bearings aeration circuit filter and the radial bearings zone
- 22: Junction between the first stage vapor-line and the the axial bearing zone
- 23: Axial bearing, impellers side
- 24: Axial bearing, radial bearings side
- 25: Physical outlet of the first stage compressor
- 26: Piping between the second stage impeller outlet and the gas bearings aeration circuit filter
- 27: Bypass of the economizer
- 28: Vapor-line of the second stage compressor inlet
- 29: Junction of the first stage vapor-line and the outlet of the axial bearing, impeller-side.

Figure 4.3: AWP model

- Increase the pressure of the refrigerant vapor through the process of compression, simultaneously increasing the temperature of the refrigerant vapor [Dinçer and Kanoglu, 2010, p. 109] in order to meet the required condensation conditions [Rapin et al., 2011].

Those two functions can not be fulfilled without the use of expansion devices on liquid lines. The compressor role in the heat pump prototype studied here is performed by a compression unit containing the two compression stages, rotating at the same speed. The prototype compression unit tested in the AWP was the *cp105* compression unit, from the *evo4* design family. Compression units from *evo1* and *evo2* families have almost not been tested in the Brine-Water twin-stage heat pump Prototype (BWP) or in the AWP, as those units were not ready for heat pump integration. Compression units from the *evo4* family were the first decently working prototypes that have been available for tests⁸. They started to be available during Spring 2012. One unit from the *evo4* family, the *cp105* unit, has been tested in the AWP in May 2012. The datasets presented in this work have been generated during that period. An other unit of this family, *cp101*, assembled before the *cp105* unit, has been tested later in the BWP, in October 2013. Because of confidentiality issues, the details of the design of the units or the differences between the different compression unit design families can not be exposed in this work and are only partially known by the author himself. However, the structure of the *cp105* unit and its connections with the heat pump main and auxiliary circuits are described in fig. 4.4. The main differences with the version tested in the BWP are:

Motor cooling configuration: The motor cooling configuration tested on the *cp105* unit was a pool-boiling configuration. In the BWP, the motor was cooled down with a flow-boiling configuration⁹.

Gas bearings aeration inlets/outlet configuration: The gas bearings aeration circuit injects cold gas at the back of the compression unit (inlet #1), after the motor (component #13¹⁰), and in the radial gas bearings cavity (component #12) (inlet #2). The gas flows through the gap between the stator and the rotor, cooling down the two parts, and evacuating windage losses. This gas flow is mixed with the flow coming from the second inlet and leaves through the axial bearing of the motor side (component #24) towards the outlet of the gas circuits, which is the middle of the set of axial bearings (component #11). A share of this flow leaves by entering the axial bearing of the impeller side (component #23)¹¹.

4.2.2 Compression stage bypass systems

Bypass circuits are mandatory auxiliary circuits in heat pumps integrating the radial compression units. In the AWP, each compression stage is equipped with a bypass circuit consisting of a manual needle valve, used to set the characteristics of the bypass, and a solenoid valve for rapid bypass activation. This solution had been chosen for cost-related reasons, and because the crucial role of the bypass circuits dynamic response had not been identified at the time. Fast electric needle valves are quite big and expensive and were not appropriate if referred to the prototype specification defined in section 4.1.1. The BWP has been equipped with such a valve for its bypass system, which is quite different from the one used in the AWP, as illustrated in fig. 5.6, page 73. The BWP bypass system bypasses both compression stages together, as described in section 5.2.2, page 71 while the AWP bypass system bypasses each compression stage independently. However, being able to open or close the bypass circuits independently in the AWP does not make them independent, as illustrated in fig. 5.6a.

4.2.3 Economizer

The AWP is equipped with glass-made separator and economizer to allow an easier monitoring and understanding of the refrigerant distribution. This configuration allows for instance to see the topology of the flow or to see if droplets appear at critical locations. To prevent liquid management issues during the tests at the laboratory, the inlet separator and the economizer should be able to contain a good share of the refrigerant charge. When the heat pump cycle is reversed for cooling or defrosting mode, part of the refrigerant charge is likely to flow from

⁸ More details about the compression unit history is given in section 5.2.1.

⁹ Details about the motor cooling parts are given in appendix A.1.6 page 92.

¹⁰ For components description and numbering, see figs. 4.2 and 4.3, page 37 and 38.

¹¹ This gas path was not the one expected and this issue is discussed with further details in section 4.5.1, page 48.

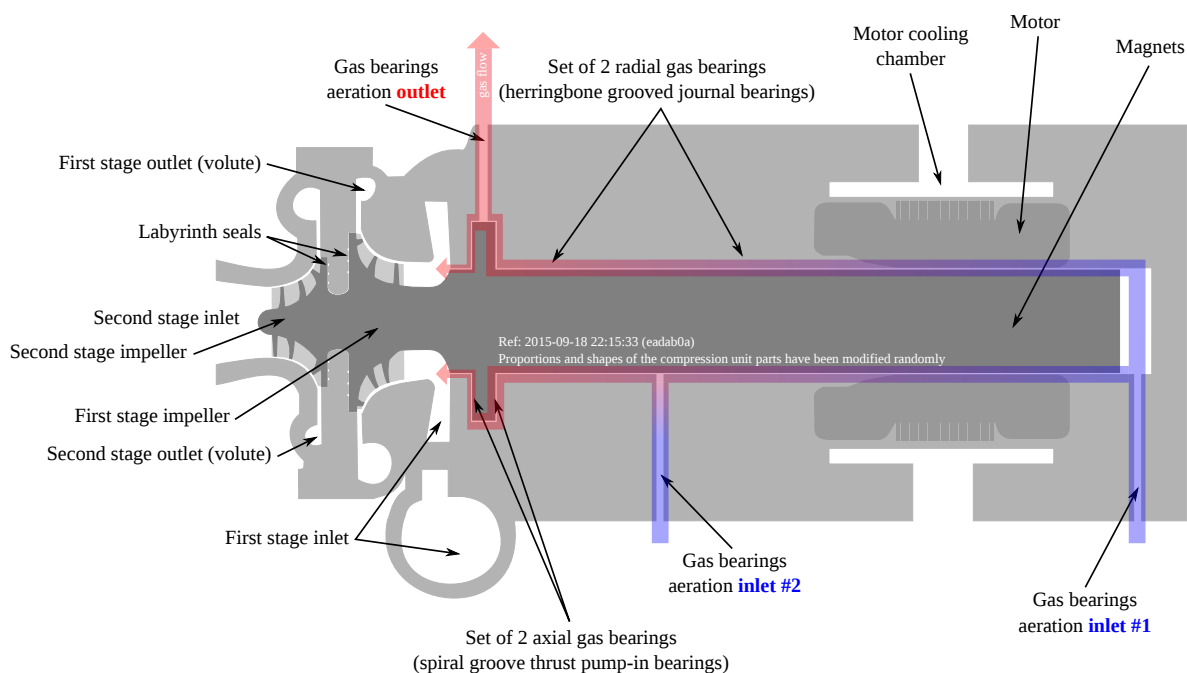


Figure 4.4: Structure of the twin-stage compressor unit with the AWP gas bearings aeration circuit inlets/outlets layout. Those inlets/outlets are different on the BWP, as illustrated in fig. 5.4, page 71. Differences are stressed with a bold font.

the condenser to the evaporator in a short time, due to the pressure difference between those two components. This volume of liquid is likely to arrive in the first stage inlet separator, consequently. In normal operation, the liquid content of each heat exchanger is determined by its flow conditions and characteristics (pinch diagram and flow pattern maps, notably). The charge which is not contained in the heat exchangers at a given time is collected in the economizer, which has to be able to contain this charge while ensuring its liquid/gas separation function properly. In order to decrease the impact of control mistakes during the experiments, the volumes of the first stage compressor inlet separator and of the economizer have been increased by a factor two by duplicating them and by mounting the duplicates and the main parts together¹² in the prototype (as illustrated in fig. 4.1b).

Gas/liquid separation issues were encountered in the economizer during the experiments, so the design of the gas/liquid separation parts in the economizer have evolved significantly during the experimental investigation. The successive versions are detailed in fig. 4.7. The data presented in this thesis work has been generated with the AWP equipped with version #4 (before May 25th, 2012) and version #5 (after May 25th, 2012) of the economizer. An other action taken to solve the separation issue was to move the second part of the economizer below the main part, in order to increase the distance between the liquid level and the second stage compressor inlet. The two components were connected with a 20cm-long 3/4-inch pipe.

4.2.4 Evaporator

The evaporator of the AWP is pictured on fig. 4.5b. The air ducting of the heat pump housing used as a base for the AWP design occurred to be designed with compactness in mind and has not been designed for optimum air streams or noise reduction. The goal of the designers was clearly to design a heat pump unit able to go through the width of a conventional domestic doorway. As a result of those design choices, the air stream distribution in the air ducting was far from being satisfactory, as detailed in section 4.5.6. In order to try to compensate for this issue, a plate drilled with holes in front of the evaporator channels which had the lowest degree of superheat at their outlets has been added at the inlet of the air ducting. This plate and its influence on the superheating profile along the height of the evaporator are detailed in section 4.5.6.

¹² See appendix A.1.4 page 91 for details.

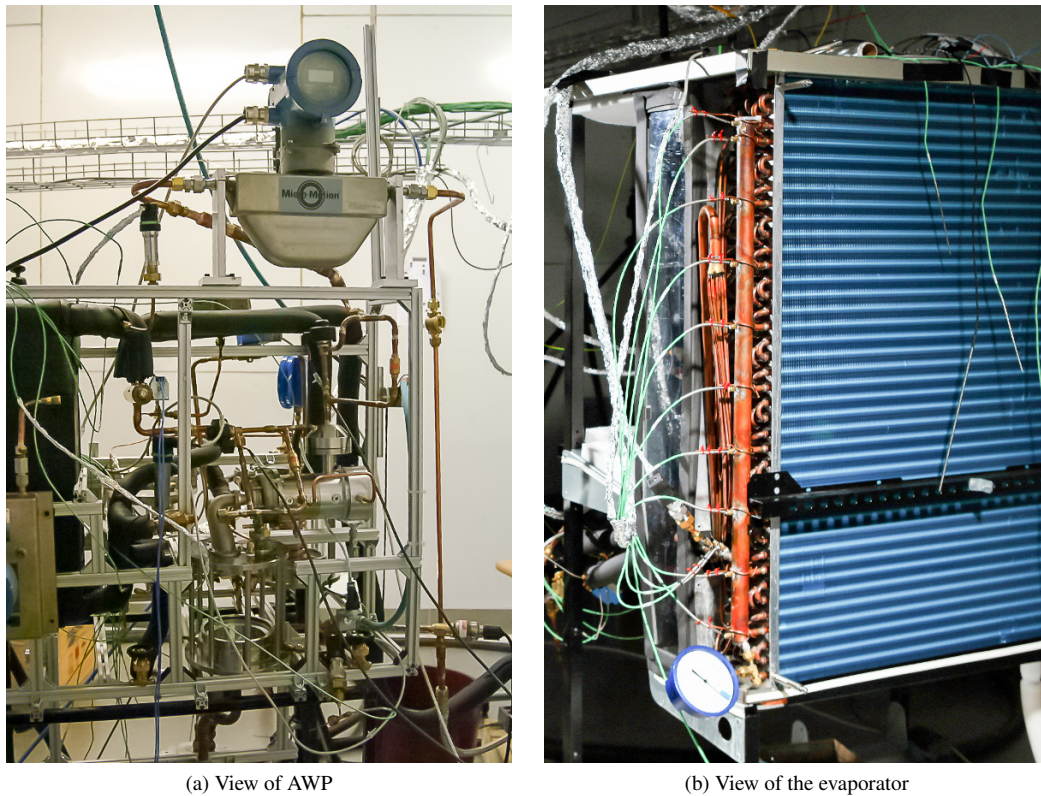


Figure 4.5: Views of the AWP. The extension of the economizer (component #8) is located below its main part. The pipe connecting the two parts is visible at the bottom of the picture. Extra flow meters (one can be seen in fig. 4.5a) have been added outside the original device housing, in order to understand the behavior of the prototype and characterize the system. The evaporator (fig. 4.5b) is instrumented with a thermocouple per channel.

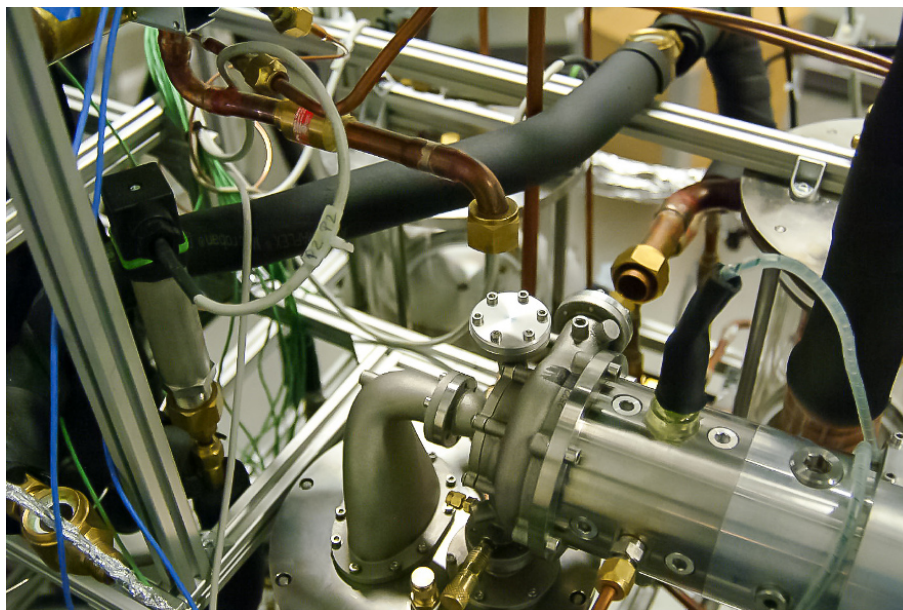
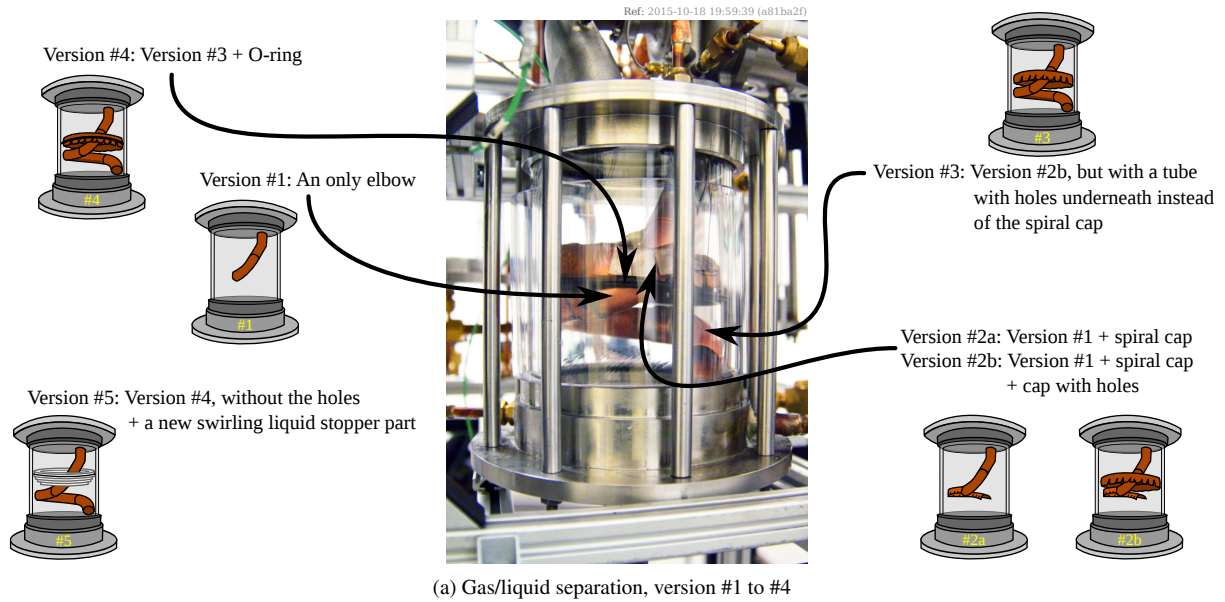


Figure 4.6: Compression unit *cp105*, being mounted in the AWP



(b) Version #5 (big central hole, with a seal and shapes to send the liquid back down the economizer on the sides)

Figure 4.7: AWP economizer version #1 to #5.

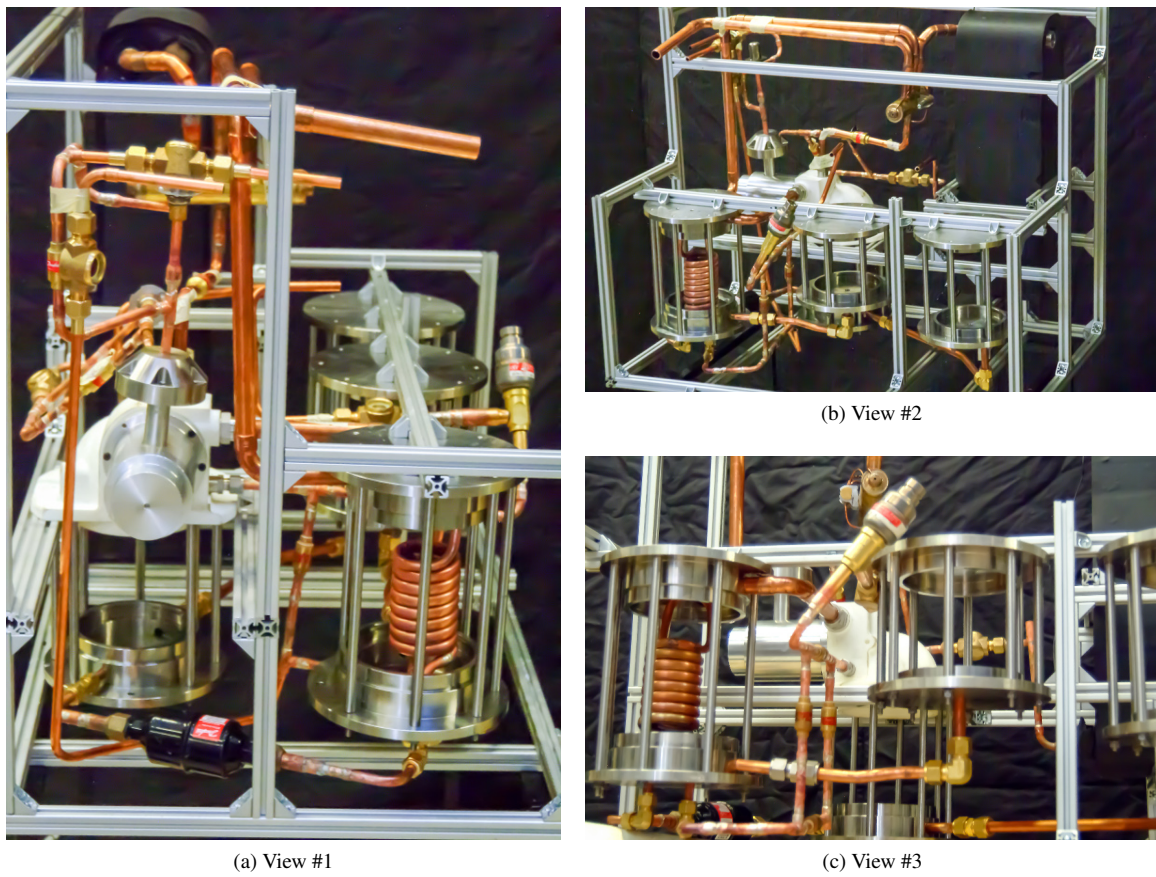


Figure 4.8: AWP assembly

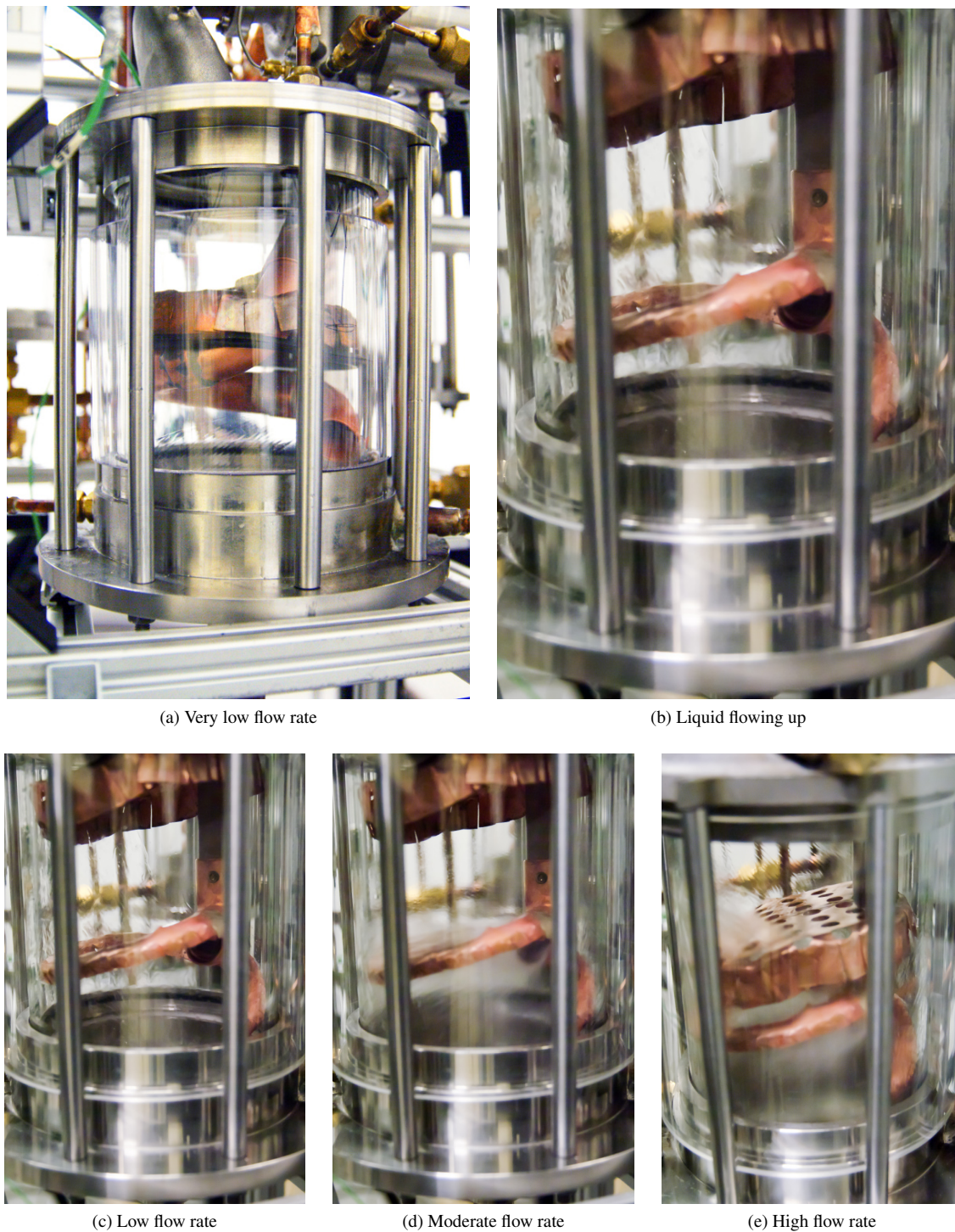


Figure 4.9: Gas/liquid stream patterns with qualitative flow velocities. The gas/liquid separation assemblies used in this illustration are assemblies version #2a, #2b, and #4.

4.2.5 4-way valve

A 4-way reversing valve is included in the heat pump circuits in order to switch between heating-mode, cooling-mode, and defrosting-mode. It can be seen in fig. 4.10. Such a valve allows the condenser and evaporator to exchange their role in the heat pump cycle, in order to defrost the evaporator during the heating period, or for space cooling application. The flow of the refrigerant in the exchangers is reversed and the roles of the exchangers are exchanged. The valve is mounted on the suction line of the first compression stage and the discharge line of the second compression stage. The slide assembly inside the valve can translate to connect the appropriate ports for the desired operation mode. It generates additional pressure drops, a leakage flow and a heat exchange between the discharge and the suction ports [Bertsch and Hubacher, 2002, p. 4]. This leakage has been measured by Bertsch and Hubacher [2002, p. 39] for a type of 4-way valve very similar to the one used in the AWP and have been measured between 1 and 3 mg s⁻¹ bar⁻¹ with R134a. The valve used in AWP has been cleaned in order to remove any lubricant contained within the valve¹³, which has certainly contributed to increase the leakage between the suction and discharge ports, as the oil acts also as a sealant. This leakage is neglected in the frame of this study. The 4-way valve in the AWP is the valve that was already present in the industrial partner heat pump delivered to EPFL. As it had been sized for R407C, this valve was slightly small to be used with R134a, as confirmed in section 4.5.5.

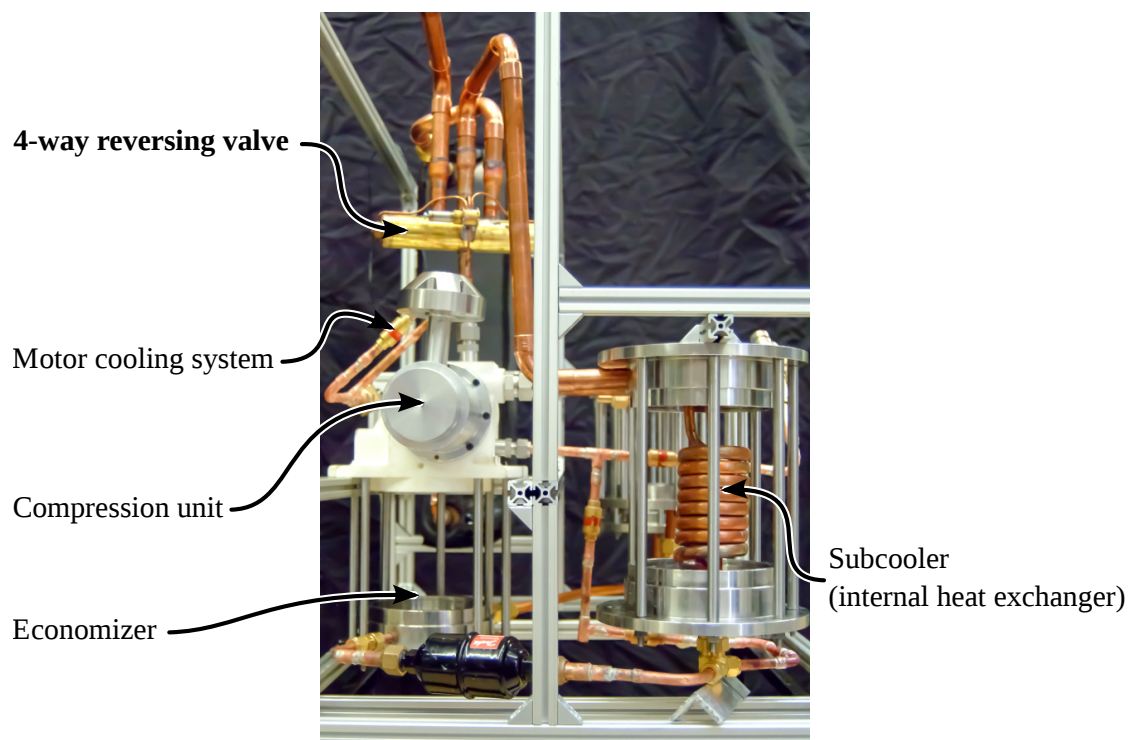


Figure 4.10: View of the 4-way reversing valve in the heat pump circuits

4.3 Modeling

The model proposed is based on the areas or physical elements of interest in the AWP. Figure 4.2 presents the AWP layout and fig. 4.3 presents the model itself. The set of equations deduced from analysis of the model in fig. 4.3 is detailed in appendix D.

Following the procedure described in section 3.4.3, the model is built with 29 components; 11 of them describe the compression unit itself.

¹³ The application here must be oil-free, as detailed in section 5.5.4, page 80.

4.4 Prototype performance

A stable¹⁴ Operating Point (OP) ensures that the experimental setup is in a steady state, which allows to use the modeling technique presented in section 3.4.3, page 25. Indeed, the data recorded were not enough to use a dynamic modeling approach, but were appropriate for a steady state modeling approach. The maximum rotor speed reached with the compressor unit is 180 krpm, which is the maximum rotor speed of the compression unit, by design, and also the maximum speed configured in the inverter. The maximum rotor speed reached for a stable OP is 171 krpm.

The first and the second OP, A-6.8/W31.3 and A-7.0/W32.3, are two similar OP¹⁵, regarding temperature levels. One has been measured with the 4-way reversing valve, one has been measured without. The consequence of this modification of the heat pump circuits is detailed in section 4.5.5. The third OP¹⁶, A-7.0/W35.6, yields the highest temperature lift between the sources. It allows a comparison of the AWP with industrial products currently on the market, since the OP A-7/W35 is common OP heat pump ranking and comparison [AFNOR, 2011c]. The next three OP¹⁷, A-0.5/W20.7, A-3.1/W29.5, and A-6.6/W22.1, illustrate the gas temperature profile behavior inside the compression unit, with the increase of the rotation speed. This issue is documented in section 4.5.3.

Table 4.1 summarizes the main performance indicators for the 6 stable OP. The inverter is considered to be inside the internal frontier in the model presented fig. 4.3, since its efficiency is not properly known. Indeed, it could be measured only once, with the compressor unit running at 120 krpm, as the laboratory was not equipped to perform high frequency three-phase power measurements on a regular basis. Consequently, this measured efficiency of 85% is considered constant in this thesis work. The heating effectiveness (ϵ_h) is consequently defined as expressed in eq. (3.8), page 31, and considers the inverter to be part of the internal system. ϵ_h , as defined in eq. (3.8), does not take into account the pumps or the fan energy consumption for the auxiliary fluids. The experimental results show differences of temperature between the sources from 28.7 to 42.6 degrees and ϵ_h ranges from 2.19 to 4.02 in the stable OP reached. The overall exergy efficiencies, defined in eq. (3.15), page 32, range from 26.3% to 32.6%. Those exergy efficiencies are considered low, as they could have reached 30 to 40% with better heat exchangers, notably with a better evaporator¹⁸, improved insulation¹⁹, better control of the auxiliary circuits²⁰, and better control of the subcooling and superheating values²¹. The most interesting OP is the OP A-7.0/W35.6²², which allows to compare the AWP performance with industrial products performance using conventional technology, even if the comparison is not very accurate, as the prototype tests were not strictly performed in the conditions imposed by the standards relative to performance measurement of heat pumps with electrically driven compressors for space heating & cooling applications [AFNOR, 2011a,b,c,d, 2012]²³. Notably, the fan and pump electrical powers were not taken in account [AFNOR, 2011c, sec. 4.1.4 and 4.1.6], the condenser water temperature difference was of 6.84K, instead of 5K [AFNOR, 2011b, tab. 12]²⁴, and the condenser inlet temperature was not exactly at 35.0°C, but at 35.6°C. Nonetheless, it appears that the AWP performs close to the devices currently on the market, as it can be seen in table 4.2. Indeed, the AWP performance is a little lower than the devices it compares with (ϵ_h is 0.2 to 0.5 points lower). Reaching this level of performance is encouraging, since even this first working prototype, far from being a complete optimized industrial version, already ranks close to the models currently on the market. In addition to the drawbacks mentioned above, the prototype topology was burst around in order to include measurement capabilities, creating pressure drop. As illustrated in fig. 4.11, about 6% of the energy was dissipated in the environment during this experiment A-7.0/W35.6. Those 6% include the heat losses of the inverter (component #14). This heat energy could be also recovered by the thermodynamic cycle, for instance, as it is already the case for the motor heat losses. Moreover, the control issues detailed in section 4.6 have also a negative influence on the

¹⁴ An OP is considered stable if it qualifies to defined conditions. See appendix G.1 page 135 for details.

¹⁵ The first and second OP are detailed respectively in appendix F.1, page 111 and appendix F.2, page 114.

¹⁶ The third OP is detailed in appendix F.3, page 117.

¹⁷ Those 3 OP are detailed respectively in appendix F.4, page 120, appendix F.5, page 123, and appendix F.6, page 126.

¹⁸ The evaporator exergy efficiency η_{ev} , in the OP detailed in table 4.1, ranges from 17% to 34% (see section 4.5.6, page 55) and is calculated with eq. (3.21a), page 33. The subcooler exergy efficiency η_{sc} ranges from 0.4% to 3% (see section 4.5.7, page 57) and is calculated with eq. (3.22), page 33.

¹⁹ The prototype was only partially insulated, as this can be seen on fig. 4.5a page 41.

²⁰ The motor cooling flow was often not appropriate, as detailed in section 4.6.5 page 59, and the gas bearings aeration flow was not easy to set at a chosen value, as described in section 4.5.7 page 57.

²¹ Those values were not easily controlled, as explained in sections 4.5.6 and 4.6.6, page 61.

²² More details about this specific OP are given in appendix F.3 page 117.

²³ Acoustic measurements conditions are detailed in other standards [AFNOR, 2008, 2009].

²⁴ The standard condenser inlet/outlet water for this OP are 30°C at the inlet and 35°C at the outlet.

prototype performance. As a consequence, even if they are comparatively low, the performance reached with this first working prototype is considered very promising and constitutes a breakthrough in the domain.

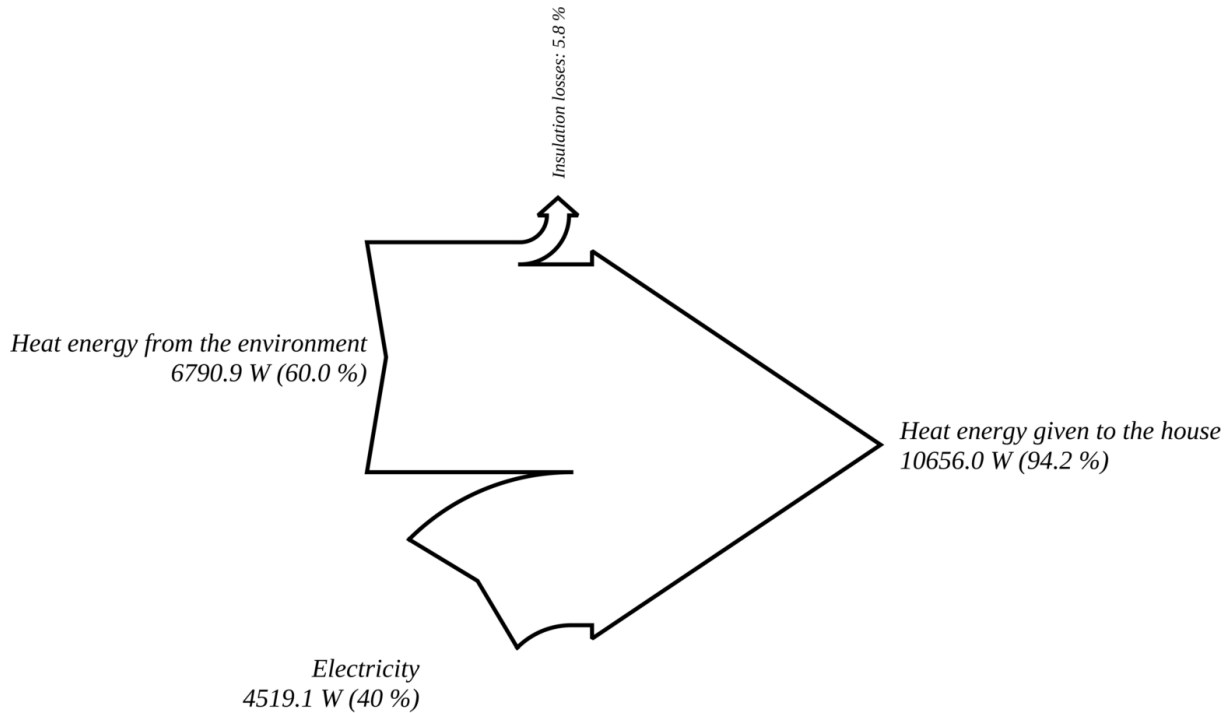


Figure 4.11: A-7.0/W35.6 - Sankey diagram for heat pump energy balance (internal frontier)

OP #		#1	#2	#3	#4	#5	#6
OP		A-6.8/W31.3	A-7.0/W32.3	A-7.0/W35.6	A-0.5/W20.7	A-3.1/W29.5	A-6.6/W22.1
Data		appendix F.1	appendix F.2	appendix F.3	appendix F.4	appendix F.5	appendix F.6
Speed		170 krpm	160 krpm	171 krpm	130 krpm	153 krpm	160 krpm
ϵ_h	-	2.19 ± 0.04	2.69 ± 0.03	2.36 ± 0.03	4.02 ± 0.06	3.10 ± 0.04	2.67 ± 0.05
$\eta_{heat\ pump}$	%	26.3 ± 0.7	32.6 ± 0.5	30.5 ± 0.5	26.6 ± 0.8	31.0 ± 0.6	25.2 ± 0.7
η_{motor}	%	<u>88.99</u>	<u>82.34</u>	<u>91.92</u>	<u>88.00</u>	<u>91.67</u>	<u>90.43</u>
η_{cp1}	%	59 ± 40	63 ± 36	62 ± 37	76 ± 23	74 ± 26	71 ± 30
$\eta_{s, cp1}$	%	88 ± 12	88 ± 12	88 ± 11	93 ± 7	92 ± 7	93 ± 7
η_{cp2}	%	83 ± 17	80 ± 19	59 ± 16	66 ± 34	75 ± 24	60 ± 30
$\eta_{s, cp2}$	%	89 ± 11	88 ± 12	82 ± 18	89 ± 11	88 ± 11	86 ± 13
η_{cd}	%	94 ± 3	92 ± 2	92 ± 3	89 ± 3	90 ± 2	93 ± 4
η_{ev}	%	17 ± 17	31 ± 31	34 ± 34	29 ± 29	20 ± 20	30 ± 30
η_{sc}	%	1 ± 1	2 ± 2	2 ± 2	3 ± 3	3 ± 3	0.4 ± 0.4
$\dot{Y}_{3 \rightarrow 15}$	W	7367 ± 138	$1.0458 \times 10^4 \pm 134$	$1.0656 \times 10^4 \pm 137$	9010 ± 130	$1.0252 \times 10^4 \pm 134$	7363 ± 125
$\dot{Y}_{16 \rightarrow 4}$	W	4278 ± 138	7144 ± 136	6791 ± 152	7102 ± 131	7398 ± 149	4875 ± 174
$\dot{E}_{el \rightarrow 14}$	W	3367.4 ± 0.5	3881.4 ± 0.4	4519.1 ± 0.4	2243.5 ± 0.4	3310.7 ± 0.4	2758.5 ± 0.4

Table 4.1: Overall performance of the AWP and its main components

4.5 Design issues

This section details the encountered issues which are related to AWP layout design or topology deficiencies. Those deficiencies have a negative influence on the prototype efficiency and performance.

Brand & Model / -	\dot{E}_{el} / kW	\dot{Y}_{cd} / kW	ϵ_h / -	Noise level / dB(A)	current type / -
LG Therma V Model HU143U31	4.27	10.69	2.5	70	400V – 50Hz
Ciat Aqualis2+ 65 HT Model 7321653	3.89	10.7	2.75	73.5	230V – 50Hz
Panasonic Aquarea Kompakt Model WH-MDC14C9E8	4	10.7	2.68	69	400V – 50Hz
Atlantic Alféa Hybrid Duo Gas 11 Tri Model WOYK112LTC	4.28	10.8	2.52	66	400V – 50Hz
Air/Water heat pump Prototype AWP	4.5	10.7	2.36	N/A	400V – 50Hz
Brand & Model / -	Refrigerant / -	Type / -	cp type / -	cp stages / -	Reversibility / -
LG Therma V Model HU143U31	R410A	Split	Rotary	Single	Not reversible
Ciat Aqualis2+ 65 HT Model 7321653	R410A	Monobloc	Scroll	Single	Reversible
Panasonic Aquarea Kompakt Model WH-MDC14C9E8	R410A	Monobloc	Rotary	Single	Reversible
Atlantic Alféa Hybrid Duo Gas 11 Tri Model WOYK112LTC	R410A	Split	Rotary	Single	Not reversible
Air/Water twin-stage heat pump Prototype AWP	R134a	Monobloc	Radial	Twin	Reversible

Table 4.2: AWP and similar industrial domestic Air/Water heat pumps, currently on the market, ϵ_h for the OP A-7/W35. Noise level corresponds to the external side sound level envelope. The Air/Water heat pumps ϵ_h takes in account the defrosting process. The AWP ϵ_h does not include the defrosting process.

4.5.1 Gas forced to flow reversely in one side of the axial bearing

The compressor thrust bearing is a two sided inward pumping spiral groove thrust bearing. Under normal operating conditions such a bearing is known for generating a gas flow from the bearings outside diameter towards the bearings inside diameter. As described in section 4.2.1, this normal behavior is not observed in component #24, which is one side of the set of axial bearings. Indeed, the gas bearings aeration circuit was set as described in fig. 4.4. The appropriate setting is described in fig. 5.4, page 71. A comparison of the normal setting and the setting used in the AWP shows that the outlet of the gas bearings aeration circuit in the compression unit is connected as an inlet. This means that the gas can only flow from the components #13 and #12 inlets to component #11 outlet through component #24, in the reverse way regarding bearing flow. The flow here is imposed by the pressure levels in the circuit. The compressor has been plugged in this way following the industrial partner requirements, and as the internal design of the compression unit was unknown by the author. The industrial partner was expecting to solve the issue documented in section 4.5.2 by plugging in the compressor this way.

4.5.2 Excess of compressor thrust forces during deceleration

In steady state operation, the heat pump circuit has 3 pressure levels. The high pressure zone is located between the outlet of the second stage compressor and the inlet of the second stage expansion valve. The intermediate pressure zone is located between the two compression stages, including the economizer, and the low pressure zone is located between the outlet of the first stage expansion valve and the inlet of the first stage compressor. The larger is the temperature difference between the condenser outlet and the evaporator inlet, the larger is the difference of pressure level between the zones.

When the compressor unit decelerates, the rotor speed decreases quite fast, since the rotor is mechanically loaded by the compressor work. In less than 2 seconds, the rotor speed drops below 100 krpm. Below 30 krpm, bearing touch-down occurs. Between 60 and 80 krpm, there is a dangerous operation zone, in particular if there is a high pressure level difference between the zones. This is typically the case in a running heat pump cycle, where the pressure levels are determined by the temperature levels of the sources. Depending on the design of the heat pump circuits, pressure level differences can also be observed in the compression unit at specific times. As differences of pressure levels in the compression unit induce thrust forces on the axial bearing, and as both the bearing stiffness

and load capacity increase with rotor speed, there are situations where the external force applied on the bearings might be high for their nominal load capacity, especially with an unexpected reversed flow on one side of the bearing.

When the AWP runs at a given OP, the pressure across the second stage compressor varies from intermediate level to high pressure level, through the second stage impeller. The pressure at the first stage compressor varies from low level to intermediate pressure level, through the first stage impeller. The pressure level in the radial bearings cavity and at the back of the compressor unit is close to low pressure level²⁵. When the compression unit decelerates abruptly (in case of uncaredful stop, which means stopping the prototype without decreasing the gap between the temperature levels of the sources, emergency stop, or power failure), the bypass circuits of the compression stages²⁶ are open in order to avoid the surge phenomenon²⁷. As the rotor speed decreases, it reaches the dangerous zone described above, the pressure level in the second compression stage rapidly becomes the intermediate pressure level. The pressure level in the first compression stage rapidly becomes the low pressure level. The radial bearings cavity and the back of the compression unit pressure level stay at the low pressure level. It happens this way because the compression stages are bypassed separately in the AWP²⁸. This situation implies a force, created from the difference of pressure levels between the compressor unit pressure zones, that loads the axial bearing. As this force is directed from the impellers zone towards the motor zone, it applies consequently on component #24, which is unfortunately the side of the axial bearing which is working with a reverse flow in the AWP piping configuration.

This gas stream can only flow from the inner diameter to the outer diameter of the axial bearing, on the motor-side of the axial bearing. Indeed, the flow only happens because of the difference of pressure between the inlet pressure level, which is the high pressure level²⁹, in the AWP, and the outlet pressure level, which is the low pressure level²⁹, in the AWP. The solving of the model presented in section 4.3 shows that mass and energy balances only close if:

- The gas stream flows from the bearings cavity (component #12) to the outer diameter of the axial bearing (component #11), through its motor-side (component #24).
- The gas stream flows from the outer diameter of the axial bearings (component #11) to the first compression stage vapor suction line (component #22), and to the inlet of the impeller (component #1) through the impeller-side of the axial bearing (component #23).

This allows to conclude that the flow through one of the sides of the axial bearing was globally reversed due to the pressure difference induced by the erroneous plugging of the aeration circuit. The industrial partner was assuming the axial bearing was not able to sustain the force induced by the difference of pressure level while decelerating. It might be possible that this problem with the axial bearing was created only by the reversed flow. Maybe a compressor correctly plugged in would easily sustain the force induced by the pressure levels. A proper connection of the gas bearings aeration circuit has been tried in the BWP, which, in addition, was equipped with an other compressor bypass system that avoid the pressure level difference, getting the whole compression unit to the low pressure level when the compressor unit is decelerating³⁰. The differences between the bypass systems and their influence on the generation of axial forces are detailed in section 5.2.2, page 71.

4.5.3 Significant increase of the temperatures in the labyrinth seal with rotation speed

A significant increase of the gas temperature in the labyrinth seal is observed for rotor speeds above 160 krpm, as illustrated in table 4.3 and fig. 4.12. This observation is possible only through the use of the model presented in section 4.3.

²⁵ This is for minimizing the bearings and motor windage losses.

²⁶ See section 4.2.2, page 39 for details about the bypass circuits.

²⁷ See appendix H.3, page 142 for details about the surge phenomenon.

²⁸ See section 4.2.2, page 39 for a description of the AWP bypass system.

²⁹ The choice of the gas bearings aeration circuit inlet and outlet pressure levels is detailed in section 6.3, page 84.

³⁰ The characteristics of this bypass system are described in section 5.2.2, page 71.

OP #		#1	#2	#3	#4	#5	#6
OP		A-6.8/W31.3	A-7.0/W32.3	A-7.0/W35.6	A-0.5/W20.7	A-3.1/W29.5	A-6.6/W22.1
Data		appendix F.1	appendix F.2	appendix F.3	appendix F.4	appendix F.5	appendix F.6
Speed		170 krpm	160 krpm	171 krpm	130 krpm	153 krpm	160 krpm
$T_{1,in}$	°C	-18 ± 7	-11 ± 6	-6 ± 12	3 ± 13	1 ± 17	-12 ± 13
$T_{1,out}$	°C	33.7 ± 0.6	31.1 ± 0.9	37 ± 3	28 ± 2	37 ± 2	26 ± 3
$T_{2,in}$	°C	8.683 ± 0.007	8.391 ± 0.006	11.945 ± 0.006	11.125 ± 0.006	11.681 ± 0.006	4.176 ± 0.007
$T_{2,out}$	°C	50.761 ± 0.007	45.140 ± 0.006	53.358 ± 0.006	32.140 ± 0.006	43.925 ± 0.006	38.933 ± 0.007
$T_{26,out}$	°C	14.472 ± 0.007	9.452 ± 0.006	2.811 ± 0.006	6.271 ± 0.006	9.002 ± 0.006	7.857 ± 0.007
$T_{13,out}$	°C	20 ± 25	28 ± 28	43 ± 33	14 ± 22	24 ± 27	17 ± 34
$T_{24,in}$	°C	41 ± 38	46 ± 37	56 ± 36	85 ± 43	44 ± 37	39 ± 39
$T_{24,out}$	°C	95 ± 43	145 ± 46	89 ± 38	125 ± 47	75 ± 40	104 ± 46
$T_{11,out}$	°C	127 ± 58	121 ± 60	135 ± 63	123 ± 57	120 ± 65	117 ± 55
$T_{23,in}$	°C	127 ± 58	121 ± 60	135 ± 63	123 ± 57	120 ± 65	117 ± 55
$T_{23,out}$	°C	150 ± 65	142 ± 65	152 ± 71	124 ± 64	139 ± 75	131 ± 64
$T_{7,in}$	°C	-11.4 ± 0.8	-11.5 ± 0.7	-12.3 ± 0.7	-6.0 ± 0.6	-12 ± 2	-12.1 ± 0.7
$T_{7,out}$	°C	-11.4 ± 0.8	-11.5 ± 0.7	-12.3 ± 0.7	36 ± 8	55 ± 8	36 ± 11
$\dot{Y}_{14 \rightarrow 13}$	W	2862.3 ± 0.4	3299.2 ± 0.3	3841.3 ± 0.3	1906.9 ± 0.3	2814.1 ± 0.3	2344.7 ± 0.4
$\dot{Y}_{13 \rightarrow 7}$	W	211.07 ± 0.03	415.44 ± 0.04	244.72 ± 0.02	169.03 ± 0.03	171.68 ± 0.02	172.96 ± 0.03
$\dot{Y}_{13 \rightarrow 12}$	W	98.71 ± 0.02	162.37 ± 0.02	59.715 ± 0.004	53.060 ± 0.008	47.578 ± 0.005	43.373 ± 0.006
$\dot{Y}_{12 \rightarrow 11}$	W	118 ± 59	164 ± 50	49 ± 49	0.03 ± 0.03	60 ± 60	59 ± 59
$\dot{Y}_{11 \rightarrow 23}$	W	5 ± 3	16 ± 5	16 ± 16	0.007 ± 0.007	13 ± 13	12 ± 12
$\dot{Y}_{11 \rightarrow 24}$	W	59 ± 59	114 ± 77	38 ± 38	47 ± 47	33 ± 33	72 ± 72
$\dot{Y}_{11 \rightarrow 1}$	W	94 ± 47	131 ± 40	17 ± 17	0.003 ± 0.003	22 ± 22	27 ± 27
$\dot{Y}_{1 \rightarrow 2}$	W	94 ± 94	131 ± 131	17 ± 17	0.003 ± 0.003	22 ± 22	27 ± 27

Table 4.3: Temperatures and heat energy exchanges inside the compression unit. The uncertainties are not all the same for every experiments because some sensors have been damaged between the different experiments. Indeed, the measurement points were equipped with one, two, or three thermocouples. Consequently, the values measured have not been measured all the time with the same number of sensors.

Facts

None of the temperatures of the compressor parts have been recorded; only the gas temperatures are known. Since only inlet and exhaust flow temperatures were measured³¹, the gas temperatures inside the compressor unit are deduced from the model presented in section 4.3. The solving of this model allows the conclusions presented in this section.

Solving the model presented in section 4.3 results in the temperature values presented in table 4.3 and table 4.4. The interpretation of those results leads to the following conclusions:

- component #24 is traveled across in the reversed way, as detailed in section 4.5.1.
- The order of magnitude of the shaft temperature in the axial bearings area of the gas is of about 150°C³², as the gas temperature approaches this temperature in this area.
- The hottest location in the whole compression unit and in the whole circuit is located in the axial bearing area, but the exact location is not known properly (see next section for details). A wide range of temperatures in the gas along the shaft can be observed, as illustrated in fig. 4.12, which let assume that the shaft temperature axial gradient is pretty strong (see next section for details).

Assumptions

Location of the hottest point: The results of the solving of the model for each of the stable OP, summarized on fig. 4.12, let assume that the location of the hottest point of the shaft is in the axial bearing area. In the OP #1, #3,

³¹ Refer to the layout in fig. 4.2, page 37 and to the values in bold in appendix F, page 111 for details about the location of the temperatures measurement points.

³² Figure 4.12 page 51 illustrates the gas temperatures location and the kind of temperature profiles that are observed.

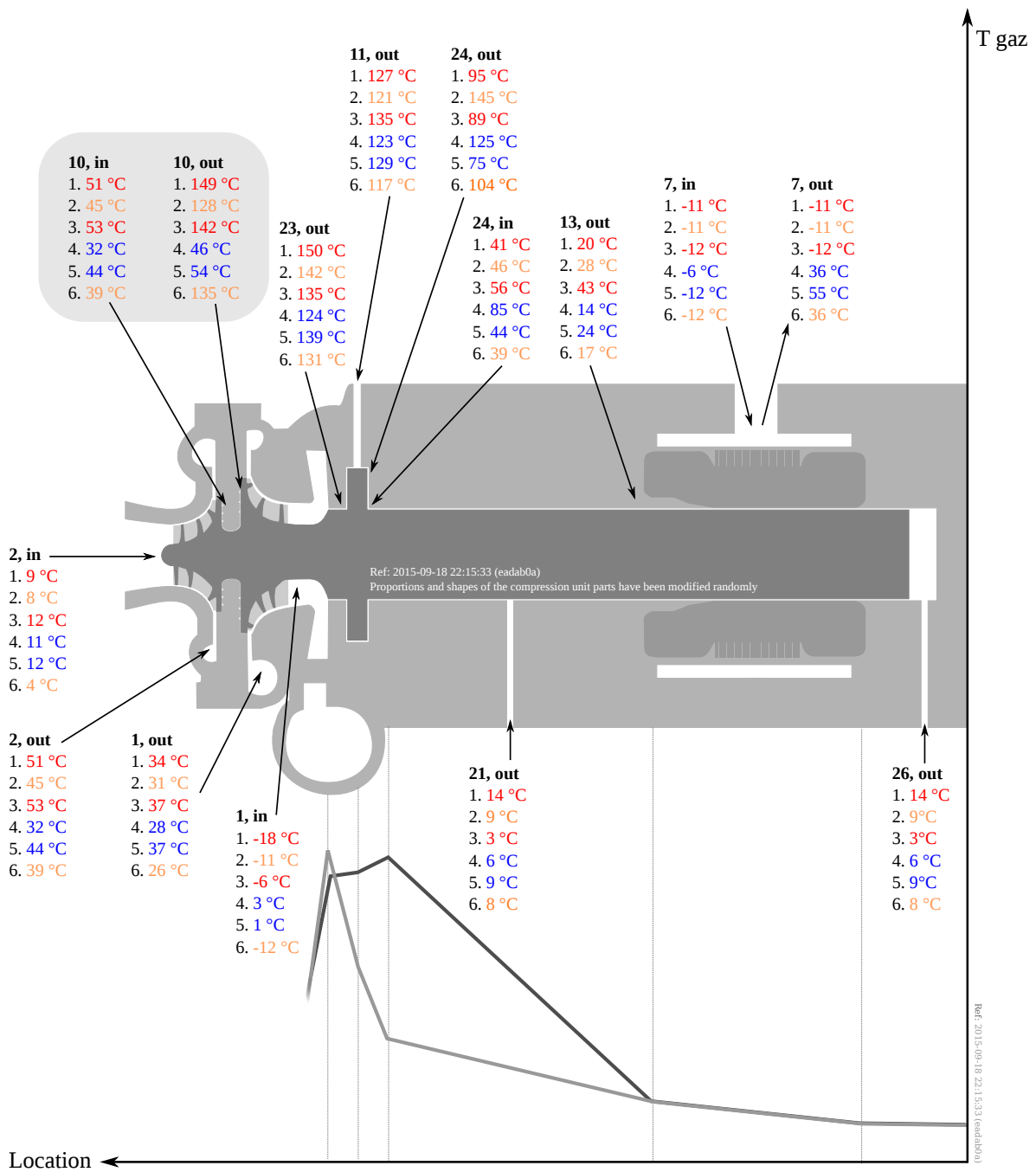


Figure 4.12: Gas temperatures inside the compression unit. The temperature values are colored according to the level of gas outlet temperature in the labyrinth seal (outlet of component #10). The lines of numbers in red have high labyrinth seal outlet temperatures, while the lines of numbers in orange have moderate outlet temperatures, and the lines of numbers in blue have low outlet temperatures. The temperature profiles at the bottom of the picture illustrate qualitatively the 2 types of profiles observed.

OP #		#1	#2	#3	#4	#5	#6
OP		A-6.8/W31.3	A-7.0/W32.3	A-7.0/W35.6	A-0.5/W20.7	A-3.1/W29.5	A-6.6/W22.1
Data		appendix F.1	appendix F.2	appendix F.3	appendix F.4	appendix F.5	appendix F.6
Speed		170 krpm	160 krpm	171 krpm	130 krpm	153 krpm	160 krpm
$\eta_{s,cp1,theory}$	%	78 ± 2	79 ± 2	77 ± 1	79 ± 2	74 ± 2	78.4 ± 0.3
$\eta_{s,cp1}$	%	88 ± 83	88 ± 59	88 ± 80	93 ± 93	92 ± 92	93 ± 93
$\eta_{cp1,s,ext}$	%	90 ± 10	94 ± 7	98 ± 3	99.20	98 ± 2	98 ± 2
$\eta_{cp2,s,theory}$	%	79.482 ± 0.002	72.37 ± 0.04	N/A	N/A	65.0 ± 0.1	73.00 ± 0.05
$\eta_{cp2,s}$	%	89 ± 89	88 ± 72	82 ± 82	89 ± 89	88 ± 88	86 ± 86
$\eta_{cp2,s,ext}$	%	82 ± 19	81 ± 19	68 ± 32	39 ± 39	80 ± 20	47 ± 47
$\dot{M}_{29 \rightarrow 1}$	g s ⁻¹	33 ± 2	38.3 ± 0.9	29.4 ± 0.9	35.4 ± 0.8	43 ± 2	23 ± 1
$\dot{M}_{10 \rightarrow 25}$	g s ⁻¹	<u>0.19</u>	<u>1.01</u>	<u>6.69</u>	<u>9.52</u>	<u>4.78</u>	<u>3.66</u>
$\dot{M}_{1 \rightarrow 25}$	g s ⁻¹	33 ± 2	38.3 ± 0.9	29.4 ± 0.9	35.4 ± 0.8	43 ± 2	23 ± 1
$\dot{M}_{28 \rightarrow 2}$	g s ⁻¹	41 ± 2	59 ± 2	65 ± 2	57 ± 2	58 ± 2	43 ± 2
$\dot{M}_{2 \rightarrow 20}$	g s ⁻¹	39.2 ± 0.8	56.8 ± 0.8	57 ± 1	46.0 ± 0.8	52.3 ± 0.8	37.7 ± 0.8
$\dot{M}_{2 \rightarrow 26}$	g s ⁻¹	1.20 ± 0.06	1.20 ± 0.06	1.20 ± 0.06	1.20 ± 0.06	1.20 ± 0.06	1.20 ± 0.06
$T_{1,out}$	°C	33.7 ± 0.6	31.1 ± 0.9	37 ± 3	28 ± 2	37 ± 2	26 ± 3
$T_{10,out}$	°C	149 ± 101	128 ± 88	142 ± 94	46 ± 21	54 ± 19	135 ± 98
$T_{25,out}$	°C	34.389 ± 0.007	33.701 ± 0.006	57.767 ± 0.006	31.979 ± 0.006	38.455 ± 0.006	42.561 ± 0.007

Table 4.4: Isentropic efficiencies for each compression stages

#5, and #6, it seems to be between the first stage impeller and the axial bearing. In the OP #2, and #4, it seems to be just at the location of the axial bearing side where the gas stream flows reversely. This situation comes probably from the lack of available data to constrain the model proposed in section 4.3. Indeed, minimums of the objective function can currently be observed with more than one flow temperatures and heat exchange, close to the axial bearing: the temperature peak can be before or after the axial bearing without making a significant difference in term of objective function. This situation occurs because no mass or energy rates and no temperatures are known in this area. Consequently, as soon as the global balances with the group of components [#11, #12, #23, #24] are respected, it makes no difference for the objective function and it exists more than one configuration that satisfy the balances. This uncertainty about the gas thermal profile could be solved easily by introducing a more detailed thermal monitoring of the compression unit and its flows, as it would allow to add more constraints in the model objective function.

Gradient of temperature along the shaft: The temperatures observed through the solving of the AWP model let think that the shaft axial thermal gradient is quite strong close to the bearings area. It could be that the shaft temperature is a lot higher when the rotor speed is above 160 krpm as a result from increased windage and parasitic electro-mechanical losses. Perhaps the shaft temperature, between the impellers and the axial bearing, is a function of the rotor speed. The shape of this function could be exponential toward the rotor speed. This assumption can not be checked in the frame of this work due to a lack of data. If this assumption appears to be true, it may be that the axial bearing, traveled across in the reversed way on one of its side, performs badly. It may be that the relative location of the axial bearing in its gaps is not appropriate, with this configuration of flow.

Improvement of the thermal design of the compression unit: Thermal management is an important area of the design of such compression units, since the gaps between the parts are very small and consequently, the dilatation phenomena have to be taken in account very carefully. Schiffmann and Favrat [2010, p. 3] state that the thermal design and management of the compression unit is very important to reach a good performance of the device and the integrated multi-objective design method they propose takes the thermal management into account through a lumped parameter approach. The unit has been designed to sustain such high temperatures, but with the idea in mind that the refrigerant used in the heat pump circuits would be cleared from every trace of lubricant oil. Reaching such high temperatures could create troubles due to the lubricant pollution observed in the heat pump circuits³³. Indeed, the synthetic lubricant oil, heated up to those temperatures, might start to deteriorate. The degradation of the lubricant oil creates uncondensable gases which decrease the heat pump performance, as those

³³ The lubricant oil pollution issue is detailed in section 5.5.4, page 80.

uncondensable gases are pumped in the cycle by the compression stage without transferring heat energy efficiently from the evaporator to the condenser.

Scenarios to test in future work

Improved thermal management of the unit: In 2013, Schiffmann [2013, p. 1–2] highlights the importance of the thermal management in small scale radial compressors. He shows that the gas bearings losses increase in proportion when the shaft power decreases [Schiffmann, 2013, p. 1 & fig. 1 p. 2] and proposes design guidelines to decrease significantly the bearing losses [Schiffmann, 2013, tab. 4 p. 6]. Consequently, a first improvement would be to use bearings geometries which generate less windage losses. It could also be possible to decrease the pressure drop of the filter on the gas bearings aeration circuit, for example by expanding its surface or set some of them in parallel, in order to increase the mass flow rate in this aeration circuit. This increase would result in a better heat dissipation in the unit. The shaft could also maybe be redesigned in order to offer more surface to the aeration flow, which would result in a better heat dissipation.

Moreover, having such a dissipation of energy in the axial bearing area implies a high temperature of the impeller, and especially of the first stage impeller. Part of the heat energy given to the impellers is dissipated in the gas being compressed and this consequently decrease the isentropic efficiency of the compression stages. In the same spirit, the leak mass flow rate from the compression second stage outlet to the first stage outlet, and the heat exchange happening inside the seal, imply that the first compression stage isentropic efficiency appears quite low ($\eta_{cp1,s,ext}$ in table 4.4). In fact, the first compression stage isentropic efficiency is quite high ($\eta_{cp1,s}$ in table 4.4), but is decreased a lot by the leakage and the heat exchange. Those phenomena decrease the efficiency of the compression unit, and consequently, the efficiency of the whole heat pump cycle.

Correlation of the thermal profile with the rotor speed: So far, no direct correlation could be found between the energy rate flowing from the shaft to the impellers $\dot{Y}_{11 \rightarrow 1}$ and the labyrinth seal (component #10) outlet temperature $T_{10,out}$. It would be interesting to study the behavior of the labyrinth seal more thoroughly. It may be that the design of the seal is not appropriate to the conditions in the cycle, which would explain at least partly the huge leaks observed between the two compression stages. Those leaks are detailed in table 4.4 with the mass flow rate $\dot{M}_{10 \rightarrow 25}$.

4.5.4 Mixing and separating gas and liquid in the economizer:

Figure 4.7 shows the different versions of the economizer gas/liquid separation parts. Figure 4.9 illustrates the separation issues:

- The liquid is sucked up with a rotative gas flow bringing some of the liquid phase at the second stage compressor inlet.
- The incoming superheated gas from the first stage compressor is not mixed properly with the incoming saturated gas/liquid flow coming from the second stage expansion valve. The gas in the economizer stays slightly superheated.

Those separation and mixing issues have mostly been solved through different versions of the economizer mixing part. This part has been improved through the experiments. 5 successive versions have been used. The final version, the version #5, can be seen on fig. 4.7b and allows a satisfactory gas/liquid mixing, resulting in a gas stream with less than 2 degrees of superheating leaving the economizer, and a satisfactory gas/liquid separation, blocking the swirling liquid phase streaming up along the walls of the economizer.

4.5.5 Decreasing the performance by using a 4-way valve

The experiments were performed in heating mode. Some of those experiments were performed with the normal circuit, through the 4-way valve, and some were performed with a bypass around the 4-way valve. Figure 4.13

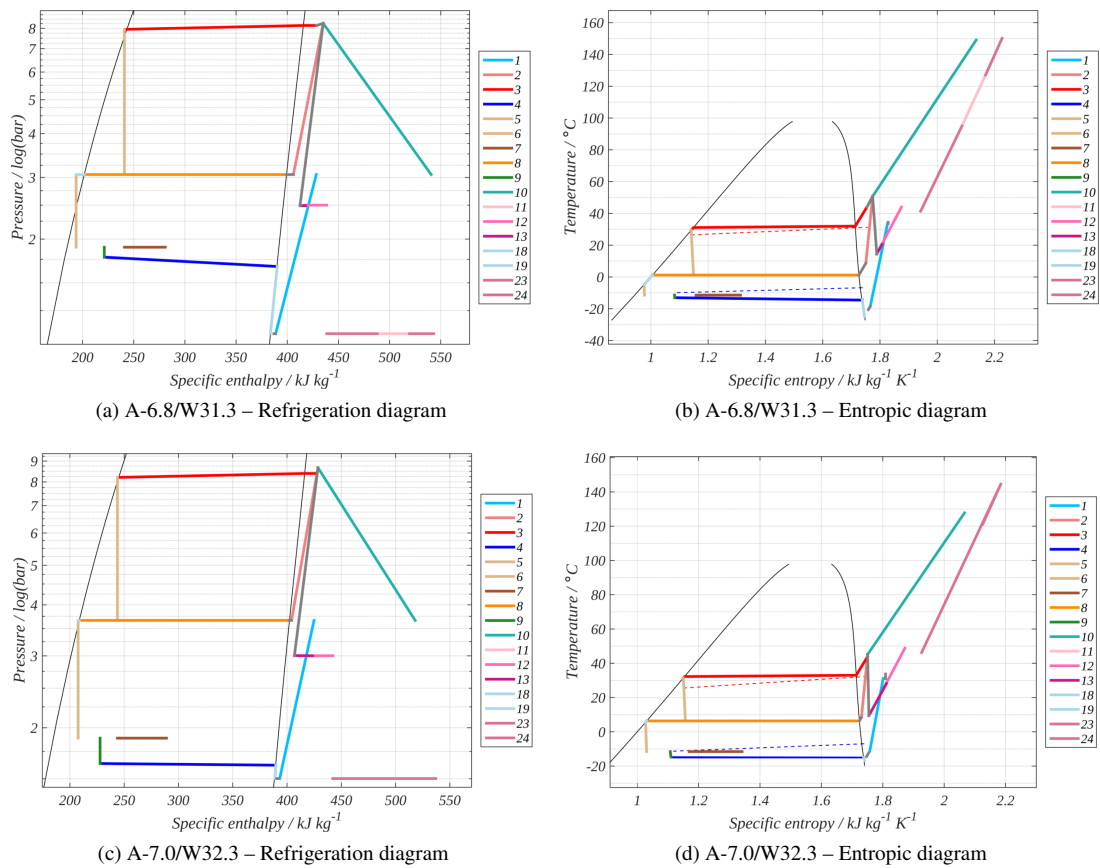


Figure 4.13: Thermodynamic diagrams with and without 4-way valve. OP A-6.8/W31.3 has been recorded with the 4-way in the circuit while OP A-7.0/W32.3 has been recorded without the 4-way valve.

shows the thermodynamic diagrams for two similar OP, with and without 4-way valve. The OP are similar in term of level of temperatures but there are some significant differences, stressed out in table 4.5³⁴. The pressure drop difference on the vapor lines can be observed on the enthalpy diagram and is detailed in table 4.5. This example makes the disadvantage of using a reversing 4-way valve very clear. Indeed, the valve creates significant pressure drops before and after the compression stages, decreasing the temperature difference potential of the device, and generating exergy losses on vapor lines, which are the worst location to create such losses.

OP	speed / krpm	\dot{Y}_{cd} / kW	\dot{Y}_{ev} / kW	\dot{M}_{ev} / g s ⁻¹	COP / -	ΔP_{4-way} / bar
A-6.8/W31.3	170	7.4 ± 0.2	4.3 ± 0.1	32 ± 2	2.19 ± 0.04	0.597 ± 0.002
A-7.0/W32.3	160	10.5 ± 0.2	7.1 ± 0.2	37.1 ± 0.9	2.69 ± 0.03	0.118 ± 0.002

Table 4.5: OP comparison with and without 4-way valve

4.5.6 Poor exergy efficiency of the evaporator and fluids maldistribution

Maldistribution of the refrigerant and/or of the air in the evaporator channels has been observed during the experiments. Indeed, superheating values at the outlet of each evaporator channel vary a lot, as illustrated fig. 4.14e. Difference of superheat at the outlet of the evaporator circuits can be as high as 8K. Consequently, in order to get no liquid phase at the outlet of the evaporator, high overall superheat values at the inlet of the first stage compressor had to be imposed. The situation observed when trying to decrease the superheat value is a good example of the phenomenon observed by [Chen et al. \[2002\]](#): indeed, the superheat may decrease suddenly when it goes down below a certain value, even if the opening of expansion valve is not changed in the process. If that amount of superheat was decreased below 4°C, as illustrated on fig. 4.14c, some liquid was starting to flow into the first stage separator. Indeed, the liquid and gas were not mixing together properly after the collector, and a residual liquid flow was present even with some degrees of overall superheat in the gas flow.

The maldistribution observed in the refrigerant flow is caused by 2 factors:

- a non-ideal distribution of the liquid/gas flow coming from the lower stage expansion valve, implying that the distribution capillaries were not receiving the same mass flow rate and/or the same vapor fraction in the flow.
- a non-ideal distribution of the air flow in the air ducting implying uneven speed profiles in the evaporator section. According to the location of the fan in the air flow, upper channels are exposed to a higher air mass flow rate. Clearly, the design of this air ducting emphasizes on compactness, not on effectiveness of the heat exchange.

None of these two factors could be quantified and studied in depth. The problem seems to come more from the air ducting than from the refrigerant distributor, in the experimenter's opinion. In an attempt to decrease the air flow maldistribution phenomena, a plate drilled with holes located in front of the evaporator circuits with the lower superheat values was added 5cm away from the fins, upstream to the air ducting inlet. The experiments performed after May 11th 2012 have been performed with this plate fixed upstream to the air ducting inlet. As illustrated in fig. 4.14f, this attempt was a failure. It even had the tendency to move the average overall superheat value necessary to ensure the presence of gas only at the first stage separator to a value increased by about 2K. The use of such plate would have been a temporary solution, in any case, as the plate added a significant pressure drop in the air flow, and consequently, increasing the fan energy consumption.

It is possible that the control issue described in section 4.6.6 has an influence on the maldistribution issue, as the refrigerant flow in the evaporator was controlled in an attempt to get enough superheating at the first compression stage, but the demonstration performed in section 4.6.6 shows that the mass flow rate in the first stage heat pump circuit is a function of the second stage heat pump circuit mass flow rate and not a value chosen independently using the first stage expansion valve. Those elements are detailed further in section 4.6.6.

³⁴ More details about those OP are available in appendices F.1 and F.2 page 111 and page 114.

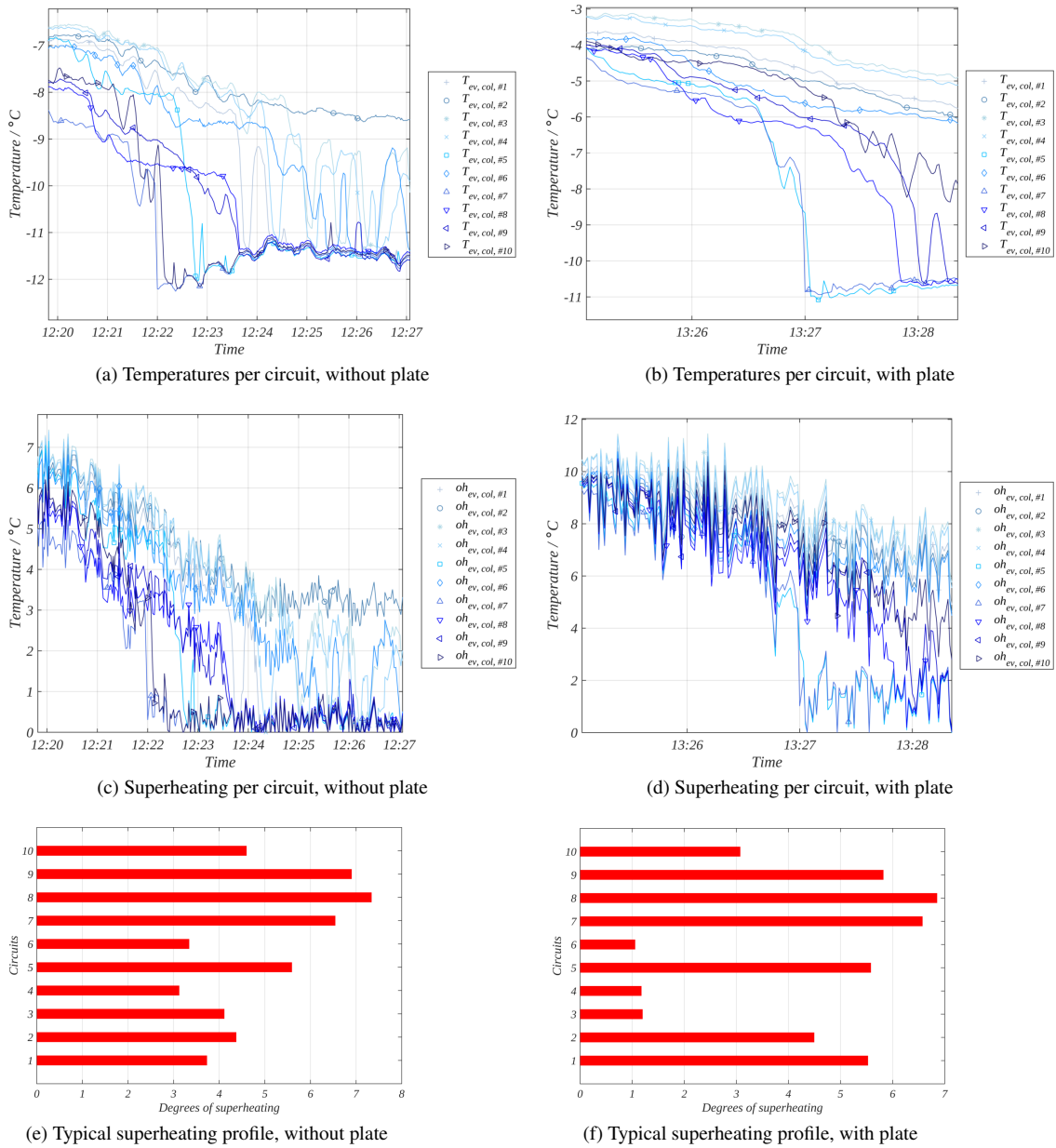


Figure 4.14: Refrigerant and air flow maldistribution in the evaporator

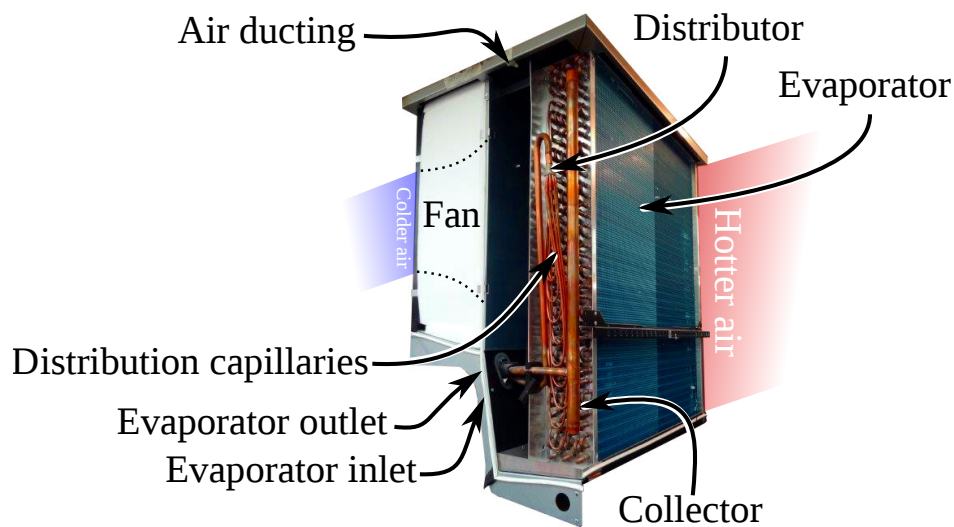


Figure 4.15: Air ducting with the fan and the fin-and-tube evaporator

4.5.7 Poor exergy efficiency of the subcooler

The exergy efficiency of the subcooler η_{sc} is defined in eq. (3.22), p. 33, and is particularly low. As detailed in table 4.1, η_{sc} ranges from 0.4% to 3%. The low performance is the result of a poor design of the heat exchanger³⁵, a high temperature difference between the fluids, and a significant difference of flow rate between the two streams, as illustrated in fig. 4.3 and eq. (D.6), p. 103. As it can be seen on fig. 4.2, the location of the temperature sensors were also not ideal to quantify accurately this efficiency.

4.6 Control issues

Control issues are related to structural deficiencies and to design mistakes of the prototype or of the compression unit. As the prototypes have not been extensively tested, the control strategies offered in this section and the issues encountered remain poorly documented. They are mainly a testimony of the experimenter's experience.

4.6.1 Procedure to start the cycle

As the compression unit is a radial compression machine, it needs to be equipped with a compressors bypass system. Indeed, in order to start the installation away from the surge domain, the characteristics of the circuit needs to be contained into the operation range of the compressors³⁶, represented by the inner surface of the compressors maps. In heat pump applications, starting an installation without bypass systems is likely to yield operation outside of the radial compressor map, at least during the start-up time. Indeed, in domestic heat pumps applications the temperature levels of the sources can not be changed by the heat pump control, as those temperature levels are imposed by the environment and by the house. Having defined temperature levels imposes defined pressure levels at the main heat exchangers and consequently, at the inlet of the first compression stage and at the outlet of the second compression stage. For a radial compressor, starting up with no mass flow rate and an already existing pressure ratio would result in surge which might damage the compressor. In order to avoid this situation, the compression unit is started within a bypass circuit which provides flow resistance characteristics compliant with the compressor maps. Namely, this implies that the characteristics of the bypass circuits always fits into the compressors maps, as illustrated fig. 5.6c.

The implemented procedure to start the heat pump prototype is:

³⁵ This heat exchanger design is detailed in appendix A.1.5, page 92.

³⁶ See fig. 5.6c, page 73 for an illustration of the bypass circuits flow characteristics in compression maps.

1. Liquid is present at the bottom of the condenser, at the bottom of the economizer, and at the inlets of the expansion valves, ideally. As the AWP have two separated bypass circuits (one per compression stage), it is possible to start with no liquid in the economizer, as it was the case in most of the experiments performed. In that case, the upper part of the cycle is started first while the first compression stage is being bypassed. When liquid arrives in the economizer, the lower part of the cycle is also started.
2. The compression unit is started at 60 krpm with fully open bypass circuits and fully closed expansion valves.
3. The second stage bypass circuit is closed and the second stage expansion valve is open, but not much. A typical value is 20% of opening for this valve in this situation. As the bypass circuits are made of a manual needle valve and a solenoid valve, in the AWP, the upper part of the cycle switches from the bypass circuit to the main circuit instantly, inducing an instantaneous change of pressure ratio and mass flow rate in the compression unit. This might induce surge at the second stage impeller, if pressure ratio is already too high between the economizer (which is approximately at the climate chamber temperature and consequently probably at a low pressure level as the room temperature might be low) and the condenser (which might be at a temperature much higher as the house space heating water flows into it). In that case, the compression unit rotor speed is increased until the second compression stage leaves the surge domain. This happens below 120 krpm in the tested cases.
4. As the upper part of the heat pump cycle stabilizes, saturated liquid and gas enters the economizer. The second stage expansion valve is set to an opening small enough to increase the pressure level at the condenser and get some degrees of subcooling at the condenser outlet.
5. The first stage expansion valve is open with a small opening and the first compression stage bypass circuit is closed. Typically, the first compression stage enters the surge domain as the pressure difference between the economizer and the evaporator is already not equal to zero anymore and no refrigerant flows yet through the valve, while some gas is being pumped in the evaporator. With no flow rate, the compression unit is not able to perform a pump down of the evaporator. This needs to be done gradually, and that is also why having a controllable bypass circuit has been favored for the BWP. Leaving the surge domain is more difficult in this case, since this operation implies some increase of the compression unit rotation speed, some opening of the first stage expansion valve, and depends on the liquid brought at the economizer. If there is no liquid in the economizer, it is useless to open the first stage expansion valve further. Consequently, starting the lower part of the cycle heavily depends of the situation in the upper part of the cycle.

With more experience with the setup, this procedure could be automated. First, the control system could involve level control devices, and then, with a good knowledge of the device dynamics, control levels could be removed or kept at their minimal expression (presence of liquid or not).

4.6.2 Procedure to reverse the cycle

The procedure to reverse the cycle is detailed here. It has not been properly tested as an inversion of the cycle happened only once and with a low difference between the sources temperature levels.

1. The heat pump operates at a given OP.
2. Both bypass circuits are open and expansion valves are closed.
3. The compression unit rotational speed is decreased to 120 krpm where the stiffness of the bearings is already good and the rotation speed reasonably lowered.
4. The reversing 4-way valve is activated. Liquid might flow from the condenser to the first stage separator.
5. The first stage bypass circuit is closed. The first stage expansion valve is open with a small opening. The goal is to get an opening big enough to stay away from the surge domain, but small enough to create a significant pressure ratio and decreasing this way the pressure in the separator. The second stage expansion valve is closed and the second stage bypass circuit is open. The liquid in the separator has to be evaporated before increasing the compression unit rotational speed too much, in order to prevent droplets and liquid suction into the first compression stage. The liquid evaporates with the combined action of the energy rate coming from the subcooler circuit and the decreasing of the pressure level in the evaporator, through the reduction of the first stage expansion valve opening.

6. When the liquid in the separator is evaporated, the compression unit rotational speed can be increased again.

4.6.3 Procedure to stop the cycle

During experiments: During the experiments, the sources temperature levels difference was gradually reduced in order to be below 10K. The compressor bypass circuits were open, and the compression unit rotational speed was reduced to 120 krpm and then, the unit was stopped.

Normal operation: Originally, the industrial partner had requested that the filter included in component #26 is bypassed by the activation of the solenoid valve between components #26 and #21, in order to set the pressure levels in the compression unit housing to the intermediate pressure level before the compression unit deceleration reaches the dangerous speed zone ranging between 80 krpm and 60 krpm³⁷. This procedure was dangerous, since it implied the bypass of the filter, which could imply the admission of dusts of critical sizes inside the radial bearings cavity (component #12). Practically, this procedure has been kept for emergency situations, which did not occur often, so it is untested. The favored procedure was to lower the temperature levels difference (reducing consequently the pressure level differences, which was also reducing the efforts on the axial gas bearing) and to simply stop the compression unit.

Emergency situations: In emergency situation, the procedure would be to open the solenoid valve between components #26 and #21, and as the compression unit starts to slow down, and in any case before the dangerous speed zone is reached³⁷, and to open the bypass circuits while closing the expansion valves. When the compression unit has stopped, the solenoid valve can be closed again. This procedure has not been tested during the experimental campaign.

4.6.4 Setting an appropriate gas bearings aeration circuit flow rate

Providing the needed gas flow to the gas bearings aeration circuit is problematic. As described in section 6.3, the 0.5 μm -filter is by-far the main pressure drop of the circuit, which means that the needle valve located before the filter has a low authority on the circuit flow rate. In fact, the pressure drop of the filter is too big for the pressure difference observed between the high pressure zone and the low pressure zone, which reduces the flow rate possible in the aeration circuit. Practically, the 1.2 g s^{-1} measured during the tests could not be increased significantly. Reducing the flow was also difficult, since closing the manual needle valve had no consequence with the first turns, then closing the valve was resulting very fast in a significant decrease of the flow (the valve was indeed too big and had a low authority on the flow, but a smaller valve would have decreased the flow further more). The 0.5 μm -filter is necessary to protect the set of bearings from small dusts that could block grooves in the set of bearings. The dust-size range to filter here is 0.5 to 5 μm , which is the range of dangerous dust size for the bearings. In order to decrease the filter pressure drop, increasing the surface of the filter or mounting more filters in parallel would have been valid solutions.

4.6.5 Setting an appropriate motor cooling circuit flow rate

As it can be observed in the entropy diagrams in appendix F, often, during the experiments, the flow in the motor cooling chamber was not appropriate. Ideally, the flow of refrigerant sent to the motor cooling circuit would be fully evaporated. For OP A-6.8/W31.3, A-7.0/W32.3 and A-7.0/W35.6, the flow was too high, as the vapor quality at the outlet of the motor cooling chamber was low. This phenomenon can be observed on the diagrams in figs. 4.16 and 5.8. In the contrary, in OP A-0.5/W20.7, A-3.1/W29.5, and A-6.6/W22.1, the flow was too low and the refrigerant was leaving the motor cooling chamber with too much superheat. This phenomenon can be observed in the diagrams in figs. 4.13 and 4.17. At this flow regulation problem, is added the oil separation problem, which is detailed in section 5.5.4. Indeed, in the AWP, the motor cooling chamber acts as a lubricant oil separation device. The compression unit *cp101*, after being removed from one of the industrial partner installations which used the same motor cooling system as for the one in the AWP, was partially filled with synthetic lubrication oil.

³⁷ See section 4.5.2, page 48 for more details about the dangerous rotational speed zone.

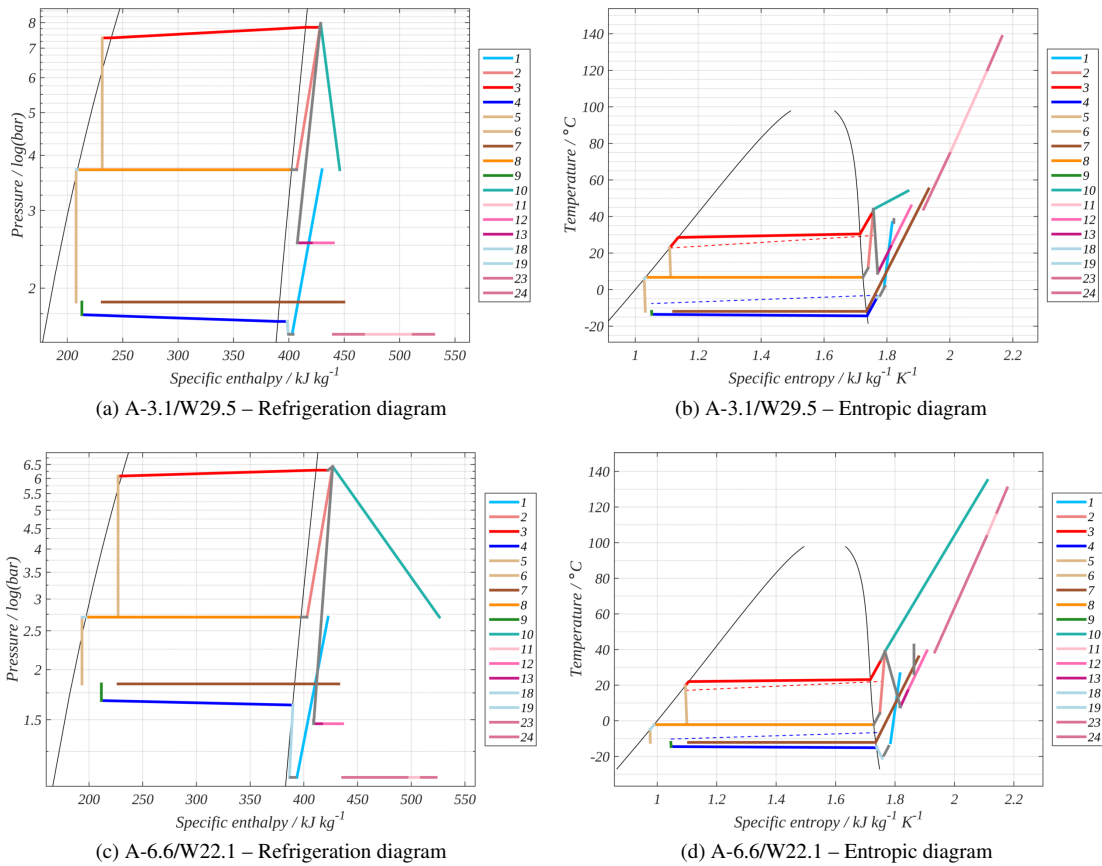


Figure 4.16: A-3.1/W29.5 & A-6.6/W22.1 – Thermodynamic diagrams. The diagrams illustrate notably a too low mass flow rate in the motor cooling chamber, as the vapor quality at the outlet of the motor cooling circuit (component #7) is too high. An other example of this situation can be observed for the OP A-0.5/W20.7 in fig. 5.8.

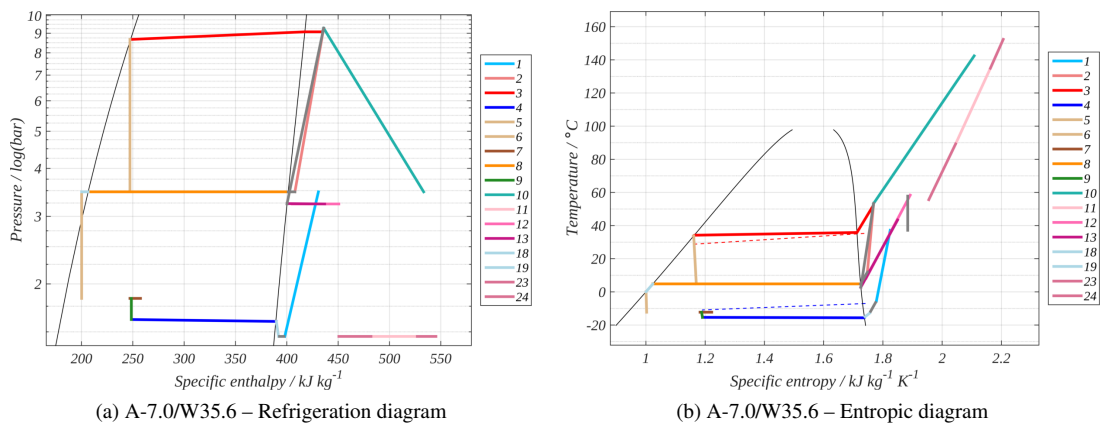
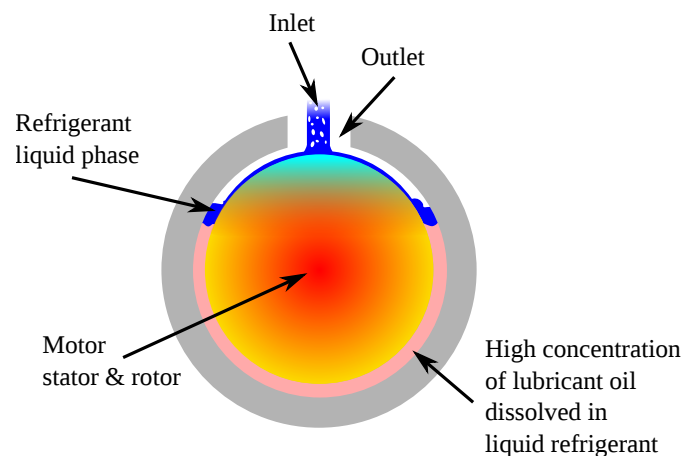


Figure 4.17: A-7.0/W35.6 – Thermodynamic diagrams. The diagrams illustrate notably a too high mass flow rate in the motor cooling chamber, as the vapor quality at the outlet of the motor cooling circuit (component #7) is low. Others examples of this situation can be observed for the OP A-6.8/W31.3 and A-7.0/W32.3 in fig. 4.13.

Figure 4.18 illustrates how the motor cooling chamber was probably performing with an effective cooling of the upper part of the motor and a defective cooling of the lower part, mainly surrounded by refrigerant liquid saturated of lubricant oil. Of course, the presence of this oil significantly decreases the performance of the motor cooling system, as the gap between the two walls of the motor cooling chamber is small, and because there is no circulation of the refrigerant around the motor. A defective motor cooling system can result in unexpected deformations of the motor parts, and especially of the shaft and can also result in an overheat of those parts, damaging them heavily. The mounting of the magnets on the shaft is also sensitive to overheat. Consequently, a flow boiling motor cooling system might be a better option for the motor cooling circuit until clean and lubricant-free refrigerant can be obtained and guaranteed by the industry supply chain.



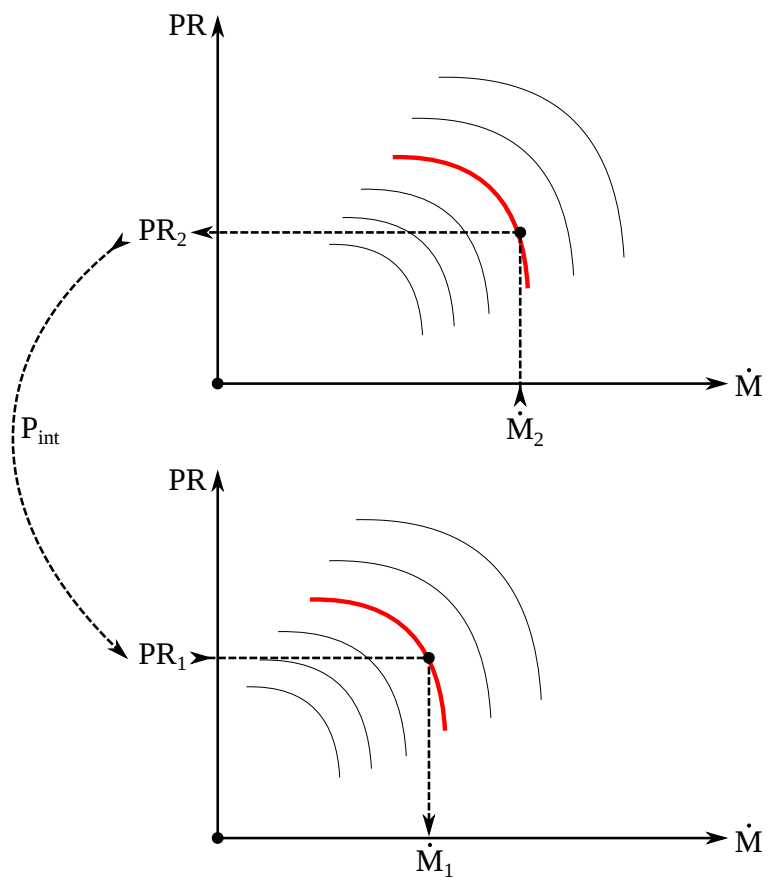
Ref: 2015-09-18 22:15:33 (eadab0a)

Figure 4.18: Schematics of the motor cooling chamber filled up with lubricant oil. The cooling down of the motor, symbolized qualitatively with the red to blue colors, is not isosymmetric which could cause dilatation differences and a motor failure.

4.6.6 Controlling the heat pump to reach stable OP

- Absolute pressure in the economizer (component #8) was barely affected during the experiments by the settings of the prototype, including compressor speed and valves settings.
- The subcooling value was stabilizing itself around an almost fixed value and was almost independent of the setting of the second stage expansion valve.

Those two phenomena are explained by the nature of the control system needed for such a heat pump. If the economizer is perfectly insulated, the intermediate pressure level is defined by the balance of the economizer inlet and outlet mass flow rates and enthalpies. Being external conditions, hot source inlet and outlet temperatures are imposed. The second compression stage provides the heating service to the house, so its mass flow rate and pressure level is set by the external conditions. The intermediate pressure level and the choice of the compressor rotation speed sets the first stage compressor mass flow rate, as shown in fig. 4.19. However, the main function of the first stage expansion valve is to maintain an overheating value at the first stage compressor inlet. So, the valve, trying to reach the desired level of overheating, will influence the first stage mass flow rate and the intermediate pressure level together. This will imply the setting of the second stage expansion valve in order to maintain the second stage mass flow rate, needed to perform the heating service (change of the intermediate pressure level implies a change of the mass flow rate if there is no change of the rotational speed). Consequently, the intermediate pressure level can not be controlled independently and is a consequence of the choice of the compression unit rotation speed and the setting of the valves. The control system needs to control the valves and the rotation speed all together. Designing such a control algorithm is foreseen as the only way to control the heat pump in order to reach a stable OP for every



Ref: 2015-09-18 22:15:33 (eadab0a)

Figure 4.19: The mass flow rates of the two compression stages are bound together through the pressure levels and compression unit current rotational speed.

external conditions. This explanation tends to prove that there is one and only one setting of the valves and rotation speed that allows to reach a given intermediate pressure level and overheating value for given external conditions. Of course, this reasoning implies that the two compressor maps provide a common working point where the energy and mass balances on the economizer can be satisfied. During the experiments, the sources temperatures and mass flow rate have been modified to stabilize the OP, as the heat pump was controlled manually. Moreover, mass flow rates in the auxiliary circuits, which have been neglected in this argumentation, have to be taken in account in the control law and the first assumption of a perfectly insulated economizer is obviously wrong, which implies that the heat energy exchanges of the economizer with its environment have an influence on the control of the heat pump. Finally, it could be also necessary to modify one of the compression stages with a variable geometry set up. This modification would allow to adapt the matching of the maps of the compressors, and to give an additional degree of freedom to the heat pump controller in order to modulate the heating power.

In order to control the heat pump to reach stable OP, the control law needs to control simultaneously the rotation speed of the compression unit, and the settings of the motor cooling valve, the gas bearing aeration valve, and the two expansion valves. It is mandatory that the control law controls all those settings together because the intermediate pressure level is a function of the inlet and outlet mass flow rates in the economizer and their enthalpies, but the dynamic of this is very slow. Indeed, what really control the economizer pressure level is the temperature of the liquid it contains. Consequently, the intermediate pressure level can not really be set at a chosen value directly. A control strategy is proposed in section 4.6.7.

4.6.7 Control of an industrialized version of the AWP

In an industrialized product, no mass flow rate is measured. Only absolute pressures and temperatures are measured.

Pressure levels at the inlets and outlets of the compression stages are measured, which means that the first and the second pressure ratios are known. As the compression unit rotation speed is known through the inverter control, the mass flow rates in the impellers are known through the use of the compressor maps. But, knowing the mass flow rates in the impellers does not imply that the mass flow rates in the different circuits of the heat pump are known. In particular, the main and auxiliary flows are not quantified, but there is no need to know then to control the heat pump, as demonstrated in the paragraphs below.

The second stage flow rate is unknown. This flow rate secures the product service which is to transfer heat energy to the house. Functionally, the flow needs to be subcooled when it leaves the condenser, but the amount of subcooling at the outlet of the condenser is not controlled properly by the second stage expansion valve, as explained in section 4.6.6. The experimenter recommend to control the second stage expansion valve with the liquid level in the economizer. The valve has different control modes. The starting mode is used if there is no liquid in the economizer or if the subcooling value is close to zero. In this mode, the valve needs to be almost fully closed (minimum value, allowing a small flow, and implying an increase of the second compression stage outlet pressure through an increase of the pressure level inside the condenser). While being in this mode, the rotor speed needs to be increased up to a value high enough to maintain the compression stage outside the surge domain. This mode can not be used for a long time, as the motor of the compression unit might not be cooled down efficiently during those periods for reasons detailed further in this section. As soon as some liquid flows in the economizer through the valve, the valve control law switches to normal mode. In normal mode, the subcooling value is above zero and the valve is regulated through the level of liquid in the economizer. If the level decreases, the valve opens. If the level increases, the valve closes. If the subcooling value falls to zero, in this case, the valve control switches to starting mode again.

The first stage expansion valve has also different control modes. If there is liquid in the economizer, the control of the expansion valve is a classical control which function is to secure a chosen value of superheat at the outlet of the evaporator (and not at the inlet of the compression stage). If the level of superheat is too low, the valve closes, if it is too high, the valve opens. If no liquid is detected in the economizer, the valve is in starting mode and is fully open.

With the settings presented above, the intermediate pressure is defined as the pressure level associated to the temperature of the liquid refrigerant in the economizer, which is mainly defined by the second stage expansion valve setting. This implies that the compression unit can not be used in its more effective range systematically. If the compression maps and the refrigerant charge in the installation are correctly optimized, the compression stages

perform in the highest efficiency domains of the compressor maps during most of the operation time, but this is a consequence of the optimization of the compressor maps and of the refrigerant charge in order to get the proper amount of liquid in the economizer when operating the heat pump at different OP. As explained in section 4.2.3, the liquid refrigerant which is not in the heat exchangers at a given time is mainly recovered in the economizer. This implies that the control law relative to the liquid level management in the economizer need to be investigated. Indeed, what is the proper liquid level in the economizer for a given OP is something to be determined in order to create a good control law. It is important to note that this proper level is also dependant of the specific compressor maps of the compression unit powering the heat pump circuit at the time, which suggests that the controller embeds the maps of the specific compressor being mounted in the installation and that the control law are parametrized with parameters of the compressor maps. A mathematical model of compressor maps is proposed in appendix H, page 141. If such models are used, the parameters of those map models could eventually be used to parametrize the control laws for the economizer liquid level. Moreover, those control laws might be dependant of the refrigerant charge being filled up in the circuits and this might be a parameter to include in the control laws.

The motor cooling valve in starting mode is fully closed³⁸. In normal mode, it regulates the temperature of the motor around a chosen value. If the motor temperature is below the chosen value, the valves closes. If the motor temperature is above the chosen value, the valve opens. If the motor temperature gets too high, in any mode, the heat pump shuts down³⁹ and issues an error. The chosen value needs to be determined with performance tests. It only needs to be high enough to be sure that no condensation occurs in the compression unit housing.

The gas bearings aeration valve (which is manual for now, but that would be in the future replaced by an electric valve with a high authority on the gas bearings aeration circuit⁴⁰) in starting mode is fully open. In normal mode, it is controlled with the temperature of the gas at the outlet of the compression unit gas bearings aeration circuit. If the temperature is above the chosen value, the valve opens, if it is below the chosen value, the valve closes. The chosen value needs to be determined with performance tests. It only needs to be high enough to be sure that no condensation occurs in the compression unit housing.

The compression unit rotation speed is determined using the two following rules:

- If the control system is in starting mode, the compressor speed increases.
- If the control system is in normal mode, which means that the compression unit speed is high enough to not be in starting mode, the compression unit speed is chosen with the compressor maps to get the highest efficiency. The highest efficiency can be defined, at first, as the best global compression unit isentropic efficiency (being the product of the isentropic efficiencies of each compression stages), and ultimately, defined as the best accessible heat pump effectiveness or, even better, in the author opinion, as the best accessible global exergy efficiency for the heat pump⁴¹. Those best efficiencies can be obtained for the controller using a model-based or predictive control approach [Fallahsohi et al., 2010].

Bibliography

AFNOR. NF EN 12102: Air conditioners, liquid chilling packages, heat pumps and dehumidifiers with electrically driven compressors for space heating and cooling - Measurement of airborne noise - Determination of the sound power level, 07 2008. URL <http://sagaweb.afnor.org/fr-FR/sw/consultation/notice/1405770>.

AFNOR. ISO 9614-1: Acoustics - Determination of sound power levels of noise sources using sound intensity - Part 1 : measurement at discrete points, 11 2009. URL <http://sagaweb.afnor.org/fr-FR/sw/consultation/notice/1287190>.

AFNOR. NF EN 14511-1: Air conditioners, liquid chilling packages and heat pumps with electrically driven compressors for space heating and cooling - Part 1 : terms, definitions and classification, 12 2011a. URL <http://sagaweb.afnor.org/fr-FR/sw/consultation/notice/1405768>.

³⁸ The starting mode is used if there is no liquid in the economizer or if the subcooling value is close to zero at the condenser outlet.

³⁹ Shutting down the heat pump means closing the expansion valve, opening the bypass circuits, shutting down the compression unit. Eventually, it means bypassing the filter in the gas bearings aeration circuit. This later action is discussed in section 4.6.3, page 59.

⁴⁰ This would imply to have a lower pressure drop in the 0.5 μ m-filter.

⁴¹ Those efficiencies and effectiveness are defined in section 3.4.4, page 30.

- AFNOR. NF EN 14511-2: Air conditioners, liquid chilling packages and heat pumps with electrically driven compressors for space heating and cooling - Part 2 : test conditions, 12 2011b. URL <http://sagaweb.afnor.org/fr-FR/sw/consultation/notice/1405767>.
- AFNOR. NF EN 14511-3: Air conditioners, liquid chilling packages and heat pumps with electrically driven compressors for space heating and cooling - Part 3 : test methods, 12 2011c. URL <http://sagaweb.afnor.org/fr-FR/sw/consultation/notice/1405766>.
- AFNOR. NF EN 14511-4: Air conditioners, liquid chilling packages and heat pumps with electrically driven compressors for space heating and cooling - Part 4 : operating requirements, marking and instructions, 12 2011d. URL <http://sagaweb.afnor.org/fr-FR/sw/consultation/notice/1405843>.
- AFNOR. NF EN 14825: Air conditioners, liquid chilling packages and heat pumps, with electrically driven compressors for space heating and cooling - Testing and rating at part load conditions and calculation of seasonal performance, 05 2012. URL <http://sagaweb.afnor.org/fr-FR/sw/consultation/notice/1407222>.
- S. Bertsch and P. Hubacher. Verbesserung des Abtauens bei luftbeaufschlagten Verdampfern - Phase 2: Bewertung der Abtauprozesse. Technical report, Swiss Federal Office of Energy, 2002. URL <http://www.bfe.admin.ch/php/modules/enet/streamfile.php?file=000000007564.pdf>.
- W Chen, Chen Zhijiu, Zhu Ruiqi, and Wu Yezheng. Experimental investigation of a minimum stable superheat control system of an evaporator. *International Journal of Refrigeration*, 25(8):1137 – 1142, 2002. ISSN 0140-7007. doi:[10.1016/S0140-7007\(01\)00107-4](https://doi.org/10.1016/S0140-7007(01)00107-4).
- I. Dinçer and M. Kanoglu. *Refrigeration Systems and Applications*. Wiley, 2nd edition edition, 2010. ISBN: 978-0-470-74740-7.
- H. Fallahsohi, C. Changenet, S. Placé, C. Ligeret, and X. Lin Shi. Predictive functional control of an expansion valve for minimizing the superheat of an evaporator. *International Journal of Refrigeration*, 33(2):409–418, 2010. ISSN 0140-7007. doi:[10.1016/j.ijrefrig.2009.10.008](https://doi.org/10.1016/j.ijrefrig.2009.10.008).
- P. Rapin, P. Jacquard, and J. Desmons. *Technologie des Installations Frigorifiques*. Dunod, 9th edition edition, 2011. ISBN: 978-2-10-055760-8.
- J. Schiffmann. Enhanced Groove Geometry for Herringbone Grooved Journal Bearings. *Journal of Engineering for Gas Turbines and Power*, 135(10), 2013. doi:[10.1115/1.4025035](https://doi.org/10.1115/1.4025035).
- J. Schiffmann and D. Favrat. Design, experimental investigation and multi-objective optimization of a small-scale radial compressor for heat pump applications. *Energy*, 35(1):436–450, 2010. doi:[10.1016/j.energy.2009.10.010](https://doi.org/10.1016/j.energy.2009.10.010).

Credits

Fig. 4.1a, page 36 © 2015 Julien Ropp, licensed under [CC BY 4.0](https://creativecommons.org/licenses/by/4.0/).

Fig. 4.15, page 57 © 2015 Julien Ropp, licensed under [CC BY 4.0](https://creativecommons.org/licenses/by/4.0/).

Brine-Water heat pump Prototype (BWP)

This chapter presents the Brine-Water twin-stage heat pump Prototype (BWP) designed to demonstrate the statement detailed in chapter 3. It presents the prototype specifications and design, its results, and the encountered issues.

5.1 Design of the BWP

5.1.1 Specifications

Modularity with the components: The Brine-Water twin-stage heat pump Prototype (BWP) components can be changed and many different possibilities can be tested.

Modularity with the thermodynamics cycles and circuits: The BWP can test different single and twin-stage heat pump cycles, and tolerates modifications of the motor cooling and gas bearings aeration circuits.

Liquid refrigerant location monitoring: The BWP is expected to allow the tracking of the liquid refrigerant location within the cycle. The amount of refrigerant in the heat exchangers and in the economizer needs to be known.

Those 3 guidelines led to the following design choices:

Many assemblies, as few brazings as possible: Ideally, the whole setup would have been designed with fittings and assemblies, in order to keep as few brazings as possible, but it would have exceeded the budget allowed for the manufacturing of the prototype. As a compromise, the setup was built with brazed components, connected to assembly fittings at their interfaces. The system was built around modules which could be relocated or connected differently, using straight flexible or conventional pipes, and fittings.

Flexible pipes to connect the weighted elements: In order to weight the heat exchangers and the economizer properly, those components have been hang up to load cells, and connected to the main circuits using straight flexible pipes. This configuration can be observed in fig. 5.1.

Inline components with selection of the active component: Different types of inline components, such as the expansion valves, could be mounted together in parallel in the experimental setup and could be operated, alone, or together with the other components of the line. This possibility allows to test during the same experiment different technologies of valves and active components, in order to observe the dynamic response of the cycle¹. As radial compression units have continuous dynamic behavior, changing the dynamics of

¹ An example of a test section of expansion devices mounted in parallel can be seen in appendix B.4.1, page 97.

the valves response with different technologies² can be interesting to develop control strategies for the prototypes.

5.1.2 Description

The Brine-Water twin-stage heat pump Prototype (BWP) is designed to be modular and allows to test different heat pump layouts. Indeed, each component test section is connected to other components using fastened fittings and flexible pipes. The components can be moved and spatially rearranged in the housing. Their order can also be modified. The experimental setup has been designed to test single and twin-stage heat pump cycles. The setup is equipped with load cells to measure the weight of the elements which are subject to variations of their overall refrigerant vapor quality. Those weighted components are the condenser, the evaporator, and the economizer. The weight of the elements was intended to be used to track the location of the liquid charge in the installation and would have allowed to compare the observed liquid location behavior with the predicted behavior using a model of the heat pump integrating nowadays modeling techniques such as components dynamic modeling and other techniques listed by Ding [2007]. The model in question would have been based on moving boundaries heat exchanger modeling, such as the one implemented by Bell et al. [2015], and on mass and energy balance equations. The inline components, such as the expansion valves, can be mounted in parallel in order to be tested sequentially or together during the same experiment. Before the experiment presented in this chapter, the BWP had been modified in order to get a new bypass circuit which was likely to solve the issues encountered with the Air-Water twin-stage heat pump Prototype (AWP) and detailed in section 4.5.2. As explained in section 5.2.1, the compression unit crashed soon after the beginning of the experiment because of an assembly issue in the compression unit. Before the crash of the unit, a small B8.0/W11.0 Operating Point (OP) was being stabilized, with the compressors being connected in series, bypassed with the new bypass system. This experiment is interesting as it confirms that the new bypass circuit, described in section 5.2.2, is functional and could consequently maybe solve the issue described in section 4.5.2, page 48. It also shows a thermal behavior of the compression unit very different of the one observed in the AWP.

The BWP has been designed vertically for liquid management reasons. Indeed, when the heat pump is stopped:

- Liquid refrigerant tends to condensate at the evaporator, which is the coolest location in the heat pump cycle. Consequently, if no insulation valve stops this phenomenon, the evaporator tends to fill up with liquid when the installation is stopped.
- Pumping down the evaporator using radial compression units is a difficult operation, as a pump down of the evaporator requires to decrease its pressure level, and consequently to support a pressure ratio at the first compression stage, which implies to have a flow there, but there can be enough flow, as the expansion valve is not loaded with liquid refrigerant. Section 5.5.3 presents the issue relative to the pump down of the evaporator.

5.2 BWP components

This section gives details about of the main components in order to make the understanding of the sections 5.3 to 5.5 easier. Further details about the components and the topology of the circuits are given in appendix B, page 95.

5.2.1 Compression unit

The compression unit mounted in the BWP for the experiment which has been used to generate the data presented in section 5.4 was the *cp101* unit, from the *evo4* design family³. This compression unit has been mounted in the

² Modulating refrigerant valves equipped with a magnetic actuator have a response time shorter than stepper-motor valves, but are more expensive, for instance. The later valves also have a continuous setting behavior while pulse width modulation electric expansion valves have a discreet setting behavior. Thermostatic expansion valves are cheap but can not be set interactively for the needs of the cycle control. Those different technologies have different dynamic responses which can have an influence on the dynamic behavior of the whole prototype, as the compression unit is a dynamic compressor.

³ Details about the previous design families are given in appendix B.1, page 95.

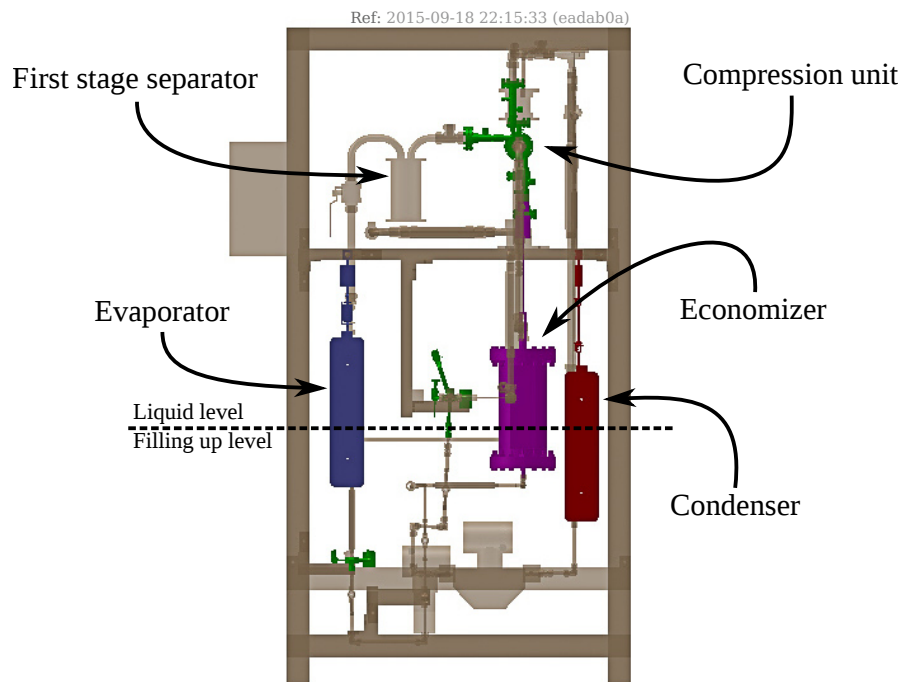


Figure 5.1: BWP topology, after the first set of heavy modifications mentioned in appendix B.1.1.

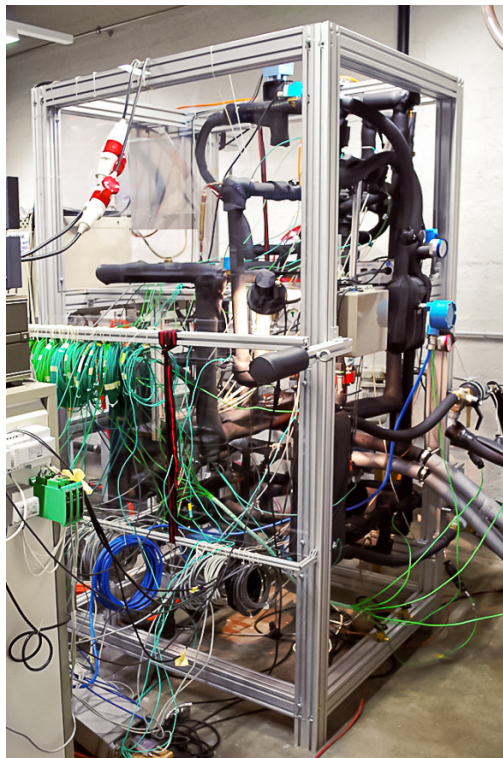


Figure 5.2: View of the experimental setup in the laboratory.

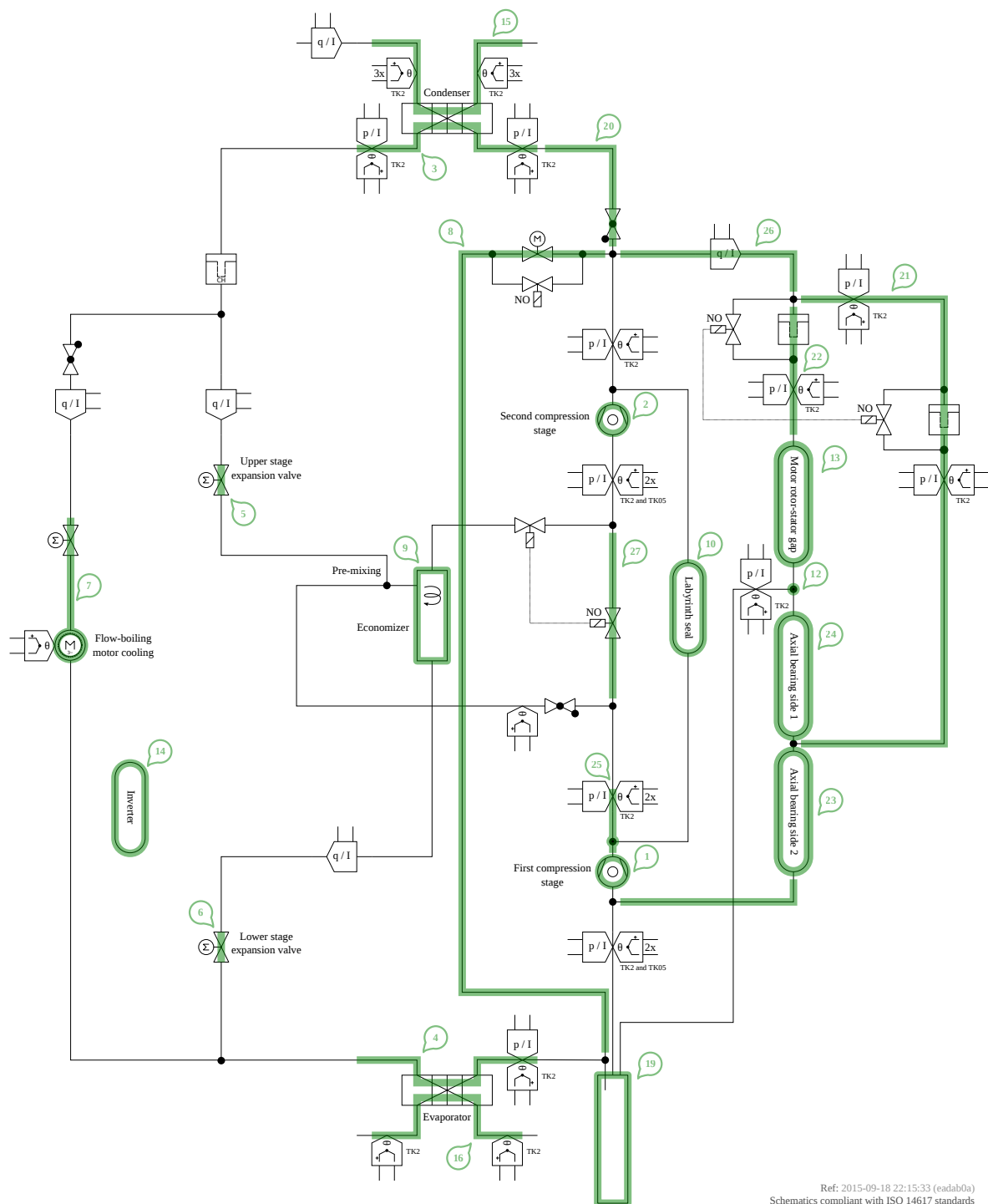


Figure 5.3: Layout of the Brine-Water heat pump test-rig.

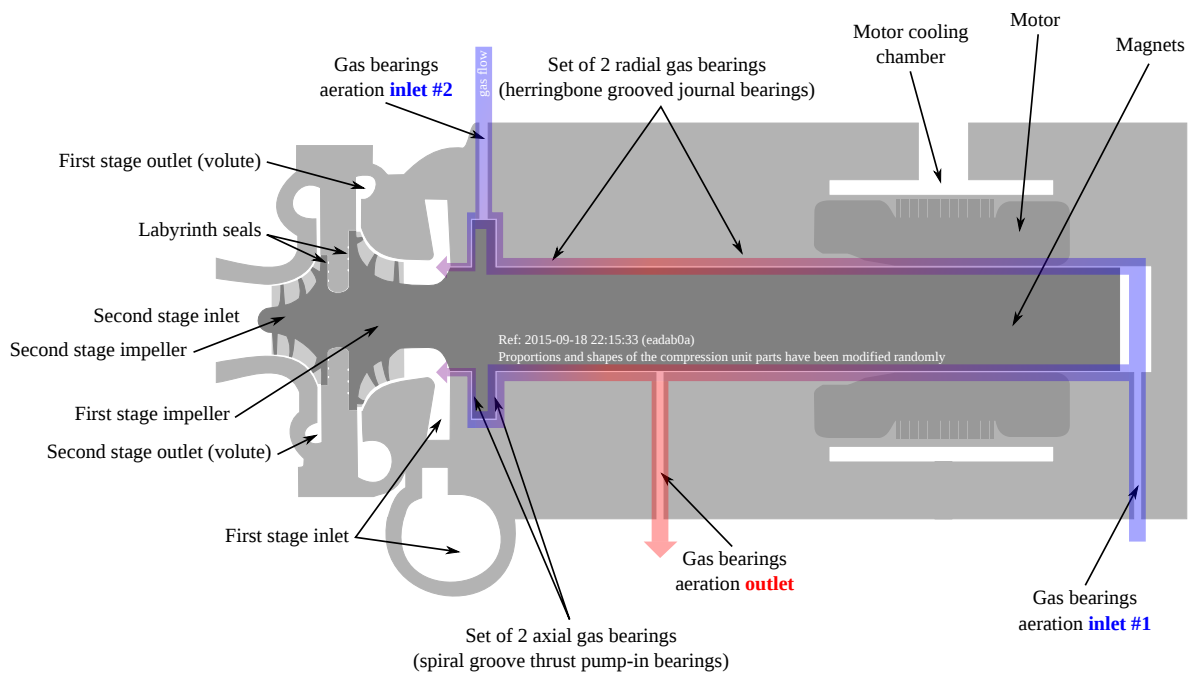


Figure 5.4: Structure of the twin-stage compressor unit with the BWP gas bearings aeration circuit I/O layout

BWP following the piping layout detailed in fig. 5.4. The compression unit mounted in the circuits can be seen in fig. 5.5. This piping layout is very different from the one used with *cp105* in the AWP. Indeed, the unit *cp101* has been plugged in the heat pump circuits with the proper inlets and outlets connections. Unfortunately, due to an assembly issue, the unit crashed soon after the start of the experiment. After dismantling and investigation at the industrial partner facility, it appeared that the unit would have broken in any case due to the mounting defect and the experiment itself is not responsible for the crash.

5.2.2 Bypass system

The bypass circuit connects the outlet of the second compression stage to the first stage separator (component #8⁴). When the bypass circuit is used, the solenoid valve in component #27 is open and no gas from the vapor line flows into the economizer (component #9). The economizer is consequently, in bypass-mode, a simple tank located after the second-stage expansion valve, ensuring that the first stage expansion valve is filled up with liquid. In that mode, the economizer has only one inlet and one outlet⁵. In the AWP, each compression stage has its own bypass-mode and can be bypassed separately. In the BWP, in bypass-mode, the two compression stages are in series. The two compression stages have the same mass flow rate and the intermediate pressure is kept at the economizer pressure using the second expansion valve only⁶, as the first expansion valve is dedicated to the setting of the superheat at the outlet of the evaporator. Figure 5.6 shows the complexity of the configuration of the flows when being in bypass-mode, for the AWP (fig. 5.6a) and BWP (fig. 5.6b). It shows also that the bypass circuit resistance flow characteristic needs to always be contained in the compressor maps in order for the bypass to ensure their function. Those characteristics are illustrated in fig. 5.6c. The layout of the bypass circuit can be observed in fig. 5.3. The circuit is the component #8.

5.2.3 Motor cooling circuit

The motor cooling circuit in the BWP takes in account the motor cooling issue encountered with the AWP and detailed in section 4.6.5, page 59. The motor cooling strategy in the BWP is based on a flow-boiling heat exchange

⁴ Components numbering is detailed in fig. 5.3, page 70 and fig. 5.7, page 75

⁵ In the AWP, the economizer has 2 inlets and 2 outlets in every modes.

⁶ See issues in section 4.6.6, page 61, and section 5.5.2, for details about keeping the intermediate pressure at a chosen value.

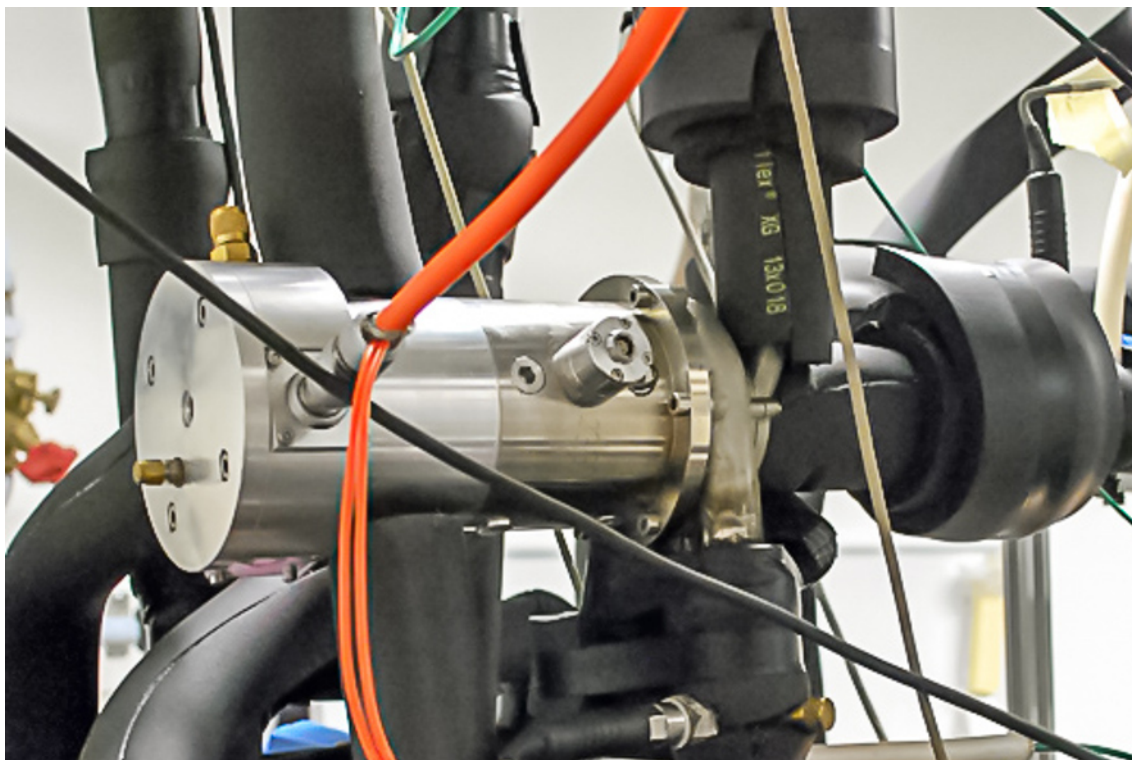


Figure 5.5: Compression unit *cp101*, mounted in the BWP

while the strategy in the AWP is a pool-boiling strategy. Pool boiling is easier to control as a simple liquid level management would be enough to ensure the proper cooling down of the motor. As lubricant pollution is encountered in the heat pump circuits⁷, flow boiling was a better technical solution in polluted circuits⁸. The compression unit inlets and outlets could be closed with ball valves, in order to be able to remove the unit from the circuit without recovering the refrigerant from the installation. The layout of the motor cooling circuit can be observed in fig. 5.3. The circuit is the component #7.

5.2.4 Gas bearings aeration circuit

The BWP gas bearings circuit⁹ is similar to the AWP, but has the following main differences:

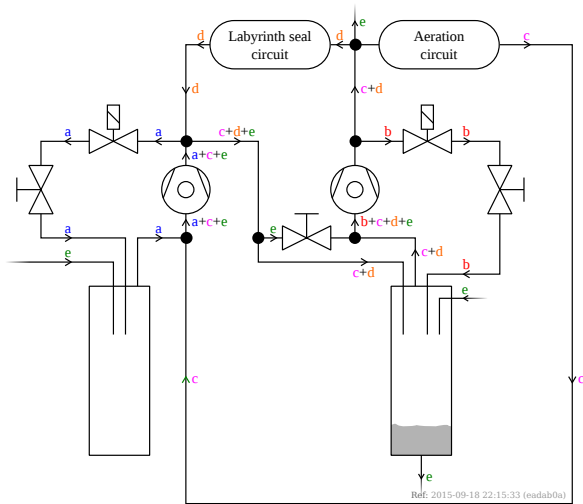
- The topology of the circuit is more vertical than in the AWP, and the pipes are longer. As a result, the pressure drop in the pipes is higher, and the chances of gas condensation in the pipes are also higher. However, the risk of condensation is decreased by the fact that the BWP is kept at room temperature, while the AWP was in the climate chamber, and was consequently at the environment temperature.
- There are two 0.5 μ m-filters (one per circuit branch). Consequently the pressure drop created by the filtration process is lower.

The layout of the gas bearings aeration circuit can be observed in fig. 5.3. The circuit is made of the components #21, #22, #26, and of the pipe connecting component #12 to component #19. The new layout was expected to solve the issue detailed in section 4.5.2, page 48. Unfortunately, the data collected and the test performed did not allow to confirm the solving of the issue with the new system, as the compression unit broke before a proper stop sequence could be studied. Consequently, further tests with new compression units and the next version of the experimental setup need to be performed with the improved bypass circuit in order to document the new system and its results.

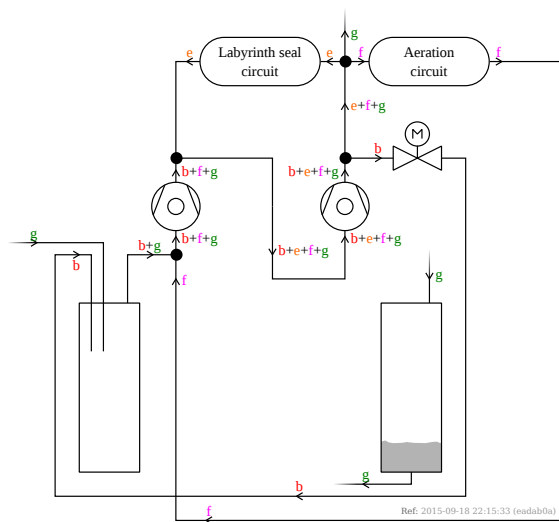
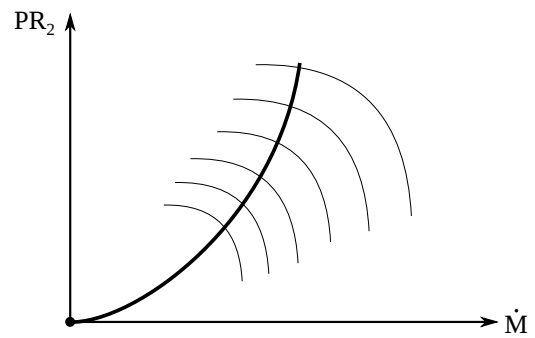
⁷ This motor cooling issue is detailed in section 5.5.4, page 80.

⁸ Details about the design and layout of the BWP motor cooling circuit are given in appendix B.3, page 97.

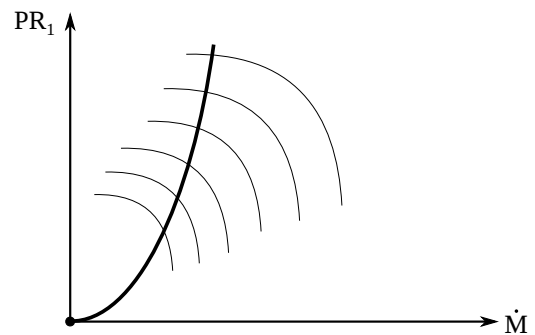
⁹ Further details about the BWP gas bearings aeration circuit can be found in appendix B.2, page 96.



(a) AWP simplified bypass circuits layout



(b) BWP simplified bypass circuit layout



Ref: 2015-09-18 22:15:33 (eadab0a)

(c) Bypass circuits characteristics in compressor maps

Figure 5.6: Compressors bypass systems in the AWP and the BWP. Those schematics are simplified layouts. The complete layouts are available in figs. 4.2 and 5.3.

5.3 Modeling

The model proposed is based on the areas or physical elements of interest in the BWP. Figure 5.3 presents the BWP layout and fig. 5.7 presents the model itself. The set of equations deduced from analysis of the model in fig. 5.7 is detailed in appendix E. Following the procedure described in section 3.4.3, page 25, the model is built with 27 components; 10 of them describe the compression unit itself.

5.4 BWP results and observations

The compression unit failed after 25 minutes of experiment, while an OP B8.0/W11.0 was being stabilized. The OP in question was not really a conventional OP, as the compression unit was still bypassed. The experimenter was stabilizing the conditions before closing the bypass circuit furthermore. Using the model proposed in section 5.3, the amount of the flow being bypassed could be computed. At the time when the compression unit broke, 61% of the flow was being bypassed¹⁰, which explains the high level of superheat observed at the outlet of the first stage separator (component #19).

Using the model, the mass flow rates and the energy rates between the components of the prototype could be computed. They are detailed in tables 5.2 and 5.3¹¹. Observing the data collected from the experiment or determined with the model leads to the following general observations:

- Changing the gas bearings aeration circuit inlets/outlets configuration used for the AWP to the proper configuration, applied in the BWP, seems to change the temperature behavior in the compression unit, as it can be observed in fig. 5.8b, compared with the behavior observed with the closest AWP OP, represented in fig. 5.8d, where the temperature was increasing a lot less in the aeration circuit.
- The motor cooling flow was too high. This was done on purpose, in order for the experimenter to be able not to worry about the cooling of the motor during the start-up phase of the experiment. The compression unit internal temperature was monitored with a PT100 inside the compression unit. The PT100 was located on a metal part surrounding the radial bearings cavity. At the time of the break, the temperature was of about 35°C¹².
- Table 5.2 shows that there was approximately no flow in the labyrinth seal¹³, and that this flow was almost adiabatic, which seems to indicate that the shaft was not at a high temperature at the time and that the impellers were at a temperature close to the second stage gas outlet temperature.
- The gas in the bypass circuit (component #8) was not increasing its temperature too much despite the relatively long period of bypassing involved¹⁴.

Table 5.1 and fig. 5.8 allow to compare the situation between the lower OP from the AWP, the OP A-0.5/W20.7, and the OP from the BWP, to some extents and on specific topics¹⁵. The temperature values from table 5.1 illustrate that the compression unit thermal behavior is very different in the BWP and in the AWP. The two OP can not be compared easily as the following important differences can be observed:

- The heat energy rate from the motor to the shaft is 5 times higher in the AWP OP than in the BWP OP.
- The BWP OP is recorded at a rotor speed of 110 krpm while the AWP OP is recorded at a rotor speed of 130 krpm.

¹⁰ Ratio of $M_{8 \rightarrow 19}$ over $\dot{M}_{1 \rightarrow 25}$. The values of those mass flow rate are available in table 5.2, page 76.

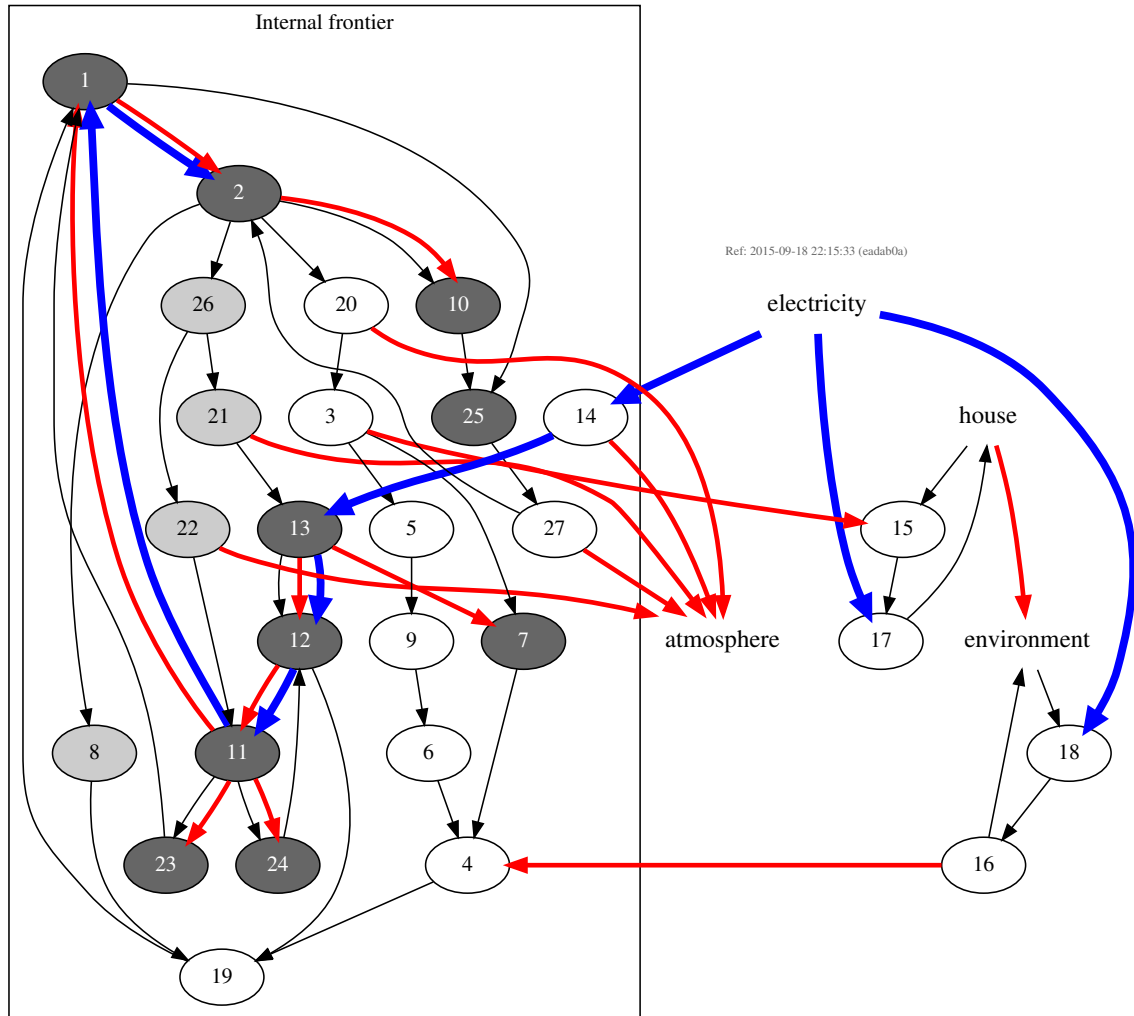
¹¹ The thermodynamic points, the performance indicators, and the graphs of some key values right before the break are available in appendix F.7, page 129.

¹² This temperature was screened on an independent device and was not recorded by the data acquisition system.

¹³ Component #10.

¹⁴ The bypass circuit has been partially open for the whole time of the experiment: 25 minutes. Despite this, the gas temperatures were reasonable, as it can be observed in table F.25, page 130.

¹⁵ Original values can be retrieved from table F.14, page 122, table F.16, page 123, table F.25, page 130, and table 5.3.



Legend

Ref: 2015-09-18 22:15:33 (eadab0a)

- 24 Elements from the compression unit
- 22 Elements from the auxiliary circuits
- 6 Elements from the main circuit
- Flow rate
- Work energy
- Heat or transformation energy

- 1: First stage impeller
- 2: Second stage impeller
- 3: Condenser, refrigerant stream
- 4: Evaporator, refrigerant stream
- 5: Second stage expansion
- 6: First stage expansion
- 7: Motor cooling chamber
- 8: Bypass circuit
- 9: Economizer
- 10: Labyrinth seal
- 11: Axial bearing zone
- 12: Radial bearings zone
- 13: Rotor/stator zone
- 14: Inverter
- 15: Condenser, hot source stream
- 16: Evaporator, cold source stream
- 17: Hot source circuit and pumps
- 18: Cold source circuit and pumps
- 19: First stage separator
- 20: Piping and fittings between the second stage impeller and the condenser
- 21: Piping, fittings, and filter between the second stage impeller and the axial bearing zone
- 22: Piping, fittings, and filter between the second stage impeller and the rotor/stator zone
- 23: Axial bearing, impellers side
- 24: Axial bearing, radial bearings side
- 25: Physical outlet of the first stage compressor
- 26: Piping between the second stage impeller outlet and the gas bearings aeration mass flow meter
- 27: Piping between the physical outlet of the first stage compressor and the physical inlet of the second stage compressor

Figure 5.7: Modeling of the BWP in bypass mode. The bypass mode implies that the two compression stages are connected in series.

Those differences do not formally allow the author to compare the thermal behavior of the two units. Indeed, the gas inlet temperatures and rotor speeds are comparable but the heat energy rates from the motor to the shaft are very different. Consequently the following comparisons are trends that need to be evaluated with further experiments, with new compression units in a next version of the BWP. If the OP would strictly be comparable, the following interesting points would be interesting to stress:

- The maximum temperature, occurring in the AWP compression unit in the axial bearing, occurs in the BWP compression unit at the outlet of the gap between rotor and stator.
- The maximum gas temperature in the AWP is more than 7 times higher than in the BWP. The gas temperature at the outlet of the axial bearing sides is only few degrees hotter in the BWP compression unit while it is several tenths of degree hotter in the AWP compression unit, even despite of the flows in the bearings that are in the same order of magnitude in the two experimental setups, as the inlet mass flow rate between the two experiments had been kept at the same value¹⁶.
- The temperature of the flow in the labyrinth seal of the BWP compression unit is almost constant and is very close to the temperature hottest gas flowing in the impellers. This allows to think that the impellers temperature was close to 51°C during the BWP OP, as the gas temperature reaches 51°C at the seal outlet and as the flow in the labyrinth seal is very small. As stressed in section 4.5.3, page 49, the temperature of the impellers in the AWP were probably much higher.

OP and speed	Motor		Gas bearings aeration			Labyrinth seal	
	$\dot{Y}_{13 \rightarrow 12}$ / W	$T_{13, out}$ / °C	In #1 / °C	In #2 / °C	Out / °C	In / °C	Out / °C
B8.0/W11.0, 110 krpm	11.685 ± 0.003	17 ± 19	7.90 ± 0.01	7.98 ± 0.01	18.95 ± 0.01	50.7 ± 0.2	51 ± 8
A-0.5/W20.7, 130 krpm	53.060 ± 0.009	14 ± 23	6.271 ± 0.007	6.271 ± 0.007	123 ± 57	32 ± 2	46 ± 21

Table 5.1: Key values for the comparison of the AWP and the BWP gas bearings aeration circuits, regarding thermal management.

Name	Value / g s ⁻¹	Name	Value / g s ⁻¹	Name	Value / g s ⁻¹
$\dot{M}_{1 \rightarrow 25}$	29.2 ± 0.3	$\dot{M}_{2 \rightarrow 8}$	17.8 ± 0.2	$\dot{M}_{2 \rightarrow 10}$	$1.88275618 \times 10^{-6} \pm 2 \times 10^{-8}$
$\dot{M}_{2 \rightarrow 20}$	10.1 ± 0.2	$\dot{M}_{2 \rightarrow 26}$	1.20 ± 0.06	$\dot{M}_{3 \rightarrow 5}$	6.94 ± 0.04
$\dot{M}_{3 \rightarrow 7}$	3.20 ± 0.02	$\dot{M}_{4 \rightarrow 19}$	10.1 ± 0.2	$\dot{M}_{5 \rightarrow 9}$	6.94 ± 0.04
$\dot{M}_{6 \rightarrow 4}$	6.94 ± 0.04	$\dot{M}_{7 \rightarrow 4}$	3.2 ± 0.1	$\dot{M}_{8 \rightarrow 19}$	17.8 ± 0.2
$\dot{M}_{9 \rightarrow 6}$	6.94 ± 0.04	$\dot{M}_{10 \rightarrow 25}$	$1.88275618 \times 10^{-6} \pm 2 \times 10^{-8}$	$\dot{M}_{11 \rightarrow 23}$	0.71 ± 0.03
$\dot{M}_{11 \rightarrow 24}$	0.151 ± 0.006	$\dot{M}_{12 \rightarrow 19}$	0.49 ± 0.02	$\dot{M}_{13 \rightarrow 12}$	0.34 ± 0.01
$\dot{M}_{19 \rightarrow 1}$	28.5 ± 0.3	$\dot{M}_{20 \rightarrow 3}$	10.14 ± 0.05	$\dot{M}_{21 \rightarrow 13}$	0.34 ± 0.01
$\dot{M}_{22 \rightarrow 11}$	0.86 ± 0.04	$\dot{M}_{23 \rightarrow 1}$	0.71 ± 0.03	$\dot{M}_{24 \rightarrow 12}$	0.151 ± 0.006
$\dot{M}_{25 \rightarrow 27}$	29.2 ± 0.4	$\dot{M}_{26 \rightarrow 21}$	0.34 ± 0.01	$\dot{M}_{26 \rightarrow 22}$	0.86 ± 0.04
$\dot{M}_{27 \rightarrow 2}$	29.2 ± 0.4				

Table 5.2: B8.0/W11.0 – Mass flow rates between the components

5.5 Additional issues

5.5.1 Getting enough power to explore the operation range

The compression unit runs at really high speed and consequently needs an inverter able to provide the needed electric power at the needed frequency. Finding such an inverter in the current inverter market is problematic, as high speed drive applications currently applies to lower electric powers than the one requested for this work¹⁷.

¹⁶ The mass flow rates in the AWP A-0.5/W20.7 OP are available in table F.15, page 123, and the mass flow rates in the BWP B8.0/W11.0 OP are available in table 5.2.

¹⁷ The twin-stage compression unit requires an electric power of 6 kW to be able to explore its whole operation range.

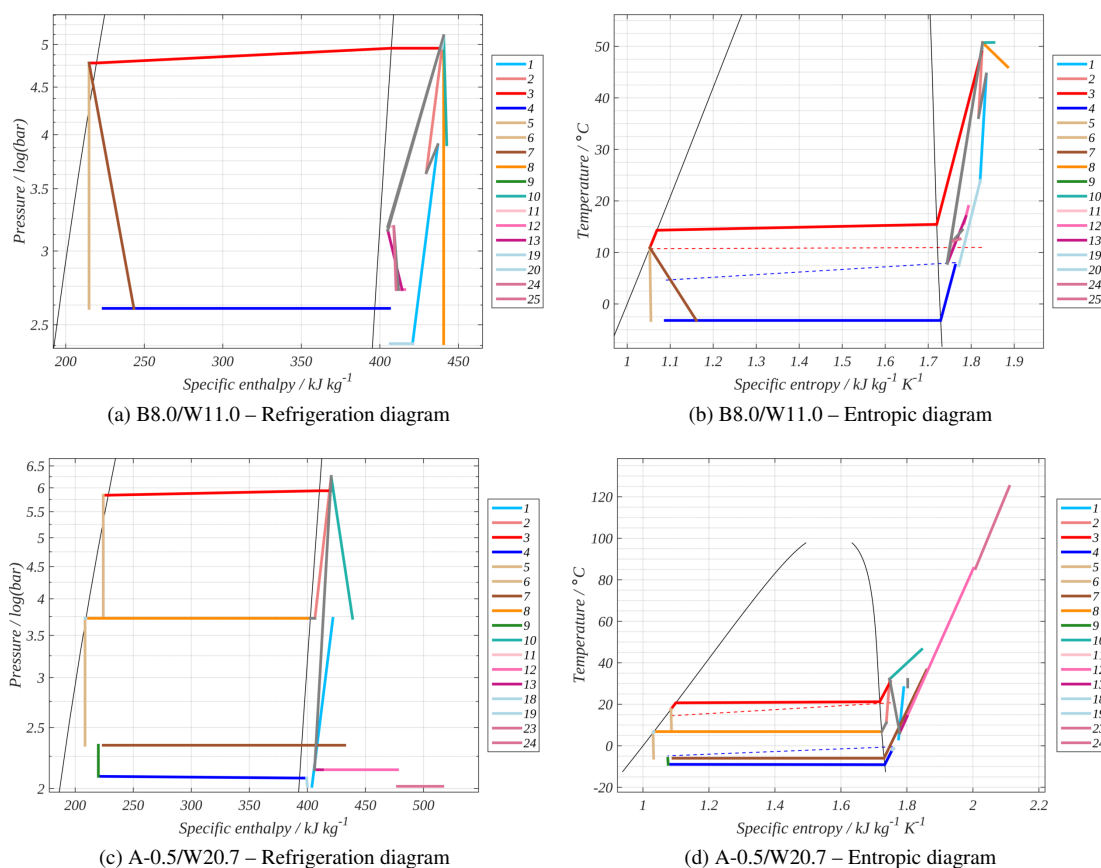


Figure 5.8: Thermodynamic diagrams of the BWP OP and of its closer AWP OP. Those diagrams are presented together in order to give comparison opportunities between the two prototypes behavior.

Name	Value / W	Name	Value / W
$\dot{E}_{1 \rightarrow 2}$	322 ± 5	$\dot{E}_{11 \rightarrow 1}$	791.8 ± 0.2
$\dot{E}_{12 \rightarrow 11}$	824.9 ± 0.2	$\dot{E}_{13 \rightarrow 12}$	844.3 ± 0.2
$\dot{E}_{14 \rightarrow 13}$	950.4 ± 0.2	\dot{E}_{cp1}	469 ± 5
\dot{E}_{cp2}	322 ± 5	$\dot{E}_{el \rightarrow 14}$	1118.1 ± 0.2
$\dot{Y}_{1 \rightarrow 2}$	$2.1718939 \times 10^{-5} \pm 1 \times 10^{-7}$	$\dot{Y}_{2 \rightarrow 10}$	$3.71518884 \times 10^{-6} \pm 2 \times 10^{-8}$
$\dot{Y}_{3 \rightarrow 15}$	2280 ± 25	$\dot{Y}_{11 \rightarrow 1}$	59.3 ± 0.3
$\dot{Y}_{11 \rightarrow 23}$	$6.315950126 \times 10^{-7} \pm 3 \times 10^{-9}$	$\dot{Y}_{11 \rightarrow 24}$	0.216 ± 0.001
$\dot{Y}_{12 \rightarrow 11}$	29.6 ± 0.3	$\dot{Y}_{13 \rightarrow 7}$	91.31 ± 0.02
$\dot{Y}_{13 \rightarrow 12}$	11.685 ± 0.002	$\dot{Y}_{14 \rightarrow at}$	167.72 ± 0.04
$\dot{Y}_{16 \rightarrow 4}$	1849 ± 53	$\dot{Y}_{20 \rightarrow at}$	10 ± 10
$\dot{Y}_{21 \rightarrow at}$	12 ± 9	$\dot{Y}_{22 \rightarrow at}$	30 ± 22
$\dot{Y}_{27 \rightarrow at}$	214 ± 189	\dot{Q}_{ax}	33.1 ± 0.3
\dot{Q}_{mo}	106.12 ± 0.02	\dot{Q}_{ra}	19.4 ± 0.3

Table 5.3: B8.0/W11.0 – Energy rates between the components

Consequently, the development of such an inverter showed up to be necessary and has been performed during an other thesis work [Rod, 2012]. Rod [2012, fig. 6.6, p. 118] has developed a prototype of inverter which could have been used to power the compression unit. This prototype needs to be developed further to become an industrial prototype, ready to used with the compression units [Rod, 2012, p. 134]. The experiments have not been performed with the inverter developed by Rod [2012], as it was still a device in development when the experiments were performed, and the heat pump prototypes had to cope with the limits of industrial inverters which were able to explore only partly the compression units operation domain. Even nowadays, the development and the industrialization of such an inverter is a critical issue for the power and control of the heat pumps equipped with such compression units [Rod, 2012, p. 135].

5.5.2 Setting the intermediate pressure to a chosen value while being in bypass-mode

When being in bypass-mode, the two compression stages have the same mass flow rate, as they are connected in series. If the flow is only partially bypassed, the overall pressure ratio is imposed by the temperature of the sources. As the compression unit rotor speed is a fixed parameter at a given time, the pressure level between the two compression stages is a consequence of the compressor maps and can not be set to a chosen value, as it can be seen in fig. 4.19, page 62, considering the same mass flow rate for the two stages. To be able to close the bypass circuit completely and to switch to normal-mode, the pressure level in the economizer has to be kept equal to the pressure level between the compression stages. If this is not done, the switch can occur nonetheless, but a pressure shock wave is likely to occur. Because of the check valve at the first compression stage outlet, the economizer pressure level can not be below the first stage outlet pressure level, even while being in bypass-mode. Consequently, the pressure level in the economizer is necessarily equal (or, eventually, slightly lower¹⁸) or higher than the pressure level at the second stage inlet. Consequently, the shock wave will be directed from the second compression stage to the economizer and will occur when the valve between components #9 and #2 opens. This counter flow shock wave can create instabilities in the flow inside the second stage impeller, damaging blades, or even produce a compression unit failure. In order to prevent such an event to occur, the pressure level in the economizer during bypass-mode needs to be kept at the pressure level of the second compression stage inlet. This also ensure that no flow comes in the economizer from the first compression stage. The pressure level in the economizer while being in bypass-mode is influenced only by the settings of the two expansion valves (considering that the economizer is properly insulated from the environment, and consequently adiabatic). As the role of the first stage expansion valve is to maintain a superheat value at the evaporator outlet, even during bypass-mode, the pressure level is maintained at the second compression stage inlet pressure level by the second stage expansion valve only. If the pressure level in the economizer decreases, the valve opens, and if it increases, the valve closes. If there is no more liquid in the economizer, the second stage expansion valve closes to a minimal value, in order to let the pressure level in the condenser increase (this is the second expansion valve starting-mode explained in section 4.6.7, page 63).

5.5.3 Pumping down of the evaporator

In a heat pump circuit, situations might happen where all the liquid refrigerant charge is located in the evaporator. This is the case, for example, when you fill in the refrigerant charge in gas phase being condensed at the coldest location of the circuit (the evaporator). It can also be the case if the expansion valves are not fully closed when the installation is shut down and if some time passes between the shutdown and the next start up (in case of power failure, for instance). With the bypass system used in the AWP¹⁹, it very difficult to pump down the liquid in the evaporator using the compression unit and the condenser, as it can be seen in fig. 5.9. Indeed, as the bypass circuits are either closed or open (no in-between position), and as there is no way to create a significant pressure difference in the heat pump main circuit without closing one of the bypass circuits (which would most likely results in moving the compression stages into the surge domain), all the liquid stays in the evaporator. The only way that could be found during the experimental campaign was to decrease the temperature at the condenser, allowing to close the second stage bypass circuit. With the second stage bypass circuit being closed, the pressure in the condenser increases and the flows starts to condense. Refrigerant is being transferred from the evaporator to the condenser. Some liquid finally arrives in the economizer and the cycle can be started.

¹⁸ Because of the pressure drop in the pipes, the pressure level at the inlet of the second compression stage can be slightly lower than the pressure level at the gas outlet of the economizer.

¹⁹ The layout of this bypass system can be seen in fig. 5.6a, page 73 and fig. 4.2, page 37.

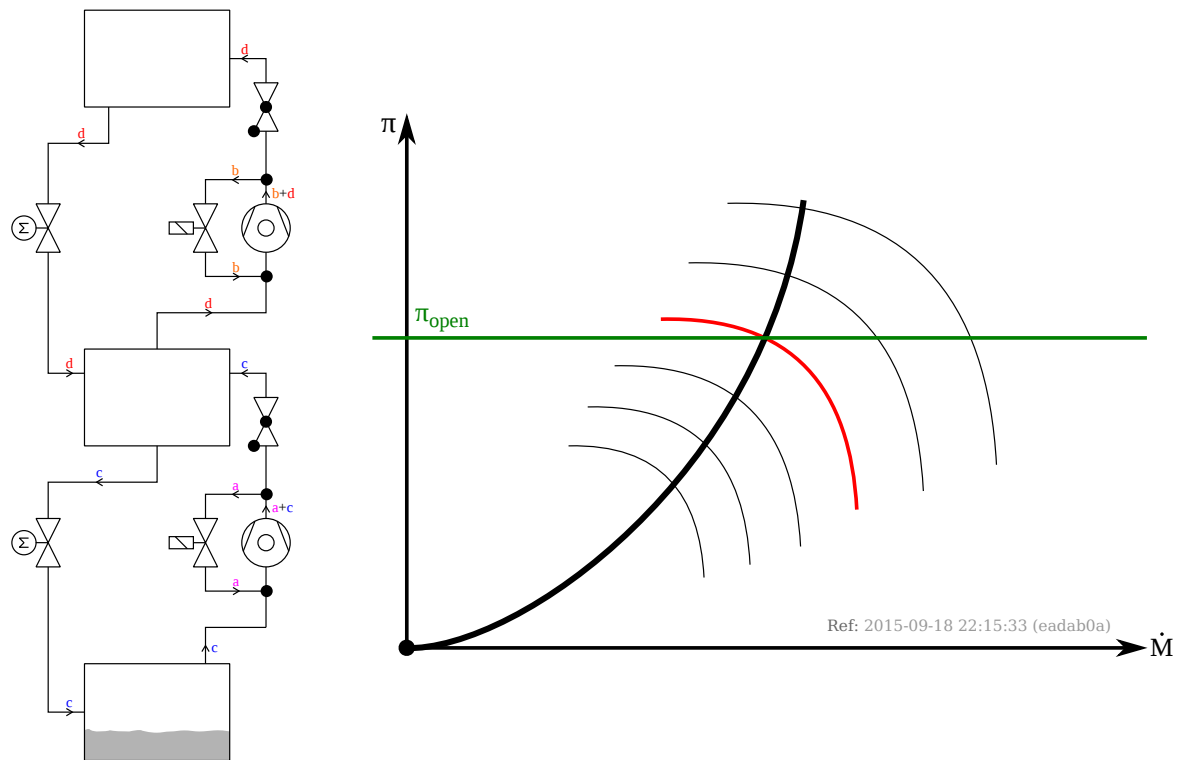


Figure 5.9: When a pump down of the evaporator is needed, most of the liquid refrigerant is in the evaporator and as there are almost no flow rate through the expansion valves (which are sized to be fed with liquid, not with gas), bypass circuits need to be open to avoid the surge domain. If the rotor speed is high enough, the pressure ratio reached allows to move the check valves and some flow enters the main heat pump circuit. Unfortunately, in order to increase the pressure ratio in the condenser (which would allow the condensation process to occur), the expansion valve needs to close, reducing further the flow. The flow is then very small, and almost no liquid is transferred from the evaporator to the condenser. Meanwhile, there is no flow in the motor cooling circuit as there is no liquid in the condenser, and the motor temperature increases. It increases even faster as the rotor speed is high. If a bypass circuit is closed, the compression stage not being bypassed enters the surge domain, as there is not enough mass flow circulating in the heat pump circuit and a too big pressure ratio. Consequently, if the temperature between the sources is not reduced, there is no way to start the heat pump in this situation. The new bypass system is expected to solve this situation.

With the new BWP bypass system, the flow of both compressors is bypassed together and pumping down the evaporator should not be a problem. Indeed, the bypass-mode transforms the twin-stage circuit in a single-stage circuit with the ability to bypass a chosen share of the flow, and consequently, it should solve the issue described above.

5.5.4 Keeping the loop clean

The prototypes tested use refrigerant with no lubricant. If there is lubricant in the refrigerant, it causes circuit pollution problems. If the pollution is not miscible in the refrigerant, it soaks the heat exchangers surfaces, which is likely to decrease their heat transfer efficiency [Bandarra Filho et al., 2009]. If it is miscible, it decreases the heat power capacity of the heat exchangers. Moreover, the lubricant is likely to enter the gas bearings and to fill their grooves, causing their failure and a crash of the compression unit. If grooves are polluted with oil, the probable consequence is a displacement of the shaft in the bearing gap, which is likely to cause a contact between the shaft surface and a fixed part. Touching a fixed surface at that speed is likely to create torsion forces far beyond the resistance of the shaft and to break it. Where the shaft touches a fixed part, the energy released locally is high enough to weld the surfaces together, damaging the unit massively. Such failures are critical events and usually imply the full replacement of the compression unit. Consequently, introducing clean refrigerant in the heat pump circuits is very important. However, industrial refrigerant cylinders often contain a small amount of synthetic lubricant oil. This lubricant oil is likely to pollute the prototype circuits if filled up with liquid refrigerant²⁰. If the prototypes are filled up with gas being condensed in one of the heat exchangers of the prototypes, some oil can also pollute the circuits, as the gas velocity is high enough to drag an oil film, flowing from the cylinder to the circuits of the prototypes, on the wall of the tubes. In order to prevent oil flowing from the cylinders to the circuits of the prototypes, gas velocity needs to be lower than a specific value which can be computed for each specific design case [Guo et al., 2011, Kesim et al., 2000]. As those design rules were not applied during the design of the heat pump prototypes, lubricant oil could be observed flowing slowly from the inlet of the first stage separator, at the top of the upper flange, to the outlet, also located at the top of the upper flange, flowing on the flange surface. The issue has been solved by adding a pipe and a deflector, inside the separator, in order to make the way from the inlet to the outlet less straightforward for the oil. The oil pollution problem has been solved by decreasing dramatically the speed of the filling up, doing it only with a low velocity, in gas phase. It is important to note that a polluted installation is very difficult to clean up, once it has been polluted. The synthetic lubricant oils have low viscosity and surface tension, so they fill every possible interstice. Consequently, every O-ring cavity, every welding, every scratch, every groove or heat exchanger improved surface is polluted and very difficult to clean up. The problem exists also with the AWP but extra care and protective behavior being applied from the start helped to prevent a too high amount of oil pollution in the circuits.

Evaporators act as oil separation devices and tend to collect a good share of the lubricant oil in the heat pumps circuits. In the AWP, the motor cooling chamber and the evaporator play such a role. In the BWP, only the evaporator plays such a role, since the refrigerant flows in the BWP motor cooling chamber from top to bottom, vertically, towards the evaporator. If the superheat value becomes too low at the evaporator outlet, refrigerant and oil might flow in the first stage separator, as illustrated in fig. 5.10, page 81. Synthetic oil is miscible in liquid R134a and will come with liquid refrigerant more or less proportionally. Mineral oil, which comes from polluting elements in the recovery cylinders, and from the vacuum pumps, stays on top of the refrigerant liquid level. When some liquid comes from the evaporator, the first amounts are heavily charged with mineral oil, if any is present in the heat pump circuits. Oil reflux from the vacuum pumps is something well known in the vacuum industry. Usually, this lubricant oil is gasified and trapped with a catalyzer containing active carbon. In the refrigeration industry, nothing is typically done against those refluxes. Most of the refrigeration professionals even ignore that such refluxes happen because they are not typically problematic for the conventional refrigeration technologies, which use lubrication, and consequently most of those professionals do not learn the existence of this issue during their certification programs.

²⁰ Liquid refrigerant can be filled in an installation either with a supply bottle put up-side-down, or with a recovery cylinder, using the liquid valve, which directly get liquid refrigerant from the bottom of the cylinder. The recovery cylinders may also contain mineral oil, leaked from the vacuum pump, for instance. This oil will be also transferred to the heat pump circuits, if they are filled up with liquid refrigerant.

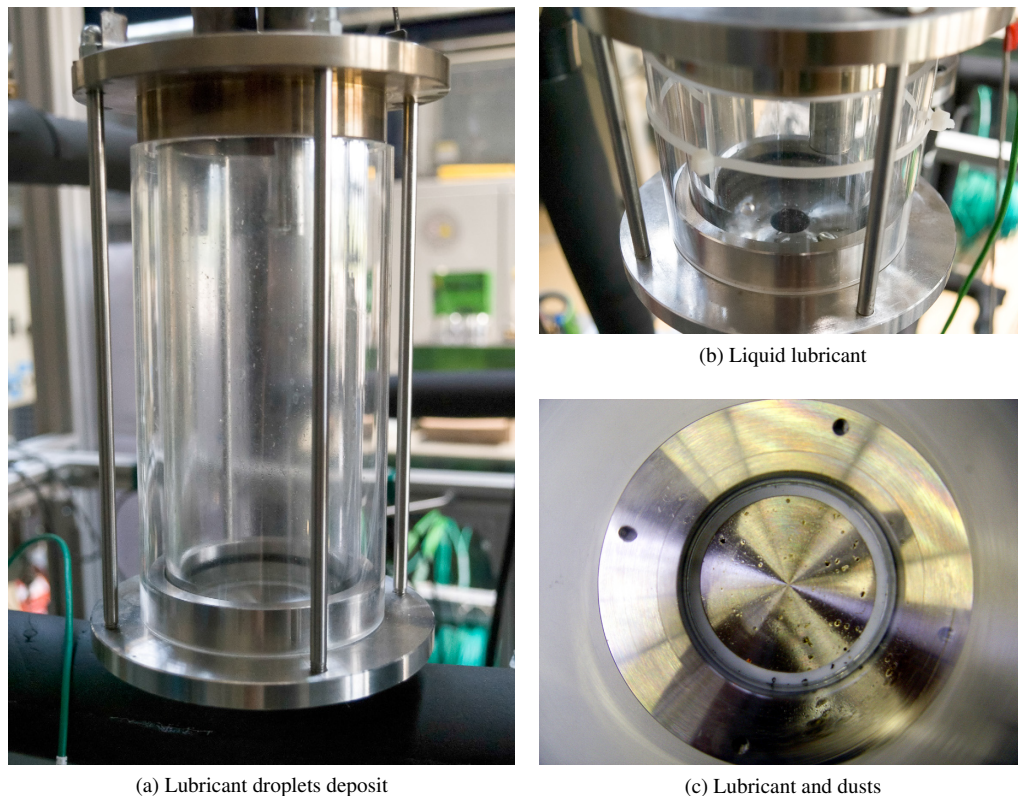


Figure 5.10: Lubricant pollution in the BWP

Bibliography

- E. P. Bandarra Filho, L. Cheng, and J. R. Thome. Flow boiling characteristics and flow pattern visualization of refrigerant/lubricant oil mixtures. *International Journal of Refrigeration*, 32(2):185–202, Mar. 2009. ISSN 0140-7007. doi:[10.1016/j.ijrefrig.2008.06.013](https://doi.org/10.1016/j.ijrefrig.2008.06.013).
- I. H. Bell, S. Quoilin, E. Georges, J. E. Braun, E. A. Groll, W. Travis Horton, and V. Lemort. A generalized moving-boundary algorithm to predict the heat transfer rate of counterflow heat exchangers for any phase configuration. *Applied Thermal Engineering*, 79(0):192 – 201, 2015. ISSN 1359-4311. doi:[10.1016/j.applthermaleng.2014.12.028](https://doi.org/10.1016/j.applthermaleng.2014.12.028).
- G.-L. Ding. Recent developments in simulation techniques for vapour-compression refrigeration systems. *International Journal of Refrigeration*, 30(7):1119 – 1133, 2007. ISSN 0140-7007. doi:[10.1016/j.ijrefrig.2007.02.001](https://doi.org/10.1016/j.ijrefrig.2007.02.001).
- Y. Guo, G. Zhang, J. Zhou, J. Wu, and W. Shen. The refrigerant oil return speed influence on the design of vertical U-Tube ground heat exchanger in the direct expansion ground-source heat pumps. In *Conference of 2011 Asia-Pacific Power and Energy Engineering Conference, APPEEC 2011, Wuhan, March, 25–28th*, 2011. ISBN 9781424462551. doi:[10.1109/APPEEC.2011.5749136](https://doi.org/10.1109/APPEEC.2011.5749136).
- S. C. Kesim, K. Albayrak, and A. Ileri. Oil entrainment in vertical refrigerant piping. *International Journal of Refrigeration*, 23(8):626 – 631, 2000. ISSN 0140-7007. doi:[10.1016/S0140-7007\(99\)00085-7](https://doi.org/10.1016/S0140-7007(99)00085-7).
- C. Rod. *Contributions au domaine de la commande des entraînements synchrones haute vitesse*. PhD thesis, EPFL, 2012. URL <http://dx.doi.org/10.5075/epfl-thesis-5352>.

Integration of the compression unit in heat pumps layouts

This chapter presents good practices and advanced proposals to integrate multistage oil-free variable-speed compression units in domestic heat pumps.

6.1 Topology

When using radial compressors, the vertical topology proposed with the Brine-Water twin-stage heat pump Prototype (BWP) and presented in fig. 5.1, page 69, is advised. Indeed, this vertical configuration makes the device more reliable and increases the chances to collect liquid refrigerant where it is functionally needed. Most companies building refrigeration circuits with radial compressors use a vertical topology. The chillers produced by Smardt¹ are good examples of this design rule. Additionally, using the vertical pipes leading to the compression unit to protect it against the possible presence of lubricant oil is a good practice. Those pipes can be sized following the sizing rules presented by Kesim et al. [2000] and Guo et al. [2011], in order to prevent that the oil is pulled up with the gas stream.

6.2 Electromagnetic perturbations

During the experiments performed with the Air-Water twin-stage heat pump Prototype (AWP), the signals of the sensors were sometimes polluted with high levels of interferences most probably caused by electro-magnetic perturbations, as the sensor cables were not shielded. Those electro-magnetic perturbations were probably generated by the three-phase inverter powering the motor of the compression unit at high frequencies. Those interferences disturb the calculation of essential values, like the superheat value. This is clearly visible in fig. 4.14d, page 56, where the superheat calculation is perturbed (high frequency, high amplitude signals) by the interferences on the pressure measurements, shown in fig. A.3, page 93. The temperature measurements are not disturbed by interferences in that specific case (as it can be seen in fig. 4.14b, page 56). This example highlights the importance to use shielded cables and grounded-sensors on this type of device.

¹ Smardt (<http://www.smardt.com/>) is a company that makes chillers powered by Turbocor compressors. It has been created by one of the founders of the Turbocor company, after the latter was bought by Danfoss. Turbocor compressors (<http://www.turbocor.com/>) are radial compressors rotating on magnetic bearings. They typically power refrigeration applications above 50kW, as the magnetic bearings technology is not easy to scale down below this value.

6.3 Gas bearings aeration circuits

The lowest possible pressure level is favored in the gas bearings cavity (component #12) in order to minimize the gas bearings losses. This implies that the outlet of the gas bearing aeration circuit is connected to the zone of the heat pump circuit where the pressure level is the lowest. The best location for this outlet is consequently in the first stage separator. The inlet of the gas bearings aeration circuit needs to be located in a zone with a higher pressure level. Two solutions exist: the inlet can be either at the intermediate pressure level, in the upper part of the economizer or between the economizer and the second compression stage inlet, or either at the higher pressure level, at the outlet of the second compression stage. In the BWP and the AWP, the safest solution has been favored: the gas bearings aeration circuit inlet is located after the second compression stage outlet. This is the safest option, since the expanded gas has a higher superheat value after its expansion, if the gas comes from the second compression stage outlet, and not from the economizer. With the pressure drop observed in the AWP aeration circuit, using the intermediate pressure level would have resulted in a lower mass flow rate, which would have been too low in the tested conditions. However, increasing the surface of the 0.5- μm -filter would certainly allow to take the aeration flow from the economizer. Taking this flow at the economizer would be better than taking it at the outlet of the second compression stage, even if it is less safe. Indeed, the aeration flow, if removed from the second compression stage flow rate, directly impacts the heat pump efficiency, as the flow rate leaving the second compression stage is used to provide the heating service. The level of superheat would decrease a little, but this could be compensated with integration strategies like the one exposed in section 6.5. Technically, it seems better to use the intermediate pressure level to provide the aeration circuit with gas, but economically, this needs to be studied further, as the filter surface and volume would increase, in order to compensate for the decrease of the pressure potential, in order to offer an equivalent flow rate. This will most probably have an influence on the price of the filter and consequently, on the price of the heat pump device.

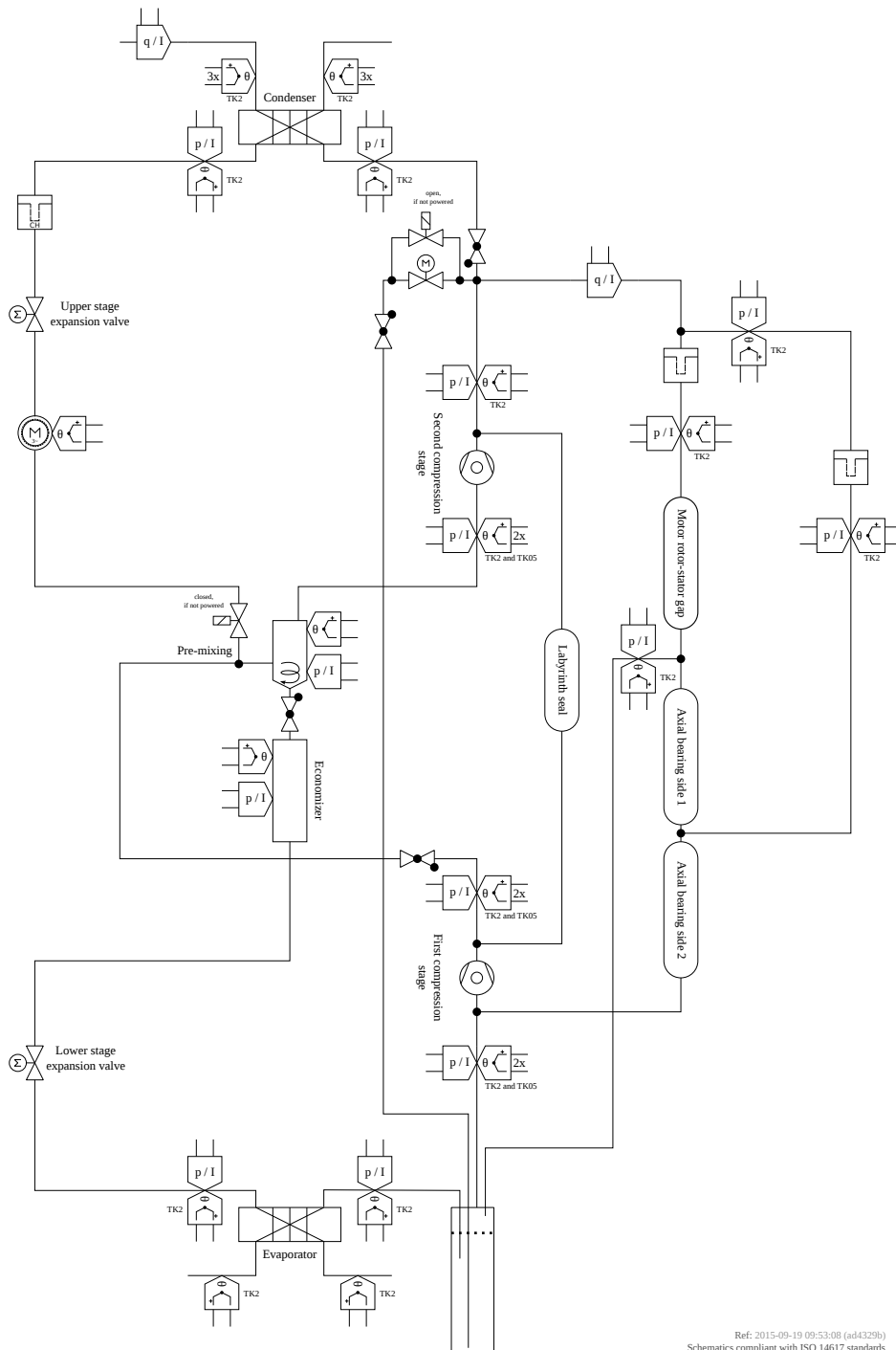
6.4 Towards new layouts with improved bypass circuits

The bypass circuits used in the AWP were far from being satisfactory, as detailed in section 4.5.2, page 48. The bypass circuit in the BWP apparently performs better but was penalized by the drawbacks highlighted in section 5.5.2, page 78. In order to solve this issue, a new bypass principle is proposed, based on the bypass system of the BWP. This bypass system is presented in figs. 6.1 and 6.2, adapted to each tested prototype. This new concept mixes the advantages observed with the economizer of the AWP, which was in two parts, and the compression stages in series of the BWP. Indeed, if the two parts of the economizer are connected with a check valve that opens if liquid weights on it (the spring of the check valve must be designed for this application, consequently), instead of a straight pipe, the component #27 of the BWP becomes unnecessary. When entering in bypass-mode, the solenoid valve above the pre-mixing device² shuts down the arrival of liquid in the economizer (during this bypass-mode, the second stage expansion valve must remain at least slightly open, in order to prevent a possible pressurization of the pipe between the expansion valve and the solenoid valve). The liquid in the economizer leaves into the lower part of the economizer (if there is any in the upper part). The two compressors are now in series. In this new bypass-mode, either the heat pump cycle is used, either the bypass circuit is used (in the contrary of the bypass circuit used in the BWP, which could be used in parallel of the heat pump circuit). If the pressure level in the lower part of the economizer changes and becomes higher than the pressure level in the upper part³, the check valve opens and the pressure level are equal again, which allows the check valve to close again. The pressure level in the upper part of the economizer is consequently higher or equal to the pressure level in the lower part. This bypass-mode can be used to start and stop the cycle, in case of emergency, but also to evaporate some liquid at the bottom of the first stage separator, as hot gas returns to the first separator with a high superheat value. As illustrated in figs. 6.1 and 6.2, the first separator can be equipped with a droplets deflector⁴, and the bypass circuit can deliver the vapor directly at the bottom of the economizer. Blowing vapor directly in the saturated liquid can result in the generation of mist. The author's advice is to use metallic mesh or foam to trap the droplets at the top of the deflector. This advice applies also to the concept presented in section 6.5. Bypass circuits need to open if there is a power failure. Consequently, that part of the circuit needs to be equipped with normally open valves.

² On the left of the economizer in figs. 6.1 and 6.2, p. 85.

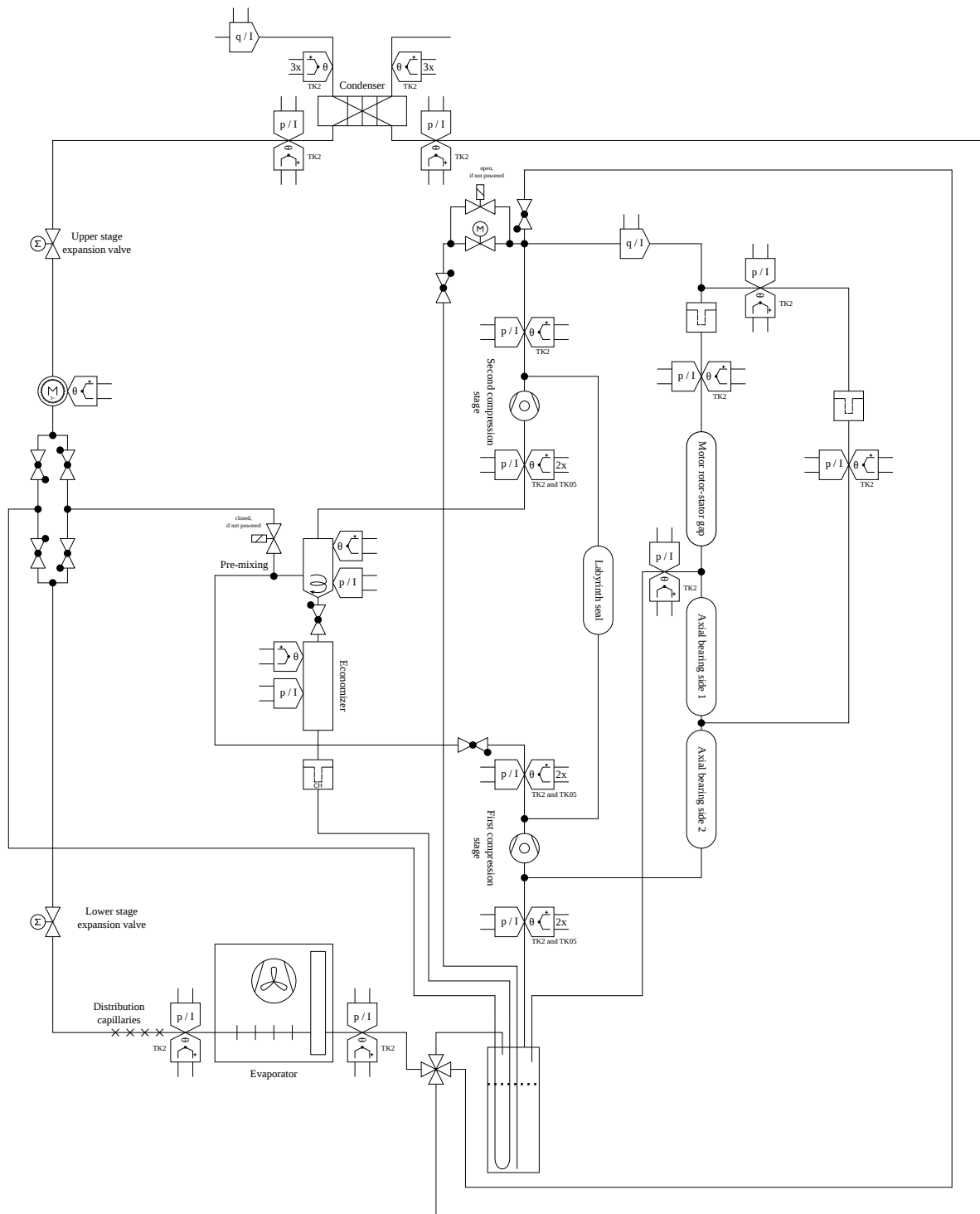
³ For instance, because some liquid evaporates, if there is any. The liquid could be used to cool down the power electronics, for instance, which would result in an evaporation of some of the fluid.

⁴ A part designed to avoid the suction of droplets in the first compression stage.



Ref: 2015-09-19 09:53:08 (ad4329b)
Schematics compliant with ISO 14617 standards

Figure 6.1: A new BWP layout



Ref: 2015-09-19 09:44:28 (b3559da)
Schematics compliant with ISO 14617 standards

Figure 6.2: A new AWP layout

6.5 Towards more integration, performance, and compactness

The compression unit may allow a more advanced integration with the heat pump cycle. This integration would lead to the creation of a compression module containing many components of the heat pump cycle. Indeed, the compression module can include easily the current compression unit, the whole economizer, and the separator. In this configuration, the only missing components to make a complete heat pump cycle would be the condenser, the evaporator, the dryer-filter, the two expansion valves, and the valves for the bypass and the gas bearings aeration circuit. The module could even include the inverter, cooled down by the liquid in the economizer. The inverter would be located directly below the economizer, in that case, and would benefit from passive convective cooling. As the inline components take almost no volume, the volume of the installation is made from the volume of the heat exchangers and of the compression unit module. As detailed in section 2.5.3, page 14, the volume of the heat exchangers can be decreased by taking advantage of the oil-free heat exchange technologies. The compression module presented in fig. 6.3 is about 50cm-wide and 30cm-high. This integration makes also the maintenance easier, as the technician can unplug the module, and replace it easily. Functionally, such integration brings many advantages:

The gas bearings aeration circuit outlet is not represented but can easily be located on the top of the compression unit.
The electric connection could be located on top of the economizer, or below it if the inverter is cooled down using liquid from the economizer.
Ref: 2015-10-18 19:59:39 (a81ba2f)

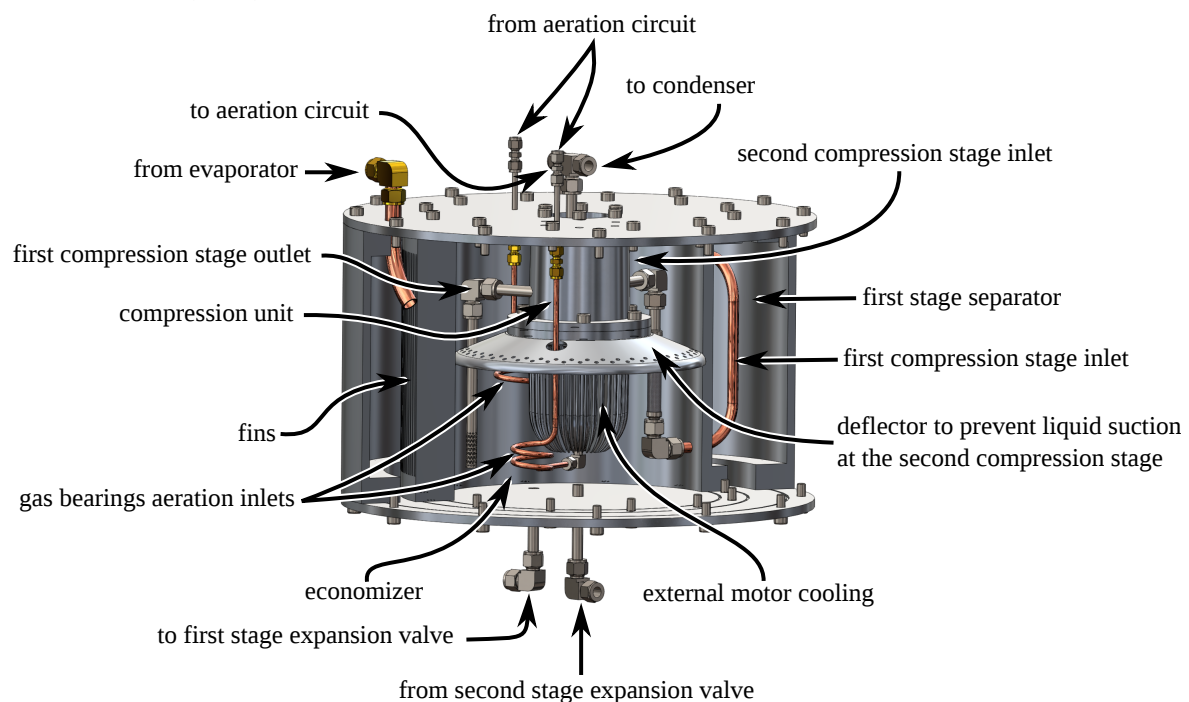


Figure 6.3: Proposal of an integrated topology for a future heat pump prototype

- There is no flow specifically taken to cool down the motor, so the heat pump controller is simpler. Moreover, the control itself is simpler, since the control of the heat pump depends on every flow rate in the cycle, as detailed in section 4.6.6, page 61.
- The check valves at the outlet of the compression stages can be integrated into the compression unit housing, like in scroll compressors.
- The bypass system can be integrated into the compression unit housing, like in the turbo-compressors in cars.

- The gas bearings aeration circuit is heated up by the liquid in the economizer. Indeed, the low pressure gas in the aeration circuit is colder than the liquid in the economizer. This protects the compression unit against the admission of droplets in the compression unit housing⁵.
- The gas from the evaporator would be heated up by the liquid in the economizer (the outside and the inside surfaces of the economizer can offer fins in order to increase the exchanges of heat energy), which protects the first compression stage against droplets. If droplets or liquid arrives in the first compression stage, it is evaporated by the heat transferred from the economizer.
- With an effective deflector, the gas coming from the first compression stage can be blown directly in the saturated liquid in the economizer. This ensures that the gas which enters the second compression stage is at a saturated state. Moreover, as the distance between the economizer and the inlet of the second compression stage is almost equal to zero, there is almost no risk of condensation.
- The flow coming from the second expansion valve, which is a two-phase flow, is ejected directly on the motor housing, which is equipped with fins, and the motor is effectively cooled down with a higher flow than in the current layouts, but with a stream at a higher temperature. This is a really good thing too, as condensation in the motor housing would be dangerous for the compression unit.

In order to secure the first tests, the author recommends the addition of a joule heater around the compression unit housing, in order to maintain the housing temperature above the condensation temperature in every situation. The author thinks that this heater will be optional in the final product, as strategies using the motor heat losses can be applied before the real starting of the heat pump cycle. For instance, when the installation is started, the cycle can stay in bypass-mode with a low rotor speed⁶ until the temperature in the motor housing and the bearings cavity is high enough. It would ensure that no liquid is present in the compression unit before the real starting up of the heat pump cycle.

Bibliography

- Y. Guo, G. Zhang, J. Zhou, J. Wu, and W. Shen. The refrigerant oil return speed influence on the design of vertical U-Tube ground heat exchanger in the direct expansion ground-source heat pumps. In *Conference of 2011 Asia-Pacific Power and Energy Engineering Conference, APPEEC 2011, Wuhan, March, 25–28th*, 2011. ISBN 9781424462551. doi:[10.1109/APPEEC.2011.5749136](https://doi.org/10.1109/APPEEC.2011.5749136).
- S. C. Kesim, K. Albayrak, and A. Ileri. Oil entrainment in vertical refrigerant piping. *International Journal of Refrigeration*, 23(8):626 – 631, 2000. ISSN 0140-7007. doi:[10.1016/S0140-7007\(99\)00085-7](https://doi.org/10.1016/S0140-7007(99)00085-7).

⁵ As the gas flow is limited in the gas bearings aeration circuits, condensation can occur, if the gas flow temperature is colder than the temperature around the pipe.

⁶ For instance, a rotor speed of 60 krpm would be appropriate.

Conclusion & outlook

7.1 Conclusion

The goal of this thesis work was to demonstrate that multistage oil-free variable-speed domestic heat pumps powered by twin-stage radial compressors are feasible and demonstrate a potential. The feasibility and the potential of the technology has been demonstrated successfully.

7.1.1 Feasible

The stable Operating Point (OP) detailed in section 4.4 and appendix F demonstrates that multistage oil-free variable-speed domestic heat pumps powered by twin-stage radial compressors are feasible. Particularly, the OP A-7.0/W35.6, presented in appendix F.3, demonstrates the feasibility of practical domestic heat pumps for space heating, as this OP is a typical domestic heat pump OP for floor heating technologies. Higher temperature lifts need to be reached and tested, but the concept has already demonstrated its feasibility.

7.1.2 Promising performance

The performance reached with the Air-Water twin-stage heat pump Prototype (AWP) is considered very promising and constitutes a breakthrough in the domain. The performance of the AWP, being a bit lower than the one of the devices on the market, with no optimization of the circuits design, with manual control, with a non-optimized refrigerant charge, and with numerous issues and avoidable energy losses, are already a great achievement. Accounting the numerous design issues which can be improved or solved in those first prototypes, the performance is really quite promising and shows that the radial compressors rotating on gas bearings technology is already a success.

7.1.3 Many challenging improvements needed

Of course, the challenges are still numerous before domestic heat pumps equipped with radial compressors reach the market. The issues to be solved are substantial but paths of solutions have already been offered all along the chapters relative to the prototypes. So far, no unsolvable problem could be identified. Control strategies have been proposed and need to be implemented and tested. Defrosting and cycle inversion are still important possible issues, but strategies and design of key components like the economizer and the first stage separator already answer to a good share of the potential problems that could occur. Consequently, what is most needed is further research, development, and tests to bring this technology to its full and greatest potential.

7.2 Perspectives

This thesis work opens the way to further development using the proposals presented in the previous chapter. A really integrated compression unit module can be developed, built, and tested, making more efficient, more compact, more silent heat pumps built with less raw material and using a lower refrigerant charge, a reality in the near future. Along with oil-free heat exchangers, this compression unit module is likely to bring further advances in the domestic heat pump field and in the oil-free refrigeration circuits as a whole.

Details about the Air-Water heat pump Prototype

A.1 Components

A.1.1 Evaporator

The evaporator of the Air-Water twin-stage heat pump Prototype (AWP) was the evaporator set in the housing provided by the industrial partner. That housing was provided with the heat exchangers and an operational air ducting and fan. Those components were kept and used to design the AWP.

A.1.2 Pipes and fittings

- Main vapor lines diameter: 3/4 inch;
- Liquid lines diameter: 1/2 inch;
- Liquid/Vapor lines: 1/2 inch;
- Auxiliary lines diameter (liquid, vapor, or both): 1/2 inch;

The fittings are Swagelok stainless steel fittings.

A.1.3 Valves

The AWP was equipped with stepper motor expansion valves. They were electric expansion valves, SER series from [Parker Sporlan](#).

A.1.4 Economizer

The economizer and the inlet separator have been designed using the maximum volume available in the housing.

- Highest height.
- Reasonable glass-tube diameter (pressure).

- Glass tubes, in order to build up onto the experience acquired with the Brine-Water twin-stage heat pump Prototype (BWP). Parallelepiped volumes and glass plates would have also been an option but this shape would have been more difficult to manufacture (assembly \Rightarrow seals \Rightarrow leaks), and less easy for subcooler and monitoring (more difficult to have a good view).

This duplication was the best solution available, since the space available in the housing was limited. Indeed, the glass-made part had already been designed using the biggest possible volume, with respect to the design constraints.

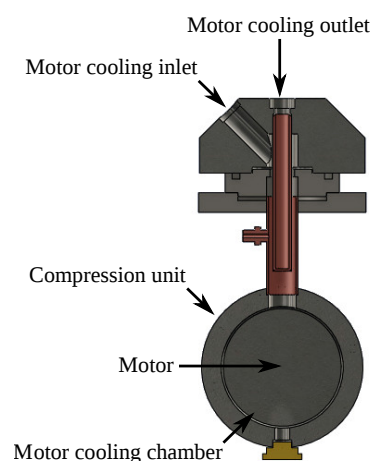
The integration of the economizer with the compression unit has increased the compactness and contributed to protect the second stage compressor against the appearance of condensates inside its inlet pipes, with cold outside conditions. The part which had been designed was expected to be made of cast aluminum or brass. Its shape can be seen on fig. 4.1b page 36. For the experiments performed in the EPFL laboratory, a conventional compression unit design, fitted with adaptation parts, has been used in order to preserve the compatibility of the manufactured units with the Brine-Water twin-stage heat pump Prototype (BWP) and the AWP. The tested unit can be seen on fig. 4.6, page 41.

A.1.5 Subcooler

The AWP is equipped with a subcooler heat exchanger. In heating mode, this heat exchanger cools down the saturated liquid refrigerant which leaves the economizer (component #8¹) using the superheated gas flow leaving the evaporator (component #4). The gas flow increases its temperature while the liquid flow gets subcooled. The liquid refrigerant flows in a pipe shaped as a coil while the gaseous refrigerant flows in the cylinder containing the coil. The inlet and the outlet of both circuits are on top of the cylinder.

A.1.6 Motor cooling chamber and circuit

The AWP was equipped with a pool-boiling motor cooling configuration.



Ref: 2015-09-18 22:15:33 (eadab0a)

Figure A.1: AWP motor cooling inlet/outlet (heating mode)

¹ The numbering and the labels of the components are detailed in fig. 4.2 and fig. 4.3, page 38.

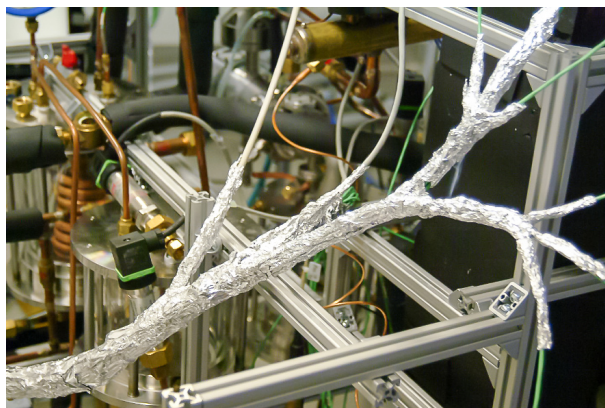


Figure A.2: Extra shielding of the AWP sensor cables

A.2 Sensors

The thermocouples are fastened on the pipes and fittings using Serto male union parts². Figure A.3 illustrates what is observed on fig. 4.14d.

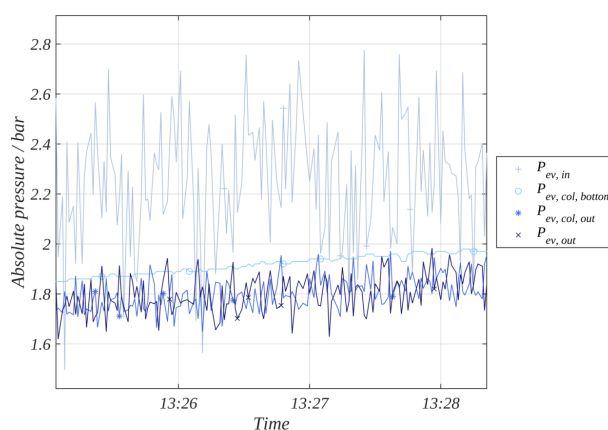


Figure A.3: Electro-magnetic perturbation of pressure sensors signals

Bibliography

Parker Sporlan. Electric expansion valves, SER series. URL <http://www.parker.com/literature/RAC%20Division%20-%20Europe/RAC%20Division%20-%20Europe%20-%20Literature%20Documents/Catalogues/100-20%20EEV-2%20Electric%20Expansion%20Valves/100-20%20EEV-2Low.pdf>. Accessed in June 2015.

² Serto male metric union M5 SO-41124-2-M5, for the 2mm-diameter-thermocouples. For the 0.5mm-diameter-thermocouples, an adaptation sleeve in Teflon, with conical shapes, was manufactured by the EPFL mechanical workshop. They were adapted, then, to the Serto fittings.

Details about the Brine-Water heat pump test-rig

B.1 History

The Brine-Water twin-stage heat pump Prototype (BWP) has been designed at the beginning of the thesis work, in 2009. It has been built between 2009 and 2010, and has been used to test compression units prototypes in 2010, 2011, and in 2013¹. In Autumn 2010, the prototype has been heavily modified, as detailed in appendix B.1.1. It has been modified again, between Winter 2012 and Autumn 2013, as detailed in appendix B.1.2.

During the tests performed between 2010 and 2011 with the BWP, the compression units from the *evo1*, the *evo2*, and the *evo3* design families failed and crashed, as the units from those design families were not ready for integration into heat pump circuits. The units from those families that have been tested have broken soon after the beginning of the tests because of design, manufacturing, balancing, or internal set up problems. Compression units from *evo3* have been tested in the BWP but failed to provide stable data or failed to develop pressure ratios or rotor speeds high enough to produce valuable datasets. Compression units from *evo3* were also breaking soon after the beginning of the test campaigns. The units from those 3 families failed before the production of any valuable datasets or stable Operating Point (OP). They had been tested first in a gas loop at the industrial partner facility, but most of the issues could only reveal themselves at production rotation speeds² and in real heat pump conditions. The compression unit mounted in the BWP for the experiment which has been used to generate the data presented in section 5.4 was the *cp101* unit, from the *evo4* design family³. This unit had been used successfully in a Brine/Water heat pump test-rig at a research center of the industrial partner and had been replaced there by a compression unit from the *evo5* design family⁴. The unit had been partially dismantled, checked, and cleaned up before being delivered to be mounted in the BWP⁵. Unfortunately the unit tested in the BWP in 2013, *cp101*, crashed soon after the beginning of the experiment. Before the crash of the unit, a small B8.0/W11.0 was being stabilized, with the compressors being connected in series, being bypassed with the new bypass system. The data collected during that experiment and their interpretation are presented in section 5.4. After the crash, the compression unit has been dismantled for analysis at the industrial partner research center. It turned out that one of the volute parts at the second compression stage had not been screwed back well in place during the maintenance operations performed before the delivery to EPFL. When the temperature rose in the circuits and in the compression unit, during the experiment, the thermal expansion phenomena have released the part, which has moved slightly, with the forces applied by the BWP pipes and circuits⁶. Consequently, the second stage impeller touched the

¹ See section 3.2, page 23 for details about the timeline of the experimental setups in the project.

² The compression units rotational speed in the industrial partner gas loops was limited due to technical limitations.

³ Details about the previous design families are given in appendix B.1, page 95.

⁴ The *evo5* design family was focused on improving the compression unit performance, which was below the models predictions due to different identified issues.

⁵ The front part, with volutes, impellers, and shaft, had been dismantled and mounted again. The motor cooling area had not been checked or dismantled.

⁶ The compression units mounting is hyperstatic due to the number of pipes and directions for the connections. This hyperstaticism creates forces when the pipes are plugged in. Moreover, the dilatation processes also influence the forces on the different parts.

volute, and a part of the labyrinth seal started to touch the impeller surface. The shaft being unbalanced by the increasing touching forces touched the set of radial bearings. The shaft broke between the radial and the set of axial bearings, due to the too big torsion forces in the shaft, and welded together with the set of radial bearings, due to the energy released by the touching.

B.1.1 First set of heavy modifications

The first set of heavy modifications was dedicated to the solving of topology issues related to weight measurements. In order to measure the weight of the heat exchangers and of the economizer, those components were connected to the main circuits using flexible pipes. In the very first version of the experimental setup, the flexible pipes were bent. When bent, the rigidity of the flexible pipes is a function notably of the pressure inside the pipe. As the pressure changes, the efforts on the flexible pipes change, which influences the value measured by the load cells. Additionally, as the flexible pipes were changing the efforts together, they were creating an hysteresis effect which could not be compensated with simple calibration processes.

B.1.2 Second set of heavy modifications

The second set of heavy modifications was dedicated to the adaptation of the BWP to the layout of the compression units of the *evo4* design family. Indeed, the BWP initial version had been designed with the inlets and outlets locations of the previous generations, *evo 1 to 3*. Those locations have changed between *evo3* and *evo4* because the industrial partner, responsible of the design and production of the devices, has redesigned the shapes and size of the volute parts. With the re-design specifications and needs, it was not possible to keep the same location for the inlets and outlets. The design of the flanges have also changed between *evo3* and *evo4*, in order for the compression unit to be mounted on the BWP or the Air-Water twin-stage heat pump Prototype (AWP) indifferently. This change of layout has implied to modify heavily the piping of the upper part of the BWP. Those piping modifications also included the new version of the bypass circuits⁷, of the motor cooling circuit⁸, and of the gas bearings aeration circuits⁹. Originally, those circuits design were close to the circuits tested in the AWP. Taking in account the issues encountered with the AWP, those circuits have been modified in the BWP before restarting the tests in 2013.

B.2 Gas bearings aeration circuit layout and topology

The Gas bearings aeration circuit starts at the top of the installation, at the second stage compression outlet. Physically, it starts downstream of the beginning of the bypass circuit, before the check valve. The beginning of the gas bearings aeration circuit is on the bypass circuit, at its very beginning, because of space constraints. The latter has to start very close from the main vapor line. Indeed, as there is no flow in the bypass circuit in normal operation, the gaseous refrigerant in this circuit may condensate. Locating the inlet of the gas bearings aeration circuit close to the main vapor line avoids that such condensate flows into the aeration circuit. The gas bearing aeration circuit goes down with a 1/2-inch pipe. The circuit is made of a manual needle valve which allows to decrease the flow if needed¹⁰, and a coriolis mass flow meter. Then, the circuit was divided into two branches of approximately the same lengths and level of sophistication, in order to get approximately the same level of pressure drop in the two branches. The two branches of 1/2-inch diameter were equipped with a 0.5mm-filter able to be bypassed by the opening of a solenoid valve. Close to the unit, the diameter of the circuits is reduced to 1/4 of inch. The two branches inject cold gas at the bottom of the compression unit and at the top of the axial bearing. An electric resistance coiled around the circuit pipe downstream of the mass flow meter allows to be sure to inject superheated cold gas in the compression unit, as no liquid droplet is allowed there. The electric resistance is used as a security measure. The gas flow leaves the compression unit with a significant superheat value and is injected through a 1/2-inch pipe into the first stage separator.

⁷ See section 5.2.2, page 71 for details about the evolution of the BWP bypass circuits.

⁸ See section 5.2.3, page 71 for details about the evolution of the BWP motor cooling circuit.

⁹ See section 5.2.4, page 72 for details about the evolution of the BWP gas bearings aeration circuit.

¹⁰ As explained in section 4.6.4, page 59, the flow in the gas bearings aeration circuit was already low, so this valve was not fully open during the experiments.

B.3 Motor cooling circuit layout and topology

The BWP motor cooling circuit starts at the bottom of the prototype, at the condenser outlet. The circuit is made of a co-tubular counter-flow heat exchanger¹¹ connected to a coriolis mass flow meter. This part of the circuit is horizontal. Then the circuit is vertical and includes a check valve located close to the top of the installation made with 1/2-inch pipes. An expansion valve is located at the top of the vertical pipe. The liquid refrigerant flow is expanded in the valve and the gas/liquid flow resulting from the expansion is spread down into the motor cooling chamber about 50 cm below, through a 1/2-inch pipe. This portion of the circuit includes a sight glass. The motor is cooled down by the 2-phase refrigerant flow which is then collected at the evaporator inlet through a 1/2-inch pipe.

B.4 Components

B.4.1 Expansion devices

BWP inline components could be mounted in parallel in the prototype housing in order to test the behavior of the cycle or of the prototype control strategies using different type of devices. Figure B.1 shows an example of inline components mounted in parallel with an expansion valve test section. The 3 valves mounted in the section are a stepper motor valve, a manual micrometer valve, and a regular thermostatic expansion valve.

The valves that could have been tested were (sorted from the cheaper to the more expensive):

- Manual micrometer valves¹², or capillary tubes;
- Thermostatic expansion valves¹³;
- Sporlan stepper-motor valves¹⁴;
- Siemens modulating refrigerant valves with magnetic actuator¹⁵.

B.4.2 Load cells

The BWP is equipped with load cells to measure the weight of the elements which are subject to variations of their overall refrigerant vapor quality. Those weighted components are the condenser, the evaporator, and the economizer.

These load cells were intended to be used to study the migration of the liquid refrigerant through the circuits during the experiments and to correlate the amount of liquid present in the different areas of the heat pump circuits with the external heat and electric powers and temperature conditions.

B.4.3 First stage separator

The first stage separator is a tank able to contain a significant share of the refrigerant charge filled in the circuits. Its role is to prevent the suction of liquid refrigerant in the first compression stage. This situation happens in case of a prototype control failure, as the superheat at the evaporator outlet is too low. In this case, mist, or even a 2-phase flow with flowing liquid, can enter the separator. This liquid refrigerant comes in with lubricant oils¹⁶, if some are present in the evaporator.

¹¹ A heat exchanger from the HE series, HE 1.5, from [Danfoss Refrigeration & Air Conditioning \[a\]](#).

¹² Bellows-sealed metering valves, BM series from [Swagelok](#), for instance.

¹³ Thermostatic expansion valves, TUA series, from [Danfoss Refrigeration & Air Conditioning \[c\]](#), for instance.

¹⁴ Electric expansion valves, SER series, from [Parker Sporlan](#), for instance.

¹⁵ Electric expansion valves for fluorinated refrigerants, AKV series, from [Danfoss Refrigeration & Air Conditioning \[b\]](#), for instance.

¹⁶ Mineral or synthetic lubricant oil, and dusts and particules can accumulate in the evaporator, as detailed in section 5.5.4, page 80.



Figure B.1: BWP expansion devices section

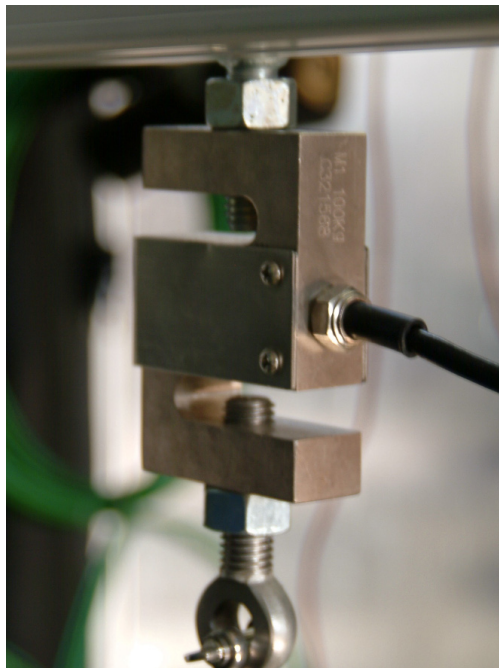


Figure B.2: Load cell used in the BWP

The separator of the BWP is glass-made, in order to allow an easy monitoring of the flow characteristics at the critical location of the circuit during the experiments. Both inlets and outlets are located at the top of the cylinder, as it is important to be able to separate this device to clean it up, which is far easier to do if all the connections with the circuits are on one side. An improvement of this design would be to add a flange at the bottom of the device, in order to be able to open the separator for cleaning operations without dismantling the glass part, which is particularly fragile and vulnerable to scratches and shocks. This flange would be equipped with a Schrader valve in order to be able to purge the separator. In the same spirit, it is a good practice to add a Schrader valve on the pipe at the lowest connection with the evaporator, in order to be able to purge the lubricant oil which accumulates in the evaporator (if the installation has been polluted, of course).



Figure B.3: First stage compressor inlet separator, in the BWP

The glass cylinder has a diameter of 10 cm and a thickness of 5 mm. It would have been interesting to increase the cylinder internal diameter, but it would have resulted in a much thicker cylinder and it would have been quite dangerous to work with the prototype. Indeed, the cylinder being pressurized, having glass parts is dangerous as a defect of the glass or its damaging during a maintenance operation could result in a glass pressure vessel explosion during an experiment. Consequently, the diameter and the thickness need to be kept at reasonable values.

B.4.4 Economizer

The BWP economizer is not glass-made, like the AWP economizer, as it was made from a stainless steel cylinder with flanges and a glass window which was part of a previous experimental setup. The big size of the cylinder was an advantage and allowed safer conditions during the experiments. Moreover, the oversizing of the parts, for the conditions of use in the BWP, was also an advantage regarding personal security. The initial parts have been modified for the needs of the prototype:

- A glass insert has been added on top of the upper flange, in order to light the inside of the cylinder.
- An inlet for the gas/liquid flow has been added at 2/3 of the height of the cylinder. This inlet is oriented towards the bottom of the cylinder with an angle of 10 degrees with the horizontal level.
- Appropriate fittings have been fastened at the 3 inlets/outlets of the economizer.

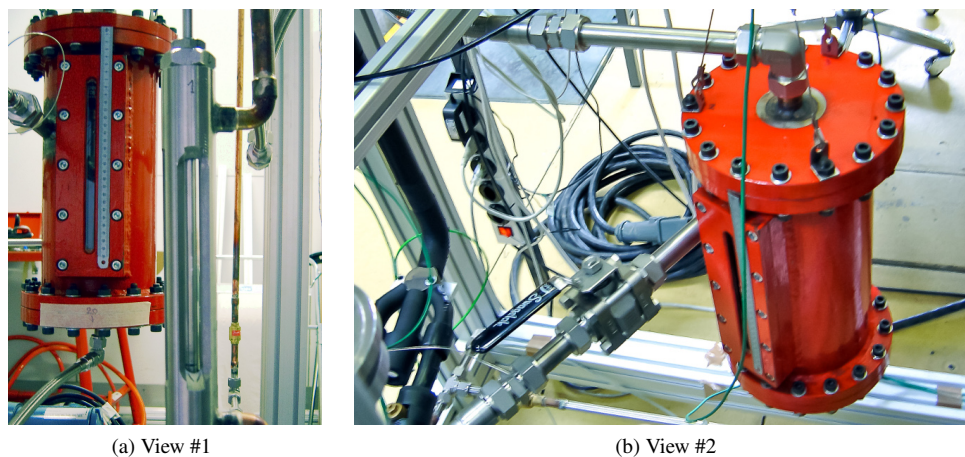


Figure B.4: Economizer of the BWP

B.4.5 Pipes and fittings

This topic is detailed in appendix A.1.2, page 91.

Bibliography

- Danfoss Refrigeration & Air Conditioning. HE 0.5 - HE 8.0 heat exchanger, solder connections, a. URL <http://products.danfoss.com/productrange/list/refrigeration/line-components/line-components-commercial-refrigeration/he-heat-exchangers/he-0-5-8-0-solder-connections/>. Accessed on June 2015.
- Danfoss Refrigeration & Air Conditioning. Electric expansion valves for fluorinated refrigerants, AKV series, b. URL <http://products.danfoss.com/productrange/refrigeration/electronically-operated-valves/akv-expansion-valves-for-fluorinated-refrigerants/>. Accessed on June 2015.
- Danfoss Refrigeration & Air Conditioning. Thermostatic expansion valves, TUA / TUAE series, c. URL <http://products.danfoss.com/productrange/refrigeration/thermostatic-expansion-valves/thermostatic-expansion-valves-exchangeable-orifice/tua-tuae/>. Accessed on June 2015.
- Parker Sporlan. Electric expansion valves, SER series. URL <http://www.parker.com/literature/RAC%20Division%20-%20Europe/RAC%20Division%20-%20Europe%20-%20Literature%20Documents/Catalogues/100-20%20EEV-2%20Electric%20Expansion%20Valves/100-20%20EEV-2Low.pdf>. Accessed in June 2015.
- Swagelok. Metering bellows valves catalog, BM series. URL <http://www.swagelok.com/downloads/webcatalogs/EN/MS-01-23.PDF>. Accessed on June 2015.

Equations set for the simple example

This appendix presents the set of equations for the model presented in section 3.4.3, page 25 with fig. 3.1, page 26. The known variables are:

- | | | | | |
|------------------------------------|----------------|----------------|----------------|----------------|
| • $\dot{E}_{el \rightarrow 02}$ | • $h_{01,in}$ | • $h_{03,in}$ | • $h_{06,in}$ | • $h_{07,in}$ |
| • $\dot{M}_{07 \rightarrow house}$ | • $h_{01,out}$ | • $h_{03,out}$ | • $h_{06,out}$ | • $h_{07,out}$ |

Specific enthalpies are determined from pressure and temperature measurements. There is one guessed parameter f_{01} which defines the proportion of the flow that leaves the component 3 to enter component 2 and component 5.

$$\begin{aligned}
 \dot{M}_{house \rightarrow 07} &= \dot{M}_{07 \rightarrow house} \\
 \dot{Y}_{03 \rightarrow 07} &= \dot{M}_{07 \rightarrow house} (h_{07,out} - h_{07,in}) \\
 \dot{M}_{01 \rightarrow 03} &= \frac{\dot{Y}_{03 \rightarrow 07}}{h_{03,in} - h_{03,out}} \\
 \dot{M}_{04 \rightarrow 01} &= \dot{M}_{01 \rightarrow 03} \\
 \dot{M}_{03 \rightarrow 02} &= f_{01} \dot{M}_{01 \rightarrow 03} && 0 < f_{01} < 1 && (C.1) \\
 \dot{M}_{03 \rightarrow 05} &= (1 - f_{01}) \dot{M}_{01 \rightarrow 03} \\
 \dot{M}_{02 \rightarrow 04} &= \dot{M}_{03 \rightarrow 02} \\
 \dot{M}_{05 \rightarrow 04} &= \dot{M}_{03 \rightarrow 05} \\
 \dot{M}_{04 \rightarrow 01} &= \dot{M}_{02 \rightarrow 04} + \dot{M}_{05 \rightarrow 04} \\
 \dot{E}_{02 \rightarrow 01} &= \dot{M}_{01 \rightarrow 03} (h_{01,out} - h_{01,in}) \\
 h_{02,in} &= h_{03,out} \\
 h_{04,out} &= h_{01,in} \\
 h_{05,in} &= h_{03,out} \\
 h_{05,out} &= h_{05,in}
 \end{aligned}$$

\dot{Y}_{mot} is equal to $(1 - \eta_{mot}) \dot{E}_{el \rightarrow 02}$, but η_{mot} is unknown. \dot{Y}_{mot} is also equal to $\dot{M}_{03 \rightarrow 02} (h_{02,out} - h_{02,in})$, but $h_{02,out}$ is unknown. We have also the equation $\dot{M}_{05 \rightarrow 04} h_{05,out} + \dot{M}_{02 \rightarrow 04} h_{02,out} - \dot{M}_{04 \rightarrow 01} h_{04,out} + \dot{Y}_{06 \rightarrow 04} = 0$ where $h_{02,out}$ and $\dot{Y}_{06 \rightarrow 04}$ are unknown. $\dot{Y}_{06 \rightarrow 04}$ needs to be determined.

$$\begin{aligned} \dot{Y}_{06 \rightarrow 04} &= \dot{Y}_{03 \rightarrow 07} - \dot{E}_{el \rightarrow 02} \\ h_{02, out} &= \frac{\dot{M}_{04 \rightarrow 01} h_{04, out} - \dot{Y}_{06 \rightarrow 04} - \dot{M}_{05 \rightarrow 04} h_{05, out}}{\dot{M}_{02 \rightarrow 04}} \\ \dot{Y}_{mot} &= \dot{M}_{03 \rightarrow 02} (h_{02, out} - h_{02, in}) \\ \eta_{mot} &= \frac{\dot{E}_{el \rightarrow 02} - \dot{Y}_{mot}}{\dot{E}_{el \rightarrow 02}} \\ h_{04, in} &= \dot{M}_{05 \rightarrow 04} h_{05, out} + \dot{M}_{02 \rightarrow 04} h_{02, out} \\ \dot{M}_{06 \rightarrow env} &= \frac{\dot{Y}_{06 \rightarrow 04}}{h_{06, in} - h_{06, out}} \\ \dot{M}_{env \rightarrow 06} &= \dot{M}_{06 \rightarrow env} \end{aligned}$$

Energy balances used for the objective function. $eb_{01 \text{ to } 05}$ values, defined need to be equal to zero.

$$eb_{01} = \dot{E}_{02 \rightarrow 01} + \dot{M}_{04 \rightarrow 01} h_{04, out} - \dot{M}_{01 \rightarrow 03} h_{01, out} \quad (C.2)$$

$$eb_{02} = \dot{E}_{el \rightarrow 02} + \dot{M}_{03 \rightarrow 02} h_{03, out} - \dot{M}_{02 \rightarrow 04} h_{02, out} - \dot{E}_{02 \rightarrow 01} \quad (C.3)$$

$$eb_{03} = \dot{M}_{01 \rightarrow 03} h_{01, out} - \dot{M}_{03 \rightarrow 05} h_{03, out} - \dot{Y}_{03 \rightarrow 07} - \dot{M}_{03 \rightarrow 02} h_{03, out} \quad (C.4)$$

$$eb_{04} = \dot{M}_{05 \rightarrow 04} h_{05, out} - \dot{M}_{04 \rightarrow 01} h_{04, out} + \dot{Y}_{06 \rightarrow 04} + \dot{M}_{02 \rightarrow 04} h_{02, out} \quad (C.5)$$

$$eb_{05} = \dot{M}_{03 \rightarrow 05} h_{03, out} - \dot{M}_{05 \rightarrow 04} h_{05, out} \quad (C.6)$$

AWP model set of equations

This appendix presents the set of equations for the model presented in section 4.3, page 45 with fig. 4.3, page 38. The known variables are:

- $\dot{E}_{el \rightarrow 14}$
- $\dot{M}_{02 \rightarrow 26}$
- $\dot{M}_{03 \rightarrow 07}$
- $\dot{M}_{17 \rightarrow 15}$
- $Cp_{15,in}$
- $Cp_{15,out}$
- $h_{02,out}$
- $h_{03,in}$
- $h_{03,out}$
- $h_{04,in}$
- $h_{04,out}$
- $h_{18,out}$
- $h_{20,out}$
- $h_{21,out}$
- $h_{25,out}$
- $h_{26,out}$
- $h_{28,out}$
- η_{in}
- η_{rad}
- η_{axi}

η_{mot} is set directly by the solver. η_{rad} and η_{axi} are determined with the gas bearings losses model implemented by Schiffmann [2008].

$$\dot{Y}_{03 \rightarrow 15} = \dot{M}_{17 \rightarrow 15} (Cp_{15,out} T_{15,out} - Cp_{15,in} T_{15,in}) \quad (D.1)$$

$$\dot{M}_{20 \rightarrow 03} = \frac{\dot{Y}_{03 \rightarrow 15}}{h_{03,in} - h_{03,out}} \quad (D.2)$$

$$\dot{M}_{03 \rightarrow 05} = \dot{M}_{20 \rightarrow 03} - \dot{M}_{03 \rightarrow 07} \quad (D.3)$$

$$\dot{M}_{05 \rightarrow 08} = \dot{M}_{03 \rightarrow 05}$$

$$\dot{M}_{02 \rightarrow 20} = \dot{M}_{03 \rightarrow 05}$$

$$\dot{M}_{07 \rightarrow 09} = \dot{M}_{03 \rightarrow 07}$$

$$\dot{M}_{26 \rightarrow 21} = f_{01} \dot{M}_{02 \rightarrow 26}$$

$$0 < f_{01} < 1$$

$$\dot{Y}_{21 \rightarrow at} = \dot{M}_{26 \rightarrow 21} (h_{26,out} - h_{21,out})$$

$$\dot{Y}_{26 \rightarrow at} = \dot{M}_{02 \rightarrow 26} (h_{02,out} - h_{26,out})$$

$$\dot{Y}_{20 \rightarrow at} = \dot{M}_{20 \rightarrow 03} (h_{02,out} - h_{20,out})$$

$$\dot{Y}_{14 \rightarrow at} = (1 - \eta_{in}) \dot{E}_{el \rightarrow 14}$$

$$\dot{Y}_{16 \rightarrow at} = \dot{Y}_{03 \rightarrow 15} - \dot{E}_{el \rightarrow 14} - \dot{Y}_{21 \rightarrow at} - \dot{Y}_{26 \rightarrow at} - \dot{Y}_{20 \rightarrow at} - \dot{Y}_{14 \rightarrow at} \quad (D.4)$$

$$\dot{M}_{09 \rightarrow 04} = \frac{\dot{Y}_{16 \rightarrow at}}{h_{04,out} - h_{04,in}} \quad (D.5)$$

$$\dot{M}_{06 \rightarrow 09} = \dot{M}_{09 \rightarrow 04} - \dot{M}_{07 \rightarrow 09} \quad (D.6)$$

$$\dot{M}_{19 \rightarrow 06} = \dot{M}_{06 \rightarrow 09}$$

$$\dot{M}_{08 \rightarrow 19} = \dot{M}_{06 \rightarrow 09}$$

$$\dot{M}_{04 \rightarrow 18} = \dot{M}_{09 \rightarrow 04}$$

$$\dot{M}_{18 \rightarrow 22} = \dot{M}_{04 \rightarrow 18}$$

$$\begin{aligned}
\dot{M}_{26 \rightarrow 13} &= (1 - f_{01}) \dot{M}_{02 \rightarrow 26} \\
\dot{M}_{21 \rightarrow 12} &= \dot{M}_{26 \rightarrow 21} \\
\dot{M}_{13 \rightarrow 12} &= \dot{M}_{26 \rightarrow 13} \\
\dot{M}_{12 \rightarrow 24} &= \dot{M}_{13 \rightarrow 12} + \dot{M}_{21 \rightarrow 12} \\
\dot{M}_{24 \rightarrow 11} &= \dot{M}_{12 \rightarrow 24} \\
\dot{M}_{11 \rightarrow 23} &= f_{02} \dot{M}_{24 \rightarrow 11} & 0 < f_{02} < 1 \\
\dot{M}_{11 \rightarrow 22} &= (1 - f_{02}) \dot{M}_{24 \rightarrow 11} \\
\dot{M}_{23 \rightarrow 29} &= \dot{M}_{11 \rightarrow 22} + \dot{M}_{18 \rightarrow 22} \\
\dot{M}_{29 \rightarrow 01} &= \dot{M}_{23 \rightarrow 29} + \dot{M}_{22 \rightarrow 29} \\
\dot{M}_{01 \rightarrow 25} &= \dot{M}_{29 \rightarrow 01} \\
\dot{M}_{cp1} &= \dot{M}_{01 \rightarrow 25}
\end{aligned}$$

The mass flow rate in the second stage impeller \dot{M}_{cp2} is equal to $\dot{M}_{02 \rightarrow 26} + \dot{M}_{02 \rightarrow 20} + \dot{M}_{02 \rightarrow 10}$. $\dot{M}_{02 \rightarrow 10}$, the leakage flow rate through the labyrinth seal, needs to be determined.

$$\dot{M}_{02 \rightarrow 10} = f_{03} \dot{M}_{cp2} \quad 0 < f_{03} < 1 \quad (\text{D.7})$$

With the introduction of the parameter f_{03} in eq. (D.7), the equation of the mass flow rate in the second stage impeller \dot{M}_{cp2} is equal to $f_{03} \dot{M}_{cp2} + \dot{M}_{02 \rightarrow 26} + \dot{M}_{02 \rightarrow 20}$. Which implies the eq. (D.8).

$$\begin{aligned}
\dot{M}_{cp2} &= \frac{\dot{M}_{02 \rightarrow 20} + \dot{M}_{02 \rightarrow 26}}{1 - f_{03}} & (\text{D.8}) \\
\dot{M}_{10 \rightarrow 25} &= \dot{M}_{02 \rightarrow 10} \\
\dot{M}_{25 \rightarrow 27} &= f_{04} (\dot{M}_{10 \rightarrow 25} + \dot{M}_{01 \rightarrow 25}) & 0 < f_{04} < 1 \\
\dot{M}_{25 \rightarrow 08} &= (1 - f_{04}) (\dot{M}_{10 \rightarrow 25} + \dot{M}_{01 \rightarrow 25}) \\
\dot{M}_{27 \rightarrow 28} &= \dot{M}_{25 \rightarrow 27} \\
\dot{M}_{08 \rightarrow 28} &= \dot{M}_{25 \rightarrow 08} + \dot{M}_{05 \rightarrow 08} - \dot{M}_{08 \rightarrow 19} \\
\dot{M}_{28 \rightarrow 02} &= \dot{M}_{27 \rightarrow 28} + \dot{M}_{08 \rightarrow 28} \\
\dot{E}_{14 \rightarrow 13} &= \eta_{in} \dot{E}_{el \rightarrow 14}
\end{aligned}$$

If we consider the energy balance on component #13, we get $\dot{E}_{14 \rightarrow 13} - \dot{E}_{13 \rightarrow 12} - \dot{Y}_{13 \rightarrow 12} - \dot{Y}_{13 \rightarrow 07} + \dot{M}_{26 \rightarrow 13} h_{26,out} - \dot{M}_{13 \rightarrow 12} h_{13,out} = 0$. $h_{13,out}$ is unknown and needs to be determined. In order to do this, $\dot{E}_{13 \rightarrow 12}$, $\dot{Y}_{13 \rightarrow 12}$ and $\dot{Y}_{13 \rightarrow 07}$ are required.

$$\begin{aligned}
\dot{E}_{13 \rightarrow 12} &= \eta_{mot} \dot{E}_{14 \rightarrow 13} & 0 < \eta_{mot} < 1 \\
\dot{Y}_{13 \rightarrow 12} &= f_{05} (1 - \eta_{mot}) \dot{E}_{14 \rightarrow 13} & 0 < f_{05} < 1 \\
\dot{Y}_{13 \rightarrow 07} &= f_{06} (1 - \eta_{mot}) \dot{E}_{14 \rightarrow 13} & 0 < f_{06} < 1 \\
h_{13,out} &= \frac{\dot{E}_{14 \rightarrow 13} - \dot{E}_{13 \rightarrow 12} - \dot{Y}_{13 \rightarrow 12} - \dot{Y}_{13 \rightarrow 07} + \dot{M}_{26 \rightarrow 13} h_{26,out}}{\dot{M}_{13 \rightarrow 12}} & (\text{D.9})
\end{aligned}$$

According to their definitions, we observe that f_{05} and f_{06} have to respect the relation $0 < f_{05} + f_{06} < 1$.

If we consider the energy balance on component #12, we get $\dot{E}_{13 \rightarrow 12} + \dot{Y}_{13 \rightarrow 12} + \dot{M}_{13 \rightarrow 12} h_{13,out} + \dot{M}_{21 \rightarrow 12} h_{21,out} - \dot{M}_{12 \rightarrow 24} h_{12,out} - \dot{E}_{12 \rightarrow 11} - \dot{Y}_{12 \rightarrow 11} = 0$. $\dot{E}_{12 \rightarrow 11}$ and $h_{12,out}$ need to be determined to get $\dot{Y}_{12 \rightarrow 11}$.

$$\begin{aligned}
\dot{E}_{12 \rightarrow 11} &= \eta_{ra} \dot{E}_{13 \rightarrow 12} \\
T_{12, out} &= (1 + f_{07}) T_{13, out} && \Rightarrow h_{12, out} \\
\dot{Y}_{12 \rightarrow 11} &= \dot{E}_{13 \rightarrow 12} + \dot{Y}_{13 \rightarrow 12} + \dot{M}_{13 \rightarrow 12} h_{13, out} \\
&\quad + \dot{M}_{21 \rightarrow 12} h_{21, out} - \dot{M}_{12 \rightarrow 24} h_{12, out} - \dot{E}_{12 \rightarrow 11}
\end{aligned} \tag{D.10}$$

If we consider the energy balance on component #11, we get $\dot{Y}_{12 \rightarrow 11} + \dot{E}_{12 \rightarrow 11} - \dot{E}_{11 \rightarrow 01} - \dot{Y}_{11 \rightarrow 01} - \dot{Y}_{11 \rightarrow 23} - \dot{Y}_{11 \rightarrow 24} - \dot{M}_{11 \rightarrow 23} h_{11, out} + \dot{M}_{24 \rightarrow 11} h_{24, out} - \dot{M}_{11 \rightarrow 22} h_{11, out} = 0$. In order to determine $h_{11, out}$, the variables $\dot{E}_{11 \rightarrow 01}$, $h_{24, out}$, $\dot{Y}_{11 \rightarrow 24}$, $\dot{Y}_{11 \rightarrow 01}$ and $\dot{Y}_{11 \rightarrow 23}$ need to be determined.

$$\begin{aligned}
\dot{E}_{11 \rightarrow 01} &= \eta_{axi} \dot{E}_{12 \rightarrow 11} \\
T_{24, out} &= (1 + f_{08}) T_{12, out} && \Rightarrow h_{24, out}
\end{aligned}$$

The energy balance on component #24 gives us the equation $\dot{M}_{12 \rightarrow 24} h_{12, out} - \dot{M}_{24 \rightarrow 11} h_{24, out} + \dot{Y}_{11 \rightarrow 24} = 0$, which gives eq. (D.11).

$$\dot{Y}_{11 \rightarrow 24} = \dot{M}_{24 \rightarrow 11} h_{24, out} - \dot{M}_{12 \rightarrow 24} h_{12, out} \tag{D.11}$$

$$\begin{aligned}
\dot{Y}_{11 \rightarrow 01} &= f_{09} \dot{Y}_{12 \rightarrow 11} && 0 < f_{09} < 1 \\
\dot{Y}_{11 \rightarrow 23} &= f_{10} \dot{Y}_{12 \rightarrow 11} && 0 < f_{10} < 1
\end{aligned} \tag{D.12}$$

$$h_{11, out} = \frac{\dot{Y}_{12 \rightarrow 11} + \dot{E}_{12 \rightarrow 11} - \dot{E}_{11 \rightarrow 01} - \dot{Y}_{11 \rightarrow 01} - \dot{Y}_{11 \rightarrow 23} - \dot{Y}_{11 \rightarrow 24} + \dot{M}_{24 \rightarrow 11} h_{24, out}}{\dot{M}_{11 \rightarrow 23} + \dot{M}_{11 \rightarrow 22}}$$

The energy balance on component #22 gives the equation $\dot{M}_{18 \rightarrow 22} h_{18, out} + \dot{M}_{11 \rightarrow 22} h_{11, out} - \dot{M}_{22 \rightarrow 29} h_{22, out} = 0$, which gives eq. (D.13).

$$h_{22, out} = \frac{\dot{M}_{18 \rightarrow 22} h_{18, out} + \dot{M}_{11 \rightarrow 22} h_{11, out}}{\dot{M}_{22 \rightarrow 29}} \tag{D.13}$$

The energy balance on components #29 and #23 give the balance equations $\dot{M}_{22 \rightarrow 29} h_{22, out} + \dot{M}_{23 \rightarrow 29} h_{23, out} - \dot{M}_{29 \rightarrow 01} h_{29, out} = 0$ and $\dot{M}_{11 \rightarrow 23} h_{11, out} + \dot{Y}_{11 \rightarrow 23} - \dot{M}_{23 \rightarrow 29} h_{23, out} = 0$ which give eq. (D.14).

$$h_{29, out} = \frac{\dot{M}_{22 \rightarrow 29} h_{22, out} + \dot{M}_{23 \rightarrow 29} h_{23, out}}{\dot{M}_{29 \rightarrow 01}} \tag{D.14}$$

The energy balance on component #1 gives the equation $\dot{E}_{11 \rightarrow 01} - \dot{M}_{01 \rightarrow 25} h_{01, out} + \dot{M}_{29 \rightarrow 01} h_{29, out} + \dot{Y}_{11 \rightarrow 01} - \dot{Y}_{01 \rightarrow 02} - \dot{E}_{01 \rightarrow 02} = 0$.

We need a relationship between $T_{01, out}$ and $T_{25, out}$, in order to go further. This results in the equation eq. (D.15). Knowing $T_{01, out}$ gives access to $h_{01, out}$ through a computation with REFPROP.

$$T_{01, out} = \frac{T_{25, out}}{1 + f_{11}} \tag{D.15} \quad 0 < f_{11} < 1$$

Equation (D.15) allows to write the equation $\dot{E}_{11 \rightarrow 01} - \dot{E}_{01 \rightarrow 02} = \dot{M}_{cp1} (h_{01,out} - h_{29,out})$, which gives eq. (D.16).

$$\begin{aligned}\dot{E}_{01 \rightarrow 02} &= \dot{E}_{11 \rightarrow 01} - \dot{M}_{cp1} (h_{01,out} - h_{29,out}) \\ \dot{Y}_{01 \rightarrow 02} &= \dot{E}_{11 \rightarrow 01} - \dot{M}_{01 \rightarrow 25} h_{01,out} + \dot{M}_{29 \rightarrow 01} h_{29,out} + \dot{Y}_{11 \rightarrow 01} - \dot{E}_{01 \rightarrow 02}\end{aligned}\quad (\text{D.16})$$

The energy balance on component #02 gives the equation $-\dot{M}_{02 \rightarrow 10} h_{02,out} - \dot{M}_{02 \rightarrow 26} h_{02,out} - \dot{M}_{02 \rightarrow 20} h_{02,out} + \dot{M}_{28 \rightarrow 02} h_{28,out} - \dot{Y}_{02 \rightarrow 10} + \dot{Y}_{01 \rightarrow 02} + \dot{E}_{01 \rightarrow 02} = 0$, which gives eq. (D.17).

$$\begin{aligned}\dot{Y}_{02 \rightarrow 10} &= \dot{Y}_{01 \rightarrow 02} + \dot{E}_{01 \rightarrow 02} - \dot{M}_{02 \rightarrow 10} h_{02,out} - \dot{M}_{02 \rightarrow 26} h_{02,out} - \dot{M}_{02 \rightarrow 20} h_{02,out} + \dot{M}_{28 \rightarrow 02} h_{28,out} \\ \dot{Y}_{19 \rightarrow 18} &= \dot{M}_{18 \rightarrow 22} (h_{18,out} - h_{04,out})\end{aligned}\quad (\text{D.17})$$

Bibliography

- J. Schiffmann. *Integrated design, optimization and experimental investigation of a direct driven turbocompressor for domestic heat pumps*. PhD thesis, Swiss Federal Institute of Technology - Lausanne, 2008. URL <http://dx.doi.org/10.5075/epfl-thesis-4126>.

BWP model set of equations

This appendix presents the set of equations for the model presented in section 5.3, page 74 with fig. 5.7, page 75. The known variables are:

- | | | | | |
|---------------------------------|---------------------------------|----------------|----------------|----------------|
| • $\dot{M}_{el \rightarrow 14}$ | • $\dot{M}_{09 \rightarrow 06}$ | • $h_{03,in}$ | • $h_{06,in}$ | • $h_{21,out}$ |
| • $\dot{M}_{02 \rightarrow 26}$ | • η_{inv} | • $h_{03,out}$ | • $h_{06,out}$ | • $h_{22,out}$ |
| • $\dot{M}_{03 \rightarrow 05}$ | • $h_{02,in}$ | • $h_{04,in}$ | • $h_{12,out}$ | • $h_{25,out}$ |
| • $\dot{M}_{03 \rightarrow 07}$ | • $h_{02,out}$ | • $h_{04,out}$ | • $h_{19,out}$ | • $h_{26,out}$ |

η_{mot} is set directly by the solver. η_{rad} and η_{axi} are determined with the gas bearings losses model implemented by Schiffmann [2008].

$$\dot{M}_{05 \rightarrow 09} = \dot{M}_{03 \rightarrow 05}$$

$$\dot{M}_{06 \rightarrow 04} = \dot{M}_{09 \rightarrow 06}$$

$$\dot{M}_{07 \rightarrow 04} = \dot{M}_{03 \rightarrow 07}$$

$$\dot{M}_{20 \rightarrow 03} = \dot{M}_{03 \rightarrow 05} + \dot{M}_{03 \rightarrow 07}$$

$$\dot{M}_{02 \rightarrow 20} = \dot{M}_{20 \rightarrow 03}$$

$$\dot{M}_{04 \rightarrow 19} = \dot{M}_{06 \rightarrow 04} + \dot{M}_{07 \rightarrow 04}$$

$$\dot{M}_{26 \rightarrow 22} = f_{01} \dot{M}_{02 \rightarrow 26}$$

$$0 < f_{01} < 1$$

$$\dot{M}_{26 \rightarrow 21} = (1 - f_{01}) \dot{M}_{02 \rightarrow 26}$$

$$\dot{M}_{21 \rightarrow 13} = \dot{M}_{26 \rightarrow 21}$$

$$\dot{M}_{22 \rightarrow 11} = \dot{M}_{26 \rightarrow 22}$$

$$\dot{M}_{13 \rightarrow 12} = \dot{M}_{21 \rightarrow 13}$$

$$\dot{M}_{11 \rightarrow 23} = f_{02} \dot{M}_{22 \rightarrow 11}$$

$$0 < f_{02} < 1$$

$$\dot{M}_{11 \rightarrow 24} = (1 - f_{02}) \dot{M}_{22 \rightarrow 11}$$

$$\dot{M}_{23 \rightarrow 01} = \dot{M}_{11 \rightarrow 23}$$

$$\dot{M}_{24 \rightarrow 12} = \dot{M}_{11 \rightarrow 24}$$

$$\dot{M}_{12 \rightarrow 19} = \dot{M}_{24 \rightarrow 12} + \dot{M}_{13 \rightarrow 12}$$

$$\dot{M}_{27 \rightarrow 02} = \frac{(\dot{M}_{02 \rightarrow 26} + \dot{M}_{02 \rightarrow 20})}{1 - f_{03} - f_{04}}$$

$$\dot{M}_{02 \rightarrow 10} = f_{03} \dot{M}_{27 \rightarrow 02}$$

$$0 < f_{03} + f_{04} < 1$$

$$\dot{M}_{02 \rightarrow 08} = f_{04} \dot{M}_{27 \rightarrow 02}$$

$$\dot{M}_{10 \rightarrow 25} = \dot{M}_{02 \rightarrow 10}$$

$$\dot{M}_{08 \rightarrow 19} = \dot{M}_{02 \rightarrow 08}$$

$$\dot{M}_{19 \rightarrow 01} = \dot{M}_{12 \rightarrow 19} + \dot{M}_{04 \rightarrow 19} + \dot{M}_{08 \rightarrow 19}$$

$$\dot{M}_{01 \rightarrow 25} = \dot{M}_{19 \rightarrow 01} + \dot{M}_{23 \rightarrow 01}$$

$$\dot{M}_{25 \rightarrow 27} = \dot{M}_{27 \rightarrow 02}$$

$$\dot{E}_{14 \rightarrow 13} = \eta_{inv} \dot{E}_{el \rightarrow 14}$$

$$\dot{Y}_{14 \rightarrow atm} = (1 - \eta_{inv}) \dot{E}_{el \rightarrow 14}$$

$$\dot{E}_{13 \rightarrow 12} = \eta_{mot} \dot{E}_{14 \rightarrow 13}$$

$$\dot{Q}_{mot} = (1 - \eta_{mot}) \dot{E}_{14 \rightarrow 13}$$

$$\dot{Y}_{13 \rightarrow 07} = f_{05} \dot{Q}_{mot}$$

$$0 < f_{05} < 1$$

$$\dot{Y}_{13 \rightarrow 12} = f_{06} \dot{Q}_{mot}$$

$$0 < f_{06} < 1$$

$$\dot{E}_{12 \rightarrow 11} = \eta_{rad} \dot{E}_{13 \rightarrow 12}$$

$$\dot{E}_{11 \rightarrow 01} = \eta_{axi} \dot{E}_{12 \rightarrow 11}$$

$$\dot{Q}_{rad} = (1 - \eta_{rad}) \dot{E}_{13 \rightarrow 12}$$

$$\dot{Q}_{axi} = (1 - \eta_{axi}) \dot{E}_{12 \rightarrow 11}$$

$$\dot{Y}_{12 \rightarrow 11} = f_{07} (\dot{Q}_{rad} + \dot{Y}_{13 \rightarrow 12})$$

$$0 < f_{07} < 1$$

$$\dot{Y}_{11 \rightarrow 01} = f_{08} (\dot{Q}_{axi} + \dot{Y}_{12 \rightarrow 11})$$

$$0 < f_{08} < 1$$

$$\dot{Y}_{11 \rightarrow 23} = f_{09} (\dot{Q}_{axi} + \dot{Y}_{12 \rightarrow 11})$$

$$0 < f_{09} < 1$$

$$\dot{Y}_{11 \rightarrow 24} = f_{10} (\dot{Q}_{axi} + \dot{Y}_{12 \rightarrow 11})$$

$$0 < f_{10} < 1$$

$$\dot{Y}_{01 \rightarrow 02} = f_{11} \dot{Y}_{11 \rightarrow 01}$$

$$0 < f_{11} < 1$$

$$\dot{Y}_{02 \rightarrow 10} = f_{12} \dot{Y}_{01 \rightarrow 02}$$

$$0 < f_{12} < 1$$

$$\dot{E}_{01 \rightarrow 02} = \dot{M}_{27 \rightarrow 02} (h_{02,out} - h_{02,in})$$

$$\dot{E}_{cp2} = \dot{E}_{01 \rightarrow 02}$$

$$\dot{E}_{cp1} = \dot{E}_{11 \rightarrow 01} - \dot{E}_{cp2}$$

$$h_{10,out} = \frac{\dot{M}_{02 \rightarrow 10} h_{02,out} + \dot{Y}_{02 \rightarrow 10}}{\dot{M}_{10 \rightarrow 25}}$$

$$h_{01,out} = \frac{\dot{M}_{25 \rightarrow 27} h_{25,out} - \dot{M}_{10 \rightarrow 25} h_{10,out}}{\dot{M}_{01 \rightarrow 25}}$$

$$h_{01,in} = h_{01,out} - \frac{\dot{E}_{cp1}}{\dot{M}_{01 \rightarrow 25}}$$

$$h_{23,out} = \frac{(\dot{M}_{19 \rightarrow 01} + \dot{M}_{23 \rightarrow 01}) h_{01,in} - \dot{M}_{19 \rightarrow 01} h_{19,out}}{\dot{M}_{23 \rightarrow 01}}$$

$$h_{07,out} = \frac{\dot{Y}_{13 \rightarrow 07} + \dot{M}_{03 \rightarrow 07} h_{03,out}}{\dot{M}_{07 \rightarrow 04}}$$

$$h_{19,in} = \frac{\dot{M}_{12 \rightarrow 19} h_{12,out} + \dot{M}_{04 \rightarrow 19} h_{04,out}}{\dot{M}_{12 \rightarrow 19} + \dot{M}_{04 \rightarrow 19}}$$

$$h_{13,out} = \frac{\dot{M}_{21 \rightarrow 13} h_{21,out} + \dot{E}_{14 \rightarrow 13} - \dot{E}_{13 \rightarrow 12} - \dot{Y}_{13 \rightarrow 12} - \dot{Y}_{13 \rightarrow 07}}{\dot{M}_{13 \rightarrow 12}}$$

$$h_{11,out} = \frac{\dot{M}_{22 \rightarrow 11} h_{22,out} + \dot{Y}_{12 \rightarrow 11} + \dot{E}_{12 \rightarrow 11} - \dot{Y}_{11 \rightarrow 01} - \dot{E}_{11 \rightarrow 01} - \dot{Y}_{11 \rightarrow 23} - \dot{Y}_{11 \rightarrow 24}}{\dot{M}_{11 \rightarrow 23} + \dot{M}_{11 \rightarrow 24}}$$

$$h_{23,in} = h_{11,out}$$

$$h_{24,in} = h_{11,out}$$

$$\begin{aligned}
h_{04,in} &= \frac{\dot{M}_{07 \rightarrow 04} h_{07,out} + \dot{M}_{06 \rightarrow 04} h_{06,out}}{\dot{M}_{07 \rightarrow 04} + \dot{M}_{06 \rightarrow 04}} \\
h_{24,out} &= \frac{\dot{M}_{11 \rightarrow 24} h_{11,out} + \dot{Y}_{11 \rightarrow 24}}{\dot{M}_{24 \rightarrow 12}} \\
h_{25,in} &= \frac{\dot{M}_{10 \rightarrow 25} h_{10,out} + \dot{M}_{01 \rightarrow 25} h_{01,out}}{\dot{M}_{10 \rightarrow 25} + \dot{M}_{01 \rightarrow 25}} \\
h_{12,in} &= \frac{\dot{M}_{13 \rightarrow 12} h_{13,out} + \dot{M}_{24 \rightarrow 12} h_{24,out}}{\dot{M}_{13 \rightarrow 12} + \dot{M}_{24 \rightarrow 12}} \\
\dot{Y}_{03 \rightarrow 15} &= (\dot{M}_{03 \rightarrow 05} + \dot{M}_{03 \rightarrow 07}) (h_{03,in} - h_{03,out}) \\
\dot{Y}_{16 \rightarrow 04} &= (\dot{M}_{06 \rightarrow 04} + \dot{M}_{07 \rightarrow 04}) (h_{04,out} - h_{04,in}) \\
h_{03,out} &= h_{05,in} = h_{05,out} \\
h_{06,out} &= h_{06,in} \\
\dot{Y}_{20 \rightarrow atm} &= \dot{M}_{02 \rightarrow 20} h_{02,out} - \dot{M}_{20 \rightarrow 03} h_{20,out} \\
\dot{Y}_{21 \rightarrow atm} &= \dot{M}_{26 \rightarrow 21} h_{26,out} - \dot{M}_{21 \rightarrow 13} h_{21,out} \\
\dot{Y}_{22 \rightarrow atm} &= \dot{M}_{26 \rightarrow 22} h_{26,out} - \dot{M}_{22 \rightarrow 11} h_{22,out} \\
\dot{Y}_{27 \rightarrow atm} &= \dot{M}_{25 \rightarrow 27} h_{25,out} - \dot{M}_{27 \rightarrow 02} h_{27,out}
\end{aligned}$$

Bibliography

- J. Schiffmann. *Integrated design, optimization and experimental investigation of a direct driven turbocompressor for domestic heat pumps*. PhD thesis, Swiss Federal Institute of Technology - Lausanne, 2008. URL <http://dx.doi.org/10.5075/epfl-thesis-4126>.

Experimental data

F.1 A-6.8/W31.3 - 170 krpm

This test has been performed on May 11th 2012, between 13:24:18 and 13:27:18.

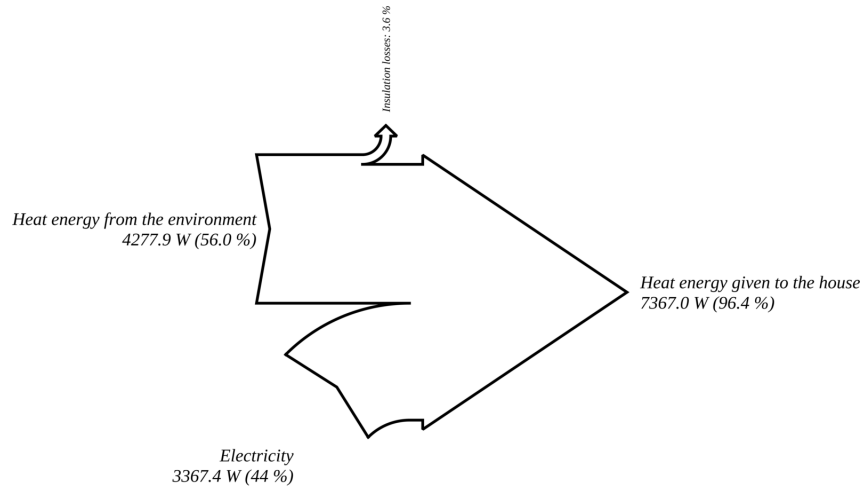


Figure F.1: A-6.8/W31.3 – Sankey diagram for heat pump energy balance (internal frontier)

Name	Value / %	Name	Value / %	Name	Value / -
$\eta_{heat\ pump}$	26.3 ± 0.7	η_{mot}	88.9 ± 0.2	ϵ_h	2.19 ± 0.04
η_{cp1}	59 ± 40	η_{cp2}	81 ± 19	π_1	2.848 ± 0.005
$\eta_{cp1,imp}$	59 ± 40	$\eta_{cp2,imp}$	83 ± 17	π_2	2.703 ± 0.002
η_{cd}	94 ± 3	η_{ev}	17 ± 17	$\pi_{1,theory}$	3.3 ± 0.2
η_{trans}	95.14 ± 0.02	η_{sc}	1 ± 1	$\pi_{2,theory}$	2.672 ± 0.001
$\eta_{s,cp1}$	88 ± 12	$\eta_{s,cp2}$	89 ± 11	η_{mot}	<u>88.99 %</u>
$\eta_{s,cp1,ext}$	90 ± 10	$\eta_{s,cp2,ext}$	82 ± 19	η_{radial}	$98.21 \pm 0.02 \%$
$\eta_{s,cp1,theory}$	78 ± 2	$\eta_{s,cp2,theory}$	79.482 ± 0.002	η_{axial}	$96.88 \pm 0.02 \%$

Table F.1: A-6.8/W31.3 – Performance indicators

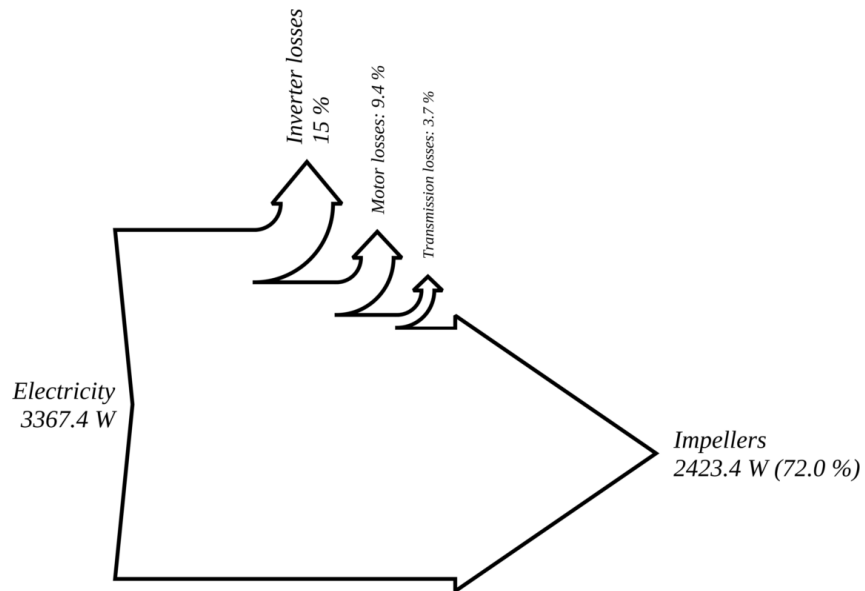


Figure F.2: A-6.8/W31.3 – Sankey diagram for the compressor unit energy balance

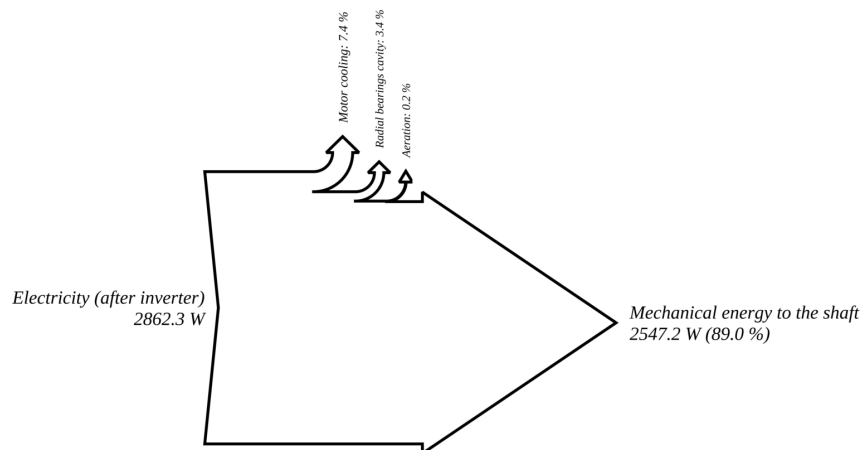


Figure F.3: A-6.8/W31.3 – Sankey diagram for the motor energy balance

Component	Location	P / bar	T / °C	h / kJ kg ⁻¹	s / kJ kg ⁻¹ K ⁻¹
1	inlet	1.073 ± 0.002	-18 ± 7	388.678 ± 0.007	1.77 ± 0.02
	outlet	3.058 ± 0.002	33.7 ± 0.6	428.3668 ± 5 × 10 ⁻⁴	1.827 ± 0.003
2	inlet	3.058 ± 0.002	8.683 ± 0.007	406.015796 ± 7 × 10 ⁻⁶	1.75057 ± 8 × 10 ⁻⁵
	outlet	8.265 ± 0.002	50.761 ± 0.007	435.116938 ± 7 × 10 ⁻⁶	1.77439 ± 5 × 10 ⁻⁵
3	inlet	8.148 ± 0.002	44.228 ± 0.006	428.645708 ± 6 × 10 ⁻⁶	1.75520 ± 4 × 10 ⁻⁵
	outlet	7.947 ± 0.002	29.426 ± 0.006	240.892167 ± 6 × 10 ⁻⁶	1.14069 ± 3 × 10 ⁻⁵
4	inlet	1.776 ± 0.002	-13.0 ± 0.8	221.2280 ± 8 × 10 ⁻⁴	1.084 ± 0.003
	outlet	1.670 ± 0.002	-14.176 ± 0.006	390.214173 ± 6 × 10 ⁻⁶	1.7379 ± 1 × 10 ⁻⁴
5	inlet	7.947 ± 0.002	29.43 ± 0.04	240.89217 ± 4 × 10 ⁻⁵	1.1407 ± 2 × 10 ⁻⁴
	outlet	3.058 ± 0.002	1.2 ± 0.5	240.8922 ± 5 × 10 ⁻⁴	1.149 ± 0.002
6	inlet	3.058 ± 0.002	-5 ± 11	193.72 ± 0.02	0.98 ± 0.06
	outlet	1.896 ± 0.002	-11.4 ± 0.8	193.7184 ± 8 × 10 ⁻⁴	0.978 ± 0.004
7	inlet	1.896 ± 0.002	-11.4 ± 0.8	240.8922 ± 8 × 10 ⁻⁴	1.158 ± 0.003
	outlet	1.896 ± 0.002	-11.4 ± 0.8	281.5177 ± 8 × 10 ⁻⁴	1.313 ± 0.002
8	inlet	3.058 ± 0.002	1.201 ± 0.007	399.302716 ± 7 × 10 ⁻⁶	1.72643 ± 2 × 10 ⁻⁵
	outlet	3.06 ± 0.06	1.2 ± 0.5	201.6155 ± 5 × 10 ⁻⁴	1.006 ± 0.003
9	inlet	1.896 ± 0.002	-11.422 ± 0.006	221.228042 ± 6 × 10 ⁻⁶	1.08263 ± 8 × 10 ⁻⁵
	outlet	1.776 ± 0.002	-13.0 ± 0.8	221.2280 ± 8 × 10 ⁻⁴	1.084 ± 0.003
10	inlet	8.265 ± 0.002	50.8 ± 0.3	435.1169 ± 3 × 10 ⁻⁴	1.774 ± 0.001
	outlet	3.058 ± 0.002	149 ± 101	540.6 ± 0.2	2.1 ± 0.3
11	inlet	1.073 ± 0.002	95 ± 43	487.85 ± 0.05	2.1 ± 0.1
	outlet	1.073 ± 0.002	127 ± 58	519.46 ± 0.06	2.2 ± 0.2
12	inlet	2.500 ± 0.002	20 ± 24	416.89 ± 0.03	1.80 ± 0.07
	outlet	2.500 ± 0.002	44 ± 37	438.58 ± 0.04	1.9 ± 0.1
13	inlet	2.491 ± 0.002	14.5 ± 0.7	412.4779 ± 7 × 10 ⁻⁴	1.789 ± 0.004
	outlet	2.491 ± 0.002	20 ± 25	417.74 ± 0.03	1.81 ± 0.08
15	inlet		26.487 ± 0.006	Cp = 4180.476 ± 0.002 J kg ⁻¹ K ⁻¹	
	outlet		31.252 ± 0.006	Cp = 4179.3369 ± 9 × 10 ⁻⁴ J kg ⁻¹ K ⁻¹	
16	inlet		-6.775 ± 0.006		
	outlet		-9.932 ± 0.006		
18	inlet	1.670 ± 0.002	-14.2 ± 0.4	390.2142 ± 4 × 10 ⁻⁴	1.738 ± 0.003
	outlet	1.073 ± 0.002	-24.77 ± 0.01	383.60197 ± 1 × 10 ⁻⁵	1.7460 ± 2 × 10 ⁻⁴
19	inlet	3.058 ± 0.002	1.2 ± 0.5	201.6155 ± 5 × 10 ⁻⁴	1.006 ± 0.003
	outlet	3.058 ± 0.002	-5 ± 11	193.72 ± 0.02	0.98 ± 0.06
20	inlet	8.265 ± 0.002	50.8 ± 0.3	435.1169 ± 3 × 10 ⁻⁴	1.774 ± 0.001
	outlet	8.148 ± 0.002	44.2 ± 0.3	428.6457 ± 3 × 10 ⁻⁴	1.755 ± 0.001
21	inlet	2.491 ± 0.002	14.5 ± 0.7	412.4779 ± 7 × 10 ⁻⁴	1.789 ± 0.004
	outlet	2.500 ± 0.002	14.472 ± 0.007	412.457806 ± 7 × 10 ⁻⁶	1.78846 ± 8 × 10 ⁻⁵
22	inlet	1.073 ± 0.002	-20 ± 5	387.658 ± 0.005	1.76 ± 0.02
	outlet	1.073 ± 0.002	-19.689 ± 0.007	387.657800 ± 7 × 10 ⁻⁶	1.7622 ± 2 × 10 ⁻⁴
23	inlet	1.073 ± 0.002	127 ± 58	519.46 ± 0.06	2.2 ± 0.2
	outlet	1.073 ± 0.002	150 ± 65	543.18 ± 0.07	2.2 ± 0.2
24	inlet	1.073 ± 0.002	41 ± 38	438.58 ± 0.04	1.9 ± 0.1
	outlet	1.073 ± 0.002	95 ± 43	487.85 ± 0.05	2.1 ± 0.1
25	inlet	3.058 ± 0.002	34 ± 28	429.02 ± 0.03	1.83 ± 0.08
	outlet	3.058 ± 0.002	34.389 ± 0.007	429.015934 ± 7 × 10 ⁻⁶	1.82866 ± 7 × 10 ⁻⁵
26	inlet	8.265 ± 0.002	50.8 ± 0.3	435.1169 ± 3 × 10 ⁻⁴	1.774 ± 0.001
	outlet	2.491 ± 0.002	14.472 ± 0.007	412.477899 ± 7 × 10 ⁻⁶	1.78880 ± 8 × 10 ⁻⁵
27	inlet	3.058 ± 0.002	33.7 ± 0.3	428.3674 ± 3 × 10 ⁻⁴	1.827 ± 0.002
	outlet	3.058 ± 0.002	33.7 ± 0.3	428.3674 ± 3 × 10 ⁻⁴	1.827 ± 0.002
28	inlet	3.058 ± 0.002	1.2 ± 0.4	399.3027 ± 4 × 10 ⁻⁴	1.7264 ± 9 × 10 ⁻⁴
	outlet	3.058 ± 0.002	8.7 ± 0.4	406.0158 ± 4 × 10 ⁻⁴	1.751 ± 0.002
29	inlet	1.073 ± 0.002	-20.6 ± 0.5	386.9432 ± 5 × 10 ⁻⁴	1.759 ± 0.005
	outlet	1.073 ± 0.002	-18 ± 7	388.678 ± 0.007	1.77 ± 0.02

Table F.2: A-6.8/W31.3 – Thermodynamic points of the heat pump cycle

Name	Value / g s ⁻¹	Name	Value / g s ⁻¹	Name	Value / g s ⁻¹
$\dot{M}_{1 \rightarrow 25}$	33 ± 2	$\dot{M}_{2 \rightarrow 10}$	0.19	$\dot{M}_{2 \rightarrow 20}$	39.2 ± 0.8
$\dot{M}_{2 \rightarrow 26}$	1.20 ± 0.06	$\dot{M}_{3 \rightarrow 5}$	34.0 ± 0.8	$\dot{M}_{3 \rightarrow 7}$	5.20 ± 0.09
$\dot{M}_{4 \rightarrow 18}$	32 ± 2	$\dot{M}_{5 \rightarrow 8}$	34.0 ± 0.8	$\dot{M}_{6 \rightarrow 9}$	27 ± 2
$\dot{M}_{7 \rightarrow 9}$	5.20 ± 0.09	$\dot{M}_{8 \rightarrow 19}$	27 ± 2	$\dot{M}_{8 \rightarrow 28}$	31 ± 2
$\dot{M}_{9 \rightarrow 4}$	32 ± 2	$\dot{M}_{10 \rightarrow 25}$	0.19	$\dot{M}_{11 \rightarrow 22}$	0.98 ± 0.04
$\dot{M}_{11 \rightarrow 23}$	0.22 ± 0.01	$\dot{M}_{12 \rightarrow 24}$	1.20 ± 0.05	$\dot{M}_{13 \rightarrow 12}$	1.01 ± 0.05
$\dot{M}_{17 \rightarrow 15}$	376 ± 5	$\dot{M}_{18 \rightarrow 22}$	32 ± 2	$\dot{M}_{19 \rightarrow 6}$	27 ± 2
$\dot{M}_{20 \rightarrow 3}$	39.2 ± 0.8	$\dot{M}_{21 \rightarrow 12}$	0.19 ± 0.01	$\dot{M}_{22 \rightarrow 29}$	33 ± 2
$\dot{M}_{23 \rightarrow 29}$	0.22 ± 0.01	$\dot{M}_{24 \rightarrow 11}$	1.20 ± 0.05	$\dot{M}_{25 \rightarrow 8}$	24 ± 1
$\dot{M}_{25 \rightarrow 27}$	9.4 ± 0.4	$\dot{M}_{26 \rightarrow 13}$	1.01 ± 0.05	$\dot{M}_{26 \rightarrow 21}$	0.19 ± 0.01
$\dot{M}_{27 \rightarrow 28}$	9.4 ± 0.4	$\dot{M}_{28 \rightarrow 2}$	41 ± 2	$\dot{M}_{29 \rightarrow 1}$	33 ± 2
\dot{M}_{cp1}	33 ± 2	\dot{M}_{cp2}	40.6 ± 0.8		

Table F.3: A-6.8/W31.3 – Mass flow rates between the components

Name	Value / W	Name	Value / W
$\dot{E}_{1 \rightarrow 2}$	1108 ± 1 × 10 ³	$\dot{E}_{11 \rightarrow 1}$	2423.4 ± 0.4
$\dot{E}_{12 \rightarrow 11}$	2501.5 ± 0.4	$\dot{E}_{13 \rightarrow 12}$	2547.2 ± 0.4
$\dot{E}_{14 \rightarrow 13}$	2862.3 ± 0.4	$\dot{E}_{el \rightarrow 14}$	3367.4 ± 0.5
$\dot{Y}_{1 \rightarrow 2}$	94 ± 94	$\dot{Y}_{2 \rightarrow 10}$	20 ± 20
$\dot{Y}_{3 \rightarrow 15}$	7367 ± 138	$\dot{Y}_{11 \rightarrow 1}$	94 ± 47
$\dot{Y}_{11 \rightarrow 23}$	5 ± 3	$\dot{Y}_{11 \rightarrow 24}$	59 ± 59
$\dot{Y}_{12 \rightarrow 11}$	118 ± 59	$\dot{Y}_{13 \rightarrow 7}$	211.07 ± 0.03
$\dot{Y}_{13 \rightarrow 12}$	98.71 ± 0.02	$\dot{Y}_{14 \rightarrow at}$	505.11 ± 0.07
$\dot{Y}_{16 \rightarrow 4}$	4278 ± 138	$\dot{Y}_{19 \rightarrow 18}$	211 ± 11
$\dot{Y}_{20 \rightarrow at}$	254 ± 11	$\dot{Y}_{21 \rightarrow at}$	0.004 ± 0.004
$\dot{Y}_{26 \rightarrow at}$	27 ± 2		

Table F.4: A-6.8/W31.3 – Energy rates between the components

F.2 A-7.0/W32.3 - 160 krpm

This test has been performed on May 31th 2012, between 10:38:42 and 19:41:43.

Name	Value / %	Name	Value / %	Name	Value / -
$\eta_{heatpump}$	32.6 ± 0.5	η_{mot}	82.1 ± 0.3	ϵ_h	2.69 ± 0.03
η_{cp1}	63 ± 36	η_{cp2}	77 ± 22	π_1	2.440 ± 0.002
$\eta_{cp1,imp}$	63 ± 36	$\eta_{cp2,imp}$	80 ± 19	π_2	2.365 ± 0.001
η_{cd}	92 ± 2	η_{ev}	31 ± 31	$\pi_{1,theory}$	3.0 ± 0.2
η_{trans}	96.04 ± 0.02	η_{sc}	2 ± 2	$\pi_{2,theory}$	1.922 ± 0.002
$\eta_{s,cp1}$	88 ± 12	$\eta_{s,cp2}$	88 ± 12	η_{mot}	<u>82.34</u> %
$\eta_{s,cp1,ext}$	94 ± 7	$\eta_{s,cp2,ext}$	81 ± 19	η_{radial}	98.54 ± 0.02 %
$\eta_{s,cp1,theory}$	79 ± 2	$\eta_{s,cp2,theory}$	72.37 ± 0.04	η_{axial}	97.47 ± 0.02 %

Table F.5: A-7.0/W32.3 – Performance indicators

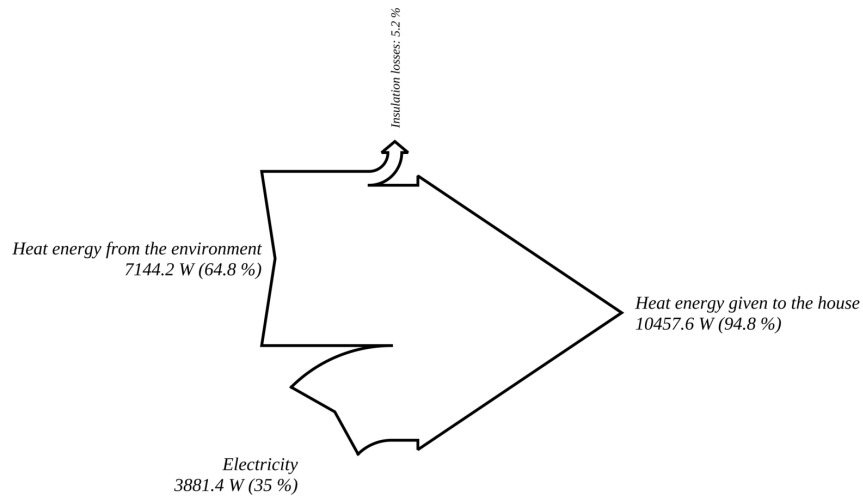


Figure F.4: A-7.0/W32.3 – Sankey diagram for heat pump energy balance (internal frontier)

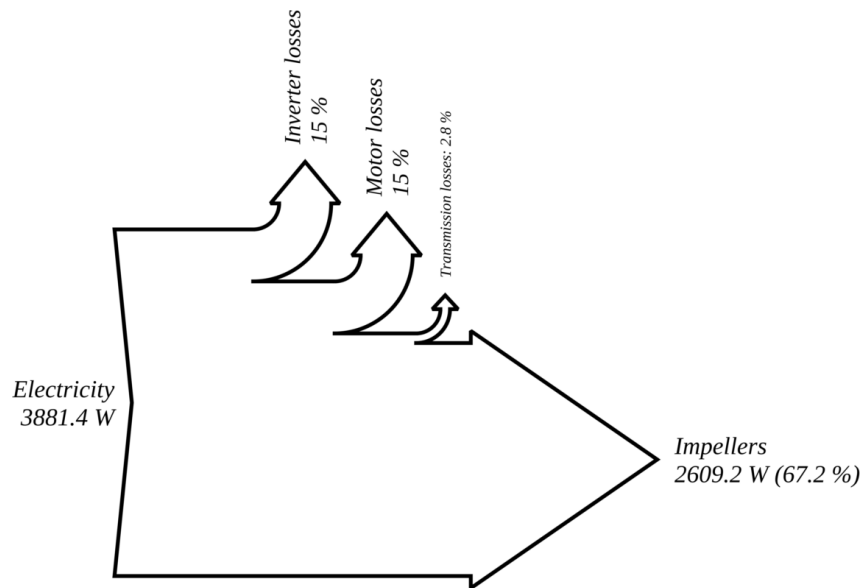


Figure F.5: A-7.0/W32.3 – Sankey diagram for the compressor unit energy balance

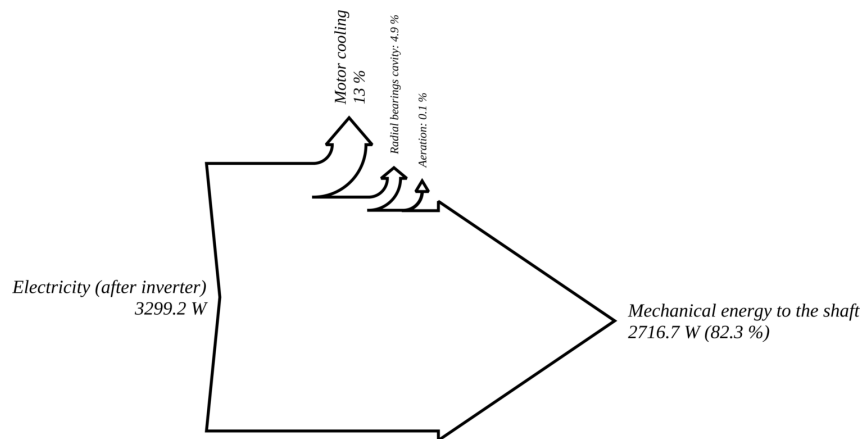


Figure F.6: A-7.0/W32.3 – Sankey diagram for the motor energy balance

Component	Location	P / bar	T / °C	h / kJ kg ⁻¹	s / kJ kg ⁻¹ K ⁻¹
1	inlet	1.502 ± 0.001	-11 ± 6	393.226 ± 0.006	1.76 ± 0.02
	outlet	3.665 ± 0.001	31.1 ± 0.9	424.8843 ± 9 × 10 ⁻⁴	1.801 ± 0.003
2	inlet	3.665 ± 0.001	8.391 ± 0.006	404.146833 ± 6 × 10 ⁻⁶	1.73050 ± 6 × 10 ⁻⁵
	outlet	8.668 ± 0.001	45.140 ± 0.006	428.511354 ± 6 × 10 ⁻⁶	1.75050 ± 4 × 10 ⁻⁵
3	inlet	8.393 ± 0.001	43.907 ± 0.005	427.803896 ± 5 × 10 ⁻⁶	1.75050 ± 4 × 10 ⁻⁵
	outlet	8.209 ± 0.001	31.449 ± 0.005	243.821366 ± 5 × 10 ⁻⁶	1.15027 ± 2 × 10 ⁻⁵
4	inlet	1.635 ± 0.001	-15.1 ± 0.7	227.7822 ± 7 × 10 ⁻⁴	1.110 ± 0.003
	outlet	1.620 ± 0.001	-15.011 ± 0.005	389.683643 ± 5 × 10 ⁻⁶	1.7382 ± 1 × 10 ⁻⁴
5	inlet	8.209 ± 0.001	31.45 ± 0.03	243.82136 ± 3 × 10 ⁻⁵	1.1503 ± 2 × 10 ⁻⁴
	outlet	3.665 ± 0.001	6.4 ± 0.4	243.8214 ± 4 × 10 ⁻⁴	1.157 ± 0.002
6	inlet	3.665 ± 0.001	6 ± 5	207.577 ± 0.004	1.03 ± 0.02
	outlet	1.886 ± 0.001	-11.5 ± 0.7	207.5766 ± 7 × 10 ⁻⁴	1.031 ± 0.003
7	inlet	1.886 ± 0.001	-11.5 ± 0.7	243.8214 ± 7 × 10 ⁻⁴	1.169 ± 0.002
	outlet	1.886 ± 0.001	-11.5 ± 0.7	288.9457 ± 7 × 10 ⁻⁴	1.342 ± 0.001
8	inlet	3.665 ± 0.001	6.357 ± 0.006	402.265796 ± 6 × 10 ⁻⁶	1.7238 ± 4 × 10 ⁻⁴
	outlet	3.66 ± 0.05	6.4 ± 0.4	208.5971 ± 4 × 10 ⁻⁴	1.031 ± 0.002
9	inlet	1.886 ± 0.001	-11.547 ± 0.005	227.782249 ± 5 × 10 ⁻⁶	1.10776 ± 7 × 10 ⁻⁵
	outlet	1.635 ± 0.001	-15.1 ± 0.7	227.7822 ± 7 × 10 ⁻⁴	1.110 ± 0.003
10	inlet	8.668 ± 0.001	45.1 ± 0.7	428.5114 ± 6 × 10 ⁻⁴	1.751 ± 0.002
	outlet	3.665 ± 0.001	128 ± 88	518.04 ± 0.09	2.1 ± 0.2
11	inlet	1.502 ± 0.001	145 ± 46	537.03 ± 0.05	2.2 ± 0.1
	outlet	1.502 ± 0.001	121 ± 60	513.38 ± 0.06	2.1 ± 0.2
12	inlet	3.002 ± 0.001	14 ± 14	410.79 ± 0.02	1.77 ± 0.04
	outlet	3.002 ± 0.001	49 ± 36	442.22 ± 0.04	1.9 ± 0.1
13	inlet	3.005 ± 0.001	9 ± 2	406.835 ± 0.001	1.755 ± 0.004
	outlet	3.002 ± 0.001	28 ± 28	423.50 ± 0.03	1.81 ± 0.08
15	inlet		25.561 ± 0.005	C _p = 4180.809 ± 0.002 J kg ⁻¹ K ⁻¹	
	outlet		32.349 ± 0.005	C _p = 4179.1934 ± 5 × 10 ⁻⁴ J kg ⁻¹ K ⁻¹	
16	inlet		-6.996 ± 0.005		
	outlet		-11.340 ± 0.005		
18	inlet	1.620 ± 0.001	-15.0 ± 0.5	389.6836 ± 5 × 10 ⁻⁴	1.738 ± 0.003
	outlet	1.502 ± 0.001	-16.405 ± 0.008	388.916580 ± 8 × 10 ⁻⁶	1.7411 ± 1 × 10 ⁻⁴
19	inlet	3.665 ± 0.001	6.4 ± 0.4	208.5971 ± 4 × 10 ⁻⁴	1.031 ± 0.002
	outlet	3.665 ± 0.001	6 ± 5	207.577 ± 0.004	1.03 ± 0.02
20	inlet	8.668 ± 0.001	45.1 ± 0.7	428.5114 ± 6 × 10 ⁻⁴	1.751 ± 0.002
	outlet	8.393 ± 0.001	43.9 ± 0.7	427.8039 ± 6 × 10 ⁻⁴	1.750 ± 0.002
21	inlet	3.005 ± 0.001	9 ± 2	406.835 ± 0.001	1.755 ± 0.004
	outlet	3.002 ± 0.001	9.452 ± 0.006	406.841635 ± 6 × 10 ⁻⁶	1.75486 ± 6 × 10 ⁻⁵
22	inlet	1.502 ± 0.001	-16 ± 1	388.934 ± 0.001	1.741 ± 0.005
	outlet	1.502 ± 0.001	-16.384 ± 0.006	388.933713 ± 6 × 10 ⁻⁶	1.7411 ± 1 × 10 ⁻⁴
23	inlet	1.502 ± 0.001	121 ± 60	513.38 ± 0.06	2.1 ± 0.2
	outlet	1.502 ± 0.001	142 ± 65	534.32 ± 0.07	2.2 ± 0.2
24	inlet	1.502 ± 0.001	46 ± 37	442.22 ± 0.04	1.9 ± 0.1
	outlet	1.502 ± 0.001	145 ± 46	537.03 ± 0.05	2.2 ± 0.1
25	inlet	3.665 ± 0.001	31 ± 15	427.27 ± 0.02	1.81 ± 0.04
	outlet	3.665 ± 0.001	33.701 ± 0.006	427.267958 ± 6 × 10 ⁻⁶	1.80915 ± 5 × 10 ⁻⁵
26	inlet	8.668 ± 0.001	45.1 ± 0.7	428.5114 ± 6 × 10 ⁻⁴	1.751 ± 0.002
	outlet	3.005 ± 0.001	9.452 ± 0.006	406.835489 ± 6 × 10 ⁻⁶	1.75478 ± 6 × 10 ⁻⁵
27	inlet	3.665 ± 0.001	31.1 ± 0.7	424.8844 ± 7 × 10 ⁻⁴	1.801 ± 0.003
	outlet	3.665 ± 0.001	31.1 ± 0.7	424.8844 ± 7 × 10 ⁻⁴	1.801 ± 0.003
28	inlet	3.665 ± 0.001	6.4 ± 0.4	402.2658 ± 4 × 10 ⁻⁴	1.724 ± 0.001
	outlet	3.665 ± 0.001	8 ± 1	404.147 ± 0.001	1.731 ± 0.003
29	inlet	1.502 ± 0.001	-14 ± 1	390.519 ± 0.001	1.747 ± 0.006
	outlet	1.502 ± 0.001	-12 ± 5	392.212 ± 0.005	1.75 ± 0.02

Table F.6: A-7.0/W32.3 – Thermodynamic points of the heat pump cycle

Name	Value / g s^{-1}	Name	Value / g s^{-1}	Name	Value / g s^{-1}
$\dot{M}_{1 \rightarrow 25}$	38.3 ± 0.9	$\dot{M}_{2 \rightarrow 10}$	<u>1.01</u>	$\dot{M}_{2 \rightarrow 20}$	56.8 ± 0.8
$\dot{M}_{2 \rightarrow 26}$	1.20 ± 0.06	$\dot{M}_{3 \rightarrow 5}$	47.6 ± 0.8	$\dot{M}_{3 \rightarrow 7}$	9.2 ± 0.2
$\dot{M}_{4 \rightarrow 18}$	37.1 ± 0.9	$\dot{M}_{5 \rightarrow 8}$	47.6 ± 0.8	$\dot{M}_{6 \rightarrow 9}$	27.9 ± 0.9
$\dot{M}_{7 \rightarrow 9}$	9.2 ± 0.2	$\dot{M}_{8 \rightarrow 19}$	27.9 ± 0.9	$\dot{M}_{8 \rightarrow 28}$	54 ± 2
$\dot{M}_{9 \rightarrow 4}$	37.1 ± 0.9	$\dot{M}_{10 \rightarrow 25}$	1.01	$\dot{M}_{11 \rightarrow 22}$	0.45 ± 0.02
$\dot{M}_{11 \rightarrow 23}$	0.75 ± 0.03	$\dot{M}_{12 \rightarrow 24}$	1.20 ± 0.05	$\dot{M}_{13 \rightarrow 12}$	0.28 ± 0.01
$\dot{M}_{17 \rightarrow 15}$	375 ± 4	$\dot{M}_{18 \rightarrow 22}$	37.1 ± 0.9	$\dot{M}_{19 \rightarrow 6}$	27.9 ± 0.9
$\dot{M}_{20 \rightarrow 3}$	56.8 ± 0.8	$\dot{M}_{21 \rightarrow 12}$	0.92 ± 0.05	$\dot{M}_{22 \rightarrow 29}$	37.5 ± 0.9
$\dot{M}_{23 \rightarrow 29}$	0.75 ± 0.03	$\dot{M}_{24 \rightarrow 11}$	1.20 ± 0.05	$\dot{M}_{25 \rightarrow 8}$	34.4 ± 0.8
$\dot{M}_{25 \rightarrow 27}$	4.9 ± 0.1	$\dot{M}_{26 \rightarrow 13}$	0.28 ± 0.01	$\dot{M}_{26 \rightarrow 21}$	0.92 ± 0.05
$\dot{M}_{27 \rightarrow 28}$	4.9 ± 0.1	$\dot{M}_{28 \rightarrow 2}$	59 ± 2	$\dot{M}_{29 \rightarrow 1}$	38.3 ± 0.9
\dot{M}_{cp1}	38.3 ± 0.9	\dot{M}_{cp2}	59.0 ± 0.8		

Table F.7: A-7.0/W32.3 – Mass flow rates between the components

Name	Value / W	Name	Value / W
$\dot{E}_{1 \rightarrow 2}$	1397 ± 670	$\dot{E}_{11 \rightarrow 1}$	2609.2 ± 0.3
$\dot{E}_{12 \rightarrow 11}$	2677.0 ± 0.3	$\dot{E}_{13 \rightarrow 12}$	2716.7 ± 0.3
$\dot{E}_{14 \rightarrow 13}$	3299.2 ± 0.3	$\dot{E}_{el \rightarrow 14}$	3881.4 ± 0.4
$\dot{Y}_{1 \rightarrow 2}$	131 ± 131	$\dot{Y}_{2 \rightarrow 10}$	90 ± 90
$\dot{Y}_{3 \rightarrow 15}$	$1.0458 \times 10^4 \pm 134$	$\dot{Y}_{11 \rightarrow 1}$	131 ± 40
$\dot{Y}_{11 \rightarrow 23}$	16 ± 5	$\dot{Y}_{11 \rightarrow 24}$	114 ± 77
$\dot{Y}_{12 \rightarrow 11}$	164 ± 50	$\dot{Y}_{13 \rightarrow 7}$	415.44 ± 0.04
$\dot{Y}_{13 \rightarrow 12}$	162.37 ± 0.02	$\dot{Y}_{14 \rightarrow at}$	582.22 ± 0.05
$\dot{Y}_{16 \rightarrow 4}$	7144 ± 136	$\dot{Y}_{19 \rightarrow 18}$	28 ± 22
$\dot{Y}_{20 \rightarrow at}$	40 ± 28	$\dot{Y}_{21 \rightarrow at}$	0.006 ± 0.006
$\dot{Y}_{26 \rightarrow at}$	26 ± 2		

Table F.8: A-7.0/W32.3 – Energy rates between the components

F.3 A-7.0/W35.6 - 171 krpm

This test has been performed on May 25th 2012, between 15:08:22 and 15:11:22.

Name	Value / %	Name	Value / %	Name	Value / -
$\eta_{heat\ pump}$	30.5 ± 0.5	η_{mot}	91.8 ± 0.2	ϵ_h	2.36 ± 0.03
η_{cp1}	70 ± 31	η_{cp2}	52 ± 14	π_1	2.381 ± 0.002
$\eta_{cp1,imp}$	62 ± 37	$\eta_{cp2,imp}$	59 ± 16	π_2	2.670 ± 0.001
η_{cd}	92 ± 3	η_{ev}	34 ± 34	$\pi_{1,theory}$	3.9 ± 0.2
η_{trans}	96.61 ± 0.02	η_{sc}	2 ± 2	$\pi_{2,theory}$	N/A
$\eta_{s,cp1}$	88 ± 11	$\eta_{s,cp2}$	82 ± 18	η_{mot}	<u>91.92</u> %
$\eta_{s,cp1,ext}$	98 ± 3	$\eta_{s,cp2,ext}$	68 ± 32	η_{radial}	98.75 ± 0.02 %
$\eta_{s,cp1,theory}$	77 ± 1	$\eta_{s,cp2,theory}$	N/A	η_{axial}	97.83 ± 0.02 %

Table F.9: A-7.0/W35.6 – Performance indicators

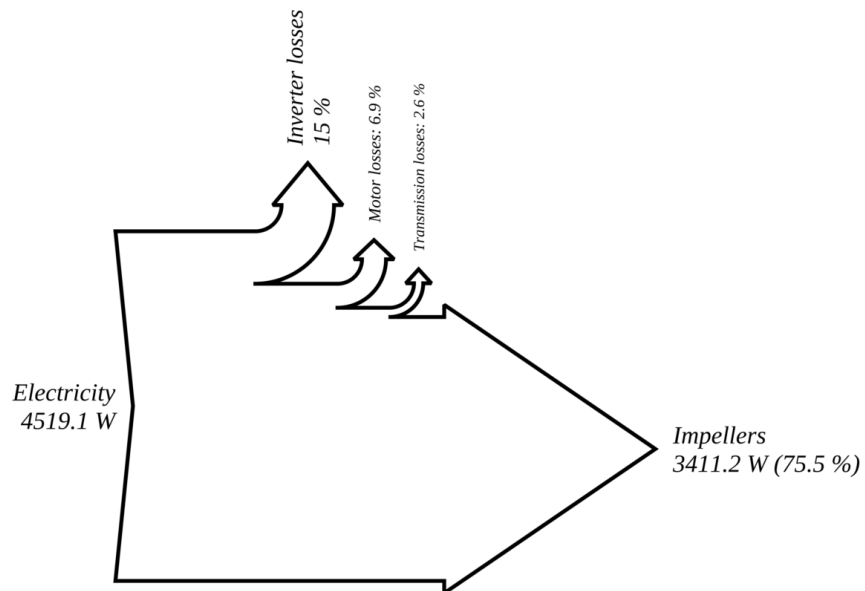


Figure F.7: A-7.0/W35.6 – Sankey diagram for the compressor unit energy balance

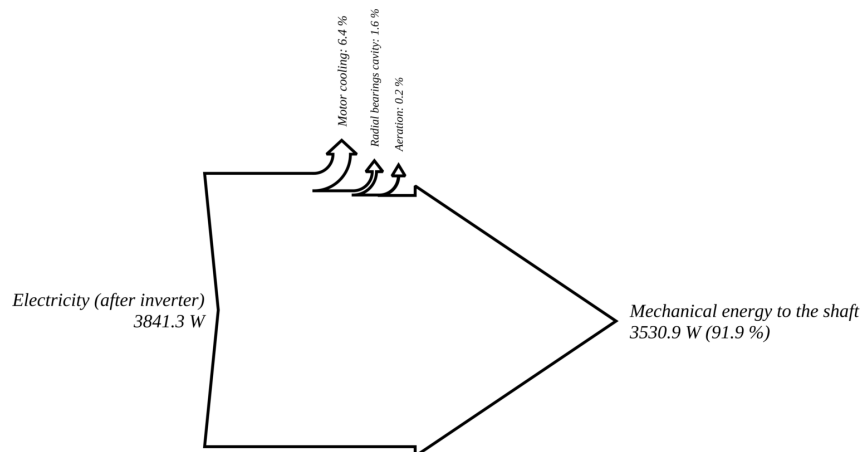


Figure F.8: A-7.0/W35.6 – Sankey diagram for the motor energy balance

Component	Location	P / bar	T / °C	h / kJ kg ⁻¹	s / kJ kg ⁻¹ K ⁻¹
1	inlet	1.459 ± 0.001	-6 ± 12	398.03 ± 0.02	1.78 ± 0.04
	outlet	3.475 ± 0.001	37 ± 3	430.787 ± 0.003	1.825 ± 0.009
2	inlet	3.475 ± 0.001	11.945 ± 0.006	407.896096 ± 6 × 10 ⁻⁶	1.74766 ± 6 × 10 ⁻⁵
	outlet	9.278 ± 0.001	53.358 ± 0.006	435.887724 ± 6 × 10 ⁻⁶	1.76869 ± 4 × 10 ⁻⁵
3	inlet	9.076 ± 0.001	51.868 ± 0.005	434.716360 ± 5 × 10 ⁻⁶	1.76661 ± 3 × 10 ⁻⁵
	outlet	8.672 ± 0.001	33.788 ± 0.005	247.229755 ± 5 × 10 ⁻⁶	1.16129 ± 2 × 10 ⁻⁵
4	inlet	1.615 ± 0.001	-15.4 ± 0.7	248.5511 ± 7 × 10 ⁻⁴	1.191 ± 0.002
	outlet	1.597 ± 0.001	-14.971 ± 0.005	389.791392 ± 5 × 10 ⁻⁶	1.7397 ± 1 × 10 ⁻⁴
5	inlet	8.672 ± 0.001	33.79 ± 0.04	247.22976 ± 4 × 10 ⁻⁵	1.1613 ± 2 × 10 ⁻⁴
	outlet	3.475 ± 0.001	4.8 ± 0.4	247.2298 ± 4 × 10 ⁻⁴	1.170 ± 0.002
6	inlet	3.475 ± 0.001	0 ± 5	200.170 ± 0.005	1.00 ± 0.02
	outlet	1.834 ± 0.001	-12.3 ± 0.7	200.1704 ± 7 × 10 ⁻⁴	1.002 ± 0.003
7	inlet	1.834 ± 0.001	-12.3 ± 0.7	247.2298 ± 7 × 10 ⁻⁴	1.183 ± 0.002
	outlet	1.834 ± 0.001	-12.3 ± 0.7	257.4993 ± 7 × 10 ⁻⁴	1.222 ± 0.002
8	inlet	3.475 ± 0.001	4.822 ± 0.006	401.390488 ± 6 × 10 ⁻⁶	1.7246 ± 4 × 10 ⁻⁴
	outlet	3.47 ± 0.05	4.8 ± 0.4	206.5105 ± 4 × 10 ⁻⁴	1.023 ± 0.002
9	inlet	1.834 ± 0.001	-12.253 ± 0.005	248.551107 ± 5 × 10 ⁻⁶	1.18783 ± 6 × 10 ⁻⁵
	outlet	1.615 ± 0.001	-15.4 ± 0.7	248.5511 ± 7 × 10 ⁻⁴	1.191 ± 0.002
10	inlet	9.278 ± 0.001	53 ± 3	435.888 ± 0.002	1.769 ± 0.008
	outlet	3.475 ± 0.001	142 ± 94	533.3 ± 0.1	2.1 ± 0.2
11	inlet	1.459 ± 0.001	89 ± 38	481.99 ± 0.04	2.0 ± 0.1
	outlet	1.459 ± 0.001	135 ± 63	527.15 ± 0.07	2.2 ± 0.2
12	inlet	3.231 ± 0.001	8 ± 6	405.190 ± 0.006	1.74 ± 0.02
	outlet	3.231 ± 0.001	58 ± 35	450.69 ± 0.04	1.9 ± 0.1
13	inlet	3.238 ± 0.001	2.81 ± 0.07	400.23505 ± 7 × 10 ⁻⁵	1.72557 ± 3 × 10 ⁻⁵
	outlet	3.231 ± 0.001	43 ± 33	436.86 ± 0.04	1.8 ± 0.1
15	inlet		28.766 ± 0.005	Cp = 4179.820 ± 0.002 J kg ⁻¹ K ⁻¹	
	outlet		35.608 ± 0.005	Cp = 4178.98964 ± 7 × 10 ⁻⁵ J kg ⁻¹ K ⁻¹	
16	inlet		-7.031 ± 0.005		
	outlet		-10.899 ± 0.005		
18	inlet	1.597 ± 0.001	-15.0 ± 0.9	389.7914 ± 9 × 10 ⁻⁴	1.740 ± 0.005
	outlet	1.459 ± 0.001	-12.867 ± 0.008	391.968568 ± 8 × 10 ⁻⁶	1.7551 ± 1 × 10 ⁻⁴
19	inlet	3.475 ± 0.001	4.8 ± 0.2	206.5105 ± 2 × 10 ⁻⁴	1.023 ± 0.001
	outlet	3.475 ± 0.001	0 ± 5	200.170 ± 0.005	1.00 ± 0.02
20	inlet	9.278 ± 0.001	53 ± 3	435.888 ± 0.002	1.769 ± 0.008
	outlet	9.076 ± 0.001	52 ± 3	434.716 ± 0.002	1.767 ± 0.008
21	inlet	3.238 ± 0.001	2.81 ± 0.07	400.23505 ± 7 × 10 ⁻⁵	1.72557 ± 3 × 10 ⁻⁵
	outlet	3.231 ± 0.001	2.811 ± 0.006	400.254898 ± 6 × 10 ⁻⁶	1.72580 ± 6 × 10 ⁻⁵
22	inlet	1.459 ± 0.001	-8 ± 10	396.05 ± 0.02	1.77 ± 0.03
	outlet	1.459 ± 0.001	-7.905 ± 0.006	396.054910 ± 6 × 10 ⁻⁶	1.7706 ± 1 × 10 ⁻⁴
23	inlet	1.459 ± 0.001	135 ± 63	527.15 ± 0.07	2.2 ± 0.2
	outlet	1.459 ± 0.001	152 ± 71	545.25 ± 0.08	2.2 ± 0.2
24	inlet	1.459 ± 0.001	56 ± 36	450.69 ± 0.04	2.0 ± 0.1
	outlet	1.459 ± 0.001	89 ± 38	481.99 ± 0.04	2.0 ± 0.1
25	inlet	3.475 ± 0.001	37 ± 25	449.78 ± 0.03	1.88 ± 0.07
	outlet	3.475 ± 0.001	57.767 ± 0.006	449.776941 ± 6 × 10 ⁻⁶	1.88384 ± 5 × 10 ⁻⁵
26	inlet	9.278 ± 0.001	53 ± 3	435.888 ± 0.002	1.769 ± 0.008
	outlet	3.238 ± 0.001	2.811 ± 0.006	400.235046 ± 6 × 10 ⁻⁶	1.725574 ± 6 × 10 ⁻⁶
27	inlet	3.475 ± 0.001	37 ± 3	430.787 ± 0.003	1.825 ± 0.008
	outlet	3.475 ± 0.001	37 ± 3	430.787 ± 0.003	1.825 ± 0.008
28	inlet	3.475 ± 0.001	4.8 ± 0.4	401.3905 ± 4 × 10 ⁻⁴	1.725 ± 0.001
	outlet	3.475 ± 0.001	12 ± 4	407.896 ± 0.004	1.75 ± 0.01
29	inlet	1.459 ± 0.001	-12 ± 5	392.867 ± 0.005	1.76 ± 0.02
	outlet	1.459 ± 0.001	-6 ± 11	397.26 ± 0.02	1.78 ± 0.04

Table F.10: A-7.0/W35.6 – Thermodynamic points of the heat pump cycle

Name	Value / g s^{-1}	Name	Value / g s^{-1}	Name	Value / g s^{-1}
$\dot{M}_{1 \rightarrow 25}$	29.4 ± 0.9	$\dot{M}_{2 \rightarrow 10}$	<u>6.69</u>	$\dot{M}_{2 \rightarrow 20}$	57 ± 1
$\dot{M}_{2 \rightarrow 26}$	1.20 ± 0.06	$\dot{M}_{3 \rightarrow 5}$	33 ± 2	$\dot{M}_{3 \rightarrow 7}$	23.8 ± 0.3
$\dot{M}_{4 \rightarrow 18}$	28.2 ± 0.9	$\dot{M}_{5 \rightarrow 8}$	33 ± 2	$\dot{M}_{6 \rightarrow 9}$	4.4 ± 0.8
$\dot{M}_{7 \rightarrow 9}$	23.8 ± 0.3	$\dot{M}_{8 \rightarrow 19}$	4.4 ± 0.8	$\dot{M}_{8 \rightarrow 28}$	50 ± 2
$\dot{M}_{9 \rightarrow 4}$	28.2 ± 0.9	$\dot{M}_{10 \rightarrow 25}$	<u>6.69</u>	$\dot{M}_{11 \rightarrow 22}$	0.31 ± 0.01
$\dot{M}_{11 \rightarrow 23}$	0.89 ± 0.04	$\dot{M}_{12 \rightarrow 24}$	1.20 ± 0.05	$\dot{M}_{13 \rightarrow 12}$	0.162 ± 0.008
$\dot{M}_{17 \rightarrow 15}$	376 ± 4	$\dot{M}_{18 \rightarrow 22}$	28.2 ± 0.9	$\dot{M}_{19 \rightarrow 6}$	4.4 ± 0.8
$\dot{M}_{20 \rightarrow 3}$	57 ± 1	$\dot{M}_{21 \rightarrow 12}$	1.04 ± 0.05	$\dot{M}_{22 \rightarrow 29}$	28.5 ± 0.9
$\dot{M}_{23 \rightarrow 29}$	0.89 ± 0.04	$\dot{M}_{24 \rightarrow 11}$	1.20 ± 0.05	$\dot{M}_{25 \rightarrow 8}$	21.8 ± 0.5
$\dot{M}_{25 \rightarrow 27}$	14.3 ± 0.4	$\dot{M}_{26 \rightarrow 13}$	0.162 ± 0.008	$\dot{M}_{26 \rightarrow 21}$	1.04 ± 0.05
$\dot{M}_{27 \rightarrow 28}$	14.3 ± 0.4	$\dot{M}_{28 \rightarrow 2}$	65 ± 2	$\dot{M}_{29 \rightarrow 1}$	29.4 ± 0.9
\dot{M}_{cp1}	29.4 ± 0.9	\dot{M}_{cp2}	65 ± 1		

Table F.11: A-7.0/W35.6 – Mass flow rates between the components

Name	Value / W	Name	Value / W
$\dot{E}_{1 \rightarrow 2}$	2447 ± 652	$\dot{E}_{11 \rightarrow 1}$	3411.2 ± 0.3
$\dot{E}_{12 \rightarrow 11}$	3486.7 ± 0.3	$\dot{E}_{13 \rightarrow 12}$	3530.9 ± 0.3
$\dot{E}_{14 \rightarrow 13}$	3841.3 ± 0.3	$\dot{E}_{el \rightarrow 14}$	4519.1 ± 0.4
$\dot{Y}_{1 \rightarrow 2}$	17 ± 17	$\dot{Y}_{2 \rightarrow 10}$	652 ± 652
$\dot{Y}_{3 \rightarrow 15}$	$1.0656 \times 10^4 \pm 137$	$\dot{Y}_{11 \rightarrow 1}$	17 ± 17
$\dot{Y}_{11 \rightarrow 23}$	16 ± 16	$\dot{Y}_{11 \rightarrow 24}$	38 ± 38
$\dot{Y}_{12 \rightarrow 11}$	49 ± 49	$\dot{Y}_{13 \rightarrow 7}$	244.72 ± 0.02
$\dot{Y}_{13 \rightarrow 12}$	59.715 ± 0.004	$\dot{Y}_{14 \rightarrow at}$	677.87 ± 0.05
$\dot{Y}_{16 \rightarrow 4}$	6791 ± 152	$\dot{Y}_{19 \rightarrow 18}$	61 ± 61
$\dot{Y}_{20 \rightarrow at}$	67 ± 67	$\dot{Y}_{21 \rightarrow at}$	0.02 ± 0.02
$\dot{Y}_{26 \rightarrow at}$	43 ± 4		

Table F.12: A-7.0/W35.6 – Energy rates between the components

F.4 A-0.5/W20.7 - 130 krpm

This test has been performed on May 31th 2012, between 09:33:53 and 09:36:53.

Name	Value / %	Name	Value / %	Name	Value / -
$\eta_{heatpump}$	26.6 ± 0.8	η_{mot}	87.9 ± 0.2	ϵ_h	4.02 ± 0.06
η_{cp1}	78 ± 21	η_{cp2}	53 ± 34	π_1	1.847 ± 0.001
$\eta_{cp1,imp}$	76 ± 23	$\eta_{cp2,imp}$	66 ± 34	π_2	$1.6787 \pm 7 \times 10^{-4}$
η_{cd}	89 ± 3	η_{ev}	29 ± 29	$\pi_{1,theory}$	1.9 ± 0.2
η_{trans}	95.81 ± 0.03	η_{sc}	3 ± 3	$\pi_{2,theory}$	N/A
$\eta_{s,cp1}$	93 ± 7	$\eta_{s,cp2}$	89 ± 11	η_{mot}	<u>88.00 %</u>
$\eta_{s,cp1,ext}$	99.20	$\eta_{s,cp2,ext}$	39 ± 39	η_{radial}	98.45 ± 0.03 %
$\eta_{s,cp1,theory}$	79 ± 2	$\eta_{s,cp2,theory}$	N/A	η_{axial}	97.31 ± 0.03 %

Table F.13: A-0.5/W20.7 – Performance indicators

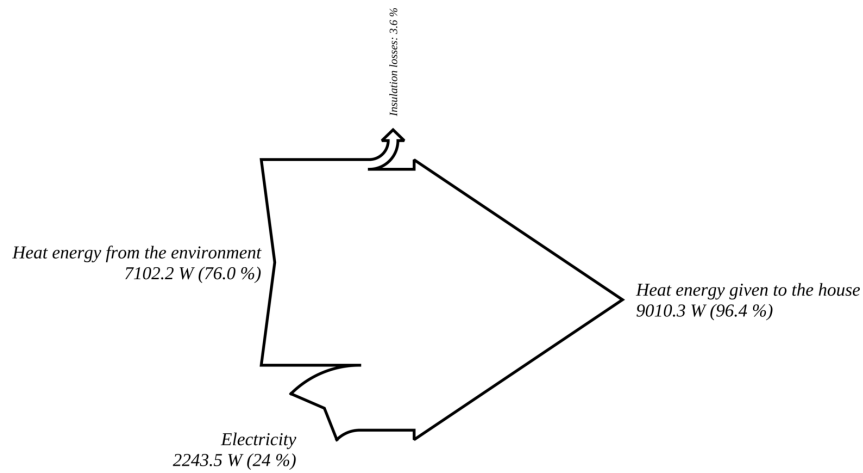


Figure F.9: A-0.5/W20.7 – Sankey diagram for heat pump energy balance (internal frontier)

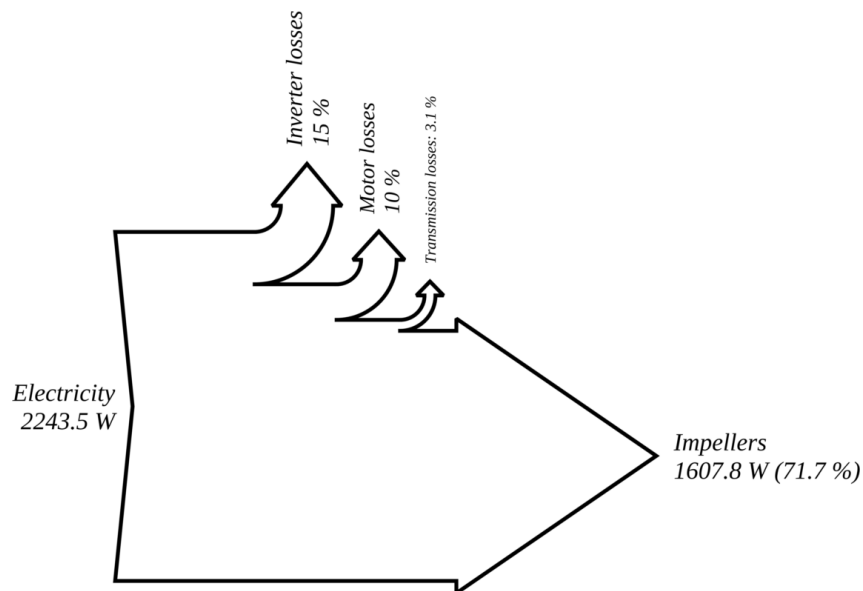


Figure F.10: A-0.5/W20.7 – Sankey diagram for the compressor unit energy balance

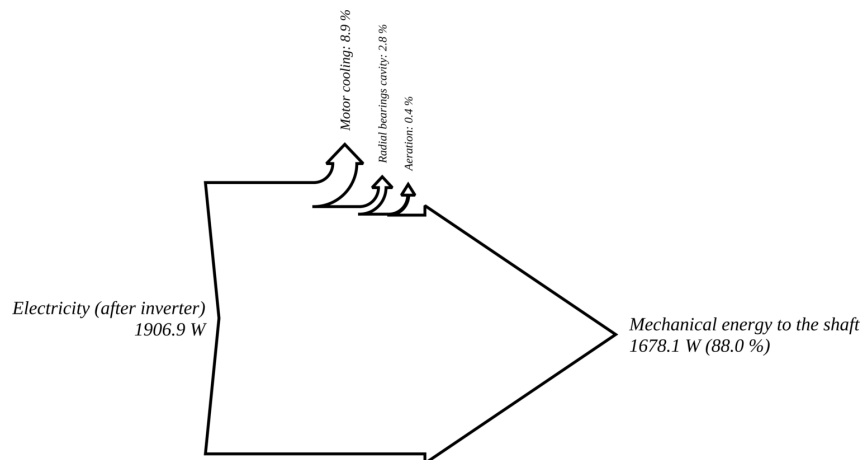


Figure F.11: A-0.5/W20.7 – Sankey diagram for the motor energy balance

Component	Location	P / bar	T / °C	h / kJ kg ⁻¹	s / kJ kg ⁻¹ K ⁻¹
1	inlet	2.017 ± 0.001	3 ± 13	403.92 ± 0.02	1.77 ± 0.04
	outlet	3.725 ± 0.001	28 ± 2	421.988 ± 0.002	1.791 ± 0.006
2	inlet	3.725 ± 0.001	11.125 ± 0.006	406.504319 ± 6 × 10 ⁻⁶	1.73763 ± 6 × 10 ⁻⁵
	outlet	6.254 ± 0.001	32.140 ± 0.006	420.500606 ± 6 × 10 ⁻⁶	1.74764 ± 5 × 10 ⁻⁵
3	inlet	5.936 ± 0.001	31.015 ± 0.005	420.101398 ± 5 × 10 ⁻⁶	1.75005 ± 4 × 10 ⁻⁵
	outlet	5.841 ± 0.001	17.638 ± 0.005	224.162130 ± 5 × 10 ⁻⁶	1.08488 ± 2 × 10 ⁻⁵
4	inlet	2.092 ± 0.001	-8.9 ± 0.6	219.9442 ± 6 × 10 ⁻⁴	1.076 ± 0.003
	outlet	2.079 ± 0.001	-1.960 ± 0.005	399.313756 ± 5 × 10 ⁻⁶	1.75553 ± 8 × 10 ⁻⁵
5	inlet	5.841 ± 0.001	17.64 ± 0.04	224.16213 ± 4 × 10 ⁻⁵	1.0849 ± 2 × 10 ⁻⁴
	outlet	3.725 ± 0.001	6.8 ± 0.5	224.1621 ± 4 × 10 ⁻⁴	1.086 ± 0.002
6	inlet	3.725 ± 0.001	6.3 ± 0.6	208.4875 ± 5 × 10 ⁻⁴	1.030 ± 0.003
	outlet	2.343 ± 0.001	-6.0 ± 0.6	208.4875 ± 6 × 10 ⁻⁴	1.032 ± 0.003
7	inlet	2.343 ± 0.001	-6.0 ± 0.6	224.1621 ± 6 × 10 ⁻⁴	1.091 ± 0.002
	outlet	2.343 ± 0.001	36 ± 8	432.166 ± 0.008	1.86 ± 0.02
8	inlet	3.725 ± 0.001	6.836 ± 0.006	402.537415 ± 6 × 10 ⁻⁶	1.7236 ± 4 × 10 ⁻⁴
	outlet	3.73 ± 0.05	6.8 ± 0.5	209.2490 ± 4 × 10 ⁻⁴	1.033 ± 0.002
9	inlet	2.343 ± 0.001	-5.994 ± 0.005	219.944179 ± 5 × 10 ⁻⁶	1.07515 ± 7 × 10 ⁻⁵
	outlet	2.092 ± 0.001	-8.9 ± 0.6	219.9442 ± 6 × 10 ⁻⁴	1.076 ± 0.003
10	inlet	6.254 ± 0.001	32 ± 2	420.501 ± 0.001	1.748 ± 0.005
	outlet	3.725 ± 0.001	46 ± 21	438.91 ± 0.03	1.85 ± 0.06
11	inlet	2.017 ± 0.001	125 ± 47	516.61 ± 0.05	2.1 ± 0.1
	outlet	2.017 ± 0.001	123 ± 57	514.63 ± 0.06	2.1 ± 0.1
12	inlet	2.143 ± 0.001	13 ± 21	411.80 ± 0.03	1.80 ± 0.06
	outlet	2.143 ± 0.001	86 ± 43	477.63 ± 0.05	2.0 ± 0.1
13	inlet	2.143 ± 0.001	6 ± 3	406.191 ± 0.002	1.778 ± 0.008
	outlet	2.143 ± 0.001	14 ± 22	412.95 ± 0.03	1.80 ± 0.07
15	inlet		14.453 ± 0.005	C _p = 4188.728 ± 0.006 J kg ⁻¹ K ⁻¹	
	outlet		20.716 ± 0.005	C _p = 4183.264 ± 0.004 J kg ⁻¹ K ⁻¹	
16	inlet		-0.495 ± 0.005		
	outlet		-4.827 ± 0.005		
18	inlet	2.079 ± 0.001	-2 ± 2	399.314 ± 0.002	1.756 ± 0.008
	outlet	2.017 ± 0.001	-1.311 ± 0.009	400.036209 ± 9 × 10 ⁻⁶	1.7605 ± 1 × 10 ⁻⁴
19	inlet	3.725 ± 0.001	6.8 ± 0.5	209.2490 ± 4 × 10 ⁻⁴	1.033 ± 0.002
	outlet	3.725 ± 0.001	6.3 ± 0.6	208.4875 ± 5 × 10 ⁻⁴	1.030 ± 0.003
20	inlet	6.254 ± 0.001	32 ± 2	420.501 ± 0.001	1.748 ± 0.005
	outlet	5.936 ± 0.001	31 ± 2	420.101 ± 0.001	1.750 ± 0.005
21	inlet	2.143 ± 0.001	6 ± 3	406.191 ± 0.002	1.778 ± 0.008
	outlet	2.173 ± 0.001	6.271 ± 0.006	406.116899 ± 6 × 10 ⁻⁶	1.77684 ± 8 × 10 ⁻⁵
22	inlet	2.017 ± 0.001	0 ± 10	401.19 ± 0.02	1.76 ± 0.03
	outlet	2.017 ± 0.001	0.041 ± 0.006	401.187210 ± 6 × 10 ⁻⁶	1.76473 ± 9 × 10 ⁻⁵
23	inlet	2.017 ± 0.001	123 ± 57	514.63 ± 0.06	2.1 ± 0.1
	outlet	2.017 ± 0.001	124 ± 64	515.10 ± 0.07	2.1 ± 0.2
24	inlet	2.017 ± 0.001	85 ± 43	477.63 ± 0.05	2.0 ± 0.1
	outlet	2.017 ± 0.001	125 ± 47	516.61 ± 0.05	2.1 ± 0.1
25	inlet	3.725 ± 0.001	28 ± 13	425.58 ± 0.02	1.80 ± 0.04
	outlet	3.725 ± 0.001	31.979 ± 0.006	425.577035 ± 6 × 10 ⁻⁶	1.80238 ± 6 × 10 ⁻⁵
26	inlet	6.254 ± 0.001	32 ± 2	420.501 ± 0.001	1.748 ± 0.005
	outlet	2.143 ± 0.001	6.271 ± 0.006	406.191435 ± 6 × 10 ⁻⁶	1.77819 ± 8 × 10 ⁻⁵
27	inlet	3.725 ± 0.001	28 ± 2	421.988 ± 0.001	1.791 ± 0.005
	outlet	3.725 ± 0.001	28 ± 2	421.988 ± 0.001	1.791 ± 0.005
28	inlet	3.725 ± 0.001	6.8 ± 0.5	402.5374 ± 4 × 10 ⁻⁴	1.724 ± 0.001
	outlet	3.725 ± 0.001	11 ± 2	406.504 ± 0.002	1.738 ± 0.006
29	inlet	2.017 ± 0.001	1 ± 11	401.80 ± 0.02	1.77 ± 0.04
	outlet	2.017 ± 0.001	1 ± 11	401.80 ± 0.02	1.77 ± 0.04

Table F.14: A-0.5/W20.7 – Thermodynamic points of the heat pump cycle

Name	Value / g s ⁻¹	Name	Value / g s ⁻¹	Name	Value / g s ⁻¹
$\dot{M}_{1 \rightarrow 25}$	35.4 ± 0.8	$\dot{M}_{2 \rightarrow 10}$	9.52	$\dot{M}_{2 \rightarrow 20}$	46.0 ± 0.8
$\dot{M}_{2 \rightarrow 26}$	1.20 ± 0.06	$\dot{M}_{3 \rightarrow 5}$	44.2 ± 0.8	$\dot{M}_{3 \rightarrow 7}$	1.75 ± 0.02
$\dot{M}_{4 \rightarrow 18}$	34.2 ± 0.8	$\dot{M}_{5 \rightarrow 8}$	44.2 ± 0.8	$\dot{M}_{6 \rightarrow 9}$	32.4 ± 0.8
$\dot{M}_{7 \rightarrow 9}$	1.75 ± 0.02	$\dot{M}_{8 \rightarrow 19}$	32.4 ± 0.8	$\dot{M}_{8 \rightarrow 28}$	45 ± 2
$\dot{M}_{9 \rightarrow 4}$	34.2 ± 0.8	$\dot{M}_{10 \rightarrow 25}$	9.52	$\dot{M}_{11 \rightarrow 22}$	1.19 ± 0.05
$\dot{M}_{11 \rightarrow 23}$	0.0148 ± 6 × 10 ⁻⁴	$\dot{M}_{12 \rightarrow 24}$	1.20 ± 0.05	$\dot{M}_{13 \rightarrow 12}$	1.00 ± 0.05
$\dot{M}_{17 \rightarrow 15}$	366 ± 4	$\dot{M}_{18 \rightarrow 22}$	34.2 ± 0.8	$\dot{M}_{19 \rightarrow 6}$	32.4 ± 0.8
$\dot{M}_{20 \rightarrow 3}$	46.0 ± 0.8	$\dot{M}_{21 \rightarrow 12}$	0.20 ± 0.01	$\dot{M}_{22 \rightarrow 29}$	35.4 ± 0.8
$\dot{M}_{23 \rightarrow 29}$	0.0148 ± 6 × 10 ⁻⁴	$\dot{M}_{24 \rightarrow 11}$	1.20 ± 0.05	$\dot{M}_{25 \rightarrow 8}$	33.3 ± 0.6
$\dot{M}_{25 \rightarrow 27}$	11.6 ± 0.2	$\dot{M}_{26 \rightarrow 13}$	1.00 ± 0.05	$\dot{M}_{26 \rightarrow 21}$	0.20 ± 0.01
$\dot{M}_{27 \rightarrow 28}$	11.6 ± 0.2	$\dot{M}_{28 \rightarrow 2}$	57 ± 2	$\dot{M}_{29 \rightarrow 1}$	35.4 ± 0.8
\dot{M}_{cp1}	35.4 ± 0.8	\dot{M}_{cp2}	56.7 ± 0.8		

Table F.15: A-0.5/W20.7 – Mass flow rates between the components

Name	Value / W	Name	Value / W
$\dot{E}_{1 \rightarrow 2}$	969 ± 605	$\dot{E}_{11 \rightarrow 1}$	1607.8 ± 0.3
$\dot{E}_{12 \rightarrow 11}$	1652.2 ± 0.3	$\dot{E}_{13 \rightarrow 12}$	1678.1 ± 0.3
$\dot{E}_{14 \rightarrow 13}$	1906.9 ± 0.3	$\dot{E}_{el \rightarrow 14}$	2243.5 ± 0.4
$\dot{Y}_{1 \rightarrow 2}$	0.003 ± 0.003	$\dot{Y}_{2 \rightarrow 10}$	175 ± 175
$\dot{Y}_{3 \rightarrow 15}$	9010 ± 130	$\dot{Y}_{11 \rightarrow 1}$	0.003 ± 0.003
$\dot{Y}_{11 \rightarrow 23}$	0.007 ± 0.007	$\dot{Y}_{11 \rightarrow 24}$	47 ± 47
$\dot{Y}_{12 \rightarrow 11}$	0.03 ± 0.03	$\dot{Y}_{13 \rightarrow 7}$	169.03 ± 0.03
$\dot{Y}_{13 \rightarrow 12}$	53.060 ± 0.008	$\dot{Y}_{14 \rightarrow at}$	336.52 ± 0.06
$\dot{Y}_{16 \rightarrow 4}$	7102 ± 131	$\dot{Y}_{19 \rightarrow 18}$	25 ± 25
$\dot{Y}_{20 \rightarrow at}$	18 ± 18	$\dot{Y}_{21 \rightarrow at}$	0.02 ± 0.02
$\dot{Y}_{26 \rightarrow at}$	17 ± 3		

Table F.16: A-0.5/W20.7 – Energy rates between the components

F.5 A-3.1/W29.5 - 153 krpm

This test has been performed on May 25th 2012, between 13:01:57 and 13:04:57.

Name	Value / %	Name	Value / %	Name	Value / -
$\eta_{heat\ pump}$	31.0 ± 0.6	η_{mot}	91.62 ± 0.05	ϵ_h	3.10 ± 0.04
η_{cp1}	73 ± 26	η_{cp2}	67 ± 32	π_1	2.361 ± 0.002
$\eta_{cp1, imp}$	74 ± 26	$\eta_{cp2, imp}$	75 ± 24	π_2	2.1463 ± 9 × 10 ⁻⁴
η_{cd}	90 ± 2	η_{ev}	20 ± 20	$\pi_{1, theory}$	2.1 ± 0.2
η_{trans}	96.19 ± 0.02	η_{sc}	3 ± 3	$\pi_{2, theory}$	1.612 ± 0.002
$\eta_{s, cp1}$	92 ± 7	$\eta_{s, cp2}$	88 ± 11	η_{mot}	<u>91.67 %</u>
$\eta_{s, cp1, ext}$	98 ± 2	$\eta_{s, cp2, ext}$	80 ± 20	η_{radial}	98.59 ± 0.02 %
$\eta_{s, cp1, theory}$	74 ± 2	$\eta_{s, cp2, theory}$	65.0 ± 0.1	η_{axial}	97.56 ± 0.02 %

Table F.17: A-3.1/W29.5 – Performance indicators

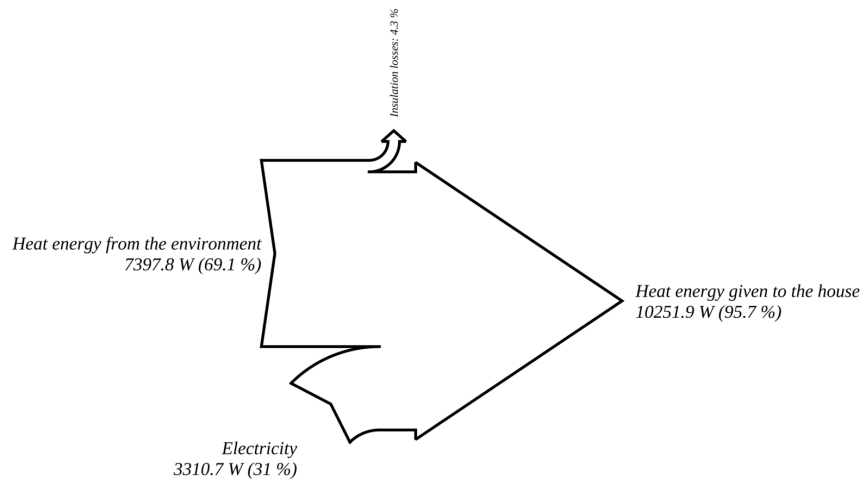


Figure F.12: A-3.1/W29.5 – Sankey diagram for heat pump energy balance (internal frontier)

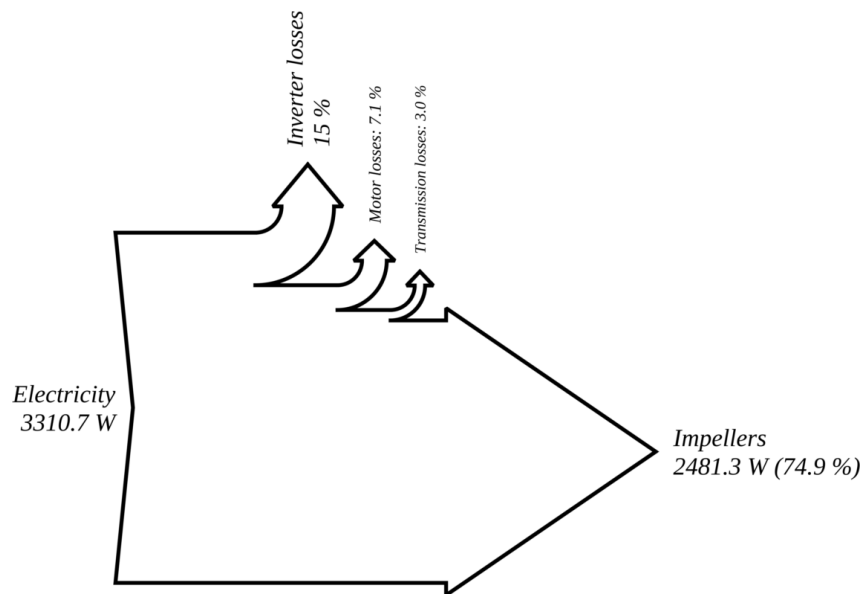


Figure F.13: A-3.1/W29.5 - Sankey diagram for the compressor unit energy balance

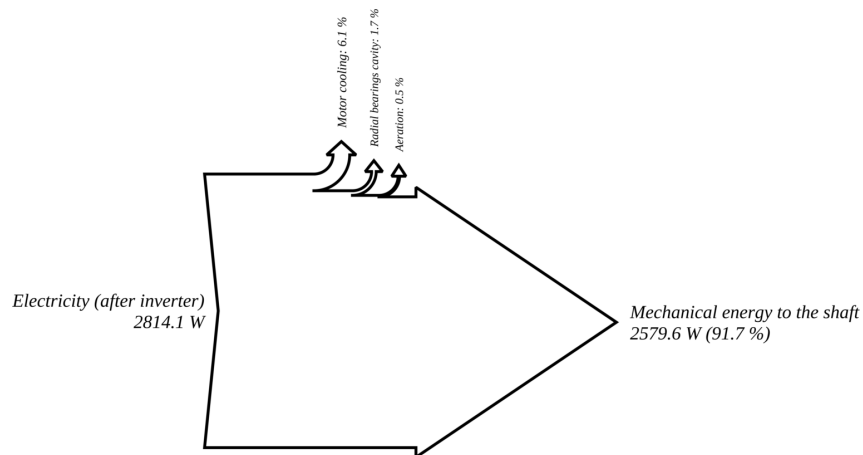


Figure F.14: A-3.1/W29.5 – Sankey diagram for the motor energy balance

Component	Location	P / bar	T / °C	h / kJ kg ⁻¹	s / kJ kg ⁻¹ K ⁻¹
1	inlet	1.572 ± 0.001	1 ± 17	402.95 ± 0.02	1.79 ± 0.05
	outlet	3.711 ± 0.001	37 ± 2	429.940 ± 0.001	1.817 ± 0.005
2	inlet	3.711 ± 0.001	11.681 ± 0.006	407.053941 ± 6 × 10 ⁻⁶	1.73985 ± 6 × 10 ⁻⁵
	outlet	7.964 ± 0.001	43.925 ± 0.006	428.713024 ± 6 × 10 ⁻⁶	1.75700 ± 4 × 10 ⁻⁵
3	inlet	7.805 ± 0.001	42.381 ± 0.005	427.463103 ± 5 × 10 ⁻⁶	1.75447 ± 4 × 10 ⁻⁵
	outlet	7.386 ± 0.001	22.827 ± 0.005	231.463726 ± 5 × 10 ⁻⁶	1.10934 ± 2 × 10 ⁻⁵
4	inlet	1.741 ± 0.001	-13.5 ± 0.7	213.0976 ± 7 × 10 ⁻⁴	1.053 ± 0.003
	outlet	1.681 ± 0.001	-4.352 ± 0.005	398.387663 ± 5 × 10 ⁻⁶	1.7684 ± 1 × 10 ⁻⁴
5	inlet	7.386 ± 0.001	22.83 ± 0.03	231.46373 ± 3 × 10 ⁻⁵	1.1093 ± 2 × 10 ⁻⁴
	outlet	3.711 ± 0.001	6.7 ± 0.4	231.4637 ± 4 × 10 ⁻⁴	1.113 ± 0.002
6	inlet	3.711 ± 0.001	5.9 ± 0.9	207.9201 ± 9 × 10 ⁻⁴	1.028 ± 0.004
	outlet	1.860 ± 0.001	-12 ± 2	207.933 ± 0.002	1.032 ± 0.008
7	inlet	1.860 ± 0.001	-12 ± 2	231.464 ± 0.002	1.122 ± 0.006
	outlet	1.860 ± 0.001	55 ± 8	449.675 ± 0.008	1.93 ± 0.03
8	inlet	3.711 ± 0.001	6.722 ± 0.006	402.473001 ± 6 × 10 ⁻⁶	1.7236 ± 4 × 10 ⁻⁴
	outlet	3.71 ± 0.05	6.7 ± 0.4	209.0942 ± 4 × 10 ⁻⁴	1.033 ± 0.002
9	inlet	1.860 ± 0.001	-11.900 ± 0.005	213.097590 ± 5 × 10 ⁻⁶	1.05178 ± 8 × 10 ⁻⁵
	outlet	1.741 ± 0.001	-13.5 ± 0.7	213.0976 ± 7 × 10 ⁻⁴	1.053 ± 0.003
10	inlet	7.964 ± 0.001	44 ± 2	428.713 ± 0.001	1.757 ± 0.004
	outlet	3.711 ± 0.001	54 ± 19	445.92 ± 0.02	1.87 ± 0.05
11	inlet	1.572 ± 0.001	75 ± 40	467.94 ± 0.04	2.0 ± 0.1
	outlet	1.572 ± 0.001	120 ± 65	512.21 ± 0.07	2.1 ± 0.2
12	inlet	2.533 ± 0.001	24 ± 27	420.30 ± 0.03	1.81 ± 0.08
	outlet	2.533 ± 0.001	46 ± 37	440.13 ± 0.04	1.9 ± 0.1
13	inlet	2.533 ± 0.001	9 ± 3	407.603 ± 0.002	1.770 ± 0.007
	outlet	2.533 ± 0.001	24 ± 27	420.31 ± 0.03	1.81 ± 0.08
15	inlet		22.756 ± 0.005	C _p = 4182.072 ± 0.003 J kg ⁻¹ K ⁻¹	
	outlet		29.550 ± 0.005	C _p = 4179.643 ± 0.002 J kg ⁻¹ K ⁻¹	
16	inlet		-3.084 ± 0.005		
	outlet		-7.645 ± 0.005		
18	inlet	1.681 ± 0.001	-4 ± 2	398.388 ± 0.002	1.768 ± 0.008
	outlet	1.572 ± 0.001	-3.376 ± 0.008	399.497252 ± 8 × 10 ⁻⁶	1.7777 ± 1 × 10 ⁻⁴
19	inlet	3.711 ± 0.001	6.7 ± 0.4	209.0942 ± 4 × 10 ⁻⁴	1.033 ± 0.002
	outlet	3.711 ± 0.001	5.9 ± 0.9	207.9326 ± 9 × 10 ⁻⁴	1.029 ± 0.004
20	inlet	7.964 ± 0.001	44 ± 2	428.713 ± 0.001	1.757 ± 0.004
	outlet	7.805 ± 0.001	42 ± 2	427.463 ± 0.001	1.754 ± 0.004
21	inlet	2.533 ± 0.001	9 ± 3	407.603 ± 0.002	1.770 ± 0.007
	outlet	2.533 ± 0.001	9.002 ± 0.006	407.603064 ± 6 × 10 ⁻⁶	1.77041 ± 7 × 10 ⁻⁵
22	inlet	1.572 ± 0.001	-3 ± 13	399.70 ± 0.02	1.78 ± 0.04
	outlet	1.572 ± 0.001	-3.134 ± 0.006	399.698150 ± 6 × 10 ⁻⁶	1.7785 ± 1 × 10 ⁻⁴
23	inlet	1.572 ± 0.001	120 ± 65	512.21 ± 0.07	2.1 ± 0.2
	outlet	1.572 ± 0.001	139 ± 75	530.82 ± 0.08	2.2 ± 0.2
24	inlet	1.572 ± 0.001	44 ± 37	440.13 ± 0.04	1.9 ± 0.1
	outlet	1.572 ± 0.001	75 ± 40	467.94 ± 0.04	2.0 ± 0.1
25	inlet	3.711 ± 0.001	37 ± 15	431.54 ± 0.02	1.82 ± 0.04
	outlet	3.711 ± 0.001	38.455 ± 0.006	431.539672 ± 6 × 10 ⁻⁶	1.82201 ± 5 × 10 ⁻⁵
26	inlet	7.964 ± 0.001	44 ± 2	428.713 ± 0.001	1.757 ± 0.004
	outlet	2.533 ± 0.001	9.002 ± 0.006	407.603064 ± 6 × 10 ⁻⁶	1.77041 ± 7 × 10 ⁻⁵
27	inlet	3.711 ± 0.001	37 ± 2	429.940 ± 0.001	1.817 ± 0.004
	outlet	3.711 ± 0.001	37 ± 2	429.940 ± 0.001	1.817 ± 0.004
28	inlet	3.711 ± 0.001	6.7 ± 0.4	402.4730 ± 4 × 10 ⁻⁴	1.724 ± 0.001
	outlet	3.711 ± 0.001	12 ± 2	407.054 ± 0.002	1.740 ± 0.006
29	inlet	1.572 ± 0.001	-3 ± 2	399.755 ± 0.002	1.779 ± 0.008
	outlet	1.572 ± 0.001	2 ± 18	403.81 ± 0.02	1.79 ± 0.06

Table F.18: A-3.1/W29.5 – Thermodynamic points of the heat pump cycle

Name	Value / g s ⁻¹	Name	Value / g s ⁻¹	Name	Value / g s ⁻¹
$\dot{M}_{1 \rightarrow 25}$	43 ± 2	$\dot{M}_{2 \rightarrow 10}$	4.78	$\dot{M}_{2 \rightarrow 20}$	52.3 ± 0.8
$\dot{M}_{2 \rightarrow 26}$	1.20 ± 0.06	$\dot{M}_{3 \rightarrow 5}$	50.4 ± 0.8	$\dot{M}_{3 \rightarrow 7}$	1.87 ± 0.02
$\dot{M}_{4 \rightarrow 18}$	42 ± 2	$\dot{M}_{5 \rightarrow 8}$	50.4 ± 0.8	$\dot{M}_{6 \rightarrow 9}$	40 ± 2
$\dot{M}_{7 \rightarrow 9}$	1.87 ± 0.02	$\dot{M}_{8 \rightarrow 19}$	40 ± 2	$\dot{M}_{8 \rightarrow 28}$	49 ± 2
$\dot{M}_{9 \rightarrow 4}$	42 ± 2	$\dot{M}_{10 \rightarrow 25}$	4.78	$\dot{M}_{11 \rightarrow 22}$	0.50 ± 0.02
$\dot{M}_{11 \rightarrow 23}$	0.70 ± 0.04	$\dot{M}_{12 \rightarrow 24}$	1.20 ± 0.06	$\dot{M}_{13 \rightarrow 12}$	1.20 ± 0.06
$\dot{M}_{17 \rightarrow 15}$	370 ± 4	$\dot{M}_{18 \rightarrow 22}$	42 ± 2	$\dot{M}_{19 \rightarrow 6}$	40 ± 2
$\dot{M}_{20 \rightarrow 3}$	52.3 ± 0.8	$\dot{M}_{21 \rightarrow 12}$	0.00063 ± 3 × 10 ⁻⁵	$\dot{M}_{22 \rightarrow 29}$	42 ± 2
$\dot{M}_{23 \rightarrow 29}$	0.70 ± 0.04	$\dot{M}_{24 \rightarrow 11}$	1.20 ± 0.06	$\dot{M}_{25 \rightarrow 8}$	38.0 ± 0.9
$\dot{M}_{25 \rightarrow 27}$	9.7 ± 0.3	$\dot{M}_{26 \rightarrow 13}$	1.20 ± 0.06	$\dot{M}_{26 \rightarrow 21}$	0.00063 ± 3 × 10 ⁻⁵
$\dot{M}_{27 \rightarrow 28}$	9.7 ± 0.3	$\dot{M}_{28 \rightarrow 2}$	58 ± 2	$\dot{M}_{29 \rightarrow 1}$	43 ± 2
\dot{M}_{cp1}	43 ± 2	\dot{M}_{cp2}	58.3 ± 0.8		

Table F.19: A-3.1/W29.5 – Mass flow rates between the components

Name	Value / W	Name	Value / W
$\dot{E}_{1 \rightarrow 2}$	1322 ± 840	$\dot{E}_{11 \rightarrow 1}$	2481.3 ± 0.3
$\dot{E}_{12 \rightarrow 11}$	2543.3 ± 0.3	$\dot{E}_{13 \rightarrow 12}$	2579.6 ± 0.3
$\dot{E}_{14 \rightarrow 13}$	2814.1 ± 0.3	$\dot{E}_{el \rightarrow 14}$	3310.7 ± 0.4
$\dot{Y}_{1 \rightarrow 2}$	22 ± 22	$\dot{Y}_{2 \rightarrow 10}$	82 ± 82
$\dot{Y}_{3 \rightarrow 15}$	1.0252 × 10 ⁴ ± 134	$\dot{Y}_{11 \rightarrow 1}$	22 ± 22
$\dot{Y}_{11 \rightarrow 23}$	13 ± 13	$\dot{Y}_{11 \rightarrow 24}$	33 ± 33
$\dot{Y}_{12 \rightarrow 11}$	60 ± 60	$\dot{Y}_{13 \rightarrow 7}$	171.68 ± 0.02
$\dot{Y}_{13 \rightarrow 12}$	47.578 ± 0.005	$\dot{Y}_{14 \rightarrow at}$	496.60 ± 0.06
$\dot{Y}_{16 \rightarrow 4}$	7398 ± 149	$\dot{Y}_{19 \rightarrow 18}$	46 ± 46
$\dot{Y}_{20 \rightarrow at}$	65 ± 65	$\dot{Y}_{21 \rightarrow at}$	8.80036 × 10 ⁻⁵ ± 9 × 10 ⁻⁵
$\dot{Y}_{26 \rightarrow at}$	25 ± 3		

Table F.20: A-3.1/W29.5 – Energy flows between the components

F.6 A-6.6/W22.1 - 160 krpm

This test has been performed on May 11th 2012, between 12:38:24 and 12:41:26.

Name	Value / %	Name	Value / %	Name	Value / -
$\eta_{heat\ pump}$	25.2 ± 0.7	η_{mot}	90.35 ± 0.09	ε_i	2.67 ± 0.05
η_{cp1}	74 ± 26	η_{cp2}	54 ± 27	π_1	2.511 ± 0.004
$\eta_{cp1,imp}$	71 ± 30	$\eta_{cp2,imp}$	60 ± 30	π_2	2.375 ± 0.001
η_{cd}	93 ± 4	η_{ev}	30 ± 30	$\pi_{1,theory}$	3.2 ± 0.2
η_{trans}	94.93 ± 0.02	η_{sc}	0.4 ± 0.4	$\pi_{2,theory}$	1.938 ± 0.002
$\eta_{s,cp1}$	93 ± 7	$\eta_{s,cp2}$	86 ± 13	η_{mot}	<u>90.43</u> %
$\eta_{s,cp1,ext}$	98 ± 2	$\eta_{s,cp2,ext}$	47 ± 47	η_{radial}	98.13 ± 0.02 %
$\eta_{s,cp1,theory}$	78.4 ± 0.3	$\eta_{s,cp2,theory}$	73.00 ± 0.05	η_{axial}	96.74 ± 0.02 %

Table F.21: A-6.6/W22.1 – Performance indicators

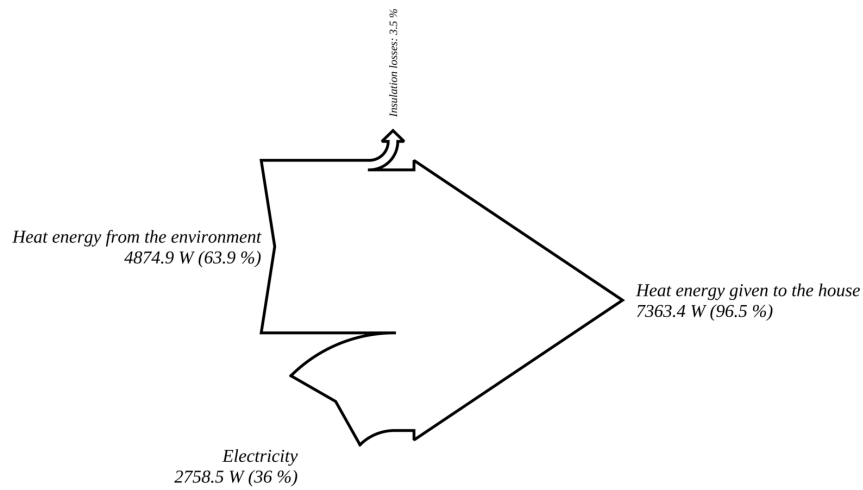


Figure F.15: A-6.6/W22.1 – Sankey diagram for heat pump energy balance (internal frontier)

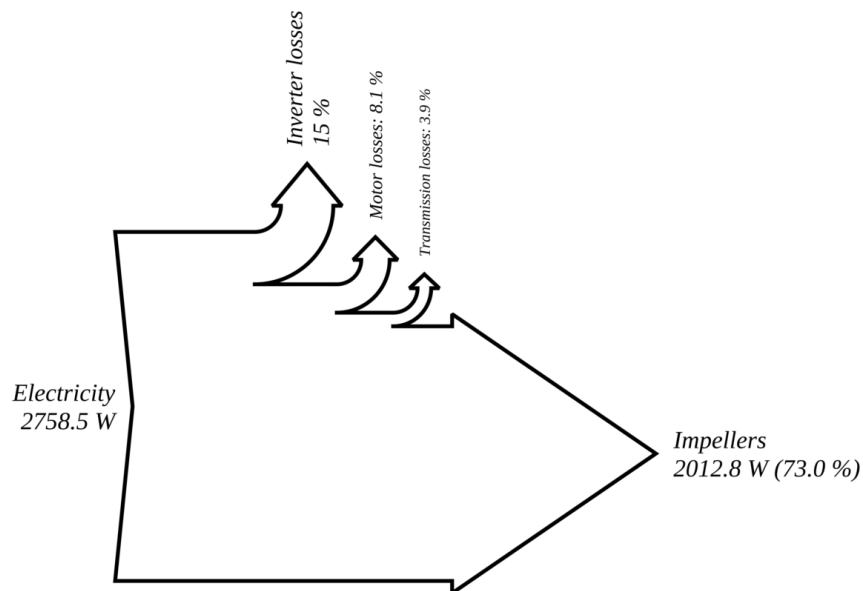


Figure F.16: A-6.6/W22.1 – Sankey diagram for the compressor unit energy balance

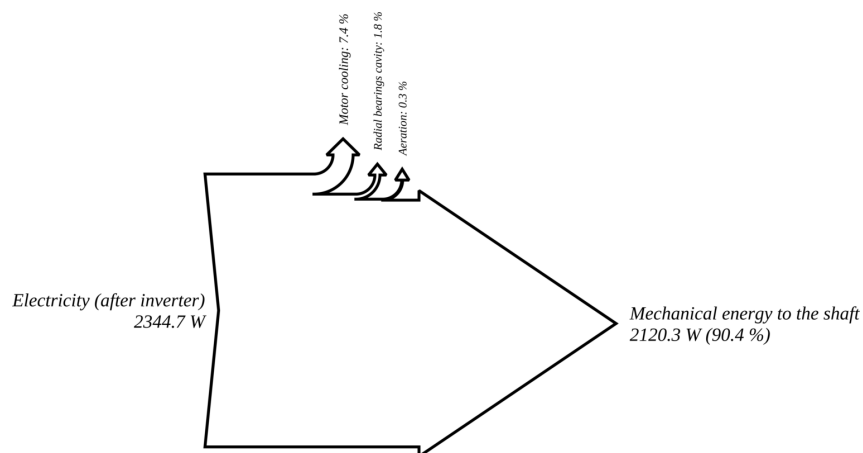


Figure F.17: A-6.6/W22.1 – Sankey diagram for the motor energy balance

Component	Location	P / bar	T / °C	h / kJ kg ⁻¹	s / kJ kg ⁻¹ K ⁻¹
1	inlet	1.077 ± 0.001	-12 ± 13	393.55 ± 0.02	1.78 ± 0.04
	outlet	2.704 ± 0.001	26 ± 3	422.594 ± 0.003	1.82 ± 0.01
2	inlet	2.704 ± 0.001	4.176 ± 0.007	402.939 191 ± 7 × 10 ⁻⁶	1.748 78 ± 8 × 10 ⁻⁵
	outlet	6.423 ± 0.001	38.933 ± 0.007	426.842 379 ± 7 × 10 ⁻⁶	1.766 28 ± 5 × 10 ⁻⁵
3	inlet	6.291 ± 0.001	34.209 ± 0.005	422.462 530 ± 5 × 10 ⁻⁶	1.753 62 ± 4 × 10 ⁻⁵
	outlet	6.083 ± 0.001	19.689 ± 0.005	227.034 683 ± 5 × 10 ⁻⁶	1.094 66 ± 3 × 10 ⁻⁵
4	inlet	1.674 ± 0.001	-14.5 ± 0.8	211.4870 ± 8 × 10 ⁻⁴	1.047 ± 0.003
	outlet	1.632 ± 0.001	-14.818 ± 0.005	389.804 601 ± 5 × 10 ⁻⁶	1.7381 ± 1 × 10 ⁻⁴
5	inlet	6.083 ± 0.001	19.69 ± 0.04	227.034 68 ± 4 × 10 ⁻⁵	1.0947 ± 2 × 10 ⁻⁴
	outlet	2.704 ± 0.001	-2.2 ± 0.6	227.0347 ± 6 × 10 ⁻⁴	1.100 ± 0.002
6	inlet	2.704 ± 0.001	-5 ± 8	193.444 ± 0.008	0.98 ± 0.04
	outlet	1.843 ± 0.001	-12.1 ± 0.7	193.4444 ± 7 × 10 ⁻⁴	0.977 ± 0.004
7	inlet	1.843 ± 0.001	-12.1 ± 0.7	227.0347 ± 7 × 10 ⁻⁴	1.105 ± 0.003
	outlet	1.843 ± 0.001	36 ± 11	432.54 ± 0.02	1.88 ± 0.03
8	inlet	2.704 ± 0.001	-2.173 ± 0.007	397.330 155 ± 7 × 10 ⁻⁶	1.728 32 ± 2 × 10 ⁻⁵
	outlet	2.70 ± 0.06	-2.2 ± 0.6	197.0870 ± 6 × 10 ⁻⁴	0.989 ± 0.003
9	inlet	1.843 ± 0.001	-12.131 ± 0.005	211.486 983 ± 5 × 10 ⁻⁶	1.045 71 ± 8 × 10 ⁻⁵
	outlet	1.674 ± 0.001	-14.5 ± 0.8	211.4870 ± 8 × 10 ⁻⁴	1.047 ± 0.003
10	inlet	6.423 ± 0.001	39 ± 3	426.842 ± 0.003	1.766 ± 0.008
	outlet	2.704 ± 0.001	135 ± 98	526.2 ± 0.1	2.1 ± 0.2
11	inlet	1.077 ± 0.001	104 ± 46	496.09 ± 0.05	2.1 ± 0.1
	outlet	1.077 ± 0.001	117 ± 55	509.36 ± 0.06	2.1 ± 0.1
12	inlet	1.466 ± 0.001	16 ± 33	415.90 ± 0.04	1.8 ± 0.1
	outlet	1.466 ± 0.001	39 ± 38	436.10 ± 0.04	1.9 ± 0.1
13	inlet	1.466 ± 0.001	8 ± 4	409.132 ± 0.004	1.82 ± 0.01
	outlet	1.466 ± 0.001	17 ± 34	416.65 ± 0.04	1.8 ± 0.1
15	inlet		17.061 ± 0.005	Cp = 4186.081 ± 0.005 J kg ⁻¹ K ⁻¹	
	outlet		22.097 ± 0.005	Cp = 4182.430 ± 0.004 J kg ⁻¹ K ⁻¹	
16	inlet		-6.647 ± 0.005		
	outlet		-10.248 ± 0.005		
18	inlet	1.632 ± 0.001	-14.8 ± 0.5	389.8046 ± 5 × 10 ⁻⁴	1.738 ± 0.003
	outlet	1.077 ± 0.001	-21.08 ± 0.01	386.536 83 ± 1 × 10 ⁻⁵	1.7575 ± 2 × 10 ⁻⁴
19	inlet	2.704 ± 0.001	-2.2 ± 0.6	197.0870 ± 6 × 10 ⁻⁴	0.989 ± 0.003
	outlet	2.704 ± 0.001	-5 ± 8	193.444 ± 0.008	0.98 ± 0.04
20	inlet	6.423 ± 0.001	39 ± 3	426.842 ± 0.003	1.766 ± 0.008
	outlet	6.291 ± 0.001	34 ± 3	422.463 ± 0.003	1.754 ± 0.009
21	inlet	1.466 ± 0.001	8 ± 4	409.132 ± 0.004	1.82 ± 0.01
	outlet	1.494 ± 0.001	7.857 ± 0.007	409.068 827 ± 7 × 10 ⁻⁶	1.8165 ± 1 × 10 ⁻⁴
22	inlet	1.077 ± 0.001	-15 ± 10	391.28 ± 0.01	1.78 ± 0.03
	outlet	1.077 ± 0.001	-15.148 ± 0.007	391.282 690 ± 7 × 10 ⁻⁶	1.7761 ± 1 × 10 ⁻⁴
23	inlet	1.077 ± 0.001	117 ± 55	509.36 ± 0.06	2.1 ± 0.1
	outlet	1.077 ± 0.001	131 ± 64	523.19 ± 0.07	2.2 ± 0.2
24	inlet	1.077 ± 0.001	39 ± 39	436.10 ± 0.04	1.9 ± 0.1
	outlet	1.077 ± 0.001	104 ± 46	496.09 ± 0.05	2.1 ± 0.1
25	inlet	2.704 ± 0.001	26 ± 29	437.00 ± 0.03	1.86 ± 0.08
	outlet	2.704 ± 0.001	42.561 ± 0.007	437.003 251 ± 7 × 10 ⁻⁶	1.863 79 ± 7 × 10 ⁻⁵
26	inlet	6.423 ± 0.001	39 ± 3	426.842 ± 0.003	1.766 ± 0.008
	outlet	1.466 ± 0.001	7.857 ± 0.007	409.132 471 ± 7 × 10 ⁻⁶	1.8182 ± 1 × 10 ⁻⁴
27	inlet	2.704 ± 0.001	26 ± 3	422.595 ± 0.003	1.82 ± 0.01
	outlet	2.704 ± 0.001	26 ± 3	422.595 ± 0.003	1.82 ± 0.01
28	inlet	2.704 ± 0.001	-2.2 ± 0.4	397.3302 ± 4 × 10 ⁻⁴	1.728 ± 0.001
	outlet	2.704 ± 0.001	4 ± 4	402.939 ± 0.004	1.75 ± 0.01
29	inlet	1.077 ± 0.001	-20 ± 5	387.589 ± 0.005	1.76 ± 0.02
	outlet	1.077 ± 0.001	-14 ± 11	391.96 ± 0.02	1.78 ± 0.04

Table F.22: A-6.6/W22.1 – Thermodynamic points of the heat pump cycle

Name	Value / g s ⁻¹	Name	Value / g s ⁻¹	Name	Value / g s ⁻¹
$\dot{M}_{1 \rightarrow 25}$	23 ± 1	$\dot{M}_{2 \rightarrow 10}$	3.66	$\dot{M}_{2 \rightarrow 20}$	37.7 ± 0.8
$\dot{M}_{2 \rightarrow 26}$	1.20 ± 0.06	$\dot{M}_{3 \rightarrow 5}$	35.5 ± 0.8	$\dot{M}_{3 \rightarrow 7}$	2.21 ± 0.03
$\dot{M}_{4 \rightarrow 18}$	21 ± 1	$\dot{M}_{5 \rightarrow 8}$	35.5 ± 0.8	$\dot{M}_{6 \rightarrow 9}$	19 ± 1
$\dot{M}_{7 \rightarrow 9}$	2.21 ± 0.03	$\dot{M}_{8 \rightarrow 19}$	19 ± 1	$\dot{M}_{8 \rightarrow 28}$	33 ± 2
$\dot{M}_{9 \rightarrow 4}$	21 ± 1	$\dot{M}_{10 \rightarrow 25}$	3.66	$\dot{M}_{11 \rightarrow 22}$	0.36 ± 0.02
$\dot{M}_{11 \rightarrow 23}$	0.84 ± 0.04	$\dot{M}_{12 \rightarrow 24}$	1.20 ± 0.05	$\dot{M}_{13 \rightarrow 12}$	1.08 ± 0.05
$\dot{M}_{17 \rightarrow 15}$	368 ± 5	$\dot{M}_{18 \rightarrow 22}$	21 ± 1	$\dot{M}_{19 \rightarrow 6}$	19 ± 1
$\dot{M}_{20 \rightarrow 3}$	37.7 ± 0.8	$\dot{M}_{21 \rightarrow 12}$	0.119 ± 0.006	$\dot{M}_{22 \rightarrow 29}$	22 ± 1
$\dot{M}_{23 \rightarrow 29}$	0.84 ± 0.04	$\dot{M}_{24 \rightarrow 11}$	1.20 ± 0.05	$\dot{M}_{25 \rightarrow 8}$	16.9 ± 0.6
$\dot{M}_{25 \rightarrow 27}$	9.4 ± 0.4	$\dot{M}_{26 \rightarrow 13}$	1.08 ± 0.05	$\dot{M}_{26 \rightarrow 21}$	0.119 ± 0.006
$\dot{M}_{27 \rightarrow 28}$	9.4 ± 0.4	$\dot{M}_{28 \rightarrow 2}$	43 ± 2	$\dot{M}_{29 \rightarrow 1}$	23 ± 1
\dot{M}_{cp1}	23 ± 1	\dot{M}_{cp2}	42.5 ± 0.8		

Table F.23: A-6.6/W22.1 – Mass flow rates between the components

Name	Value / W	Name	Value / W
$\dot{E}_{1 \rightarrow 2}$	1354 ± 659	$\dot{E}_{11 \rightarrow 1}$	2012.8 ± 0.3
$\dot{E}_{12 \rightarrow 11}$	2080.6 ± 0.3	$\dot{E}_{13 \rightarrow 12}$	2120.3 ± 0.3
$\dot{E}_{14 \rightarrow 13}$	2344.7 ± 0.4	$\dot{E}_{el \rightarrow 14}$	2758.5 ± 0.4
$\dot{Y}_{1 \rightarrow 2}$	27 ± 27	$\dot{Y}_{2 \rightarrow 10}$	364 ± 364
$\dot{Y}_{3 \rightarrow 15}$	7363 ± 125	$\dot{Y}_{11 \rightarrow 1}$	27 ± 27
$\dot{Y}_{11 \rightarrow 23}$	12 ± 12	$\dot{Y}_{11 \rightarrow 24}$	72 ± 72
$\dot{Y}_{12 \rightarrow 11}$	59 ± 59	$\dot{Y}_{13 \rightarrow 7}$	172.96 ± 0.03
$\dot{Y}_{13 \rightarrow 12}$	43.373 ± 0.006	$\dot{Y}_{14 \rightarrow at}$	413.78 ± 0.06
$\dot{Y}_{16 \rightarrow 4}$	4875 ± 174	$\dot{Y}_{19 \rightarrow 18}$	70 ± 64
$\dot{Y}_{20 \rightarrow at}$	165 ± 120	$\dot{Y}_{21 \rightarrow at}$	0.008 ± 0.008
$\dot{Y}_{26 \rightarrow at}$	21 ± 5		

Table F.24: A-6.6/W22.1 – Energy rates between the components

F.7 B8.0/W11.0 - 110 krpm

This test has been performed on October 14th 2013, at 13:57:22, just before the break of the compression unit.

Component	Location	P / bar	T / °C	h / kJ kg ⁻¹	s / kJ kg ⁻¹ K ⁻¹
1	inlet	2.39 ± 0.03	24 ± 7	420.822 ± 0.007	1.82 ± 0.02
	outlet	3.90 ± 0.03	45 ± 7	436.899 ± 0.006	1.84 ± 0.02
2	inlet	3.642 ± 0.002	36.174 ± 0.007	429.572664 ± 7 × 10 ⁻⁶	1.81710 ± 6 × 10 ⁻⁵
	outlet	5.110 ± 0.002	50.73 ± 0.01	440.61999 ± 1 × 10 ⁻⁵	1.82642 ± 6 × 10 ⁻⁵
3	inlet	4.954 ± 0.002	49.45 ± 0.01	439.66514 ± 1 × 10 ⁻⁵	1.82580 ± 6 × 10 ⁻⁵
	outlet	4.776 ± 0.002	10.91 ± 0.01	214.83703 ± 1 × 10 ⁻⁵	1.05274 ± 5 × 10 ⁻⁵
4	inlet	2.60 ± 0.03	-3.2 ± 0.3	223.8405 ± 3 × 10 ⁻⁴	1.089 ± 0.001
	outlet	2.603 ± 0.002	7.53 ± 0.01	406.14017 ± 1 × 10 ⁻⁵	1.7631 ± 1 × 10 ⁻⁴
5	inlet	4.78 ± 0.03	10.91 ± 0.03	214.83703 ± 3 × 10 ⁻⁵	1.0527 ± 1 × 10 ⁻⁴
	outlet	3.77 ± 0.02	7.2 ± 0.2	214.8370 ± 2 × 10 ⁻⁴	1.0531 ± 8 × 10 ⁻⁴
6	inlet	3.77 ± 0.02	7.2 ± 0.2	214.8370 ± 2 × 10 ⁻⁴	1.0531 ± 8 × 10 ⁻⁴
	outlet	2.60 ± 0.03	-3.2 ± 0.3	214.8370 ± 3 × 10 ⁻⁴	1.055 ± 0.001
7	inlet	4.78 ± 0.03	10.91 ± 0.03	214.83703 ± 3 × 10 ⁻⁵	1.0527 ± 1 × 10 ⁻⁴
	outlet	2.60 ± 0.03	-3.2 ± 0.3	243.3710 ± 3 × 10 ⁻⁴	1.161 ± 0.001
8	inlet	5.11 ± 0.03	50.7 ± 0.2	440.6200 ± 1 × 10 ⁻⁴	1.8264 ± 7 × 10 ⁻⁴
	outlet	2.39 ± 0.03	46.0 ± 0.2	440.6200 ± 1 × 10 ⁻⁴	1.885 ± 0.001
9	inlet	3.77 ± 0.02	7.2 ± 0.2	214.8370 ± 2 × 10 ⁻⁴	1.0531 ± 8 × 10 ⁻⁴
	outlet	3.77 ± 0.02	7.2 ± 0.2	214.8370 ± 2 × 10 ⁻⁴	1.0531 ± 8 × 10 ⁻⁴
10	inlet	5.11 ± 0.03	50.7 ± 0.2	440.6200 ± 1 × 10 ⁻⁴	1.8264 ± 7 × 10 ⁻⁴
	outlet	3.90 ± 0.03	51 ± 8	442.593 ± 0.007	1.85 ± 0.02
11	inlet	3.19 ± 0.03	8.0 ± 0.3	405.0528 ± 2 × 10 ⁻⁴	1.744 ± 0.001
	outlet	3.19 ± 0.03	12 ± 10	408.87 ± 0.01	1.76 ± 0.03
12	inlet	2.73 ± 0.03	16 ± 18	412.98 ± 0.02	1.78 ± 0.05
	outlet	2.727 ± 0.002	18.95 ± 0.01	415.89283 ± 1 × 10 ⁻⁵	1.79365 ± 9 × 10 ⁻⁵
13	inlet	3.16 ± 0.03	7.9 ± 0.3	405.0528 ± 2 × 10 ⁻⁴	1.745 ± 0.001
	outlet	2.73 ± 0.03	17 ± 19	414.15 ± 0.02	1.79 ± 0.06
15	inlet		10.729 ± 0.006	C _p = 4193.27 ± 0.05 J kg ⁻¹ K ⁻¹	
	outlet		10.961 ± 0.006	C _p = 4192.92 ± 0.05 J kg ⁻¹ K ⁻¹	
16	inlet		8.03 ± 0.01	C _p = 4197.83 ± 0.06 J kg ⁻¹ K ⁻¹	
	outlet		4.62 ± 0.01	C _p = 4205.10 ± 0.07 J kg ⁻¹ K ⁻¹	
19	inlet	2.39 ± 0.03	7 ± 7	406.594 ± 0.007	1.77 ± 0.02
	outlet	2.386 ± 0.002	24.004 ± 0.007	421.044464 ± 7 × 10 ⁻⁶	1.82142 ± 8 × 10 ⁻⁵
20	inlet	5.11 ± 0.03	50.7 ± 0.2	440.6200 ± 1 × 10 ⁻⁴	1.8264 ± 7 × 10 ⁻⁴
	outlet	4.95 ± 0.03	49.4 ± 0.2	439.6651 ± 1 × 10 ⁻⁴	1.8258 ± 7 × 10 ⁻⁴
21	inlet	5.11 ± 0.03	50.7 ± 0.2	440.6200 ± 1 × 10 ⁻⁴	1.8264 ± 7 × 10 ⁻⁴
	outlet	3.158 ± 0.002	7.90 ± 0.01	405.05280 ± 1 × 10 ⁻⁵	1.74473 ± 8 × 10 ⁻⁵
22	inlet	5.11 ± 0.03	50.7 ± 0.2	440.6200 ± 1 × 10 ⁻⁴	1.8264 ± 7 × 10 ⁻⁴
	outlet	3.188 ± 0.002	7.98 ± 0.01	405.05279 ± 1 × 10 ⁻⁵	1.74403 ± 8 × 10 ⁻⁵
23	inlet	3.19 ± 0.03	12 ± 10	408.87 ± 0.01	1.76 ± 0.03
	outlet	2.73 ± 0.03	14 ± 16	411.86 ± 0.02	1.78 ± 0.05
24	inlet	3.19 ± 0.03	12 ± 10	408.87 ± 0.01	1.76 ± 0.03
	outlet	2.73 ± 0.03	13 ± 15	410.30 ± 0.02	1.77 ± 0.05
25	inlet	3.90 ± 0.03	45 ± 8	436.899 ± 0.008	1.84 ± 0.02
	outlet	3.902 ± 0.002	44.626 ± 0.007	436.899425 ± 7 × 10 ⁻⁶	1.83521 ± 6 × 10 ⁻⁵
26	inlet	5.11 ± 0.03	50.7 ± 0.2	440.6200 ± 1 × 10 ⁻⁴	1.8264 ± 7 × 10 ⁻⁴
	outlet	5.110 ± 0.002	50.73 ± 0.01	440.61999 ± 1 × 10 ⁻⁵	1.82642 ± 6 × 10 ⁻⁵
27	inlet	3.90 ± 0.03	44.6 ± 0.2	436.8994 ± 1 × 10 ⁻⁴	1.8352 ± 8 × 10 ⁻⁴
	outlet	3.64 ± 0.03	36.2 ± 0.2	429.5727 ± 1 × 10 ⁻⁴	1.8171 ± 9 × 10 ⁻⁴

Table F.25: B8.0/W11.0 – Thermodynamic points of the heat pump cycle

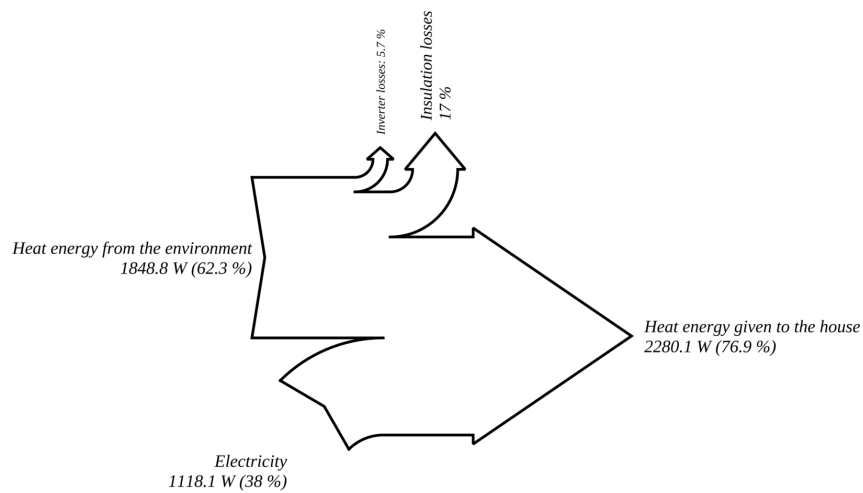


Figure F.18: B8.0/W11.0 – Sankey diagram for heat pump energy balance (internal frontier)

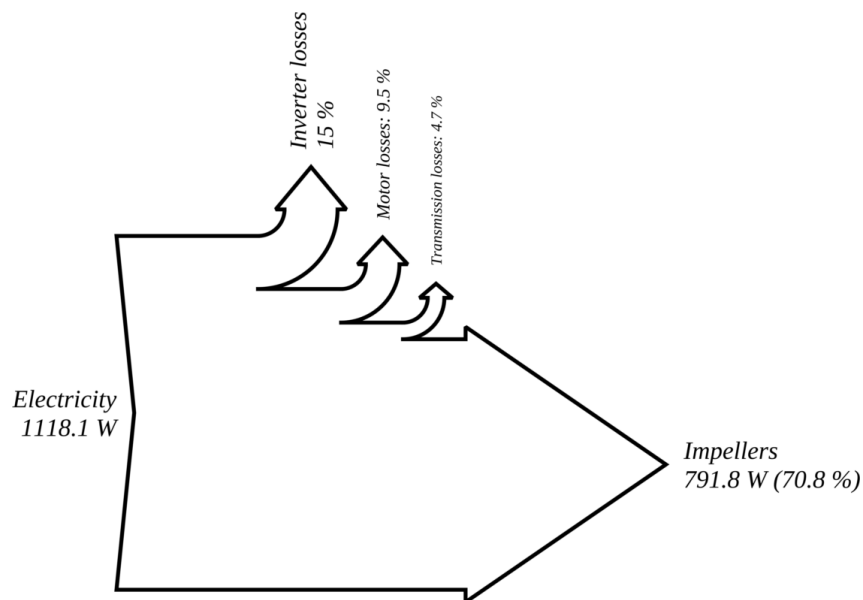


Figure F.19: B8.0/W11.0 – Sankey diagram for the compressor unit energy balance

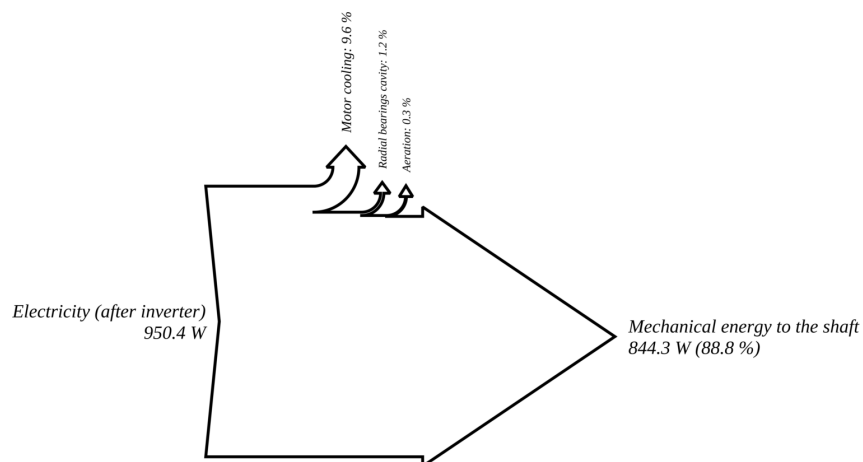


Figure F.20: B8.0/W11.0 – Sankey diagram for the motor energy balance

Name	Value / %	Name	Value / %	Name	Value / -
$\eta_{heat\ pump}$	7 ± 7	η_{motor}	88 ± 2	ε_h	1.95 ± 0.05
η_{cp1}	72 ± 1	η_{cp2}	26.1 ± 0.5	π_1	1.64 ± 0.02
$\eta_{cp1,imp}$	73 ± 26	$\eta_{cp2,imp}$	75 ± 2	π_2	$1.4032 \pm 8 \times 10^{-4}$
η_{cd}	25 ± 25	η_{ev}	58 ± 20	$\pi_{1,theory}$	1.56 ± 0.04
η_{trans}	93.78 ± 0.03	η_{sc}	N/A	$\pi_{2,theory}$	1.3 ± 0.2
$\eta_{s,cp1}$	71 ± 29	$\eta_{s,cp2}$	72.8 ± 0.3	η_{motor}	<u>86.04 %</u>
$\eta_{s,cp1,ext}$	72.6 ± 0.3	$\eta_{s,cp2,ext}$	72.8 ± 0.3	η_{radial}	$97.71 \pm 0.03 \%$
$\eta_{s,cp1,theory}$	79.0 ± 0.4	$\eta_{s,cp2,theory}$	72 ± 2	η_{axial}	$95.98 \pm 0.03 \%$

Table F.26: B8.0/W11.0 – Performance indicators

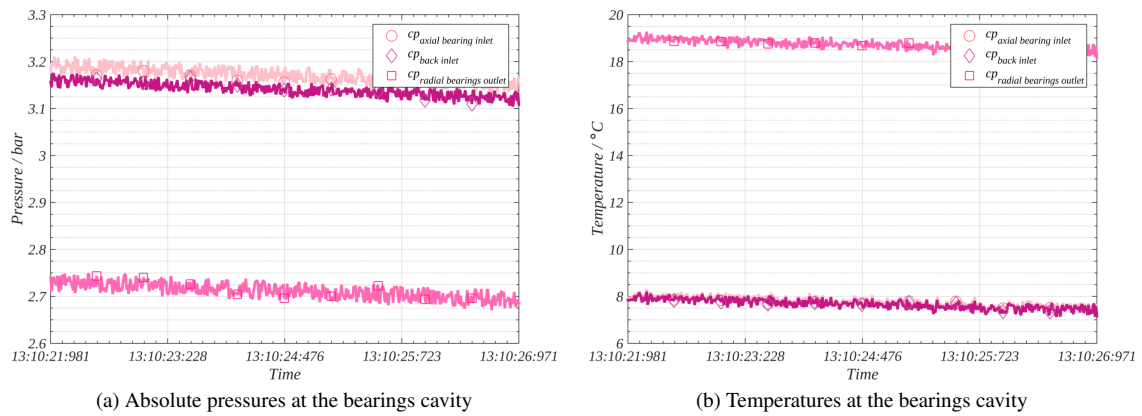


Figure F.21: Absolute pressures and temperatures at the bearings cavity when the breakdown happened

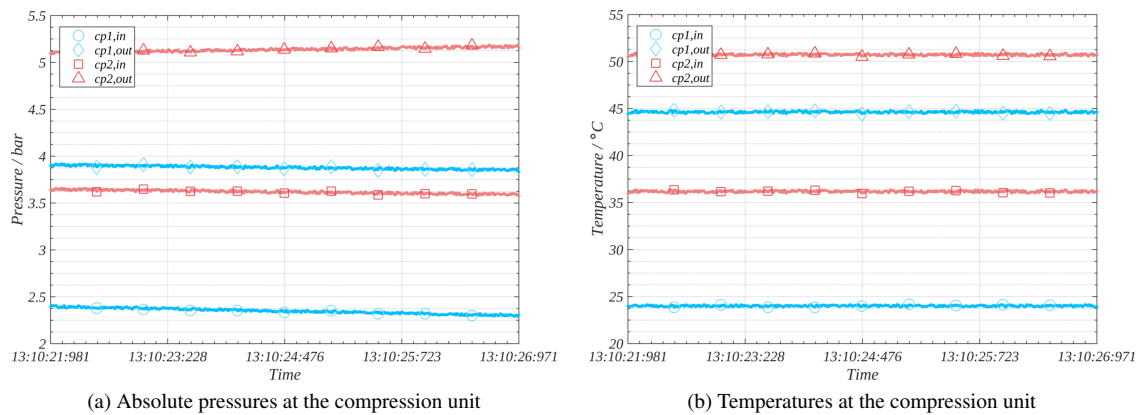


Figure F.22: Absolute pressures and temperatures at compression unit inlets/outlets when the breakdown happened

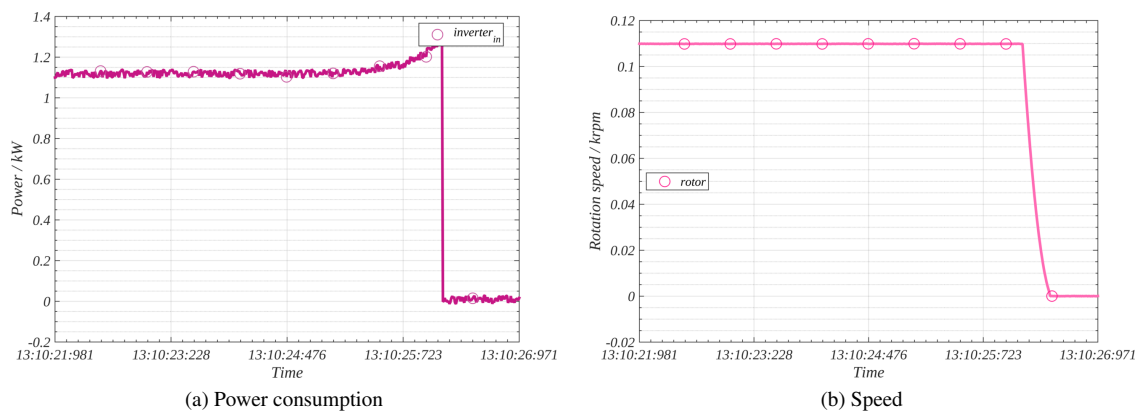


Figure F.23: Power consumption and rotational speed records when the breakdown happened

Uncertainties and sensors calibration

G.1 Stable OP

An Operating Point (OP) is considered a stable one if all the sensor values satisfy one of the following conditions:

- the value variations are bounded between the following bounds for a 3-minute period of time, with at least 100 records.

Temperature ± 0.2 °C

Absolute pressure ± 0.1 bar

Mass flow rate ± 1 %

Weight ± 1 %

- The value oscillates steadily around a fixed and stable mean value.

As stable conditions are set, the measurements are considered as independent measurements of the same physical value, which greatly decreases the uncertainty of the measurement, as the uncertainty is divided by the squared root of the number of measurements n , in this case, as illustrated by eq. (G.1).

$$a \pm \frac{\Delta a}{\sqrt{n}} \tag{G.1}$$

G.2 Sensors calibration

G.2.1 Absolute pressure transducers

The absolute pressure transducers were calibrated using a dead weight balance. Some of the pressure transducers have been calibrated independently, and some have been calibrated with an other transducer (two at a time). The dead weight balance used for the calibration is a device with two chambers: one with oil (oil chamber), which is pressurized by the application of weights on a vertical piston (weight support), and one with air (air chamber), where is mounted the transducer(s) to be calibrated (sensor plug), which is pressurized using the manual pump and the screw. The goal is to equalize the two pressures, as the pressure applied by the weights is known. The transducers signals are recorded at a frequency of 20Hz. The following procedure is followed to take each of the calibration points.

Procedure: The sensor(s) is/are mounted on the dead weight balance. Then the following protocols are applied:

At the beginning (no weight on the balance):

1. The ball valve is open and the screw is about at the middle of its range.
2. The weight support applies a pressure of 0.2 bara on the oil chamber. The pressure in the air chamber is increased using the pump until the weight support takes off and reaches its maximum position.
3. The ball valve is closed and the pressure in the air chamber is decreased by rotating the screw until the weight support lands again.
4. The air chamber is pressurized again using the screw, slowly, until the weight support takes off again by about 5 mm (so it does not reach its maximum position). The pressures are now equalized.
5. 10 seconds of stable transducer signal is recorded.

When the weight is increasing:

1. The weight is increased by adding a weight on the the weight support. The weight support lands because adding a weight increases the pressure in the oil chamber. The pressures in the two chambers are not equal anymore.
2. The ball valve is open.
3. The air chamber is pressurized using the pump until the weight support takes off and reaches its maximum position.
4. The ball valve is closed and the pressure in the air chamber is decreased by rotating the screw until the weight support lands again. The weights now need to rotate with the weight support in order to increase the accuracy of the settings. The pressure in the air chamber is increased again using the screw, slowly, while the weights rotate, until the weight support takes off again. The support rises by about 5 mm and does not reach its maximum position. The pressures are now equalized.
5. 10 seconds of stable transducer signal is recorded while the weights are rotating.

When the weight is decreasing:

1. The weight is decreased by removing a weight on the the weight support. The weight support takes off and reaches its maximum position because removing a weight decreases the pressure in the oil chamber. The pressures in the two chambers are not equal anymore.
2. The weights are rotating.
3. The pressure in the air chamber is decreased using the screw until the weight support lands (this operation is done while the weights are rotating).
4. The pressure in the air chamber is increased using the screw, slowly, until the weight support takes off again (this operation is done while the weights are rotating). The support rises by about 5 mm and does not reach its maximum position. The pressures are now equalized.
5. 10 seconds of stable transducer signal is recorded while the weights are rotating.

The pressures were corrected taking into consideration the atmospheric pressure at the time of the calibration and fitted through a linear interpolation against the voltage data. For each calibration data point, the error between the calibration and the measured pressure was calculated. From that data, the overall uncertainty of the absolute pressure data was characterized through the mean and standard deviation of the calibration errors.

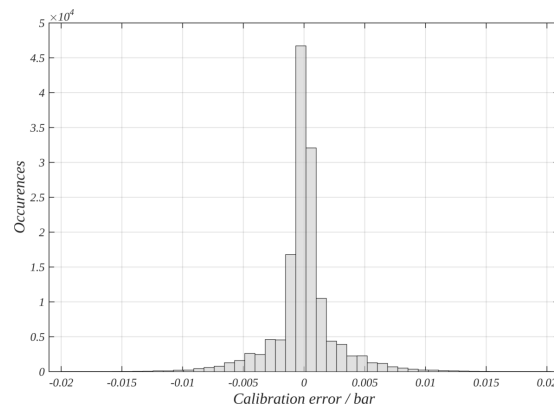


Figure G.1: Absolute pressure transducers calibration statistics

Results: Calibration statistics for the absolute pressure transducers are showed on Fig. G.1, page 137.

G.2.2 Thermocouples

The temperatures are derived from thermocouple measurements. The thermocouples used are K-type thermocouples. A thermocouple is a device made of 2 different conductive materials. In order to measure the temperature of the medium, the difference of potential created by the difference of temperature between the two ends of those two conductive wires is measured and converted into a temperature. The two ends of the two wires are welded together. In order to be converted into an absolute temperature, one of the temperatures at the ends of the wires need to be known. The latter can be measured by another temperature measurement device (usually, a PT100), or kept at a known value, for example by keeping the wire end into a mixture of ice and water (the medium is then kept at 0°C) [Rapin and Jacquard, 2010, p. 5].

Procedure: The thermocouples are calibrated against two reference thermometers PT100 and were calibrated inside a thermally controlled liquid water-glycol mixture bath. The temperature of the liquid bath has been varied by steps of 5°C, first decreasing from 20°C to -20°C, then increasing from -20°C to 80°C, then decreasing from 80°C to 20°C. Each step has last for 1 hour. The temperatures were stabilizing after about 30 minutes, then there were 20 minutes of stable signals, and 10 minutes of recording of stable signals. All the thermocouples have been calibrated together, at the same time, in the same thermally controlled bath. The sensors where kept at a homogeneous temperature being fit into a metallic part drilled to welcome thermocouples. The part was completely immersed in the thermal bath fluid.

The measured temperatures were fitted through a quadratic interpolation against the reference data. For each calibration data, the difference between the calibration and the reference was calculated. From that data, the overall uncertainty of the temperature data was characterized through the mean and standard deviation of the calibrated errors.

Results: Calibration statistics for the thermocouples are showed on Fig. G.2, page 138.

The uncertainty of all the thermocouples is set to the rounded value of the sum of the mean error, equals to zero, and twice the standard deviation, equals to 0.02°C. The uncertainty of the reference probe has been neglected and should have been added. The uncertainty is rounded above the computed value.

$$\mu + 2\sigma + \epsilon_{probes} = \pm 0.07^\circ\text{C} \quad (\text{G.2})$$

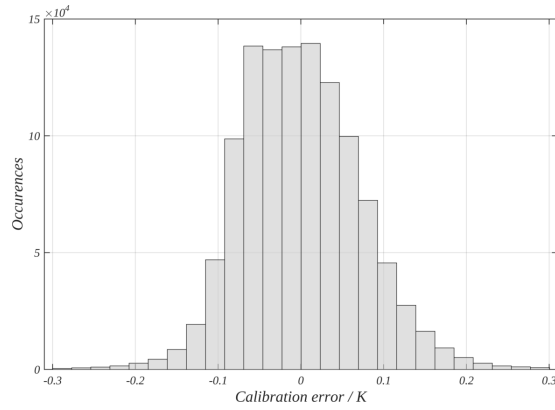


Figure G.2: Thermocouples calibration statistics

G.3 Uncertainties

G.3.1 Propagation of the uncertainties in the calculations

The propagation of the uncertainties through the sets of equations is performed automatically with the use of class of object in MATLAB, developed during the thesis [Carré, 2015]. The class includes the following propagation rules.

Addition & subtraction

$$\begin{aligned}
 &a \pm \Delta a \\
 &b \pm \Delta b \\
 &(a + b) \pm \sqrt{\Delta a^2 + \Delta b^2}
 \end{aligned} \tag{G.3}$$

$$\begin{aligned}
 &a \pm \Delta a \\
 &b \pm \Delta b \\
 &(a - b) \pm \sqrt{\Delta a^2 + \Delta b^2}
 \end{aligned} \tag{G.4}$$

Multiplication & division

$$\begin{aligned}
 &a \pm \Delta a \\
 &b \pm \Delta b \\
 &a \times b \pm \sqrt{\frac{\Delta a^2}{a} + \frac{\Delta b^2}{b}}
 \end{aligned} \tag{G.5}$$

$$\begin{aligned}
 &a \pm \Delta a \\
 &b \pm \Delta b \\
 &\frac{a}{b} \pm \sqrt{\frac{\Delta a^2}{a} + \frac{\Delta b^2}{b}}
 \end{aligned} \tag{G.6}$$

Logarithm & power

$$\begin{aligned}
 & a \pm \Delta a \\
 \ln(a) \pm & \sqrt{\frac{\Delta a^2}{a}}
 \end{aligned}
 \tag{G.7}$$

$$\begin{aligned}
 & a \pm \Delta a \\
 \log(a) \pm & \sqrt{\left(\frac{\Delta a}{\ln(10) a}\right)^2}
 \end{aligned}
 \tag{G.8}$$

$$\begin{aligned}
 & a \pm \Delta a \\
 & b \pm \Delta b \\
 a^b \pm & \sqrt{a^b \left(b \frac{\Delta a}{a}\right)^2 + (\ln(a) \Delta b)^2}
 \end{aligned}
 \tag{G.9}$$

Square root

$$\begin{aligned}
 & a \pm \Delta a \\
 \sqrt{a} \pm & \sqrt{a \left(\frac{\Delta a}{2a}\right)^2}
 \end{aligned}
 \tag{G.10}$$

Bibliography

J.-B. Carré. refprop-matlab-additions v1.0.0: A more usable backend to use NIST REFPROP in MathWorks MATLAB, August 2015. URL <https://github.com/speredenn/refprop-matlab-additions/tree/v1.0.0>. doi: [10.5281/zenodo.29424](https://doi.org/10.5281/zenodo.29424).

P. Rapin and P. Jacquard. *Aide-Mémoire - Formulaire du Froid*. Dunod, 14th edition edition, 2010. ISBN: 978-2-10-053893-5.

Compressor maps mathematical models

H.1 History

The development of the compression unit has started in 2002 with the feasibility study presented by Schiffmann et al. [2002]. The study attests of the feasibility of a twin-stage radial flow compressor with a 19.8mm and a 18.4mm-impeller rotating at 240 krpm with a total shaft power of 6kW [Schiffmann et al., 2002, p. 12 & 14]. The compression unit would be designed for domestic heating applications. From 2004 to 2008, Schiffmann [2008] has developed a single-stage compression unit of 3 kW with a 20mm-impeller. From 2008 to 2012, the company Fischer Precise Engineering Solutions AG¹ has been pushing the development of the single-stage unit to a twin-stage unit using the preliminary design and prototype developed by Schiffmann [2008]. During those 4 years, 4 design families have been issued². A working prototype, the unit *cp105* from the *evo4* design family, has successfully be tested in May 2012 in the Air-Water twin-stage heat pump Prototype (AWP). An other prototype of the same design family, the unit *cp101*, has been used in October 2013 in the Brine-Water twin-stage heat pump Prototype (BWP). Since 2013, the development of the compression unit has lifted off and the compression units are now industrial products.

H.2 Why a mathematical model of the compression maps?

In order to integrate those compression units, now technically ready, in heat pumps, the integrator needs to know how to control them in interaction with the controls of the thermodynamic cycle. Section 4.6.7, p. 63, suggests notably that using a model-based approach to control the heat pump could be the way to control the cycle properly and steadily. In order to include a model-based control in the heat pump controller, the integrator needs to include the maps of the compression stages in the model. The compressor maps are predicted with a physical model of the compressor, during the design phase, then the maps are determined by testing and measurements with each compression unit manufactured, as the maps depend on the geometrical parameters of the compression units, which slightly change with each unit. Integrating those maps in the controller is not convenient, as that implies to fill the controller with the points of the maps and to interpolate between the points. An other approach is to offer a mathematical model of the compressor maps and fit the model parameters with an identification test of the compression unit. The advantages are:

- The testing and measurement phase of each compression unit is a lot shorter, since a few points allow to identify the parameters of the model.
- The controller might need less computation power and memory to do the job.
- In the future, the compression unit could even identify its model parameters itself with a self-learning phase.

¹ Fischer Precise Engineering Solutions AG is a Swiss company based in Herzogenbuchsee, in Switzerland, <http://www.fischerspindle.com/facilities/fischer-engineering-solutions-ag/>.

² Details about the design families are given in appendix B.1, page 95.

H.3 Mathematical model of a compression map

A compressor map is a diagram which describes the link between the pressure ratio developed by the compressor and its mass flow rate, for each rotor speed. There is a compressor map per inlet conditions, being characterized by an inlet temperature and an inlet pressure. The compressor maps can be made dimensionless using Mach numbers [Haugwitz, 2002], as a Mach number is characterized notably by the pressure and the temperature of the fluid. If the map becomes dimensionless, one map only characterizes all the possible inlet conditions.

Map	Abscissa	Ordinate	Parametric speed
Classical map	Mass flow rate \dot{M}	Pressure ratio Π	Rotor speed N
Dimensionless map	Inlet Mach number $\mathcal{M}_{cp,in}$	Pressure ratio Π	Impeller tip Mach number $\mathcal{M}_{cp,tip}$

Table H.1: Characteristics of the classical and the dimensionless compressor maps

H.3.1 Modeling of the compressor iso-speed curves

The iso-speed curves are modeled using Lamé equations, also called super-ellipses equations [Haugwitz, 2002, 2003]. The generic form of a Lamé equation is given in eq. (H.1). The specific form used in this thesis work and described in eq. (H.2) uses the Lamé curves and applies them with scaled values, and with rotated coordinates, in order to decrease the prediction errors.

$$\left| \frac{x}{a} \right|^z + \left| \frac{y}{b} \right|^z = 1 \quad (\text{H.1})$$

$$\left| \frac{\mathcal{M}_{cp,in,scaled,rotated}}{a} \right|^z + \left| \frac{\Pi_{scaled,rotated}}{b} \right|^z = 1 \quad (\text{H.2})$$

The parameters a , b , and z are modeled using quadratic polynomials, as described in eqs. (H.3) to (H.5).

$$a = \sum_{i=0}^2 a_i \mathcal{M}_{cp,tip,scaled}^i \quad (\text{H.3})$$

$$b = \sum_{i=0}^2 b_i \mathcal{M}_{cp,tip,scaled}^i \quad (\text{H.4})$$

$$z = \sum_{i=0}^2 z_i \mathcal{M}_{cp,tip,scaled}^i + \kappa_{cp} \sum_{i=0}^2 z_i \mathcal{M}_{cp,tip,scaled}^i \left(\rho_{cp,in,scaled} - \frac{1}{2} \right) \quad (\text{H.5})$$

The coefficients a_i , b_i , z_i are fitted on the compressor map resulting from physical modeling or from measurements.

The inlet Mach Number $\mathcal{M}_{cp,in}$ and tip Mach Number $\mathcal{M}_{cp,tip}$ ³ are defined in eq. (H.6) and eq. (H.7).

$$\mathcal{M}_{cp,in} = \frac{C_{cp,in}}{a_{cp,in}} = \frac{\dot{M}_{cp}}{a_{cp,in} \rho_{cp,in} A_{cp,in}} \quad (\text{H.6})$$

$$\mathcal{M}_{cp,tip} = \frac{C_{cp,tip}}{a_{cp,in}} = \frac{\pi \varnothing_{cp,tip} N_{cp}}{60 a_{cp,in}} \quad (\text{H.7})$$

The inlet Mach Number $\mathcal{M}_{cp,in}$ is the ratio of the inlet fluid velocity $C_{cp,in}$ to the speed of sound in the fluid at the compressor inlet $a_{cp,in}$. $\rho_{cp,in}$ is the fluid density at the compressor inlet and $A_{cp,in}$ is the section of the compressor inlet.

³ The tip Mach number is a characteristic value, an indicator, and does not formally defines a physical phenomenon, as the number is calculated from the impeller geometry and gas characteristics. It is consequently abusive to call it a Mach Number. It is called this way for the sake of simplicity.

The tip Mach Number $\mathcal{M}_{cp,tip}$ is the ratio of the impeller rotation speed at the impeller tip $C_{cp,tip}$ to the speed of sound in the fluid at the compressor inlet $a_{cp,in}$. This Mach Number does not represent the real Mach Number of the fluid flow at the outlet of the compressor and is abusively called a Mach Number. This quantity allows a to couple the rotation speed to physical properties of the fluid at the compressor inlet.

H.3.2 Rotation of the coordinates

$$r = \sqrt{\mathcal{M}_{cp,in,scaled}^2 + PR_{scaled}^2} \quad (\text{H.8})$$

$$\phi = \begin{cases} 0 & \text{if } \mathcal{M}_{cp,in,scaled} = 0 \text{ and } PR_{scaled} = 0 \\ \arcsin\left(\frac{PR_{scaled}}{r}\right) & \text{if } \mathcal{M}_{cp,in,scaled} \geq 0 \\ -\arcsin\left(\frac{PR_{scaled}}{r}\right) + \pi & \text{if } \mathcal{M}_{cp,in,scaled} < 0 \end{cases}$$

$$\Psi = \phi - \theta_{cp} \quad (\text{H.9})$$

$$\mathcal{M}_{cp,in,scaled,rotated} = r \cos(\Psi) \quad (\text{H.10})$$

$$PR_{scaled,rotated} = r \sin(\Psi) \quad (\text{H.11})$$

The coefficients θ_{cp} and κ_{cp} are fitted on the compressor map resulting from physical modeling or from measurements.

H.3.3 Modeling of the isentropic efficiency

The isentropic efficiency can be modeled also with the inlet an tip Mach numbers. The curves are modeled with degree-four polynomials and values are scaled in order to obtain better correlations. The coefficient of those polynomials are modeled with polynomials at degrees ranging from 2 to 6, as described in eqs. (H.12) and (H.13).

$$\eta_{cp,s,scaled} = \sum_{j=0}^4 d_j \mathcal{M}_{cp,in,scaled}^j \quad (\text{H.12})$$

$$d_j = \sum_{i=0}^{2i+6} d_{ji} \mathcal{M}_{cp,in,scaled}^i \quad (\text{H.13})$$

The coefficients d_{ji} are fitted on the compressor map resulting from physical modeling or from measurements.

H.4 Errors of the correlations

The correlations are used to predict the mass flow rate, deduced from the inlet Mach number, from the measured pressure ratio. Unfortunately, at low mass flow rates, the compressor iso-speed curves become almost flat, which means that prediction of low mass flow rates with any correlation is a difficult operation. In order to keep the the errors in acceptable ranges, a rotation of the coordinates is performed. A two-objective optimization is run on the fitted parameters described in the sections above in order to keep the average error over the whole map and maximum error in acceptable ranges. From the Pareto curve obtained with the optimization, a solution is selected. The author recommends to give more weight in the decision process to low average errors, as the compressor is likely to work most of the time in low error areas. Indeed, the domain where the prediction is inaccurate is very close to the surge line.

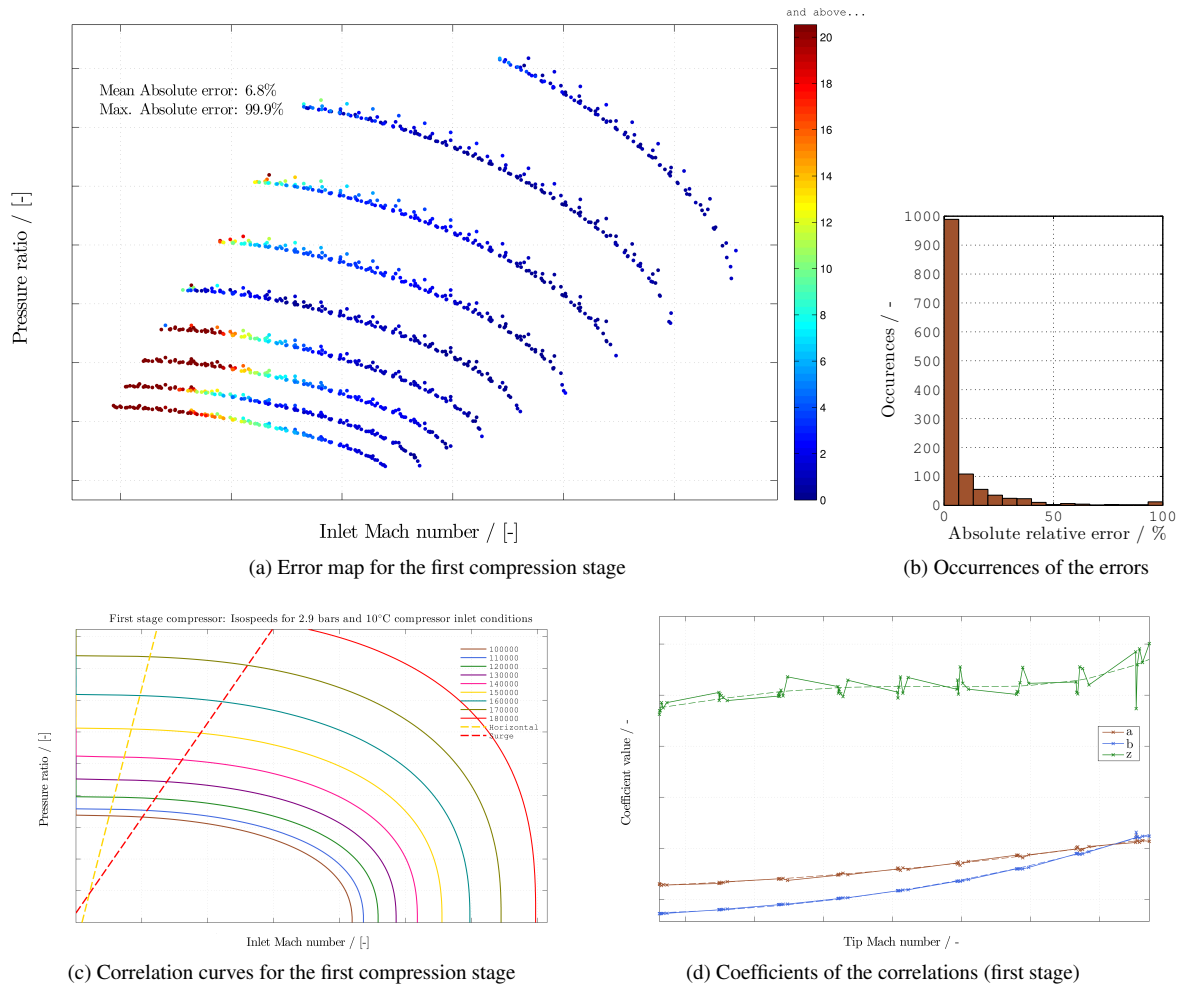
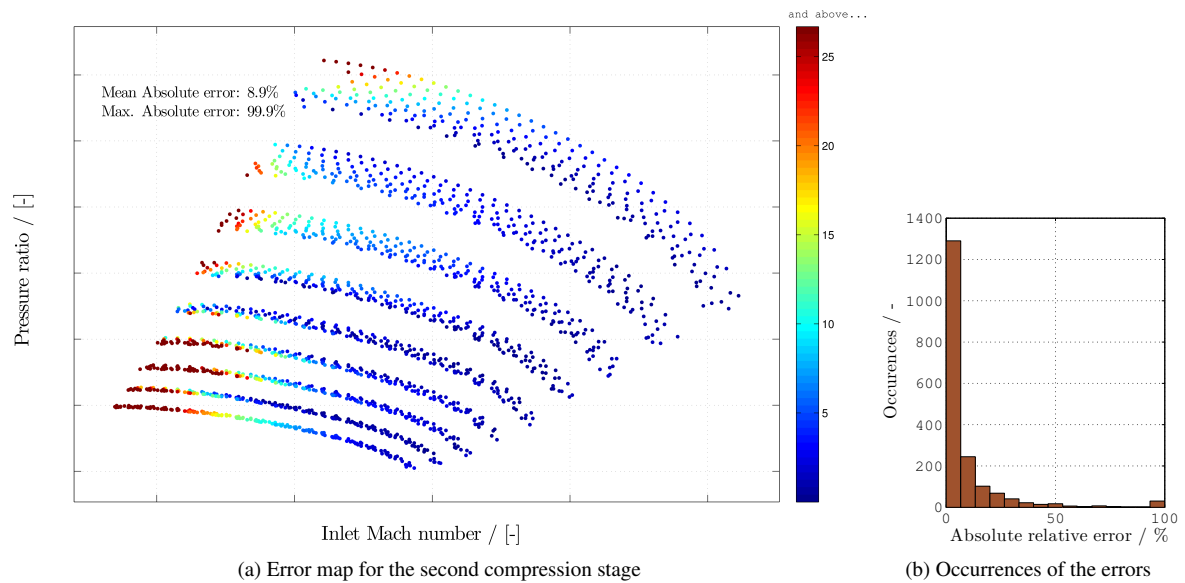
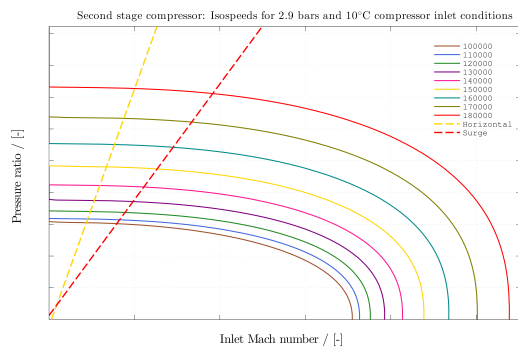


Figure H.1: Errors in the first compression stage map correlations. The axis have been removed due to confidentiality issues.

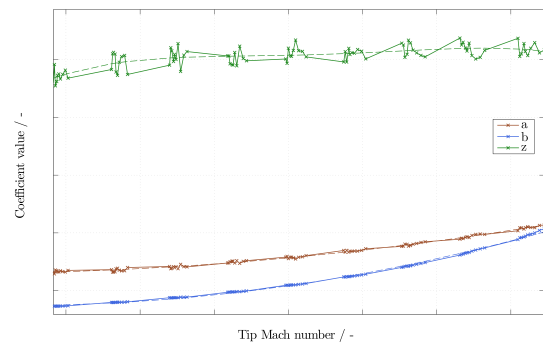


(a) Error map for the second compression stage

(b) Occurrences of the errors



(c) Correlation curves for the second compression stage



(d) Coefficients of the correlations (second stage)

Figure H.2: Errors in the second compression stage map correlations. The axis have been removed due to confidentiality issues.

Bibliography

- S. Haugwitz. Modelling of Microturbine Systems. Master's thesis, Department of Automatic Control, Lund University, Sweden, 2002. URL <http://www.control.lth.se/Publication/5687.html>.
- S. Haugwitz. Modelling of Microturbine systems. In *Proceedings of European Control Conference, Cambridge, Great Britain*, Sept. 2003. URL <http://www.control.lth.se/Publication/haug03.html>.
- J. Schiffmann. *Integrated design, optimization and experimental investigation of a direct driven turbocompressor for domestic heat pumps*. PhD thesis, Swiss Federal Institute of Technology - Lausanne, 2008. URL <http://dx.doi.org/10.5075/epfl-thesis-4126>.
- J. Schiffmann, A. Molyneaux, D. Favrat, F. Marechal, M. Zehnder, and J. Godat. Compresseur radial pour pompe à chaleur biétagée - Phase 1. Technical report, OFTEch SA, Nov. 2002. URL http://www.bfe.admin.ch/forschungwkk/02425/02724/02727/index.html?lang=en&dossier_id=03092. On the behalf of the Office Fédéral de l'Énergie (OFEN).

Jean-Baptiste CARRÉ

French - 31 years old

@ : jean-baptiste.carre@gadz.org

Main experiences

Heat pumps
Radial turbomachinery
Two-phase flow heat transfer
Refrigeration technologies



[View My LinkedIn Profile](#)

Development, experimentation, and modeling of refrigeration technologies

Profile

Heat pump specialist experienced with experimental and simulation work. Enthusiasm technophile interested in heat transfer and refrigeration technologies. Curious and passionate.





Experienced also with :

- **project communication**
Good presentation and communication skills developed through many presentations and meetings during [Exp. 1, Exp.2, and Exp.3].
- **co-worker supervision and team work**
Supervision of 3 different technicians (one at a time) for the realization of 3 heat pumps and heat transfer experimental setups [Exp.1]. Supervision of 6 semester project students and 2 interns (2 months each) [Exp.1]. **Team work** on different projects [Exp.1, Exp.2, Exp.4].
- **events and meetings organization**
Chairman role in an international conference (ECOS2010, Lausanne - Session 3.8), organization and supervision of student **meetings and brainstorming sessions** [Exp.1].
- **definition and funding of new projects**
 - The project associated with [Exp.2] has been **defined from scratch** and proposed to EDF R&D. This definition included finding the **funding** for the project and the internship position. The project associated with [Exp.4] has also been defined from scratch. It included the **finding of a partnership**.

Selected work experiences

- **Exp.1 : Research assistant (PhD Thesis project)** Oct. 2008 – Oct. 2013
Industrial Energy Systems Laboratory (LENI), École Polytechnique Fédérale de Lausanne (EPFL), Switzerland.
Development of twin-stage air/water oil-free domestic heat pumps powered by twin-stage oil-free radial compressors rotating on gas bearings. This work has included **experimental and modeling aspects**, with the development of a dynamic simulation of the tested systems.
- **Exp.2 : Thermal systems engineering assistant (intern)** Feb. – Sep. 2008
EDF R&D, Moret-sur-Loing, Seine et Marne, France.
Preliminary design of building heating and cooling systems, and of water heating systems, based on thermodynamic equipments (HVAC, heat pumps, thermodynamic cycles, etc...), for buildings in the service sector.
- **Exp.3 : Thermal engineering assistant (intern)** Jun. – Sep. 2007
EDF R&D, Moret-sur-Loing, Seine et Marne, France.
Initial mission : Sensitivity analysis of uncertain parameters in service sector buildings energy consumption diagnostics. That studying aimed at the determination of the impact of the expert's estimation mistakes on those parameters.
Extra mission : Preliminary study of different thermal simulation model adjustment methods. The goal of that study was to characterize the influence of the adjustment methods on the simulation results.
- **Exp.4 : Passive house designer (engineering school project)** Oct. 2006 – Jun. 2007
Project manager and designer roles in an engineering project consisting in the **design of passive houses characterized by low building and maintenance costs**. That project was developed in partnership with the "Office Public d'Aménagement et de Construction (OPAC)" of Saône & Loire (French agency that builds and manages housing structures for, or in collaboration with, the French Government or the local French governments).

Education

- **Master of Science in innovation, design, and engineering**  +  2008
Formalization of a generic method to control the costs along the whole product life cycle. Joint diploma at Arts & Métiers ParisTech (ENSAM) and École Centrale Paris (ECP), two of the French leading engineering schools, Paris, France.
- **Master degree in Mechanical Engineering**  2008
Arts & Métiers ParisTech (ENSAM), one of the French leading engineering schools, particularly known for its teaching in Mechanics and Manufacturing processes, Paris, France.
- **Two-year University degree in Mechanics (DUT)**  2005
Education focused on Mechanics, Product Design, and Manufacturing processes, Institut Universitaire de Technologie Grenoble 1, Université J. Fourier, S^t Martin d'Hères, Isère, France.

Languages

- **French** *Mother tongue.*
- **English** *Estimated C2 level on the European Language Council scale (Proficient level) - PhD thesis written and defended in English. TOEIC score 2008 : 920 points.*

Selected computer skills

Advanced computer skills, with various kind of software and operating systems :

- **Design** *Good skills with Catia, Pro/Engineer, and SolidWorks - Intermediate skills with CES Selector ;*
- **Simulation** *Good skills with MatLab, Octave, Maxima, Mathematica, gPROMS, and OpenModelica ; Basic skills with Dymala, ANSYS, RDM6, and Comsol ;*
- **Office** *Good skills with Microsoft Office, OpenOffice.Org, LibreOffice, and \LaTeX ;*
- **Programming** *Basic programmation skills with Microsoft VisualBasic, Python, and Rubis ;*

Strong interest for free software and open technologies. Good skills with GNU/Linux operating systems (Gentoo Linux, Debian, and more) and with many kinds of free software on GNU/Linux, Microsoft Windows, and Apple operating systems.

Extra curricular activities : Swimming, photography, hiking, mountain biking, computer sciences, free software, GNU/Linux.